

Roads Prescription-Scale Effectiveness Monitoring Project

Interim Report #2
August 2024



Charlie Luce, Tom Black, Amanda Alvis, Erkan Istanbuluoglu, Julie Dieu, Jenelle Black, Alexander Prescott

Cooperative Monitoring, Evaluation, and Research (CMER) Committee

TABLE OF CONTENTS

1	Executive Summary.....	1
2	Project Background.....	4
2.1	Critical Questions.....	5
3	Major Experiment.....	6
3.1	Study Areas.....	8
3.2	Methods.....	8
3.3	Data Collection Status.....	12
3.4	Results from WY2023 Dec-Mar Analysis.....	16
4	Continuing Model Development.....	35
4.1	Traffic-induced, erosion-enhancing processes.....	36
4.2	Spatially-lumped model.....	36
4.3	Preliminary model results.....	39
4.4	Future model development.....	42
5	Sediment Trap Efficiency Experiment.....	45
5.1	The Experiments.....	45
6	Short-Time-Scale Interactions Experiments.....	49
6.1	Short-Time-Scale Pumping Experiment.....	50
6.2	Short-Time-Scale Turbidity Experiment.....	55
7	Ditch Line Hydraulics Experiment.....	61
8	Micro-Topography Experiment.....	61
9	Cost Vs. Maintenance Survey.....	61
10	GRAIP/WARSEM.....	65
11	References.....	66
12	Appendices.....	68

ACKNOWLEDGEMENTS

This project was developed with public funding through the WA DNR Adaptive Management Program. The document was prepared for the Cooperative Monitoring, Evaluation and Research Committee (CMER) and was intended to inform and support the Forest Practices Adaptive Management Program.

The project team would like to extend our sincere appreciation to the following project partners, whom without we could not have completed this work. Westfork Environmental: Phil Peterson, Gavin Nishiyori, Sean Olsen, Heidi Barnett, Dakota Vogel, and others. DNR Pacific Cascade Region: Olivia Cantwell, Laura Cummings, Chris Harteloo, Jay Small, Kaleb Dean, Jeremiah Morris, Stan Sawyer, and others. United States Forest Service: Sam Calahan, Christa Howarth, Nathan Nelson, Erik Smith, and Zachary Holden. University of Washington: Lauren Wittkopf, Friedrich Knuth, David Shean. Green River College: Kimberlee Vezzetti. Weyerhaeuser Longview and Aberdeen tree farms: Frank Jongenburger, Wade Anderson, Jay Zillyett. Rayonier: Zane Jones, Peter Graddon, Kate McLean, Emily Elfering, Angelica Danna, Griffin Ollar, Mike Riley. Bob Daheny. American Forest Management, Manulife Investment Management, Grays Harbor County, Forest Investment Associates, Olympic Resource Management, Hancock Timberland X, and BTG Pactual.

TABLE OF FIGURES

Figure 3.1 Locations of the HTNS Major Experiment study sites in western Washington.	8
Figure 3.2 “Good” rock (i.e., relatively un-weathered basalt) is the darker rock in this picture, and “marginal” rock (i.e., slightly more weathered) appears with a lighter tan color.	9
Figure 3.3 Configuration of an 80-meter segment.	10
Figure 3.4 The upper figure shows the road surface routing water to the ditch and the collection trough.	11
Figure 3.5 V-notch weir and flow-proportional splitter in upper photo. The white blocks spread the water to ensure even flow across the splitter at the end of the flume. The lower photo shows the covered flume, debris filter and the stage measuring sensor in the white tube.	12
Figure 3.6 Rain gage data from water years 2022 and 2023. Not all sites are shown.	14
Figure 3.7 The percentage of time that reasonable field data were recorded on the tipping bucket flow gages between Oct 15 and June 15 of each water year.	15
Figure 3.8 Probability density function (pdf) of monthly runoff across site-months.	19
Figure 3.9 pdf of site slope	19
Figure 3.10 pdf of runoff times slope, roughly a measure of the average monthly stream power.	20
Figure 3.11 pdf of suspended sediment measured across site-months.	21
Figure 3.12 pdf of coarse sediment estimated across site-months from annual measurements at each site and apportioned to months on the basis of suspended sediment timing at each site.	21
Figure 3.13 pdf of total sediment, sum of suspended and coarse sediment, across site-months.	22
Figure 3.14 pdf of the suspended sediment fraction across site-months.	22
Figure 3.15 Relationship between the suspended fraction and the monthly runoff at each site, showing that site-months with greater throughflow in the sediment tubs tend to have a greater fraction in suspension.	23
Figure 3.16 pdf of the degradation resistance by site, showing bimodal distribution of rock quality.	24
Figure 3.17 pdf of the fraction of the shear stress apportioned to sediment grains (fgss) by site, showing bimodal distribution with many heavily grassed sites and several sparsely grassed sites.	24
Figure 3.18 a)-c), monthly distributions of trucks by month over sites and by classification of wetness during traffic, d) distribution of light vehicles by month over sites.	26
Figure 3.19 Correlation matrix for vehicle traffic metrics	27
Figure 3.20 pdf of fraction of trucks on wet or very wet days.	28
Figure 3.21 Relationship between stream power and sediment yield classified by high vs. low traffic, illustrating coarsely the effects of two primary drivers.	29
Figure 3.22 Relationship between stream power and sediment yield classified by high vs. low traffic and for degradation resistance (rock quality), showing the conceptual benefits of improved rock quality	30
Figure 3.23 Relationship between stream power and sediment yield.	31
Figure 3.24 Dependence of sediment yield on a simple weighted traffic loading, without consideration of other covariates.	32
Figure 3.25 Plot of predicted vs observed results using leave-one-site-out (75-fold) cross validation.	34
Figure 3.26 Relative effects of each covariate on the sediment yield (ITsed1), all axes are log transformed variable values.	35
Figure 4.1 Schematic of the pumping process.	36
Figure 4.2 Schematic of the crushing process.	36

Figure 4.3 Schematic of spatially-lumped modeling domain within an 80-m by 9-m experimental road segment. 37

Figure 4.4 Tri-layered conceptualization used to model processes occurring vertically within the road prism. 38

Figure 4.5 Fine sediment storage depth in the transport available fines (TAF) layer over time for three traffic levels..... 40

Figure 4.6 Cumulative reference transport capacity depth and cumulative actual transport depth over time for three traffic levels (mean $n_{\Delta t} = 5, 10, 20$ truck passes per day)..... 41

Figure 4.7 Sediment load per meter of road for each water year of the model run for three traffic levels (mean $n_{\Delta t} = 5, 10, 20$ truck passes per day)..... 42

Figure 4.8 Updated tri-layered conceptualization used to model processes occurring within the road prism. 43

Figure 4.9 The current modeling domain as defined in Landlab showing (a) the initial road surface and (b) the road surface after running the in-progress sediment displacement component..... 44

Figure 4.10 A cross-sectional profile of the road surface and ditch line before (gray dash-dotted line) and after (black line) running the in-progress sediment displacement Landlab component. 45

Figure 5.1 Flume and sampler configuration..... 46

Figure 5.2 Flume with sampler during run in the upper image and the retained sample in the photo below. 47

Figure 5.3 Vibratory sediment feed device applying the sediment at the upper end of the flume..... 48

Figure 5.4 Sediment trap efficiency for 5, 10 and 50 gallons a minute. 49

Figure 6.1 New fine sediment pumped from the roadbed by the passage of a loaded log truck..... 50

Figure 6.2 Surface and the photo on the right shows the surface after 6 truck passes..... 52

Figure 6.3 The fine sediment that is available for transport on the road surface due to recent traffic is carefully washed from the isolated sampling area and evacuated into a sample container for sediment analysis..... 52

Figure 6.4 The location of the 5 sampling frames within the study plot..... 53

Figure 6.5 Sampling frame before the truck passes and after the truck passes at Mel-2..... 54

Figure 6.6 Fine sediment mass sampled from 5 sample locations at Mel 12 on 2/14/ 2023 and Mel 4 on 2/19/23. 55

Figure 6.7 General layout of the water and sediment sampling locations for the turbidity experiments. 57

Figure 6.8 Gutter is sheltered from direct rainfall with a cover so that the sample is not diluted. 57

Figure 6.9 Turbidity sampling locations below the trough and ditch in the upper photo and at the Tub in the lower photo. 58

Figure 6.10 Suspended sediment concentrations from sample locations at Mel 14 on Jan 18, 2024, following truck traffic..... 59

Figure 6.11 Turbidity of samples collected for SSC from the Trough, Gutter, Ditch and Tub on 1/18/24 using a reliable ClariVue 10 in the lab..... 60

Figure 6.12 Turbidity results from the Ditch and Tub locations on January 18, 2024, with two periods of truck passes..... 61

Figure 9.1 Number of responders out of 11 for rock quality by road traffic level – A) frequent and sometimes used; B) frequent use only. 63

TABLE OF TABLES

Table 3.1 Covariates monitored in the examination of BMP performance (CMER 2017).	7
Table 3.2 List of Measurements and Covariates considered in this analysis.	18
Table 3.3 Parameter estimates and significance for (t-values greater than 1.67 are significant at the p=0.10 level).....	33
Table 5.1 Table of runs carried out the week of June 18-21, 2024.	48
Table 6.1 Summary of S-T-S Pumping Experiment Samples, Siltstone Province.	51
Table 6.2 Table of STE Turbidity runs dates and data quality.	55
Table 9.1 Number of responders out of 11 for each ditch line BMP by road traffic level.	64

1 EXECUTIVE SUMMARY

The Roads Prescription-Scale Effectiveness Monitoring Project was designed to monitor sediment production and delivery from forest roads in varying contexts of road use and design, with particular emphasis on measurement of the reductions from utilization of best management practices. In this interim report, we present updates on both the Parameterization Experiments and the Major Experiment. Substantial new results and analysis are presented with respect to 1) Major Experiment data completeness and quality, 2) Major Experiment results, 3) Model design and testing, 4) Sediment Trap Efficiency Experiment, 5) Short-Time-Scale Pumping Experiment, 6) Short-Time-Scale turbidity Experiment, 7) Ditch Line Hydraulics Experiment, 8) Micro-Topography Experiment, 9) Cost Vs. Maintenance Survey, and 10) GRAIP/WARSEM Experiment.

Data collection from the Major Experiment has always been the most challenging part of this experiment. Essentially, we are sampling 78 small-catchment studies for both flow and flow-proportional water quality—this is one of the largest small-catchment studies comprising both flow and quality metrics currently operating. It has been very successful in raw data capture, with only a few sites having persistent (though decreasing) problems in raw data acquisition. With the extent of successful data capture, imputation of data allowed use of 76 of 78 of the plots in the example analysis provided in this report, and further work on imputation may be able to reasonably represent these data, particularly as new years of successful data are added to generate more information for training and validation relationships.

With a subset of the data from the rainy season, December-March of Water Year 2023 (WY2023) on 76 plots, we attempted analyses intended for the Major Experiment data. We attempted these analyses to see if we could identify signals related to sediment yield from a few key best management practices (BMP) tests: augmented ditch line roughness, improved rock quality, and traffic timing relative to rainfall, all in the context of varying flow and traffic conditions. Per earlier experiments (e.g., Van Meerveld et al., 2014), the signal was dominated by sediment transport capacity (as indexed by flow \times slope) with a substantial effect from traffic. No effect was discernible with respect to the fraction of traffic under wet conditions; however, clear and statistically significant effects were found for both the added ditch line roughness (i.e., how much the added roughness reduces grain shear stress) and the gravel degradation score (i.e., how strong the rock is under wet conditions). Based on preliminary results from this study, fairly common treatments (typical of what exists or is applied on managed forest land, per a survey that was sent to landowners), sediment yields appear to be halved for each treatment type such as topping with higher quality rock or installing ditch line BMP. Further examination of data will be looking for improved statistical significance on interaction effects between contextual variables (stream power and traffic) and BMP effects, and interactions between road surface BMP and ditch line BMP. Some of these interaction effects were marginally significant in the continuous-variable analyses and showed up as strong effects when some contextual or test covariates were used in binned rather than continuous analyses, so we expect to learn more about these. A key message from the test analyses in this report is that the experiment is working well to measure the BMP effectiveness as intended and, with the planned BMP changes in the Study Design and implemented for WY2024, we expect yet sharper distinctions and greater capacity to detect contextual effectiveness from the WY2024 and WY2025 data.

Additional progress has been made on Model Development in terms of representing traffic-induced, erosion-enhancing processes for varying levels of traffic. The model is also able to describe, in mechanistic terms, the asymptotic decline in surface sediment storage and sediment output rates over the course of a rainy season. Preliminary efforts presented below have not shown a relationship between sediment production and haul as it occurs on days of significant rainfall. As modeling efforts continue, we hope to better understand this unexpected empirical result with respect to traffic timing and sediment yield. Answers may lie in the effects of continued rock crushing, and possibly pumping, as these processes occur when sediment is damp but rainfall is insufficient for transport.

The initial Sediment Trap Efficiency Experiment showed very strong results, with nearly complete sediment retention under lower flow conditions (very common within our observations) and linearly reduced efficiency with added flow rate for a large range of rates. Retention was strong even with relatively high flow rates. These measurements were done with well aggregated soils, typical of what is available in a recently graded ditch, but questions remain about finer sediments, such as may be sourced from the road surface during heavy haul, and a replicate set of tests using finer material is being completed this fall.

The amount of sediment generated by traffic and its disposition during short time scales is being evaluated in the two components of the Short-Time-Scale Experiment. In the S-T-S Pumping Experiment, the road is wetted and cleaned, and the new sediment appearing at the surface after traffic has passed is measured. Across several replications of the experiment conducted to date, an average of about 0.01 kg of fine sediment has been generated per m² of tread per truck pass. That we can obtain a relatively consistent and measurable value using relatively novel and potentially imprecise methods indicates that pumping is an important process for bringing sediment to the road surface. The S-T-S Turbidity Experiment measures turbidity change over time from the starting and stopping of traffic during storm events. The results suggest that the pumped fine sediments are “washed off” in a relatively short time during a storm after traffic stops. Together, these experiments support a general concept that traffic during wet conditions leads very directly to pumping and transport of sediment. Questions remain about how much pumping occurs under “damp,” as opposed to “wet” conditions, and very specifically how much sediment might be brought to the surface to be washed off during the next potential event. Related questions exist about how much rock crushing occurs while the roadbed is still damp or dry, leading to increased subsurface storage of fines rather than pumped and surface-stored fines.

The Ditch Line Hydraulics Experiment measured the reduction in grain shear stress associated with common ditch line BMP and demonstrated that reductions in sediment transport were directly related to the reductions in grain shear stress. The results are published and attached here in Appendix B. These results provide a basis for generalizing the expected benefits of ditch line BMP to other contexts and conditions based on the distributions of grain sizes and flows. The fractional grain shear stress metric produced in this experiment was used in the analysis of the Major Experiment, revealing a statistically significant effect on empirical measurements of sediment production from road segments. This allows use of a continuous variable in place of a class or “name” variable for ditch line treatments, by which we mean that the effects of a specific ditch line BMP can be characterized as a measure of roughness rather than each BMP being individually parameterized.

The Micro-Topography Experiment examined the spatiotemporal evolution of ruts and the effects of these ruts on flow pathways and erosion potential of the road surface. The results will be submitted for publication within the next month, and a draft of the paper is attached here in Appendix C. Using an unoccupied aerial vehicle and structure-from-motion technology, we investigate the evolution of rut incision as caused by traffic over time. We found that: (1) the relationship between our measure of rut incision and time since grading was nonlinear at both sites for all seasons with sufficient data; (2) as ruts develop, the overall flow pathways shift down-road; and (3) the erosion potential of our road surfaces tended to increase overall as ruts developed. Our analyses of rut evolution effects on flow pathway alterations and increases in erosion potential demonstrate the utility of using three-dimensional road surface data from SfM, rather than a few two-dimensional cross sections.

The central question that the Adaptive Management Program is asking from this study is: “Are road prescriptions effective at meeting site-scale water quality standards and performance targets for sediment and water?” There are many contexts across a forest road network, so two different ways of answering this question are “it depends” or “in some places, yes, in others, no.” The longer list of questions developed during the Study Design, however, produces slightly more straightforward answers. In terms of “How effective are road sediment BMP, individually and in combination, at minimizing production?” a few relatively concrete answers are developing. For example, the Ditch Line Hydraulics Experiment shows that in relatively low flow or low gradient conditions, we might expect quite strong, if not near elimination of sediment by introducing high roughness (e.g., heavy grass or wattles). Empirically we see a halving of the sediment production as we range from bare to heavily grassed plots as integrated across all other plot contexts. The Ditch Hydraulics Experiment tells us that this effect results from increased water storage along the ditch and resultant decreases in shear stress or “erosion potential.” There is some sense from the empirical analysis that the effect is stronger with less traffic and greater stream power, but more testing is needed to sharpen the interaction estimate as well as the mean estimate. Similarly, moving from marginal to good rock in this study nominally halved sediment production, integrated across all other contexts. The effect of rock quality appears much stronger under high traffic, as one might expect and where it would be most critical. These different contributors seem to affect erosion amounts independently and are additive in log-space, indicating that strong improvements in both rock quality and ditch line roughness could each halve the sediment yield (e.g., a multiplicative effect), on average across many plot types. Further study, and hopefully the data from WY2024 and WY2025 reflecting the BMP changes will more strongly highlight the contexts in which each kind of treatment is most valuable.

In contrast, our understanding of wet-weather haul did not follow initial expectations. There are clear responses to wet-weather traffic during individual events, both in terms of pumping sediment from the roadbed to the surface and in generating short-lived turbidity pulses, that are clearly caused by traffic events. At the same time, the fraction of traffic during wet weather seems to have no effect on monthly sediment yields. This seeming paradox across time scales speaks to fine sediment production and storage within the roadbed and maybe at the surface. We expect the modeling study to point toward resolution of this paradox and future experiments that could test understanding.

In summary we have useful, practical, theoretically-and-mechanistically-supported, and statistically-detectable answers to basic questions about BMP effectiveness already. These support strong utility of basic BMP already in wide use, and others that could be used for temporary construction or maintenance circumstances. At the same time, there are limits to the effectiveness of the treatments.

Completing the planned study should improve and clarify these results further and help better identify the contexts where effects are strongest and weakest. We also have unexpected results with different answers when we look at different time scales of traffic, and we have planned modeling work that we expect will illuminate the seeming paradox.

This being an “interim report” it is worthwhile to highlight that a principal challenge in many studies is not having high enough data quality to elucidate differences across several treatments in a large-dimensional study. Here we are working with a relatively small data set with respect to the number of dimensions we are trying to find effects from. The fact that we are able to detect statistically significant changes for the key variables we hoped to test speaks highly for the team of people taking the measurements and keeping the measurement system operating at its highest performance. While there is fundamentally not much unique or clever about the overall statistical design or analysis (though there are some features that are helping), the overarching driver of the success we are seeing in measuring these effects derives from a well-coordinated and competent team collecting, collating, and managing the data.

2 PROJECT BACKGROUND

Forest roads provide many functions such as transportation of timber products, emergency access, and access for recreationists, hunters, and fishermen. At the same time, road erosion is a large source of anthropogenic sediment in watersheds managed for timber production. Fine-grained sediment has the potential to adversely affect water quality and aquatic resources at the site, channel reach, and watershed scales.

Increased inorganic sediment loads—beyond quantities or frequencies that occur naturally—can influence the stream biota in many ways. Turbidity can reduce stream primary production by reducing photosynthesis, which affects other organisms in the food web. In addition, turbidity impacts gill function and respiration and limits feeding success of fish. Deposited sediments may affect fish or amphibians directly by smothering eggs in redd or oviposition sites, altering spawning or early rearing habitat, and reducing overwintering habitat for fry. Fish or amphibians may also be affected indirectly by deposited sediments that limit invertebrate species composition thereby decreasing abundance of preferred prey (Suttle et al., 2004).

Recognizing that roads are persistent sources of fine sediment to forest streams, forest managers have made substantial improvements in water quality in recent decades through their diligent application of best management practices (BMP). Cross-drain culverts to relieve roadside ditch line water before it reaches a stream crossing have become a common practice. Recent monitoring results in western Washington indicate that 10-11% of the total forested road length directly delivers sediment to the channel network (Dubé et al., 2010; Martin, 2009). This 10-11% of the total forest road length is stream-adjacent, cannot be successfully drained onto a hillslope, and, where this situation coincides with heavy traffic, leads to increased delivery of sediment to streams (Dubé et al., 2010).

A focal question in this project is: What combinations of surfacing, ditch line management, traffic control, and drainage management will most efficiently and effectively mitigate sediment yields from high-traffic, near-stream (HTNS) roads? Many previous studies have tested individual BMP, but landowners are more likely to implement multiple BMP simultaneously (e.g., reconstructing an old road

by adding better quality rock, increasing the number of cross-drain culverts, putting the tread into a crowned configuration, and grassing the ditch line). Thus, studying multiple BMP as a set is a logical approach. In fact, one BMP may even reduce the effectiveness of another one. For example, paving a road reduces sediment delivered from the surface but contributes more water to the ditch line and, if the ditch is bare soil, erosion can increase relative to that expected in a ditch adjacent to a gravel road.

HTNS roads are important to the transportation network as key mainline roads but are more likely to deliver sediment to streams. To meet stewardship goals and effectively address operational needs, HTNS roads warrant additional investment by landowners to increase BMP beyond those in common use. Road upgrades and enhanced BMP, however, can incur a significant cost. Therefore, improved knowledge regarding the effectiveness of both individual and integrated combinations of BMP is useful for understanding the return on BMP investments.

2.1 CRITICAL QUESTIONS

The Roads Prescription-Scale Effectiveness Monitoring Project has one guiding CMER Work Plan critical question and seven specific study design critical questions. These study design critical questions were developed as targeted and answerable questions, nested under the one CMER Work Plan critical question. Both the Major Experiment and all Parameterization Experiments were designed to specifically address one or more critical questions. As described below, significant progress has been made in addressing these questions. Completion of the Major Experiment and the remaining Parameterization Experiments (i.e., Short Time Scale Interactions, GRAIP/WARSEM) is expected to lead to solid conclusions.

CMER Work Plan Critical Question

1. Are road prescriptions effective at meeting site-scale water quality standards and performance targets for sediment and water? (Exclusive of mass wasting prescriptions, which are covered in the Unstable Slopes Rule Group.)

Study Design Critical Questions (framing the primary critical question in answerable terms).

1. How effective are road sediment BMP, individually and in combination, at minimizing production and delivery of coarse and suspended sediments from forest roads to streams (DNR Typed Waters)?
 - Total sediment yields were roughly halved by each rock quality improvement and by each increase in ditch line roughness. Reduced fractions of haul during wet weather had little influence. WY2024 and WY2025 data from the Major Experiment will provide better parameterization of specific ditch line BMP.
2. What is the comparative effectiveness of BMP in minimizing the production, routing, and delivery of sediment to streams (defined as DNR Typed waters)? And what are the comparative installation cost effectiveness, and maintenance cost effectiveness and frequency, of these BMP?
 - Total sediment production was roughly halved by each rock quality improvement and by each increase in ditch line roughness. Delivery and routing measurements, fundamental to understanding the impacts of road erosion on public resources, require completion of the GRAIP/WARSEM Experiment (see below). BMP that are being tested are in common use and relatively inexpensive (if not less expensive); our choices of which BMP to test have been informed by the Cost Vs. Maintenance Survey (see below).
3. For individual or combinations of BMP, are increases in turbidity minimized?

- Sediment reductions from rock quality and ditch line treatment effects were best modeled as mathematically independent, though multiplicative in nature. It is not clear that the effects of these basic BMP absolutely minimized production, but the reductions were substantial in magnitude. Data from WY2024 and WY2025 with the elevated ditch line BMP in place may document further sediment reductions.
4. Are the effects of combined BMP for the road surface and ditch lines additive, multiplicative, synergistic, or antagonistic with respect to runoff and sediment production from road segments?
 - The WY2023 data used here as a sample suggests that sediment reductions from rock quality and ditch line treatment effects were best modeled as mathematically independent, though multiplicative in nature.
 5. To what extent do road BMP affect water storage and erosion potential at site-scale road segments?
 - Sediment reductions from ditch line treatments fundamentally result from increased water storage in the ditch during storms, as demonstrated by the Ditch Line Hydraulics Experiment (see Appendix B).
 6. How do different characteristics of topography and lithology affect the selection and design of road BMP?
 - While there are some hints about contextual differences with respect to varying flow or slope for ditch line treatments, those are not statistically significant with this sample data set. We are anticipating statistically significant results by using all of the Major Experiment data, including WY2024 and WY2025 (i.e., since the BMP changeover). Analysis of the WY2023 data suggests that lithology has no effect on sediment yields.
 7. How quickly after installation or removal of BMP does the post-construction disturbance that temporarily increases sediment production and delivery abate?
 - Treatment changes were made in summer of 2023. WY2024 data have been collected but not yet analyzed (although our field crew anecdotally described increases in sediment during the June tub cleaning). The WY2025 data will help us understand how BMP installation effects abate and clarify how those BMP reduce sediment transport after the BMP have been in place for a while.

3 MAJOR EXPERIMENT

Three main treatment variables are being investigated for the Major Experiment: lithology (volcanic or siltstone), rock quality (marginal, good, or quality) and ditch line BMP (vegetated, bare, or elevated). Straw wattles and catch basins were applied to selected ditch lines and quality rock was applied to selected segments in WY2024 as the elevated BMP.

During the first four years of the study, per the study design (CMER, 2017) half of the sites in each lithology were treated with marginal rock and the other half were treated with good rock in both lithologies. Most ditch lines were grassed during this period, but a few segments were bare or in an elevated BMP. The variables of traffic loading, observed rainfall, and watershed contributing area are being measured for use as covariates. The variables of road length (80 m), width (3.66 m.), road slope (2-13%), and tread configuration are being controlled (Table 3.1).

Table 3.1 Covariates monitored in the examination of BMP performance (CMER 2017).

Covariate	Measured/Controlled	Measurement	Range/Condition
Segment Length	Controlled	---	Steel troughs and cross-drains isolate 80-m road segment
Tread Configuration	Controlled	---	Graded to crowned
Road Width	Controlled	---	Crest graded 3.66 m from ditch line
Road Gradient	Measured	---	Limited to 2-13%
Traffic	Measured	Inductance Loop Traffic counters, Motion-sensing cameras	Heavy traffic was anticipated but not always achieved (5+ log trucks per day)
Grading Frequency	Measured	Landowner reporting and motion-sensing cameras	---
Rainfall	Measured	Rain gauges	Hourly Precipitation
Catchment Area	Measured	Mapping catchment area above segment cutslope	---
Cutslope Interception	Measured/Estimated	Ditch line flow observations compared to hourly rainfall minus estimated tread contribution	---

3.1 STUDY AREAS

The study sites were selected to include high traffic mainline forest roads in regions of western Washington that receive heavy winter rainfall. The selected areas typically receive an average annual precipitation of 60 to 100 inches or more (PRISM Climate Group, 2023). Groups of roads were selected in the western portion of the study area that occur on fine grained sedimentary lithologies which are referred to as the Siltstone Province. These include sites on the Delezenne, Melbourne, Newkah, Bishop and Naselle road systems (Figure 3.1). Sites were selected on mainline roads in the North and South Forks of the Toutle River on volcanic lithologies and are referred to as the Volcanic Province. Road segments were selected on these private timber land roads that had scheduled timber haul during the course of the study.

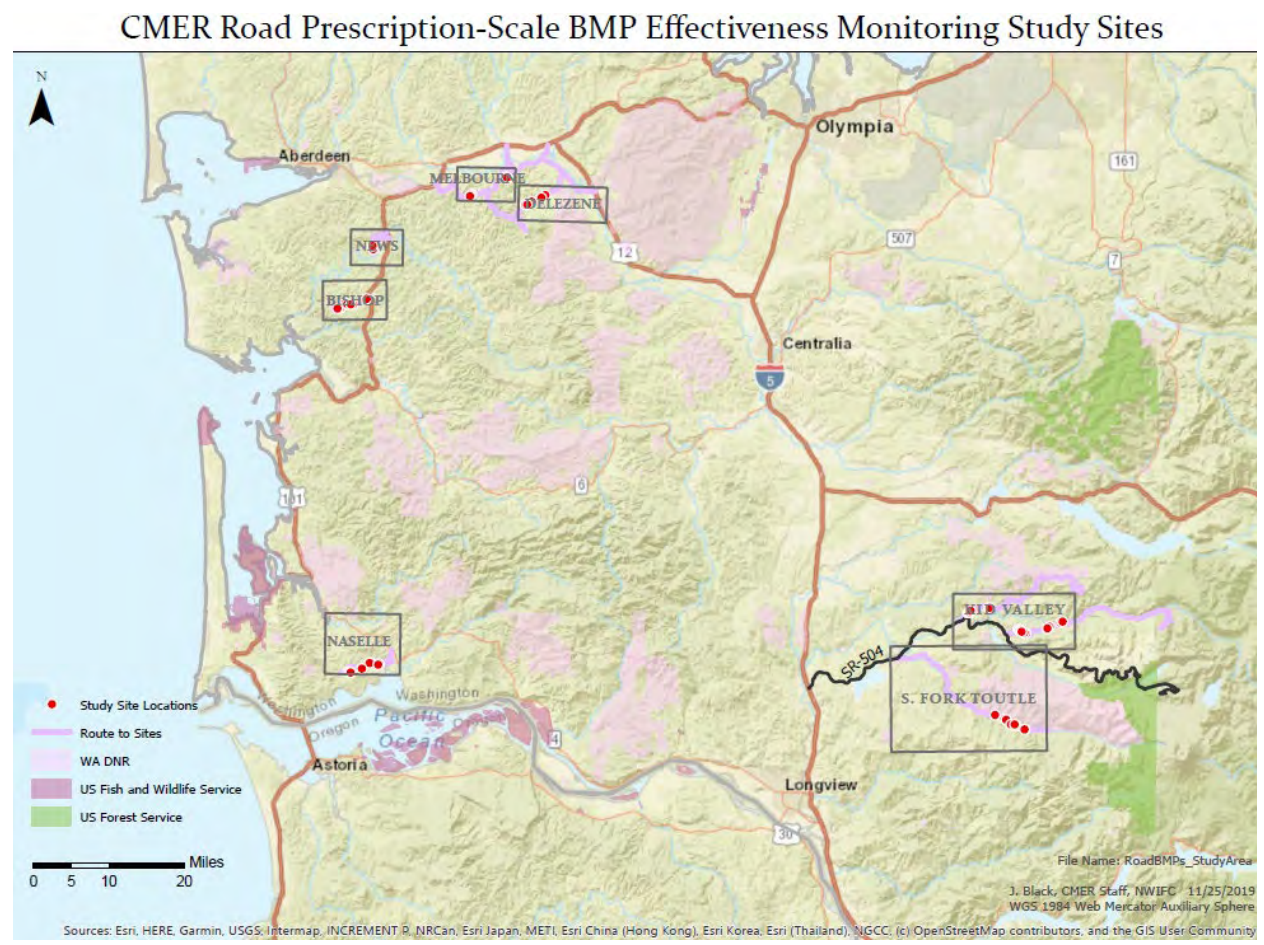


Figure 3.1 Locations of the HTNS Major Experiment study sites in western Washington.

3.2 METHODS

We constructed 78 sites, specifically targeting HTNS roads—39 in each of the two lithologies with overlapping ranges of rainfall typical of forested land in Western Washington. Each site consists of an 80-meter segment of road with a cutslope, a ditch line, and a road tread surfaced with crushed rock of a selected quality (Figure 3.2).



Figure 3.2 “Good” rock (i.e., relatively un-weathered basalt) is the darker rock in this picture, and “marginal” rock (i.e., slightly more weathered) appears with a lighter tan color. Good rock is used at most sites in practice, and marginal rock has been applied at half of the sites to test the effects of rock quality on sediment yield.

The tread surface of each 80-meter segment of road is isolated by steel troughs. The upper end of the ditch line of each segment is isolated by a cross-drain culvert with an earthen headwall that passes the ditch and road tread water captured by the upper steel trough under the forest road and onto the forest floor. This ensures that the sediment collection equipment is only collecting water from the 80-meter study site (i.e., the 80-m road segment). At the lower end of each 80-meter segment, the lower steel trough directs the water from the ditch-side tread crown (always 3.66 m.) into the ditch. Water collected in the ditch from the cutslope and the 80 meters of crowned tread passes through the lower cross-drain culvert under the road to the sediment collection equipment (Figure 3.3 and Figure 3.4).

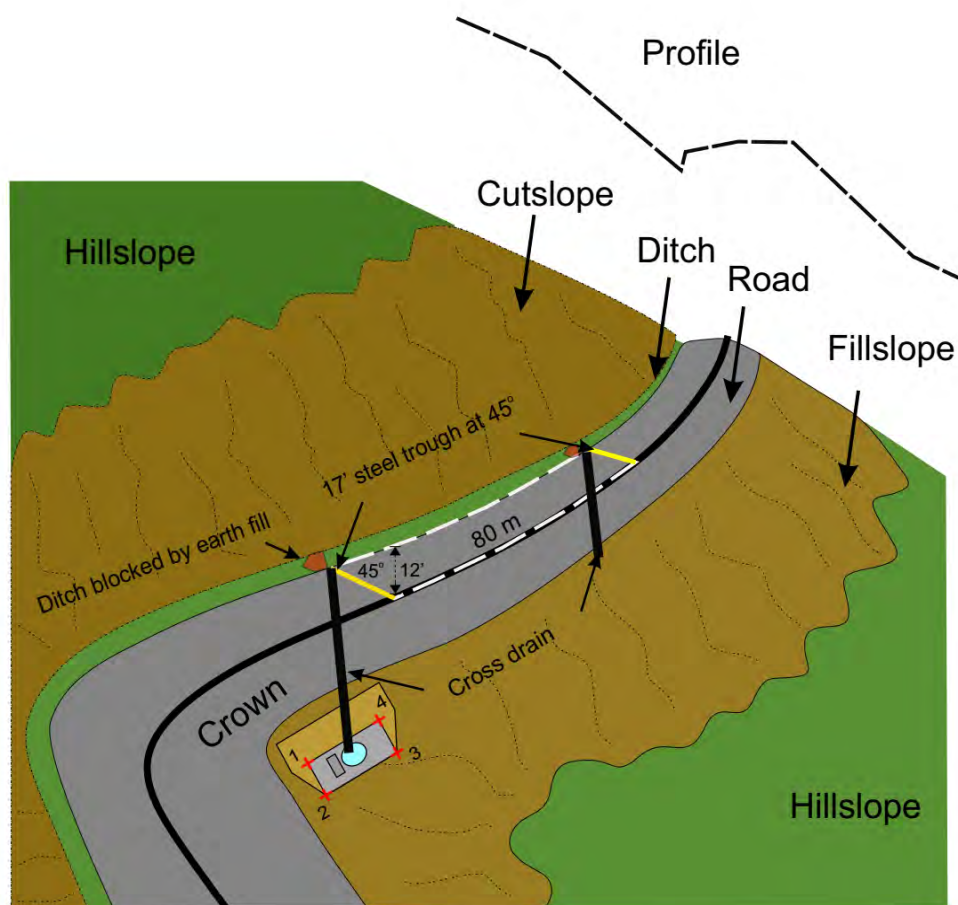


Figure 3.3 Configuration of an 80-meter segment. Ditch (in light green) is blocked below cross-drain culvert by earthen headwall. Steel trough is 5.2 m-long and placed on a 45-degree angle up the road to capture 3.66 m of the crowned road tread and drain into the ditch line .3 m above the cross-drain culvert inlet. The cross-drain culvert is on a strong skew to create a 5% gradient in the pipe, and it extends several feet beyond the edge of the tread to a platform that holds the sediment tub, tipping bucket and SST.

On a 200 ft² platform dug into the fillslope or hillslope below the road, road sediment collection equipment collects both larger-sized sediment (i.e., primarily sand) and finer material (i.e., the turbid fraction) with different methods. The cross-drain culvert that is located at the bottom end of the site will move water and sediment that is captured from the road and ditch line within the site into a tub at the outlet of the cross-drain culvert that collects sediment. The larger particles will accumulate in the sediment tub (developed by Black & Luce, 2013). Water exiting the sediment tub will pass through a tipping bucket with a data logger, measuring total water flow from the sediment tub. Finer suspended sediment escaping the sediment tub is sampled with every other tip of the tipping bucket. During these alternate tipping bucket tips, a nominally 10 ml sub-sample of discharge is captured in a small pipe with holes mounted on one wall of the tipping bucket. This flow-proportional split fraction is routed to the suspended solids tank located below the tipping bucket (SST) where the finer sediment accumulates until periodic sampling occurs.

Field visits occur at all the sites at least monthly during the wet months. Samples are taken by downloading the data logger to determine the discharge of water. During the field visit, the sediment collected in the SST is resuspended by hand mixing by a crew member and then a one-liter

representative sample is collected in a bottle. SST water samples are sent to an accredited lab for determination of suspended sediment concentration by vacuum filtration (ASTM D3977B).



Figure 3.4 The upper figure shows the road surface routing water to the ditch and the collection trough. Water and sediment then are routed through a culvert pipe to the sediment tub. The lower figure shows the platform with the sediment tub collecting road sediment, the tipping bucket measuring discharge and the suspended sediment tank (SST) sampling the fine sediment that is not settled in the tub.

The sediment tubs are emptied and measured at the end of the runoff producing season in June. The monthly suspended sediment volume is determined by multiplying the monthly tipping bucket tips by the tip calibration volume and applying the monthly average suspended sediment concentration value. The annual suspended sediment mass is the sum of the monthly masses. The sum of the monthly suspended sediment masses and the sediment tub mass can be expressed as total mass per year (kg/yr.) or divided by road surface area for $\text{kg/m}^2/\text{yr}$.

In the 2019-2020 water year, several sites produced higher than expected flows or total water volumes due to the interception of abundant shallow groundwater. The existing equipment and staff were unable to collect full runoff records for these high flow sites, as tipping buckets were being damaged and data loggers were filled as quickly as six days. An improved flow sampling method was prototyped and constructed in fiscal year 2021 to subsample the high flow sites that behaved like small streams. A 7" V-notch weir was designed, attached to a tub, and tested to measure flow with an Onset MX 2001 pressure transducer system to measure the depth of flow through the weir. The flow exiting the weir

passes through a flow-proportional splitter that samples approximately 17% of the discharge. This reduced water volume then passes through the tipping bucket and, as usual, the split volume for suspended sediment is stored in the standard SST. The equipment improvements allow us to collect data on a critical portion of the road system that is intercepting and transporting large amounts of water in the roadside ditch. This is important because these roads are more likely to be routing water and sediment from their culvert discharge points overland to the nearby stream channel.

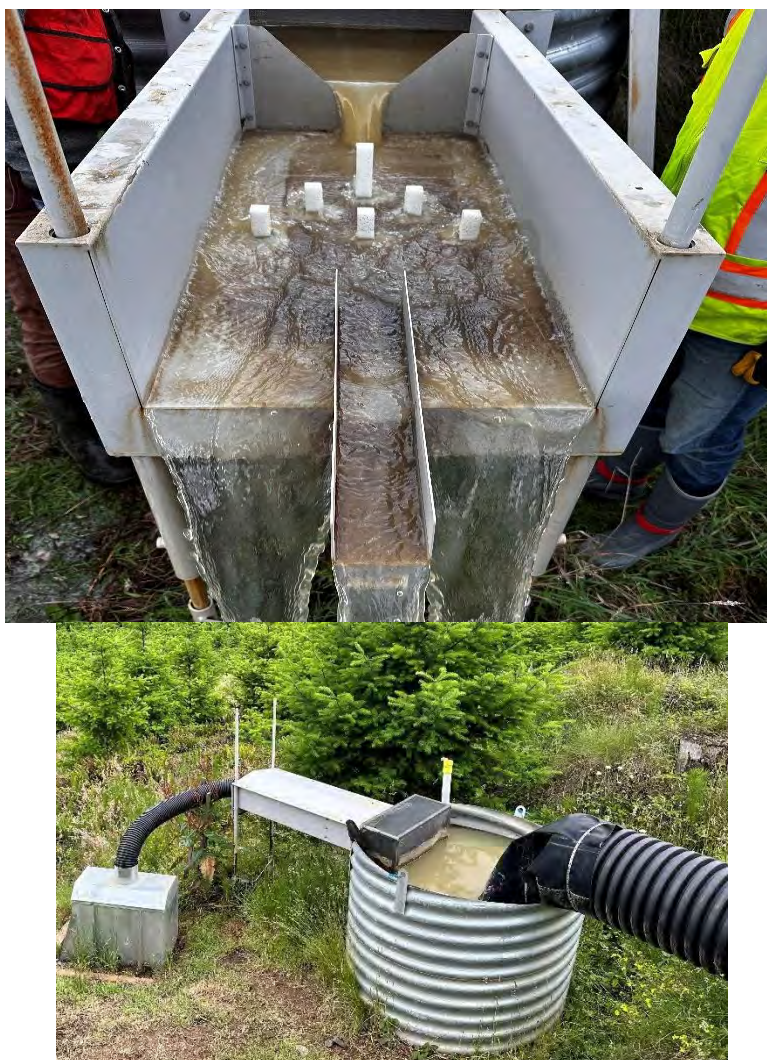


Figure 3.5 V-notch weir and flow-proportional splitter in upper photo. The white blocks spread the water to ensure even flow across the splitter at the end of the flume. The lower photo shows the covered flume, debris filter and the stage measuring sensor in the white tube. The black material at the end of the culvert is a flow diffuser that prevents water from overtopping the tub at high flows.

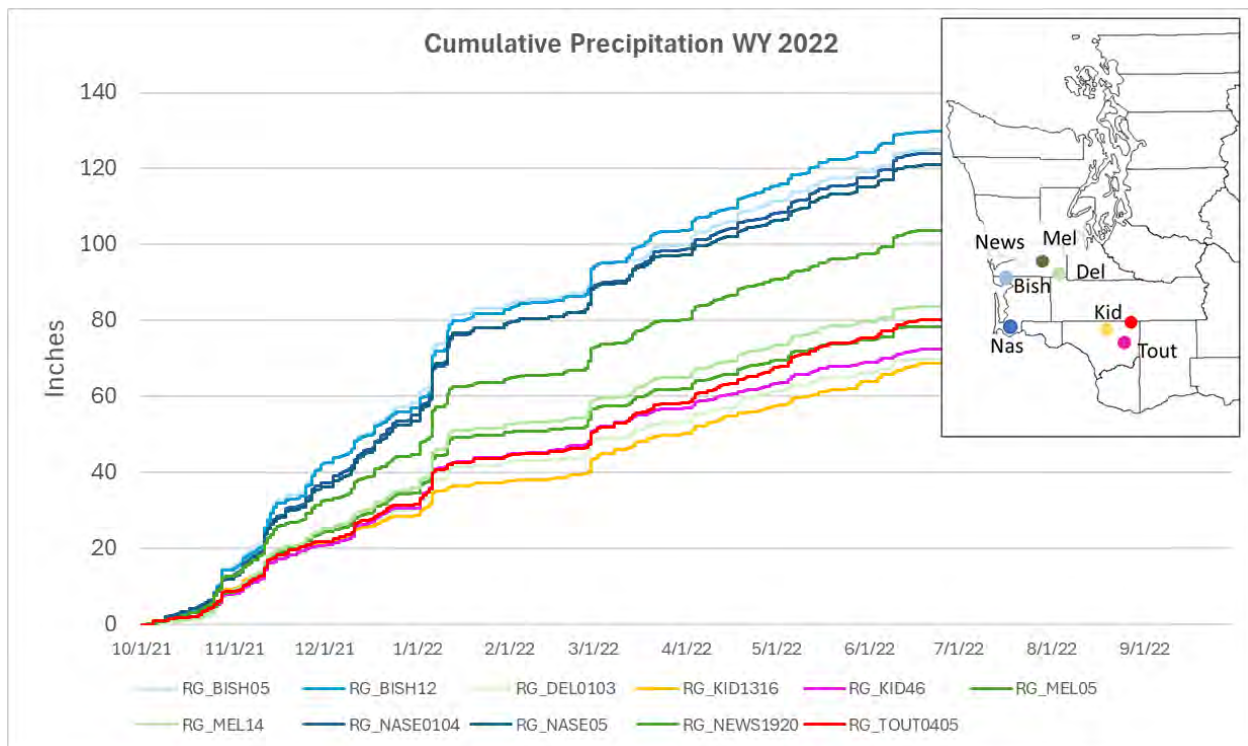
3.3 DATA COLLECTION STATUS

We are currently completing data collection for the fifth water year, WY2024 (10/01/2023-09/30/2024). Data processing for the previous water years is ongoing and all results should be considered preliminary. For the purposes of this report, we have processed the entire WY2023 dataset, as well as much of the

WY2022 dataset. We present those preliminary results here as examples of imputation of missing flow data and analyses of data from the Major Experiment.

Measured precipitation in WY2023 was 70-80% of that observed in WY2022. Precipitation in the Volcanic Province was 60-70% of that in the coastal Siltstone Province (Figure 3.6). Rainfall in the western part of the Siltstone Province has been in the expected range of 80-120 inches per year, while the eastern part of the Siltstone Province (on the Melbourne and Delezenne roads) has been experiencing slightly lower amounts of rainfall than expected. The interior Volcanic Province has been experiencing 50-80 inches of rainfall per year. These Volcanic sites are located at slightly higher elevations in the Cascade foothills, and as such, are colder in the winter. The colder temperatures of these interior sites result in a greater portion of the precipitation falling as snow and the snow persisting on the roads for longer periods of time.

In water years 2022 and 2023 of the Major Experiment, we collected annual sediment tub, flow, and fine sediment data at 78 sites and precipitation data (Figure 3.6) at 11 locations representing subsets of those sites. However, a few sites experienced periodic technical problems due to higher-than-expected flows, data logger battery issues, and equipment wear, so the flow—and subsequently fine sediment—records are not complete for every month at all sites (Figure 3.7). In WY2022, three sites had large gaps in flow data. In WY2023, only one site had less than 60% of the WY flow represented. Procedures were modified and work was completed to improve the performance of the tipping bucket flow measuring equipment and data loggers. High-quality flow data is now being collected from most sites, including the 11 highest flow sites that have flumes with flow splitters and are measured with V-notch weirs and pressure transducers. (Figure 3.5). Flow data was imputed to replace the missing flow records where a reasonable regression model could be established between the missing site and adjoining sites.



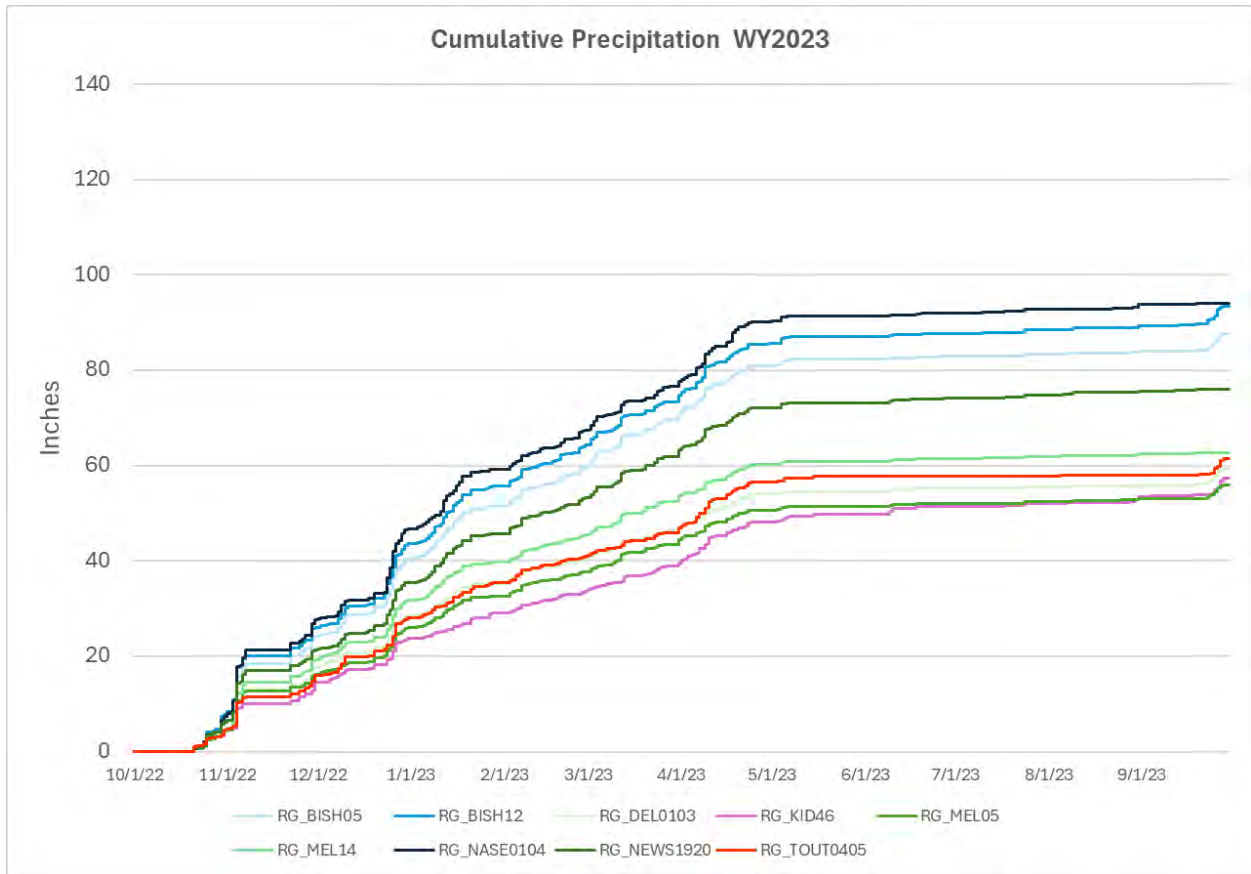
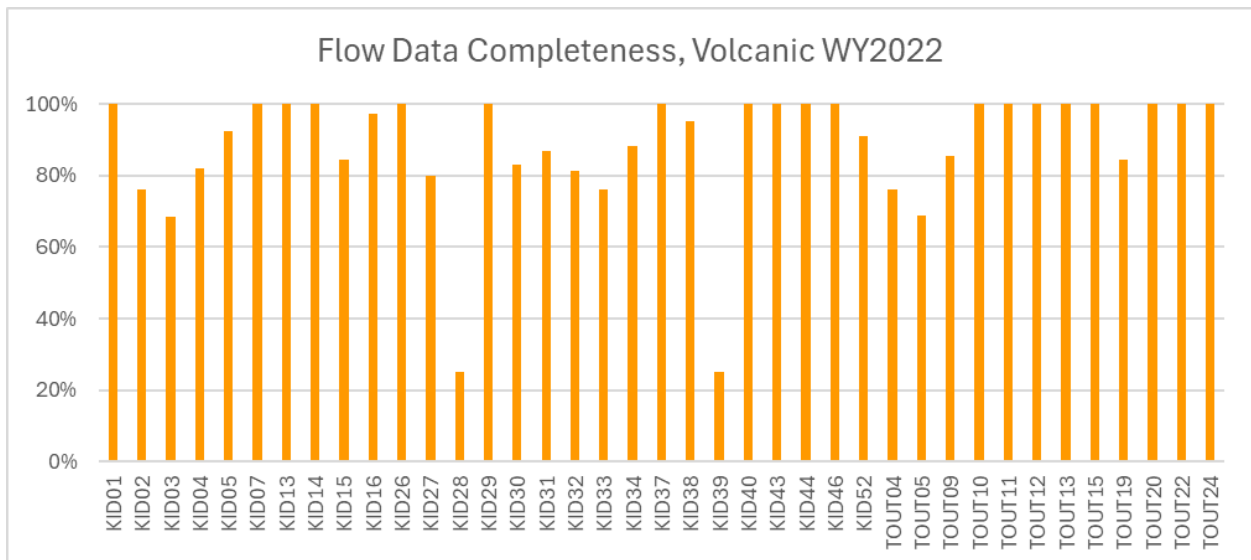


Figure 3.6 Rain gage data from water years 2022 and 2023. Not all sites are shown.



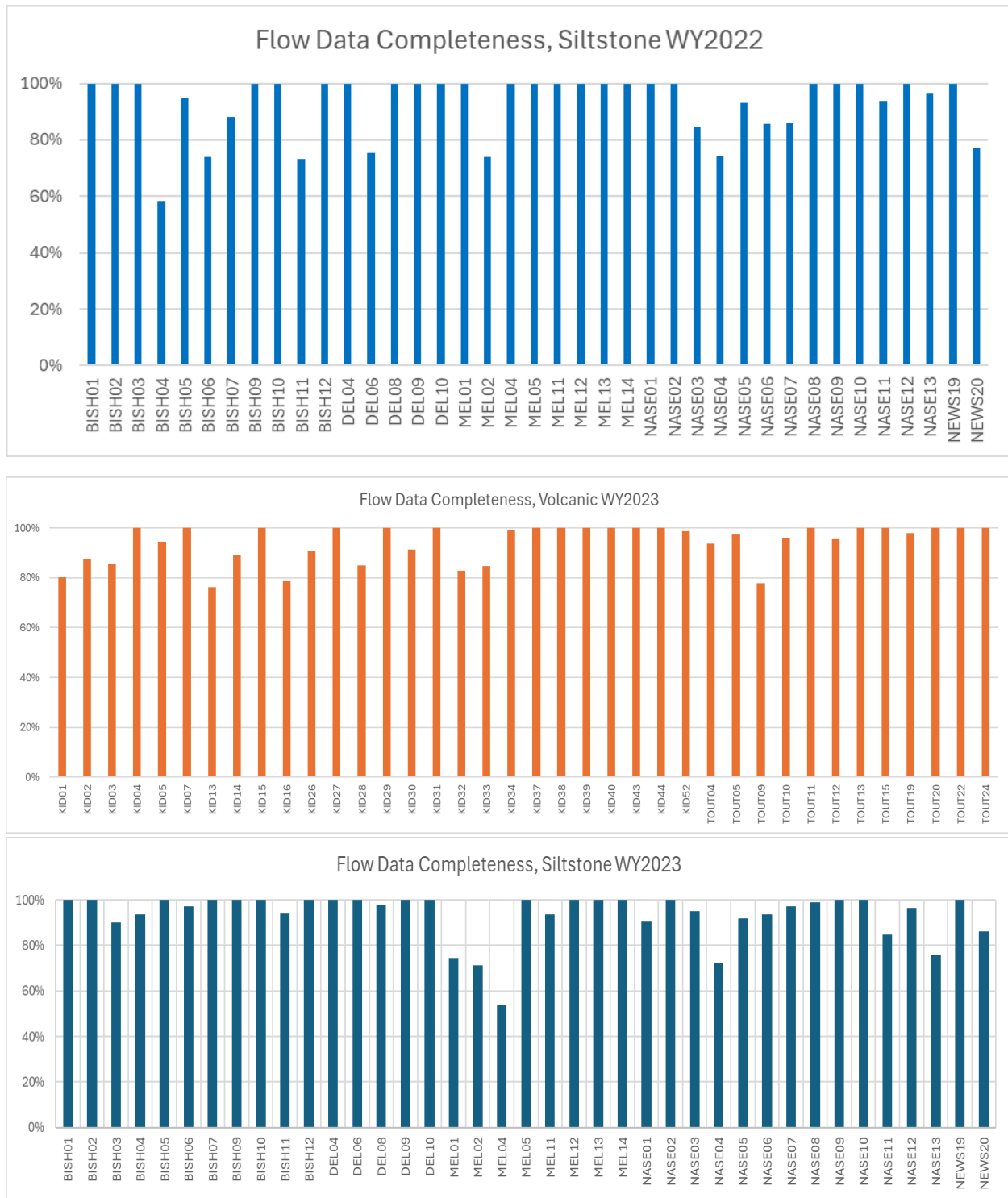


Figure 3.7 The percentage of time that reasonable field data were recorded on the tipping bucket flow gages between Oct 15 and June 15 of each water year. This represents the initial data quality. Most missing values were later imputed using regression models built from similar neighboring sites.

3.3.1 Flow Data Processing and Imputation Overview

The raw tipping bucket data are downloaded during each site visit and a suspended sediment concentration sample is taken from the suspended sediment tank (see Figure 3.4). Double tip counts in the raw tipping bucket data due to mechanical issues (i.e., bounces of the magnet, within 1 second of the previous count) are removed from the record. The cleaned data are combined into an annual continuous tip record. The record is binned using R code to create an hourly tip record. Missing hourly data are identified and verified with field notes. When a site had a mechanical problem, the data logger filled up prematurely, or the battery ran low, a data gap is coded into the record. When precipitation conditions were such that tips should have occurred, and did occur at similar, adjacent sites, then we began the process of filling flow data gaps. If no tips are expected during the data gap (e.g., mid-August), then no such effort is needed.

Neighboring sites with similar hydrographs are selected to model missing data. These predictor sites are sorted by the p-value of their linear relationships with the fitted site, and the sites with the lowest p-values are used to create a new model for that site.

A linear regression model is constructed using the fitted site and predictor sites, and statistics for the relationships between each predictor and the fitted site are tabulated. Objective function values for each model are calculated. These include: observed and residual means, Nash-Sutcliffe Efficiency (NSE), NSE-1 (NSE with sums of squares in numerator and denominator raised to 1 instead of 2 to reduce sensitivity to extreme values), coefficient of determination, sum of absolute errors, root-mean-square error, peak-weighted RMSE, and peak percent error. The data for the candidate models are plotted along with the observed data to check the model fit and select the best model. If the model is acceptable, the imputed data is used to replace the data gap.

The hourly tip data are next converted to flow by applying the annual tip calibration function. Field calibration is performed each year in June or when a tipping bucket is replaced or significantly modified. The starting and ending calibration values (liters/ tip) are used to create a sigmoidal tip calibration function. This function is applied to the data to create the hourly flow record or hydrograph.

3.4 RESULTS FROM WY2023 DEC-MAR ANALYSIS

The basic questions of this study are about effectiveness of best management practices in reducing erosion from forest roads. General hypothesized techniques include adding ditch line roughness, improving road rock quality, and reducing wet weather traffic, as outlined in the opening sections of this Interim Report. This analysis uses data from the 76 sites that had relatively complete data for at least one month during this period. The intentions are to provide draft expected results for communication with CMER stakeholders, test alternative analysis approaches, explore limits of the data and study design, and identify aspects of the analysis that could be strengthened with sampling choices.

3.4.1 Methods

Brief Review of the Data

The measurements and data reduction discussed in previous sections were analyzed for the 76 sites, considering repeated measurement over four months December, January, February, and March of water year 2023. Substantial effort was put into quality checking the data, resulting in the removal of 12

month-site records from across 10 sites (1 month at 8 sites, and 2 months at 2 sites), leaving 288 records covering 76 sites.

Since the intention of this experiment is to test how covariates affected sediment yields from each site over time, we are providing some characterization of the covariates as well as basic characterization of the response variable to describe the experiment and explain some choices for modeling approaches. While some of these might traditionally be classified as “results” of the experiment, these quantitative descriptions provide information about the experimentally imposed variables as well as the context in which they were measured. Very cursory information about the response variable (total sediment yield) is more reasonably described as a “result;” however, some cursory information about its calculation is useful in the context of setting up the modeling analysis.

For each site-month, 17 variables were compiled or calculated for analysis (Table 3.2). Most were from the measurements outlined above. Tub-captured sediment was measured annually and partitioned across months at a site based on the suspended load received at the site that year. Total sediment was calculated as the sum of suspended and trapped sediment. The monthly averaged stream power was computed as the total monthly flow multiplied by the road slope. The fraction of trucks on days exceeding thresholds were computed as the ratio of the number exceeding threshold over the total number. We also considered the 98th percentile daily runoff as a covariate, but it was so strongly correlated to the total monthly flow that it was removed from consideration.

Table 3.2 List of Measurements and Covariates considered in this analysis. Other measurements have been made, but this subset represents the ones of preliminary utility and interest.

Basic site, flow, and sediment information

Monthly runoff, liters
Slope
Geology (Volcanic and Siltstone Provinces)
Monthly average stream power (flow*slp)
Suspended load (fine sediment)
Mass trapped in tub (coarse sediment)
Total sediment

Road surface disturbance

Number of trucks in a month
Number of cars in a month
Number of trucks on days with at least 0.1 in of rain
Number of cars on days with at least 0.1 in of rain
Number of trucks on days with at least 0.25 in of rain
Number of cars on days with at least 0.25 in of rain
New road-grading occurred during the month (T-F variable)
Fraction of trucks on days with >0.1 inch of rain
Fraction of trucks on days with >0.25 inch of rain

Rock quality and ditch treatment covariates

Degradation score, resistance to degradation when wet
Fraction of shear stress partitioned to sediment grains

Runoff and slope are key causal variables for erosion, and monthly runoff ranged from a few liters to a few thousand cubic meters over a month and was somewhat lognormally distributed (Figure 3.8). With slopes ranging from 2 to 13% with less skew (Figure 3.9), the resultant monthly streamflow multiplied by slope (a scalar of the monthly averaged stream power) ranged from 0.002 to 200 m³ and is sufficiently skewed in distribution to be best represented with a log transform (Figure 3.10).

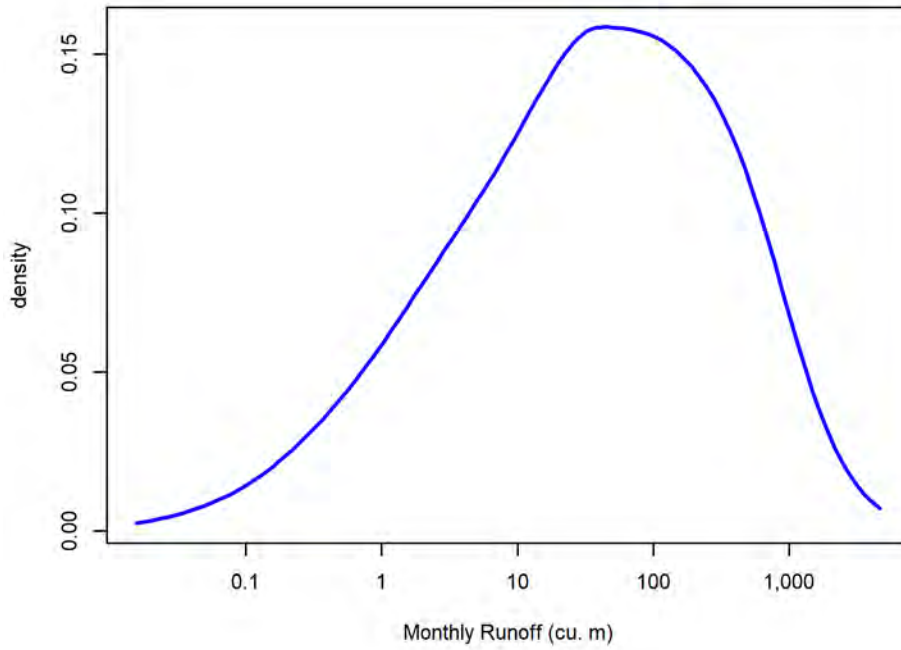


Figure 3.8 Probability density function (pdf) of monthly runoff across site-months.

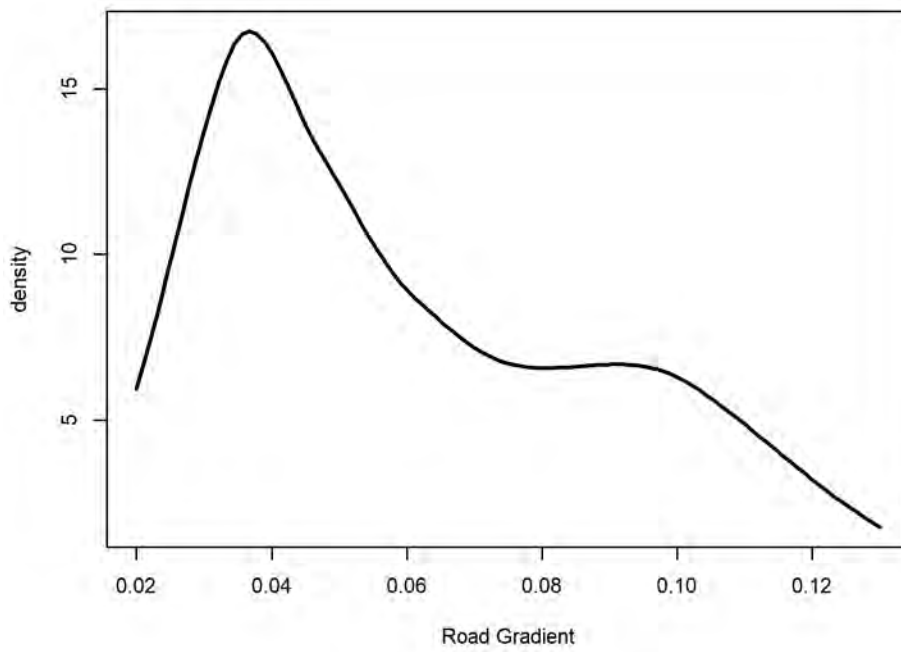


Figure 3.9 pdf of site slope

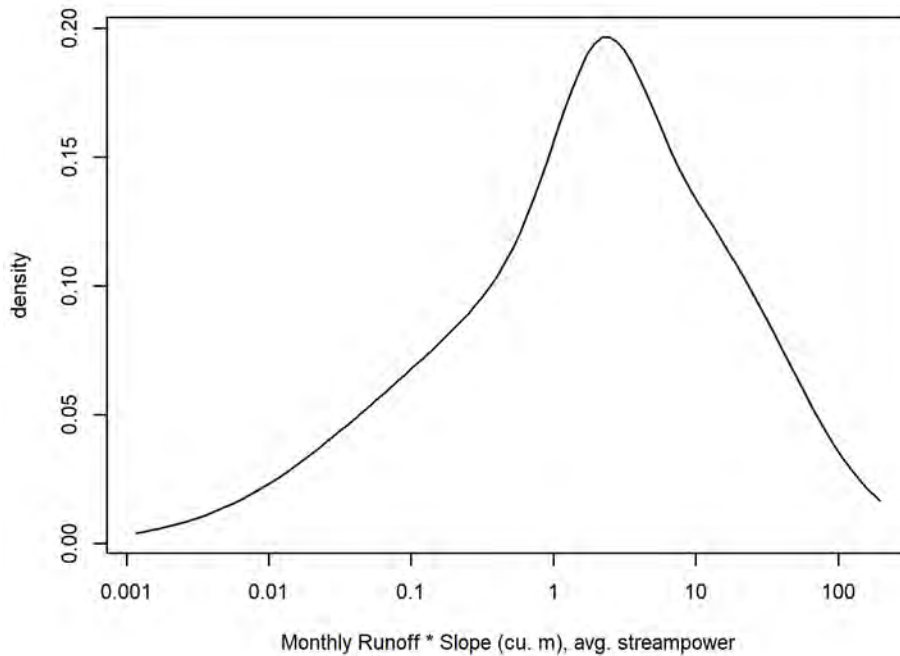


Figure 3.10 pdf of runoff times slope, roughly a measure of the average monthly stream power.

Monthly suspended sediment yields ranged from about 0.1g to about 85 kg (Figure 3.11), and coarse sediment yields estimated on a monthly basis ranged from 6g to about 200 kg (Figure 3.12), with a resultant total sediment yield ranging from 6g to about 200kg (Figure 3.13), noting that large suspended loads and large coarse loads did not necessarily occur in the same place. All distributions are substantially skewed. The suspended sediment fraction ranged from about 1 to 100% (Figure 3.14) and showed clear dependence on the flow rate through the sediment tub (Figure 3.15).

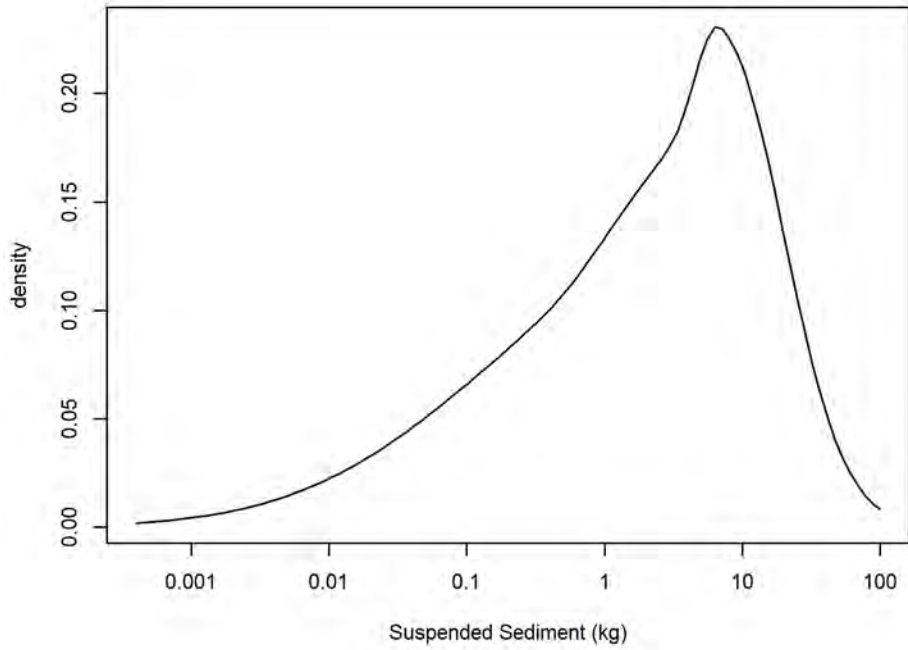


Figure 3.11 pdf of suspended sediment measured across site-months

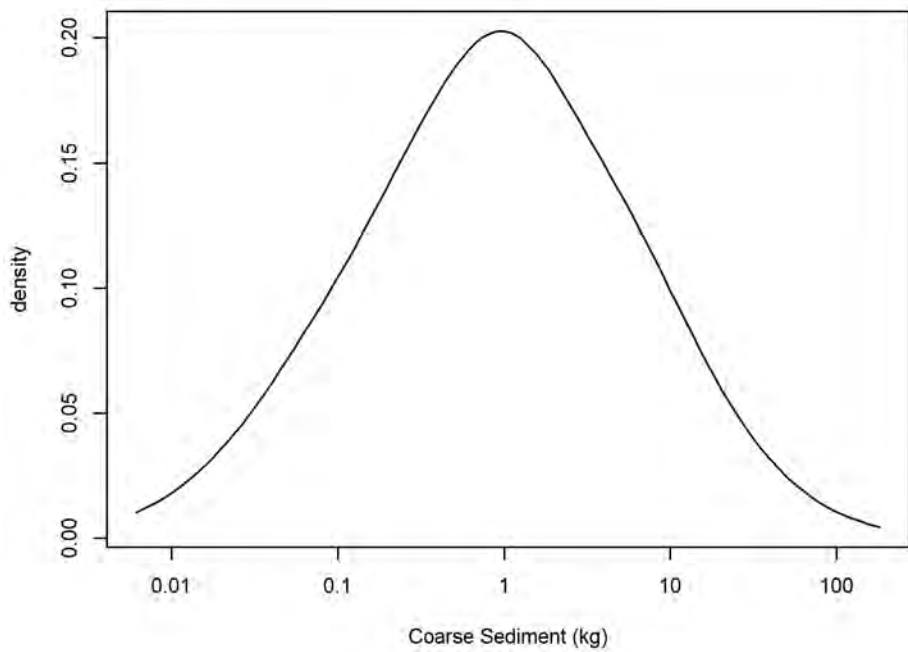


Figure 3.12 pdf of coarse sediment estimated across site-months from annual measurements at each site and apportioned to months on the basis of suspended sediment timing at each site.

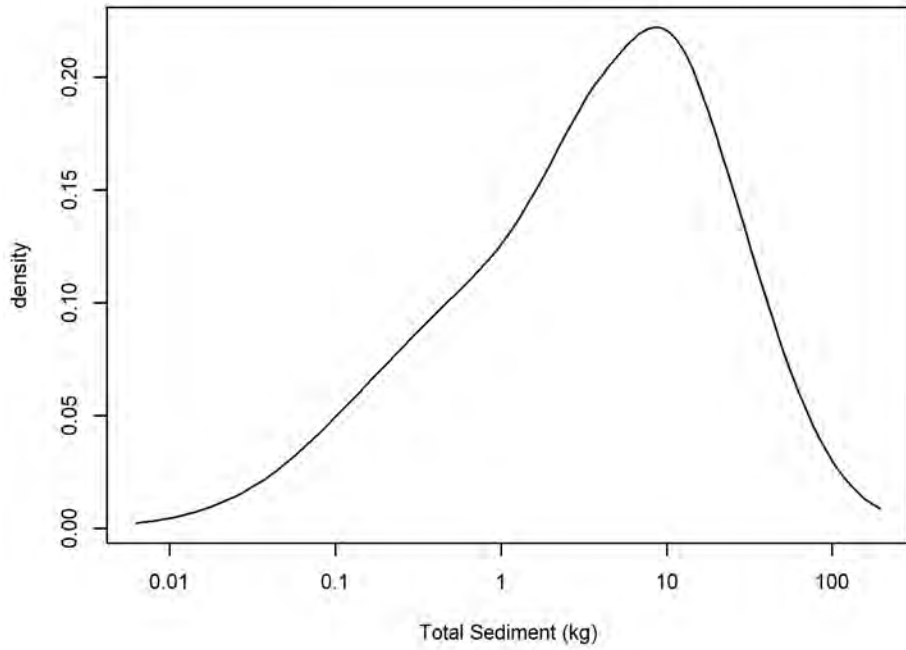


Figure 3.13 pdf of total sediment, sum of suspended and coarse sediment, across site-months.

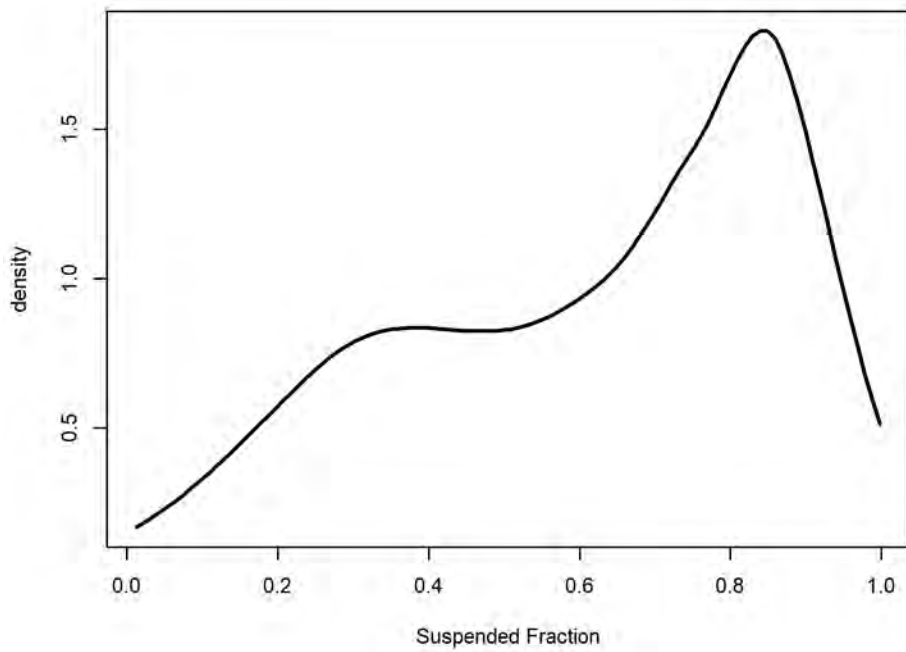


Figure 3.14 pdf of the suspended sediment fraction across site-months.

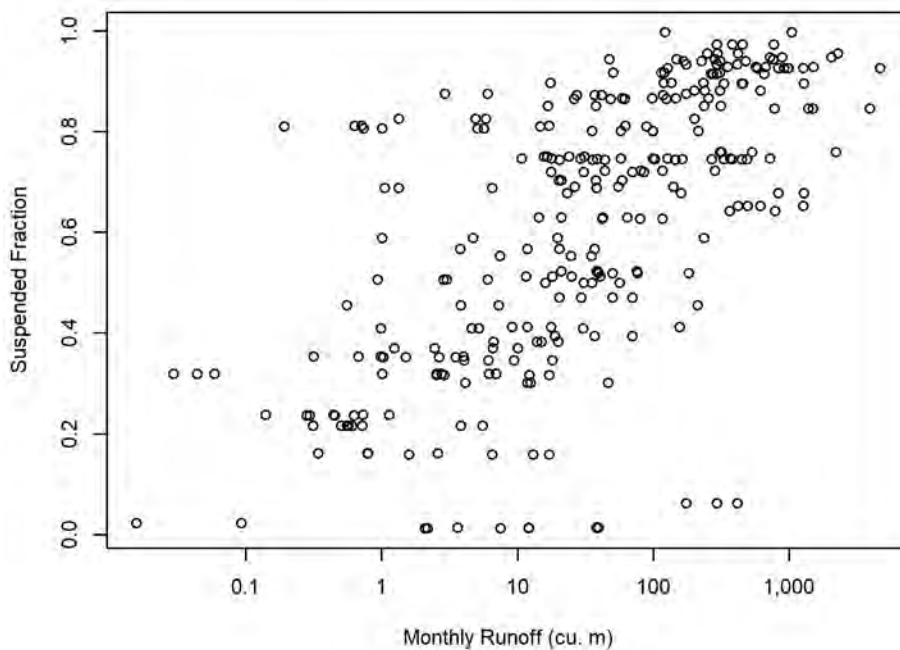


Figure 3.15 Relationship between the suspended fraction and the monthly runoff at each site, showing that site-months with greater throughflow in the sediment tubs tend to have a greater fraction in suspension.

Two key variables representing best management practices are the rock degradation resistance score (Degr) and fraction of shear stress partitioned to sediment grains (fgss). The rock degradation resistance score has larger values for stronger rocks, those more resistant to crushing by traffic, and ranged from 2 to 84 across the sites, with a bimodal distribution (Figure 3.16). A score of 50 or greater is considered good (Minor, 1960). Fgss values ranged from 0.03 for sites with wattles or thick grass cover, to 1 on freshly bare ditch segments (Alvis et al., 2024), and were bimodally distributed with the majority being thick grass or wattle-protected segments and a second mode around segments with sparse grass cover (Figure 3.17).

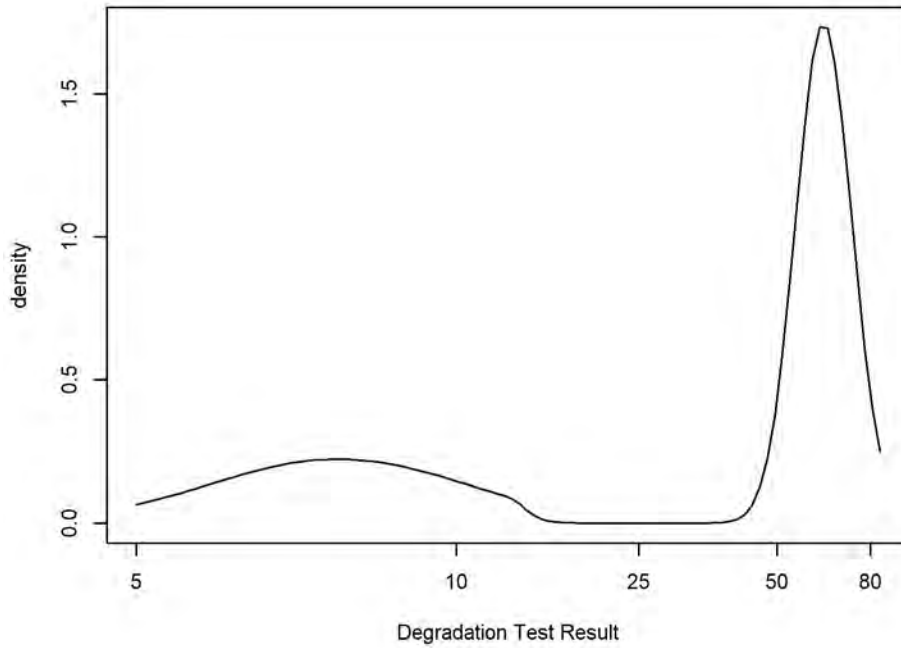


Figure 3.16 pdf of the degradation resistance by site, showing bimodal distribution of rock quality.

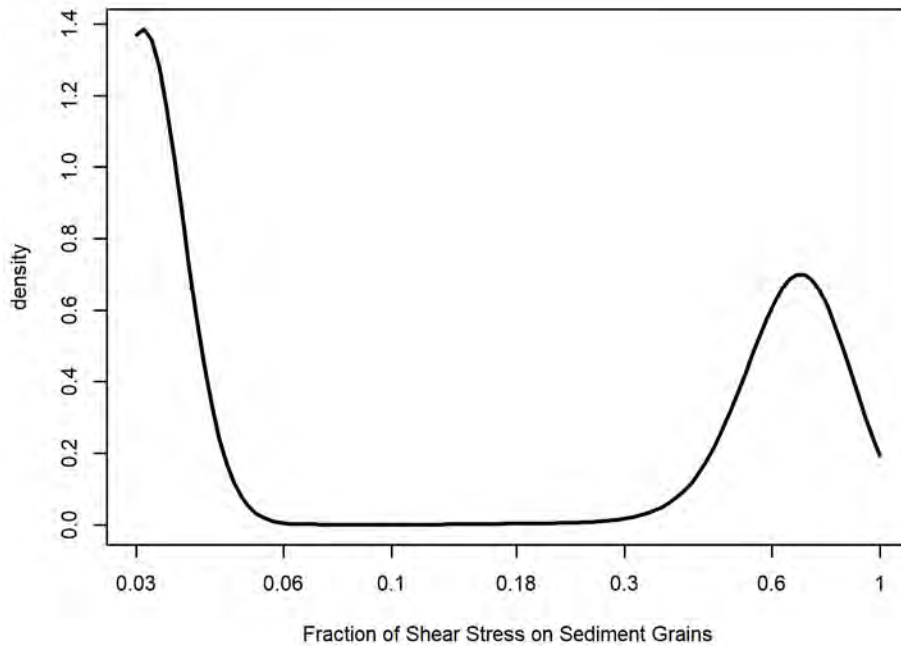


Figure 3.17 pdf of the fraction of the shear stress apportioned to sediment grains ($fgss$) by site, showing bimodal distribution with many heavily grassed sites and several sparsely grassed sites. See *Alvis et al. 2024 (Appendix B)* explaining how specific treatments relate to added roughness and how added roughness relates to the fraction of the shear stress available to transport sediment.

Traffic is expected to have substantial effects on sediment yield (Alvis et al., 2023), and there are questions about whether traffic under wet conditions might increase sediment yields by causing increased pumping and transport of sediment. As a consequence, many of the covariates of interest relate to traffic (Table 3.1), with total counts and counts of traffic broken down by vehicle type (truck vs. car), whether the traffic occurred on a wet (>0.1 inch precipitation) or very wet (>0.25 inch precipitation) day, and whether the segment experienced grading of the road surface during the month. The number of trucks is considered one of the stronger potential effects, and the distribution of truck traffic values across site-months is bi-modal, depending on whether the site is experiencing haul in that month from a harvest unit (Figure 3.18a). While the distribution of the total number of trucks is relatively consistent, it changes from month to month for different precipitation thresholds (Figures 3.18b, c). Metrics within particular vehicle types (only varying the wetness filter) are strongly correlated (Figure 3.19), particularly for trucks. Similarly, correlations across vehicle types but for varying wetness filters are still fairly strong (0.73 to 0.8).

High correlations can confound the ability to discern between potential alternative variables when testing models, so another variable, relatively uncorrelated to overall monthly traffic levels, was calculated; the fraction of trucks on wet or very wet days (Figure 3.20) offers the potential for a different analysis approach. The question became one of—with the amount of traffic being equal—whether it matters what fraction of the traffic occurred on wet days. This allowed entering the fraction of traffic on wet days as an independent variable where we could test for the significance of diverting traffic to dry days vs. wet days.

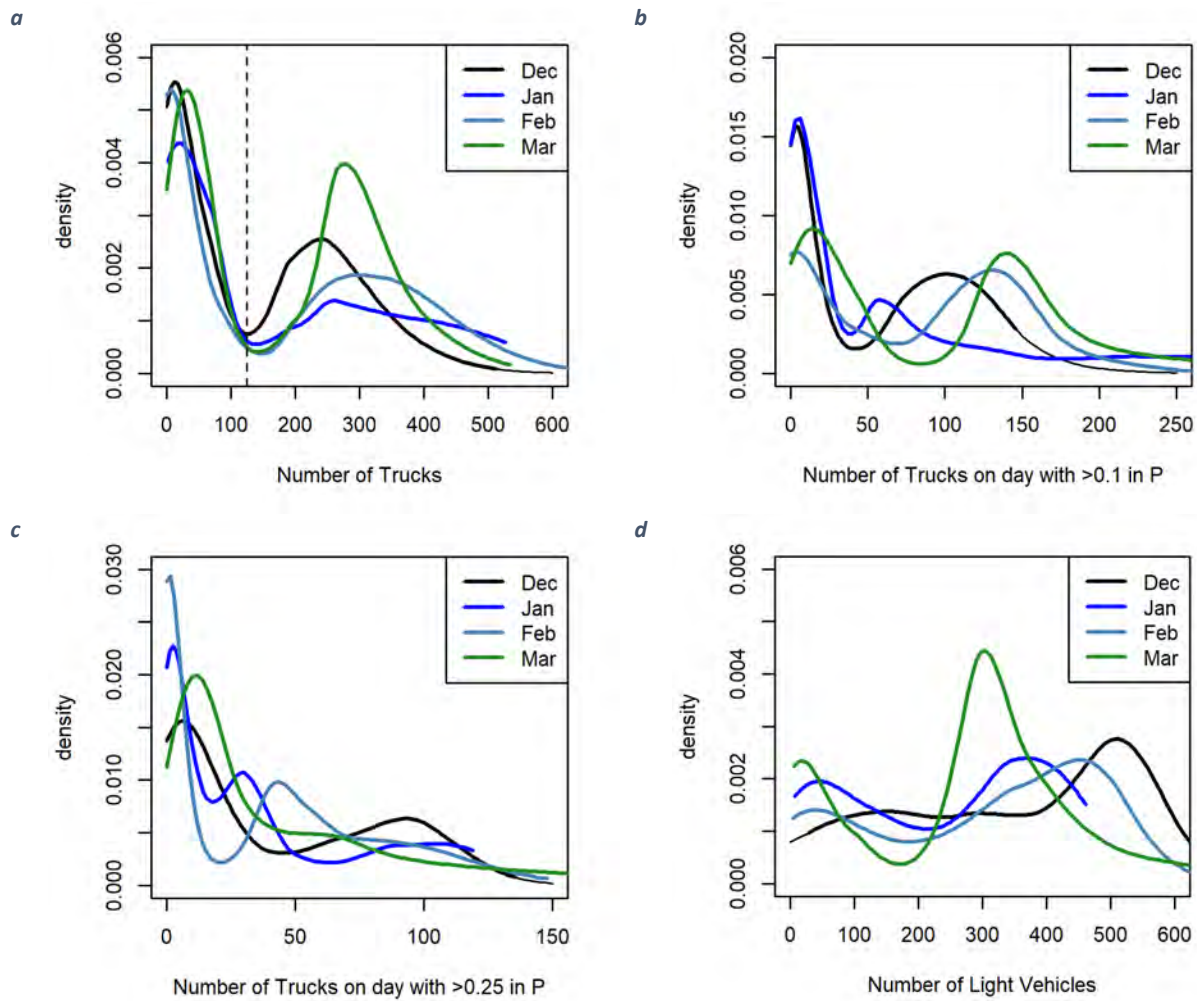


Figure 3.18 a)-c), monthly distributions of trucks by month over sites and by classification of wetness during traffic, d) distribution of light vehicles by month over sites. The dashed line in (a) shows a useful separation threshold for light vs heavy truck traffic levels that is applied in later graphics to visually portray traffic effects in a binary approximation.

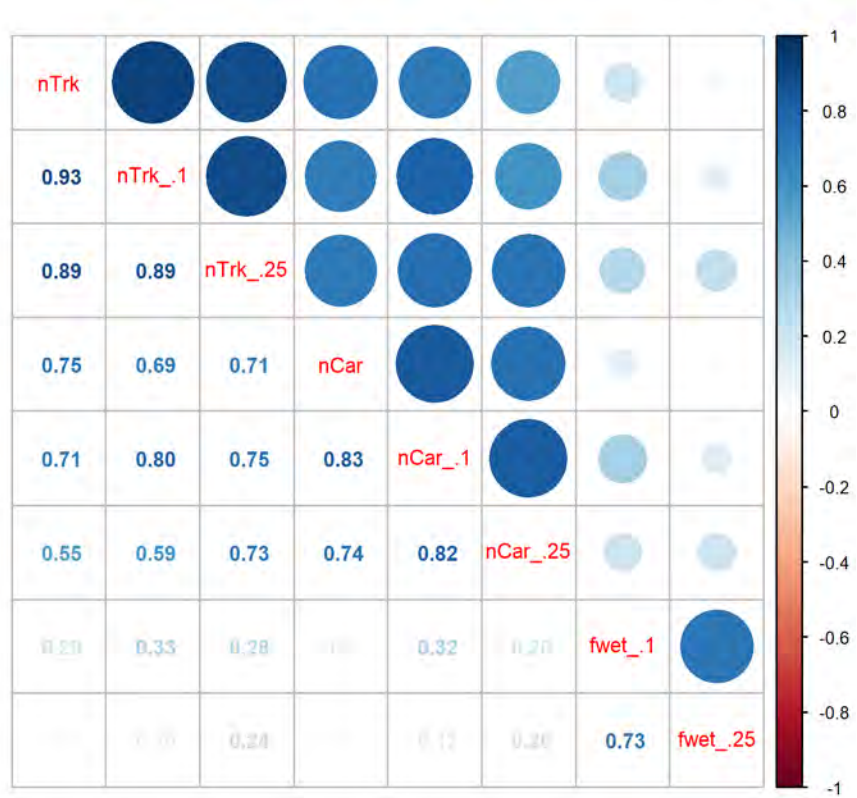


Figure 3.19 Correlation matrix for vehicle traffic metrics

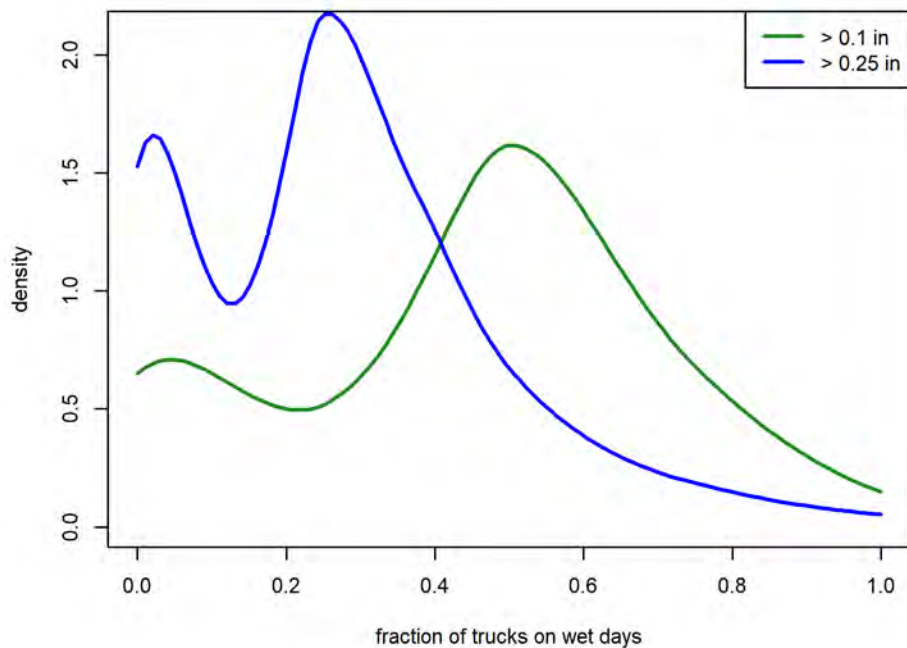


Figure 3.20 pdf of fraction of trucks on wet or very wet days.

Brief overview of modeling approach

The primary focus of the analysis approach was linear mixed-effects (lme) modeling to examine the magnitude and significance of effects in the context of repeated measures. In addition, linear modeling using a combination of continuous and classified variables is used for visualization and conceptualization of the primary model and contextual effects.

3.4.2 Results

The modeling began from the context of the limiting-conditions analysis explored in the previous Biennial report (2022) and explained in Alvis et al. (2022). The concept is that both the supply of mobile sediment, and the energy used to transport it down the road segment or ditch play a role in determining the sediment that arrives at the bottom of the site. A key control on supply is the traffic level, while the stream power analog describes the transport capacity. If there is substantial capacity but inadequate traffic to generate mobile sediment, the sediment yield is limited by the supply. Though to an extent, high slope-flow combinations can mobilize some sediment from the ditch, this is generally much smaller than the traffic-generated supply. Similarly, substantial supplies can be generated that deposit on the road surface or ditch line if the stream power or shear stress are not available to continue its movement.

A basic framing or illustration of this concept is in Figure 3.21, where traffic is classified as “high” or “low” based on a split at 125 trucks per month (split at the minimum traffic level in the bimodal distribution of Figure 3.18A). There is a clear pattern of increasing sediment delivery according to slope and runoff as well as a substantial effect of traffic, even when described in this very coarse quantification of “high” vs. “low.” We can explore effects of best management practices using this

framing and classification approach as well. Noting that the degradation resistance score is also bimodally distributed, we can classify it at a value of 50 or greater representing strong rock (Minor, 1960) and see a shift in expected sediment yield, with a stronger effect under higher traffic (Figure 3.22). Similarly, we can see an effect of added ditch line roughness (Alvis et al., 2024) driving a decline in erosion (Figure 3.23). Though there is a suggestion within the data of a greater effect of roughness under high stream power situations, the sampling is somewhat unbalanced where high traffic with low roughness (red circles) has little representation under low stream power.

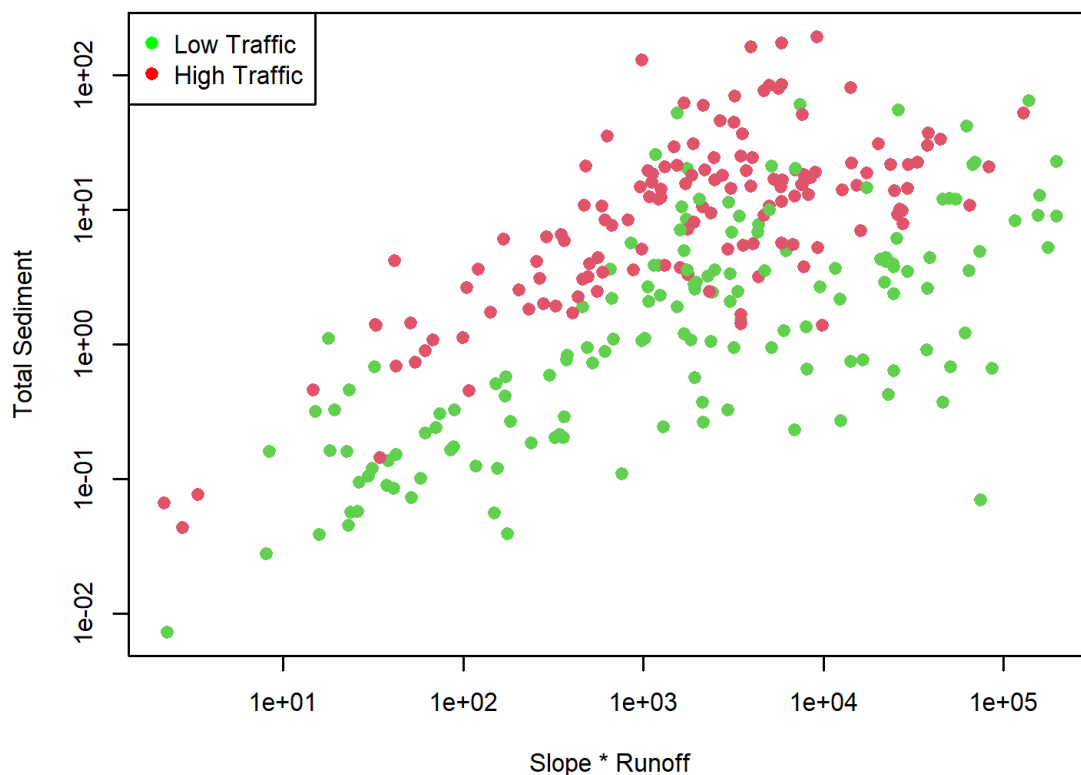


Figure 3.21 Relationship between stream power and sediment yield classified by high vs. low traffic, illustrating coarsely the effects of two primary drivers.

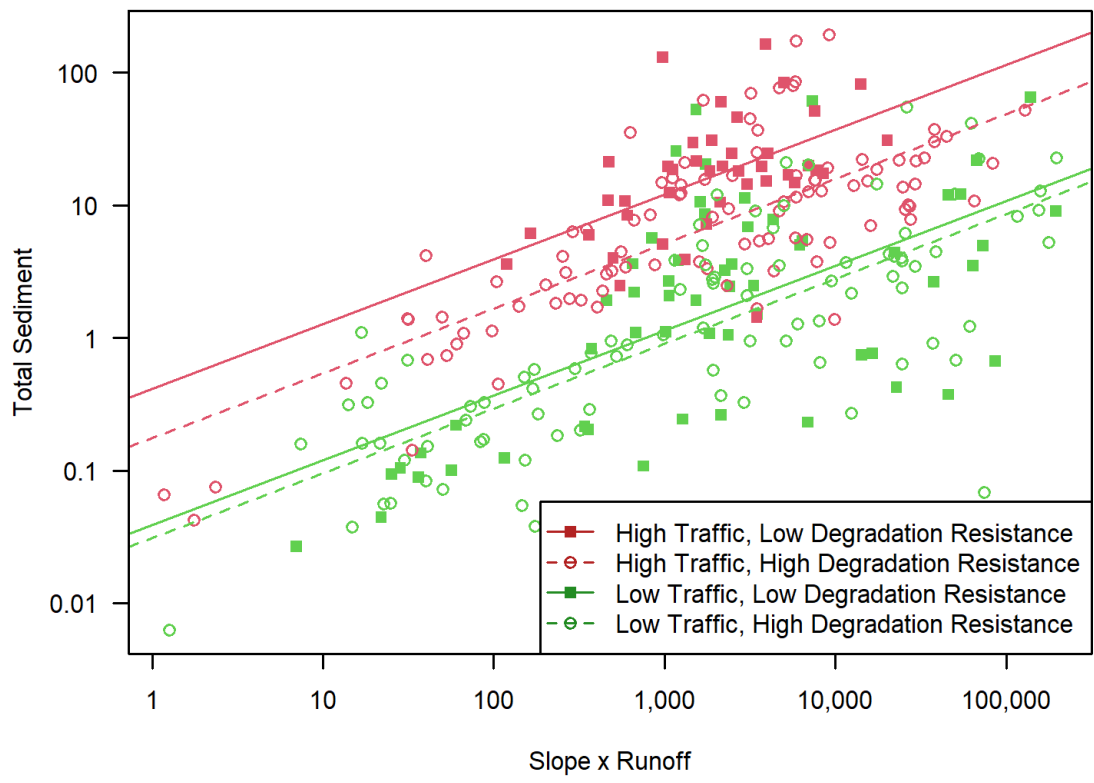


Figure 3.22 Relationship between stream power and sediment yield classified by high vs. low traffic and for degradation resistance (rock quality), showing the conceptual benefits of improved rock quality which shows some dependence on the traffic level in this classification model.

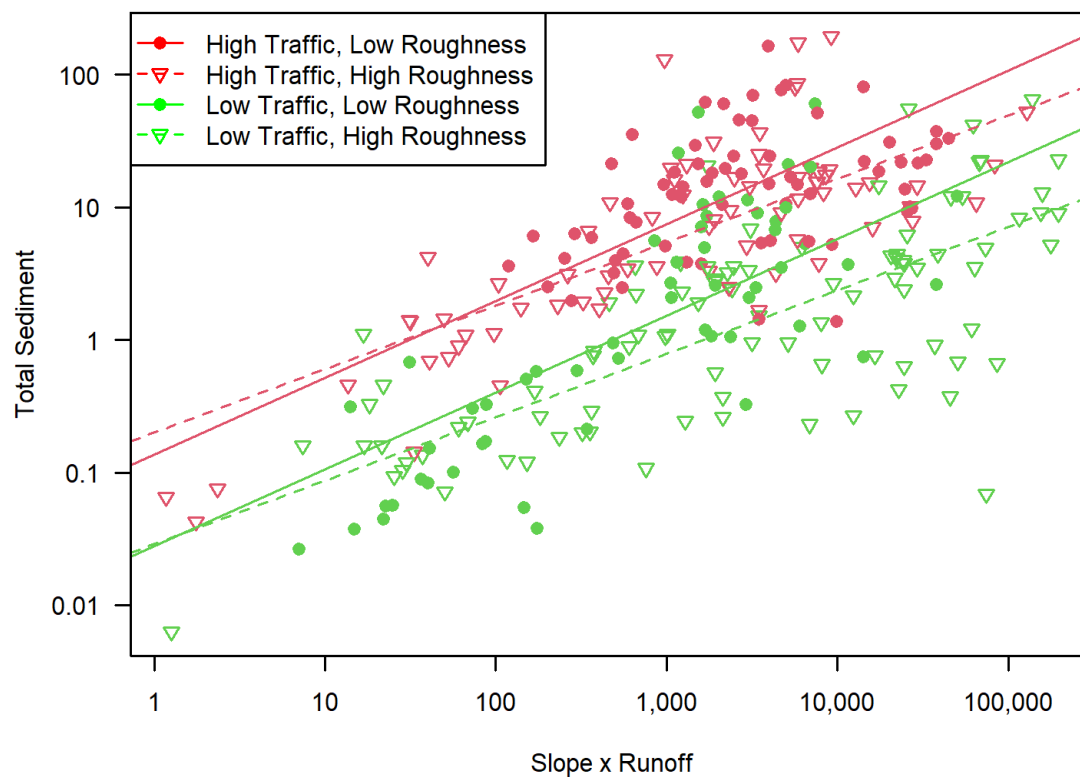


Figure 3.23 Relationship between stream power and sediment yield classified by high vs. low traffic and for the roughness (inversely related to fractional grain shear stress), showing the conceptual benefits of ditch line best management practices that slow water and reduce the shear stress available for grain transport. This classification model shows some dependence of the effect on roughness on traffic level and stream power.

Moving toward a continuous variable relationship with traffic, the number of potential covariates, along with their degree of correlation, means that there is some need for consolidating variables to prevent overfitting or confounding effects. An approach like principal components, for example, could be one useful way to explore the dimensions available across these data. PC analysis draws from correlation matrices, such as Figure 3.19, so we can see that 1) there are strong correlations across metrics of the same type (cars or trucks) across moisture conditions; 2) within a moisture condition, correlations across types are still fairly strong correlations (0.73-0.8); and 3) the fraction of traffic during wet or very wet conditions is poorly correlated with the counts. This would argue for two to three variables to describe the different kinds of traffic and their effects under different moisture conditions.

Testing of model fitting across alternative sets of surface disturbance metrics produced two points: 1) metrics trying to distinguish traffic during wet conditions compared to all conditions were not significant and some fits even gave physically implausible parameter estimates, and 2) though some improvement in overall model fit could be made separating car and truck traffic, a potentially more useful fit could be obtained by a single lumped variable. To the first point, attempted fits using all of the traffic count variables as unique variables only gave the “all” traffic counts as significant variables, and models using

them individually were strongest for the same variables. In some ways this is unsurprising, as some of the lighter traffic sites had more “zeroes” rather than a scalar value representing the traffic (Figures 3.18b, c), essentially censoring some of the variability in traffic. Neither of the fractional traffic during wet conditions produced significant fits and, within the best model for all covariates, fraction wet (fwet) traffic covariates produced negative coefficients. One issue discovered was that extreme values of fwet (near 0 or 1) occurred only at sites with low traffic, as such traffic that occurred fell on either wet or dry days. High traffic sites tended to be more constrained (between 20 and 80%). Retesting under strictly high traffic gave no improvement, and further examination of partial dependency plots using Random Forests gave no consistent effect.

To the second point, using separate counts of cars and trucks as covariates gave coefficients that indicated equivalent effects for the two metrics. Such equivalency does not coincide with physical expectations or anecdotal observations around the effects of trucks (Alvis et al., 2023; Luce & Black, 2001; Reid & Dunne, 1984; Van Meerveld et al., 2014). Combining the counts of cars and trucks into a weighted sum and then tuning the weighting for an overall “traffic” effect gave a weight of 1/8 to the car count relative to the truck count for the best fit. Sensitivity to that weighting parameter was not particularly high. Figure 3.24 shows a plot of just the traffic effect versus sediment yield.

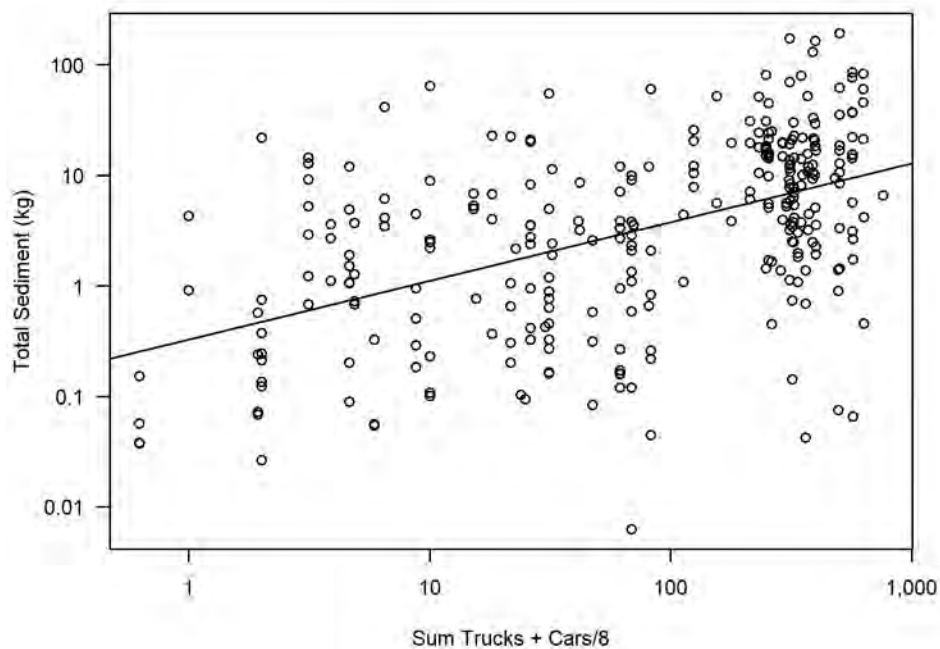


Figure 3.24 Dependence of sediment yield on a simple weighted traffic loading, without consideration of other covariates.

The best linear mixed effect model gave significant parameters for each of the main fixed effects (Table 3.3). The strongest was the mix of slope and flow, followed by traffic. The two variables reflecting surfacing and ditch line effects were both statistically significant with lesser effect and significance of effect compared to the other two independent variables. No interaction effects were statistically

significant, though the direction and magnitude of parameters were consistent with physical expectation. Geology showed no significant effect. The best LME model had a calibration R^2 of 0.68, and 75-fold cross validation (leaving one site out for each iteration) had a validation R^2 of 0.65 (Figure 3.25). Effects of the individual covariates and their uncertainty are summarized in Figure 3.26, giving a visual sense of the relative effectiveness of ditch line (fgss) and rock quality (degr) treatments.

Table 3.3 Parameter estimates and significance for (t-values greater than 1.67 are significant at the $p=0.10$ level)

	Estimate	Std. Err.	t value
Log(stream power)	0.52	0.034	15.57
log(traffic)	0.51	0.048	10.63
log(fraction grain shear stress)	0.14	0.07	2.18
log(degradation)	-0.15	0.08	-1.76

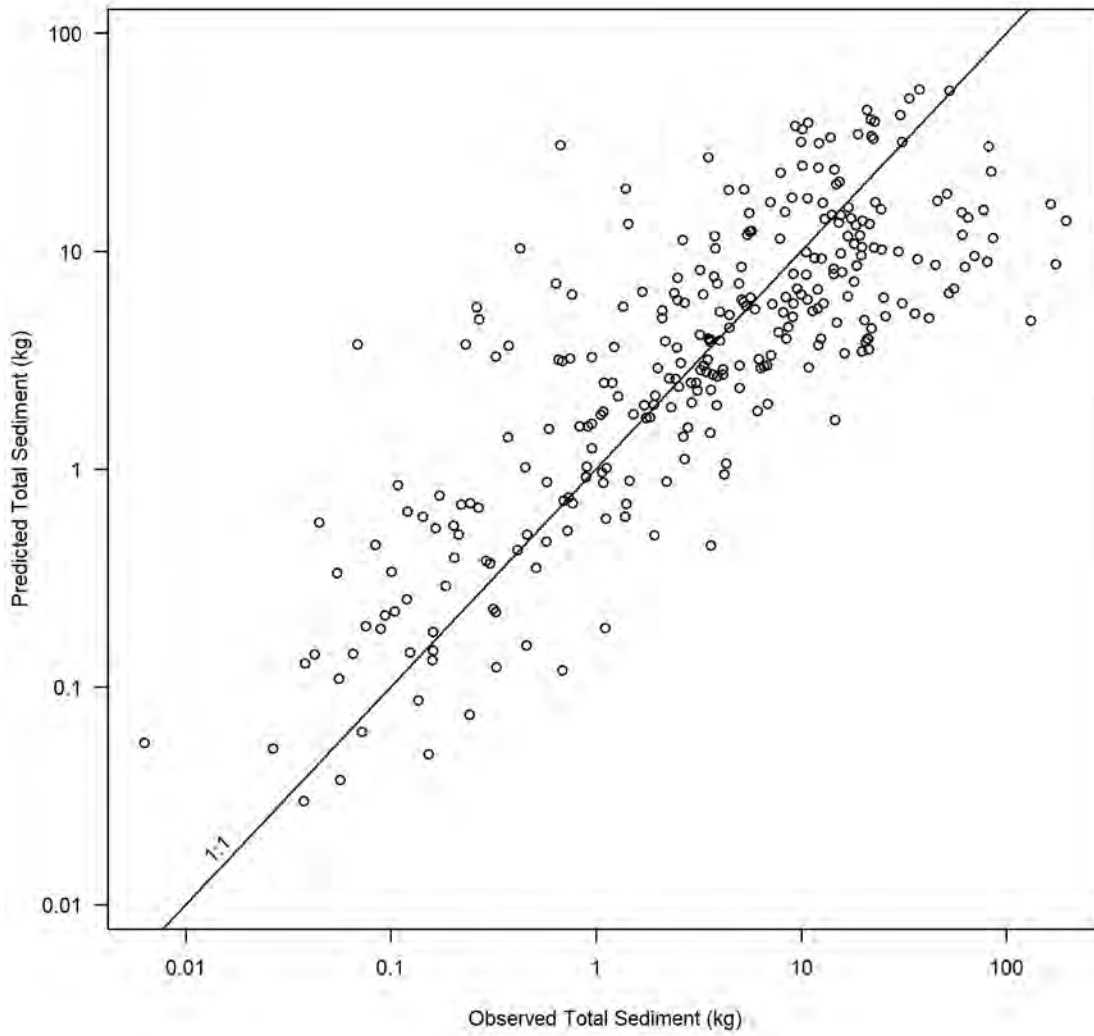


Figure 3.25 Plot of predicted vs observed results using leave-one-site-out (75-fold) cross validation.

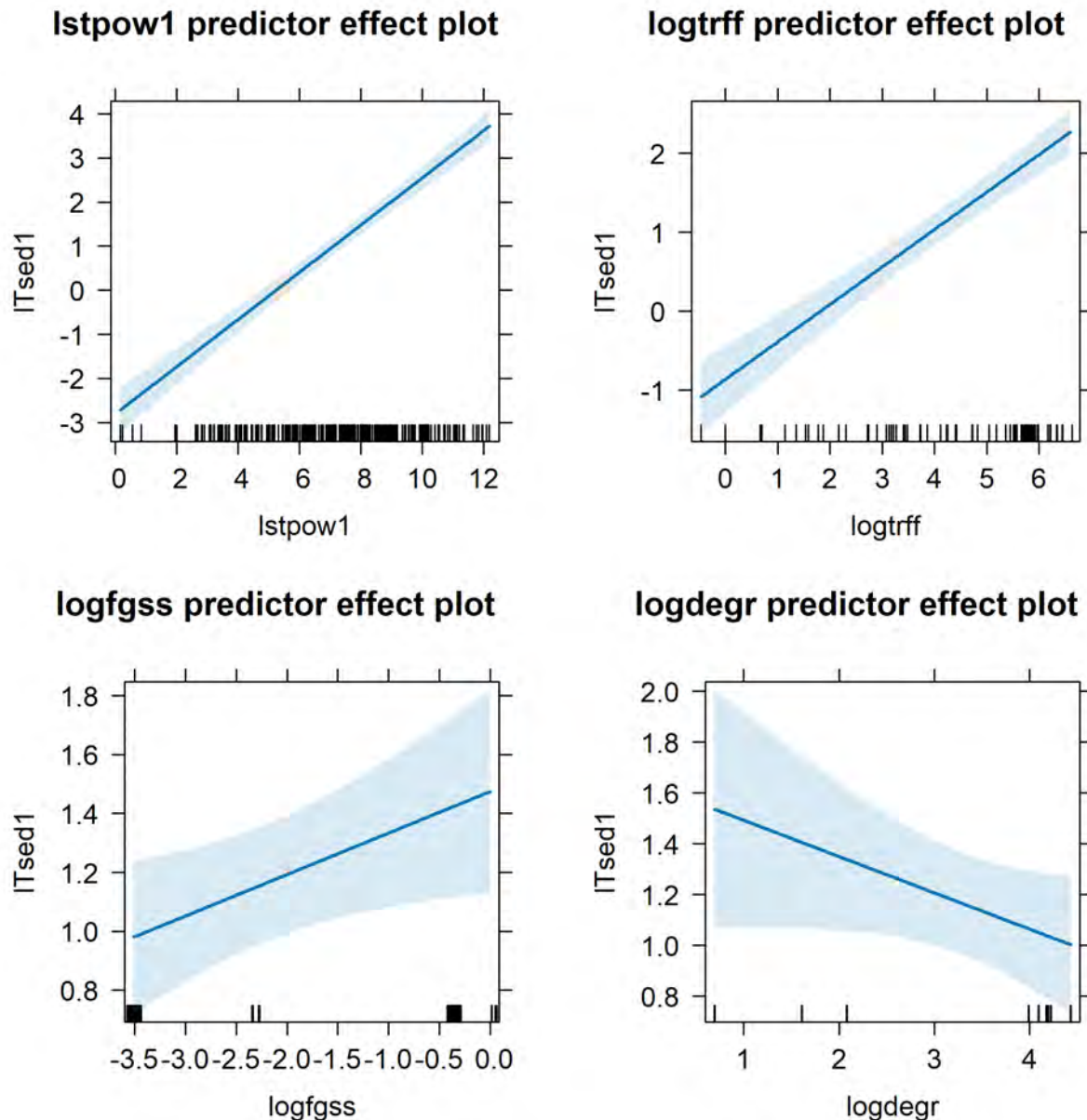


Figure 3.26 Relative effects of each covariate on the sediment yield ($ITsed1$), all axes are log transformed variable values. Recall that the rock degradation resistance score ($degr$) has higher quality with higher scores, and the fractional grain shear stress ($fgss$) partitioning is greater on bare ditches than on highly vegetated ditches. Small ticks at bottom of each graph show distributions of the predictor variable.

4 CONTINUING MODEL DEVELOPMENT

Since the previous interim report, the majority of work has focused on the Major Experiment and Parameterization Experiments to obtain more data for the Model Development. Additionally, members of the Project Team carried out a literature synthesis to aid in the framing of the model. As such, Model Development was put on a brief hiatus, and further development of the model is the goal for the rest of

this biennium. Here, we provide some background information from the literature synthesis and a detailed review of the model status (for full synthesis, see Appendix A).

4.1 TRAFFIC-INDUCED, EROSION-ENHANCING PROCESSES

Four main traffic-induced, erosion-enhancing processes have been anecdotally and experimentally described but not elaborately modeled in the literature. These four processes include: pumping, crushing, scattering, and rutting. Pumping is posited to occur when larger sediment that is layered over finer sediment gets pushed down by traffic, forcing the finer sediment to be “pumped” upwards (Figure 4.1). Crushing is caused by traffic breaking down larger sediment into finer sediment (Figure 4.2). Scattering is the lateral displacement of larger sediments armor the road surface due to traffic, exposing the finer sediment below. Rutting is the deformation of the road surface caused by similar traffic patterns eroding and compacting wheel paths, which increases the capacity of water within those ruts to move sediment.

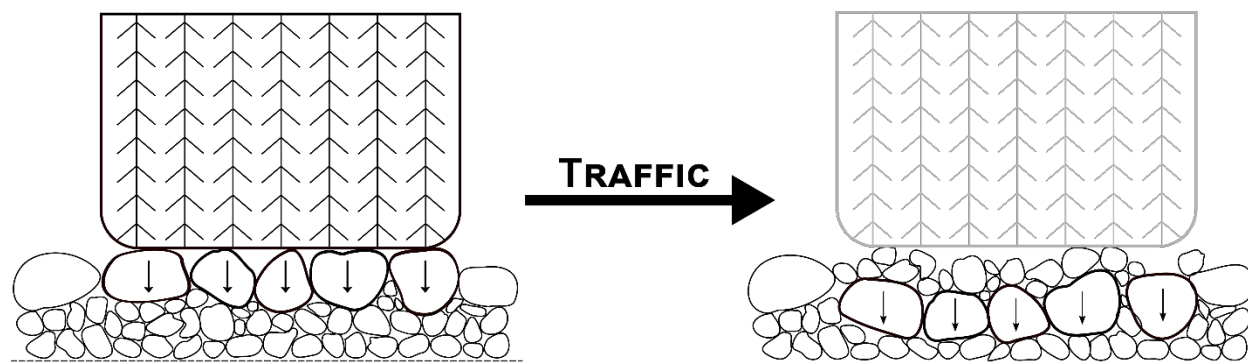


Figure 4.1 Schematic of the pumping process. Larger sediment is layered over finer sediment (left) and when traffic is applied (center) the larger sediment gets pushed down which forces the finer sediment upwards (right). Image not to scale.

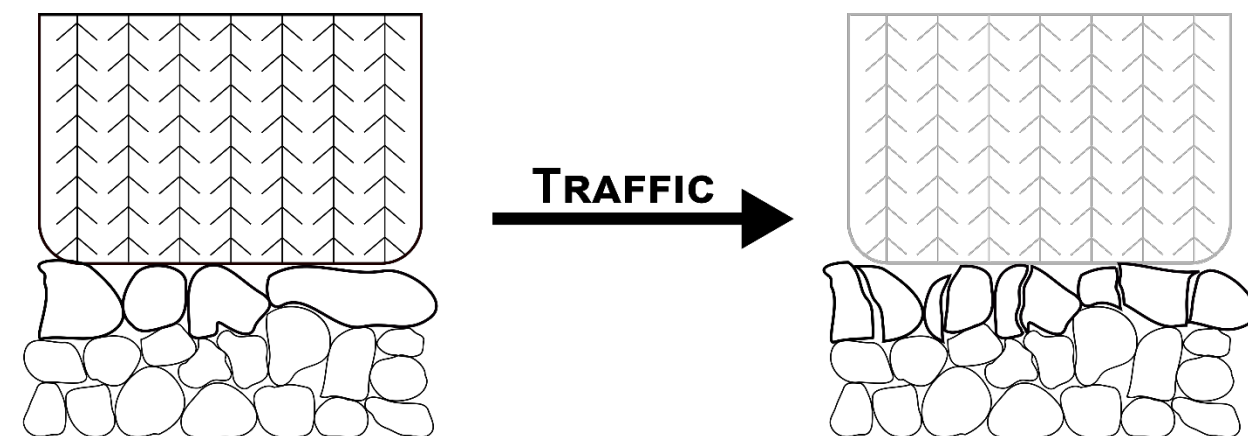


Figure 4.2 Schematic of the crushing process. On a typical road surface aggregate (left) when traffic is applied (center) the larger sediment breaks down into finer sediment (right). Image not to scale.

4.2 SPATIALLY-LUMPED MODEL

We have hypothesized and developed a preliminary, spatially-lumped forest road sediment balance model that demonstrates the vertical sediment exchange among conceptual layers and the supply for

lateral sediment transport on a representative road surface. The current spatially-lumped model incorporates the traffic-induced, erosion-enhancing processes of pumping (Figure 4.1) and crushing (Figure 4.2). The domain of the topic spatially-lumped model is a 1-meter by 4.5-meter section within a larger road segment (Figure 4.3). Every meter-long section is assumed to have the same characteristics such that sediment production in one section can be extrapolated to every other section and summed to obtain the total sediment yield.

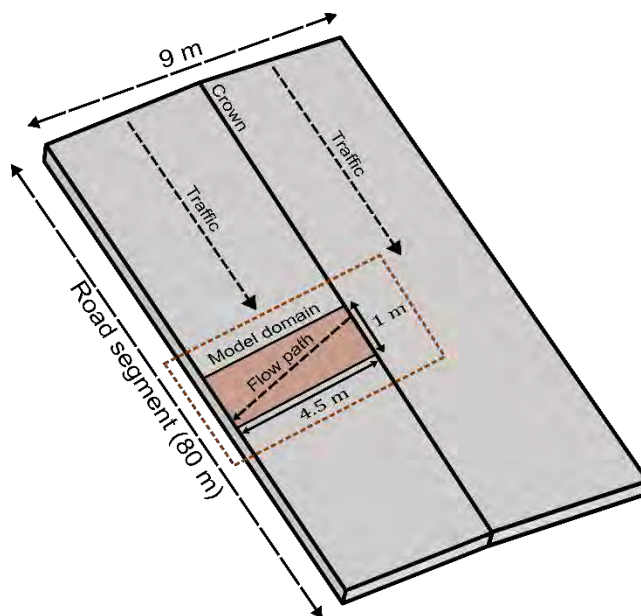


Figure 4.3 Schematic of spatially-lumped modeling domain within an 80-m by 9-m experimental road segment.

Because pumping and crushing occur vertically within road prism, we use a vertical tri-layered conceptualization (Figure 4.4) to model these processes. Scattering and rutting, however, occur laterally, and will be integrated to a future iteration of the model using a laterally distributed conceptualization. In addition to these erosion-enhancing processes, we incorporate water-driven sediment transport to model the erosion process itself.

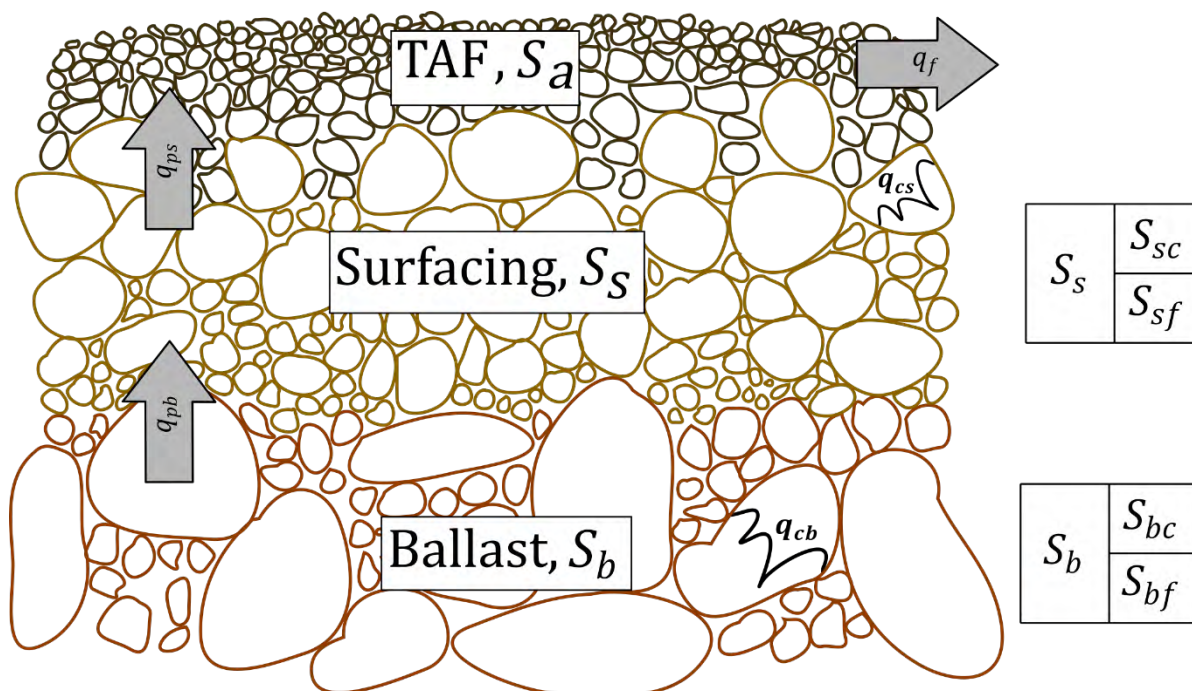


Figure 4.4 Tri-layered conceptualization used to model processes occurring vertically within the road prism.

The spatially-lumped tri-layered model conceptualization includes three layers for storage and five sediment fluxes. The three storage layers in this conceptualization are, from top to bottom: the theoretical transport available fines (TAF) layer, S_a ; the road surfacing layer, S_s ; and the ballast layer, S_b (Figure 4.4). The five sediment fluxes include the pumping of fine sediment upwards between each of the layers of the road prism, crushing of larger sediments to form fine sediment in each of the layers, and the lateral transport of fine sediment from the transport available fines layer. This conceptualization is used to ensure conservation of mass.

For the lower storage layers, S_s and S_b are further divided into fine and coarse fractions of material such that:

$$S_s = S_{sf} + S_{sc}$$

$$S_b = S_{bf} + S_{bc}$$

where the f subscript denotes the fine fraction of material, and the c subscript denotes the coarse fraction of material. These sediment size fractions are grouped into buckets of “small enough for overland flow transport” (i.e., sand size or smaller) and “too big for overland flow transport” (i.e., larger than sand size) to simplify parameters.

The theoretical TAF storage layer is the uppermost road layer that contains only fine material (sand size or smaller) available for water-driven transport. This layer can be likened to an active layer of a riverbed (Hirano, 1971). The TAF layer connects the vertical conceptualization to the laterally-distributed conceptualization and is the layer in which sediment transport occurs. The two main fluxes acting on this layer are the TAF lateral transport flux, $q_{f,out}$, and the vertical surfacing pumping flux, $q_{ps} \cdot q_{f,out}$

describes the fine sediment leaving the road prism and is governed by a common sediment transport equation. q_{ps} is an inter-layer transportive flux that describes the pumping of fine sediment from the surfacing layer, S_{sf} , into the TAF layer, S_a .

The surfacing storage layer is the middle layer of the cross-section and is typically a mixture of approximately 80% gravel and 20% finer material that is between six and twelve inches deep. This layer couples to both the TAF and the ballast and is the most active layer in terms of the number of fluxes acting on and within it. The three fluxes acting on this layer are the surfacing pumping flux, q_{ps} ; the surfacing crushing flux, q_{cs} ; and the ballast pumping flux, q_{pb} . As described above, q_{ps} is an inter-layer transportive flux that describes the pumping of fine sediment from the surfacing layer, S_{sf} , into the TAF layer, S_a . q_{cs} is an intra-layer generative flux that describes the crushing of coarse surfacing material, S_{sc} , into fine surfacing material, S_{sf} (Figure 4.4). q_{pb} is an inter-layer transportive flux that describes the pumping of fine sediment from the ballast layer, S_{bf} , into the fine sediment of the surfacing layer, S_{sf} .

The ballast storage layer is the lowest layer of this conceptualization and is typically larger material with interstitial space occupied by a fine material matrix. The ballast transitions to native material as you move farther down the stratigraphic column, but the native material is not considered in this analysis. This layer couples to the surfacing via one of two fluxes. The two fluxes acting on this layer are the ballast crushing flux, q_{cb} , and the ballast pumping flux, q_{pb} . q_{cb} is an intra-layer generative flux that describes the crushing of coarse ballast material, S_{bc} , into fine ballast material, S_{bf} . q_{pb} is an inter-layer transportive flux that describes the pumping of fine sediment from the ballast layer, S_{bf} , into the fine sediment of the surfacing layer, S_{sf} .

The pumping and crushing fluxes— q_{ps} , q_{pb} , q_{cs} , and q_{cb} —are modeled via equations we developed based on hypotheses developed from literature and field observations (e.g., Foltz & Truebe, 2003; Reid & Dunne, 1984; Rhee et al., 2018; Ziegler et al., 2001), while the transport flux is modeled by Govers' equation for shallow overland flow (Govers, 1992). The transport flux also includes a shear stress partitioning component that changes based on how “full” the TAF layer is. If the fine sediment of the TAF layer only fills some of the voids between larger rocks in the surfacing, the shear stress available to transport the sediment will be less because the larger sediment acts as an “obstruction.”

These processes, plus a simple stochastic model representing truck passes, are the basis of the spatially lumped model. Each layer is a depth of storage because the value has been normalized by the length (1 m) and width (4.5 m) of road.

4.3 PRELIMINARY MODEL RESULTS

Below are preliminary results from example spatially-lumped model runs forced using rainfall data from a gage at Elk Rock near Mount St. Helens in Washington state. We carried out three model runs, each of which used a different level of traffic per day. The traffic level is modeled using a stochastic Poisson distribution centered around 5, 10, and 20 truck passes per day. Aside from the rainfall data, the model parameters are currently estimates based on limited information available in the literature, road surfacing practices, and field inferences. As the model is further developed, the equations and

parameter estimates used in the following results will be refined. Refinement of both will be determined based on Parameterization Experiments.

In our model runs, the TAF layer has been initialized at “full” depth—a condition that corresponds to a road that has had many truck passes and no sediment transport due to rainfall—such that the model does not require a spin-up period (i.e., time to fill up the TAF layer to produce any sediment transport). A large storm occurs at the beginning of the period which flushes a lot of the fine sediment away—this is also called the “first flush” phenomenon (Van Meerveld et al., 2014). The ups and downs of the fine sediment storage are due to traffic running over the road surface, causing a disturbance (increase), and then rainfall occurring, washing the fine sediment away (decrease) (Figure 4.5). As the traffic level increases, we see a higher overall TAF layer storage depth.

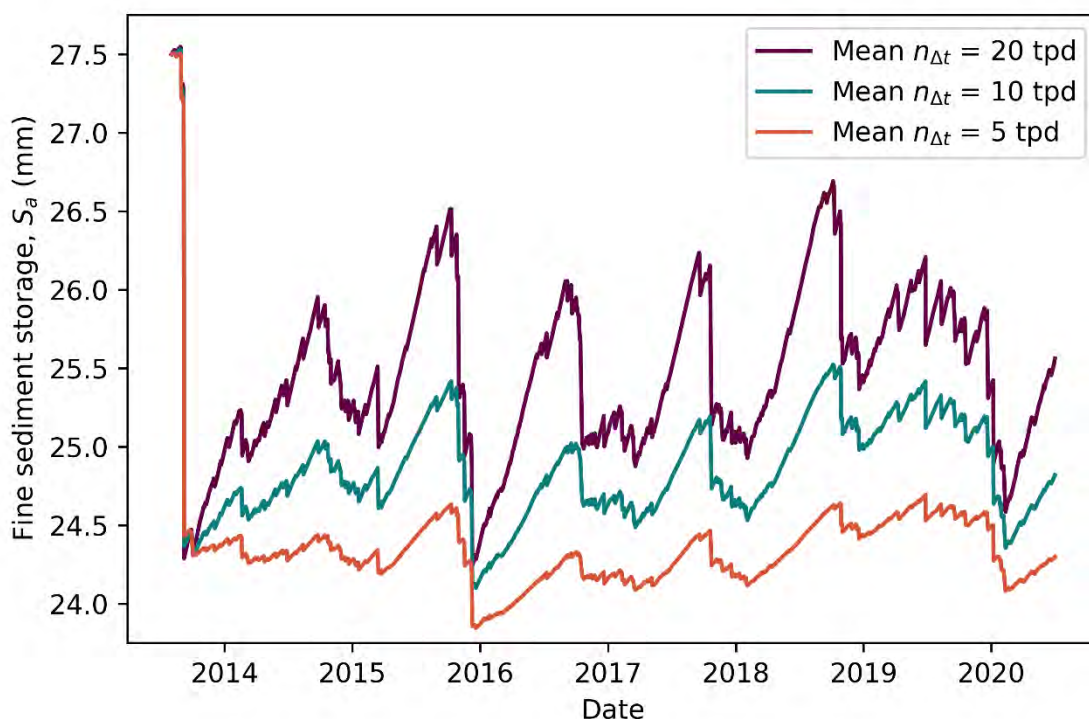


Figure 4.5 Fine sediment storage depth in the transport available fines (TAF) layer over time for three traffic levels (mean $n_{\Delta t} = 5, 10, 20$ truck passes per day). The TAF layer was initialized at 27.5 mm to avoid a model spin-up period.

The next figure (Figure 4.6) demonstrates the use of shear stress partitioning when modeling sediment transport. Here, we look at both the cumulative reference transport capacity and the cumulative actual transport. The cumulative reference transport capacity is the theoretical cumulative depth of domain-averaged erosion per storm had the shear stress not been partitioned. The red lines represent the cumulative reference transport capacity, and the bronze lines show the cumulative depth of sediment actually transported per storm. The values of cumulative actual transport are much lower than the cumulative reference transport capacity because of shear stress partitioning. We see that as traffic level increases, the cumulative reference transport capacity decreases and the cumulative actual transport

increases. In other words, as traffic increases, the supply of readily-available fine sediment increases, which also causes an increase in actual sediment transported.

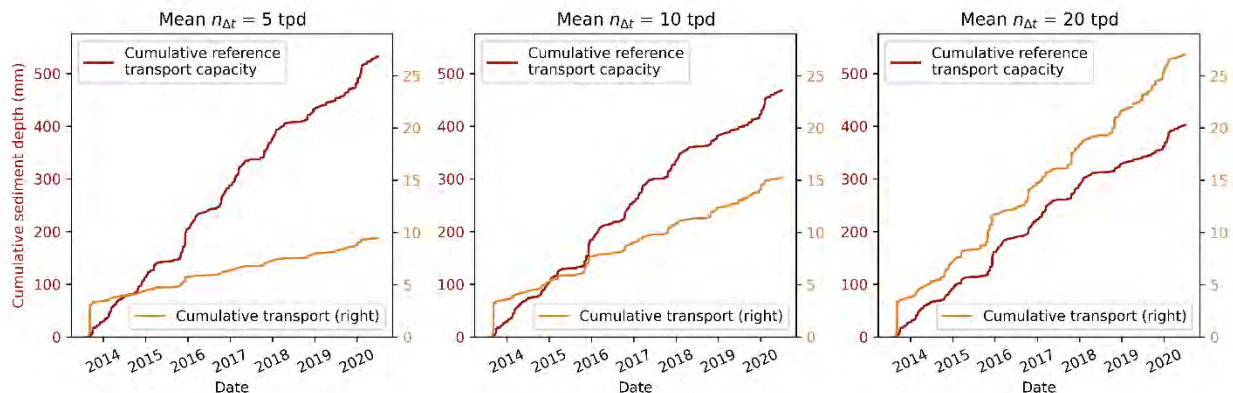


Figure 4.6 Cumulative reference transport capacity depth and cumulative actual transport depth over time for three traffic levels (mean $n_{\Delta t} = 5, 10, 20$ truck passes per day).

The final plot (Figure 4.7) shows the annual sediment load per meter of road for differing traffic levels. Overall, the values of sediment mass per meter of road yielded by this model run are high compared to data collected as part of the Major Experiment. This overestimation is likely due to a couple issues: (1) our parameters are currently only estimates and (2) this iteration of the spatially-lumped model includes only the road prism, whereas the data collected as part of the Major Experiment includes the roadside ditch lines, which have grass linings serving as an erosion control treatment for sediment-laden water entering the ditches.

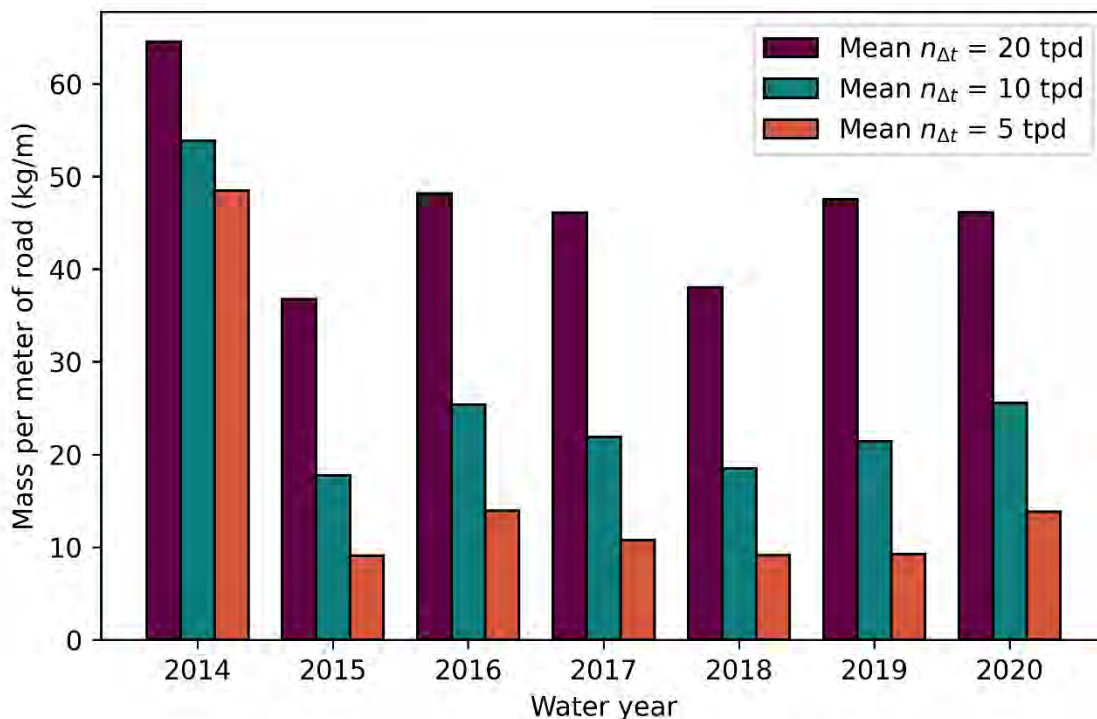


Figure 4.7 Sediment load per meter of road for each water year of the model run for three traffic levels (mean $n_{\Delta t} = 5, 10, 20$ truck passes per day).

4.4 FUTURE MODEL DEVELOPMENT

The next version of our process-based model will incorporate the final two traffic-induced, erosion-enhancing processes: scattering and rutting. The incorporation of scattering (and, implicitly, rutting) can be seen in Figure 4.8. This updated conceptualization includes the pumping of fine sediment upwards between layers of the road prism, crushing of larger sediments to form fine sediment in each of the layers, scattering of larger sediments in the active layer, and the lateral transport of fine sediment from the active layer out of the system. Scattering occurs laterally and is denoted as q_{sa} in the updated tri-layered conceptualization. Rutting, rather than being a process caused by a specific flux, is caused by a combination of vertical and lateral movement of sediment and the presence of ruts enhances erosion. Ultimately, scattering and rutting will be the main link to the more spatially-distributed processes of the model.

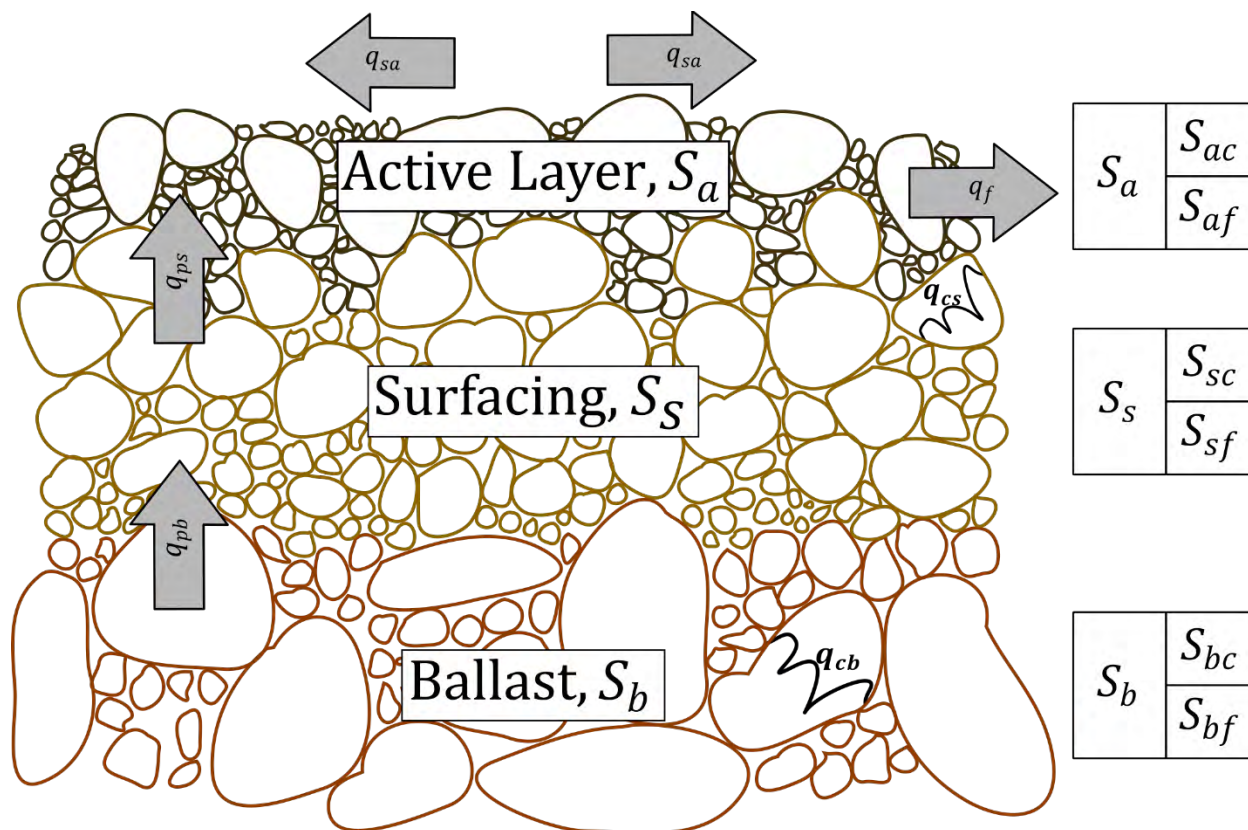


Figure 4.8 Updated tri-layered conceptualization used to model processes occurring within the road prism.

With the incorporation of scattering and rutting, we will fully convert the model to a spatially-distributed representation of the road surface, including the roadside ditch line. The spatially-distributed model will be developed using Landlab—an Earth surface dynamics modeling framework (Barnhart et al., 2020; Hobbey et al., 2017). Landlab is an open-source modular framework, offering different components to model earth surface processes that are easily combined to create a more complicated model. The road prism has numerous processes occurring therein, including, but not limited to: (1) the four traffic-induced, erosion-enhancing processes described in Alvis et al. (2023) (Appendix A) and the beginning of this section; (2) overland flow sediment transport; and (3) channelized flow in wheel ruts and the roadside ditch line. As such, Landlab is an ideal modeling framework for our spatially-distributed model.

In early conversations regarding the spatially-distributed model, we developed a sediment displacement component in Landlab. This component is a preliminary attempt at modeling scattering and rutting of the road surface using a stochastic traffic model in which the number of vehicle passes is a random number based on an exponential distribution with a mean of 5 vehicle passes per day. As a truck passes over the road, sediment is displaced to either side of and behind the tire, and when the road is not driven on, slight amounts of linear diffusion occur. As a proof-of-concept, we used a synthetic modeling domain (Figure 4.9a) of the road surface and roadside ditch line and ran the sediment displacement component for 10 model days. Wheel ruts develop on either side of the crown of the road surface (Figure 4.9b, Figure 4.10).

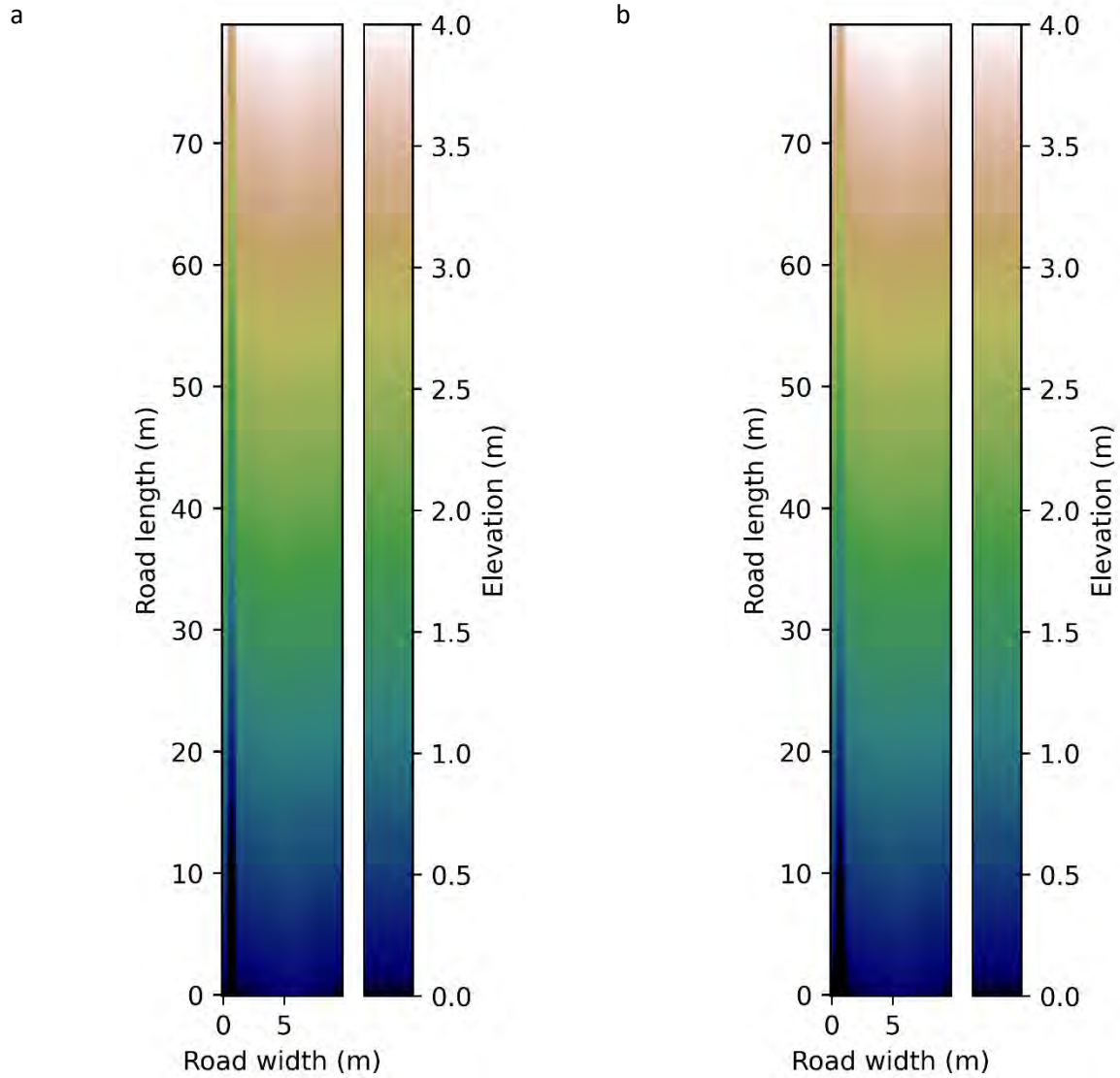


Figure 4.9 The current modeling domain as defined in Landlab showing (a) the initial road surface and (b) the road surface after running the in-progress sediment displacement component. Wheel ruts develop on either side of the road crown.

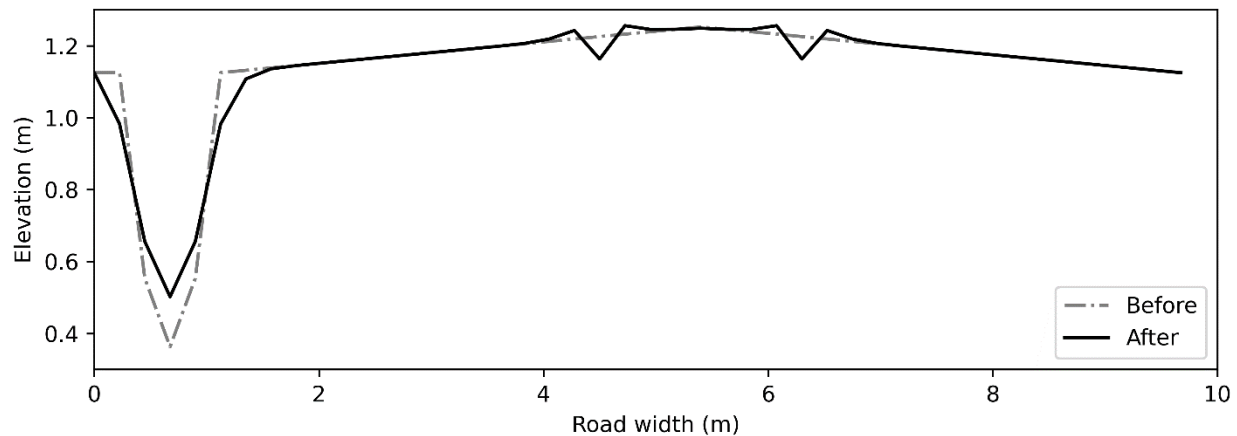


Figure 4.10 A cross-sectional profile of the road surface and ditch line before (gray dash-dotted line) and after (black line) running the in-progress sediment displacement Landlab component.

In addition to the processes described above, the spatially-distributed model will incorporate components modeling the effects of different erosion control treatments on road sediment yield. Once the spatially-distributed model is finalized, we will apply the model to various locations in western Washington using a range of climate and traffic conditions to examine estimates of forest road erosion. The model runs will be compared to sediment and runoff data collected during the Major Experiment. These data will help calibrate and validate the model.

Because the Project Team is utilizing a large number of field sites (78) to study multiple covariates affecting sediment production, we anticipate carrying out numerous model runs. Covariates that contribute to sediment production include traffic levels (high, medium, low), rainfall rates (high, medium, low), lithologies (volcanic, siltstone), road slopes (2.5–13%), rock surfacing qualities (marginal, good, high quality), and ditch line erosion control treatments (bare, eroded, grassed, wattled). We plan to run the process-based model using combinations of covariates in line with those seen at the 78 field sites, as well as a few other combinations.

The final model results from across sites will be presented in the limiting factor framing that relates erosion, supply, and energy seen in Alvis et al. (2023) (Appendix A) to begin thinking about how different locations behave based on traffic and other covariates. If the energy is less than the supply, the erosion of the system will be dependent on energy, making the erosion process energy limited (e.g., a fully muddy road). However, once the energy is greater than the supply, the erosion of the system will be equal to the amount of supply available, making the erosion process supply limited (e.g., a rocky road). Based on this framing, we can classify roads and think of potential mitigation strategies in terms of the road system type.

5 SEDIMENT TRAP EFFICIENCY EXPERIMENT

5.1 THE EXPERIMENTS

Two main experiments were conducted at the Rayonier office/yard in Forks, WA. during the week of June 17-June 21, 2024.

We investigated two central questions:

- How does sediment trap efficiency change with changes in water flow?
- How does sediment trap efficiency change with changes in sediment trap volume?

We followed the methods outlined in the detailed experimental plan and further described below.

The basic design of the experimental apparatus is shown in Figure 5.1. We used a steel half-cylinder with a nominal volume of 34 gallons as the sediment trap (see Figure 5.2). It is constructed with 2-inch higher sides on the flume end, so that water flows relatively smoothly through a sampler out the exit end, to simulate a typical sediment trap in a roadside ditch. The sediment trap was positioned nearly level with a 16-foot length of 18-inch-wide wooden flume set on a 3% grade (Figure 5.3). Water is supplied to the flume from a water truck through a flow meter. Local siltstone-derived sediment was sieved to less than 4.5 mm. Sediment was introduced at a known rate to simulate field conditions (3-5 grams/liter). Sediment was applied using a vibratory delivery device over a sediment mixing zone from where sediment was delivered to the flume and then to the sediment trap (Figure 5.4). The sediment trap was suspended from hooks and weighed before and after each run using two digital hanging scales.

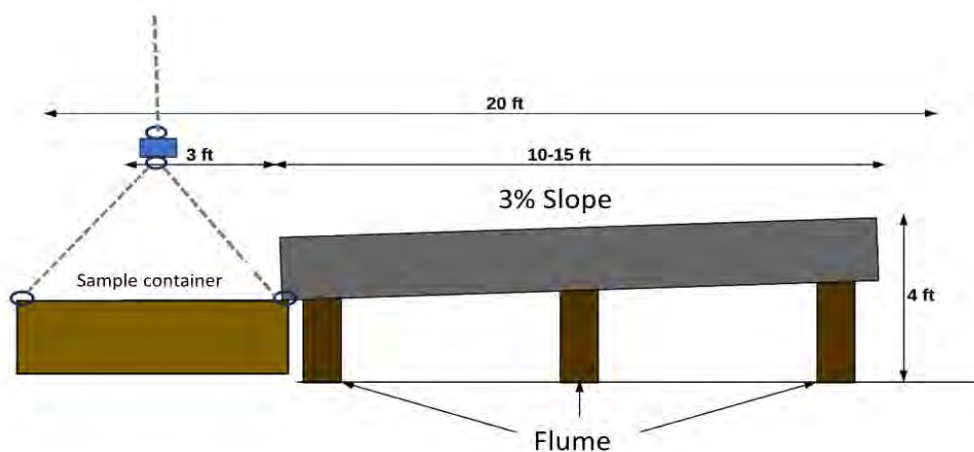


Figure 5.1 Flume and sampler configuration.



Figure 5.2 Flume with sampler during run in the upper image and the retained sample in the photo below.



Figure 5.3 Vibratory sediment feed device applying the sediment at the upper end of the flume.

On June 18-21, 2024, seven runs were conducted to answer the first question concerning the relationship between flow rate and sediment trap efficiency (Table 5.1; rows 1-6, 13). Six runs were conducted to investigate the relationship between sediment trap volume and sediment trap efficiency (Table 5.1; rows 7-12).

Table 5.1 Table of runs carried out the week of June 18-21, 2024.

Run	Nominal flow (gal/min)	Nominal % of capacity	Nominal open Volume (gal)	Target sed conc. grams moist soil/l	Target feed rate grams moist soil/min
1	10	100	34	5	189
2	10	100	34	5	189
3	5	100	34	5	95
4	5	100	34	5	95
5	50	100	34	5	945
6	50	100	34	5	945
7	10	75	25.5	5	189
8	10	75	25.5	5	189
9	10	50	17	5	189

10	10	50	17	5	189
11	10	25	8.5	5	189
12	10	25	8.5	5	189
13	10	100	34	5	189

The laboratory work is not yet complete for the June 2024 experimental runs, but preliminary results show a strong relationship between the discharge and sediment trap efficiency.

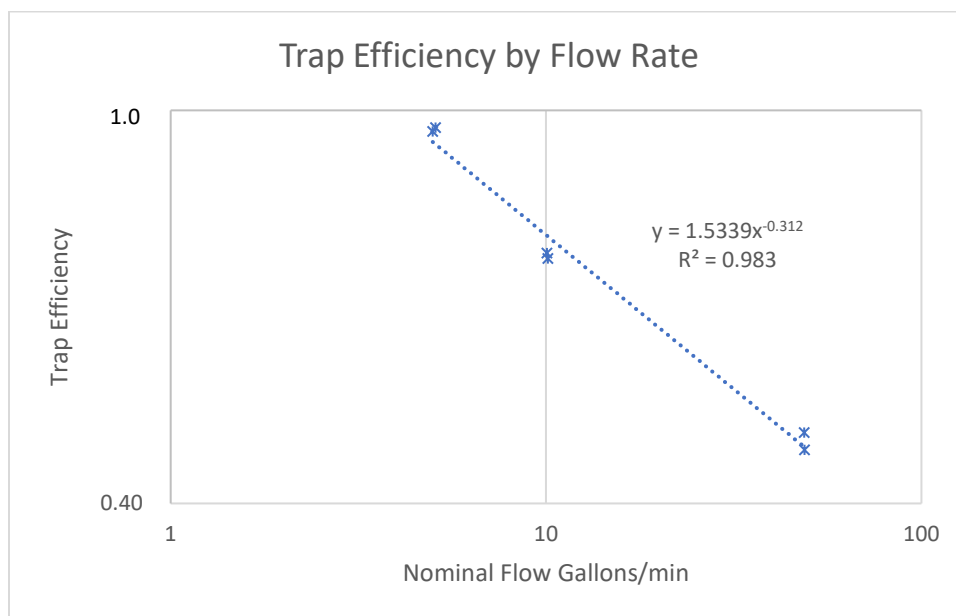


Figure 5.4 Sediment trap efficiency for 5, 10 and 50 gallons a minute.

6 SHORT-TIME-SCALE INTERACTIONS EXPERIMENTS

To better understand how to efficiently control road-derived sediment, we need to study the contribution of fines at a short-time scale in the context of overall annual plot sediment production. The goal of this experiment is to measure sediment detached and transported from the road tread under variable surfacing rock quality, truck frequency, and rainfall intensity (Figure 6.1). This experiment will determine how much sediment is produced from the road surface, where the sediment goes during a rain event after a truck pass, and how quickly the sediment moves through the road drainage system.



Figure 6.1 New fine sediment pumped from the roadbed by the passage of a loaded log truck.

The experiment is divided into two portions. The first series of experiments investigates the generation of fine sediment associated with the passage of a loaded truck, referred to as the Short-Time-Scale Pumping Experiments.

The second experimental series examines how sediment moves across the road surface within the 80-meter plot. The Short-Time-Scale Turbidity Experiments examine the within-plot contribution of sediment from traffic relative to that from ditch and cutslope by sampling water from tread, ditch and combined locations.

Presented below are preliminary protocols and results from our efforts in the Siltstone Province. We have not made a final decision but are considering doing additional runs of each of these two S-T-S experiments in the Volcanic Province.

6.1 SHORT-TIME-SCALE PUMPING EXPERIMENT

To determine the mass of sediment that is generated by the passage of a loaded truck, we selected plots on actively used mainline roads in the Siltstone Province near Elma, WA. The experimental segments were closed to the public and log haul to allow the team to work safely. We used 4-inch by 4-inch timbers with soft gasket material on the bottom side to hydrologically separate a 48-inch-wide and 50-foot-long wheel rut from the rest of the road prism. We sampled the existing road surface sediment to determine the particle size. We then used a water truck and rinsed the surface repeatedly to expose a freshly armored gravel surface that was relatively free of excess fine sediment (Figure 6.2). We sampled this cleaned surface as a control. A loaded gravel truck was then driven through the plot a total of six times, accelerating to approximately 20 mph, which represents a typical speed for a loaded gravel truck. Clean filter fabric (100 feet) was placed at each end of the plot such that the side of the truck that would next pass through the plot was lined up on the fabric. The side of the truck lined up on the fabric was

thoroughly rinsed for 10-15 minutes to remove excess sediment from the tires and wheel wells. After the six truck passes (Figure 6.2), we sampled the plot again.

For each sample—the original road surface, the control after washing, and the sample after the six truck passes—the following procedure was followed. At five locations, a 30-cm by 30-cm sampling frame was used to isolate and sample portions of the surface (Figure 6.3, 6.4, 6.5). Low pressure water from a hand sprayer was used to rinse the mobile sediment from the surface within the sampling frame for a set time. The sediment and water were gently sampled from the corner of the frame using a vacuum system and separatory chamber. The sediment extracted from the control (i.e., after cleaning and before traffic) and after traffic pairs were differenced to show the amount of sediment that became available due to the six truck passes - this reasonably represents pumping during a typical “heavy haul” day of 5+ trucks.

The Short-Time-Scale Pumping Experiment has been conducted twice with a total of 8 runs at 3 road segment locations (Table 6.1). The results from the experiments conducted February 2023 are considered good quality and are likely sufficient to answer the question about the rate of sediment pumping on these haul routes in the Siltstone Province.

Table 6.1 Summary of S-T-S Pumping Experiment Samples, Siltstone Province.

Site	Sample Date	Data Quality	Runs	Samples	Comment
Mel 2	2/16/2022	Fair	3	28	First run of 4 samples needed a cleaner road; runs 2 and 3 good
Mel 12	2/17/2022	Fair	2	20	Variable water spray and recovery
Mel 12	2/14/2023	Good	2	20	Final run had lower water recovery and higher variability
Mel 4	2/19/2023	Good	1	10	Few samples but good results



Figure 6.2 Surface and the photo on the right shows the surface after 6 truck passes.



Figure 6.3 The fine sediment that is available for transport on the road surface due to recent traffic is carefully washed from the isolated sampling area and evacuated into a sample container for sediment analysis.

Truck Initiated Sediment Pumping Mass

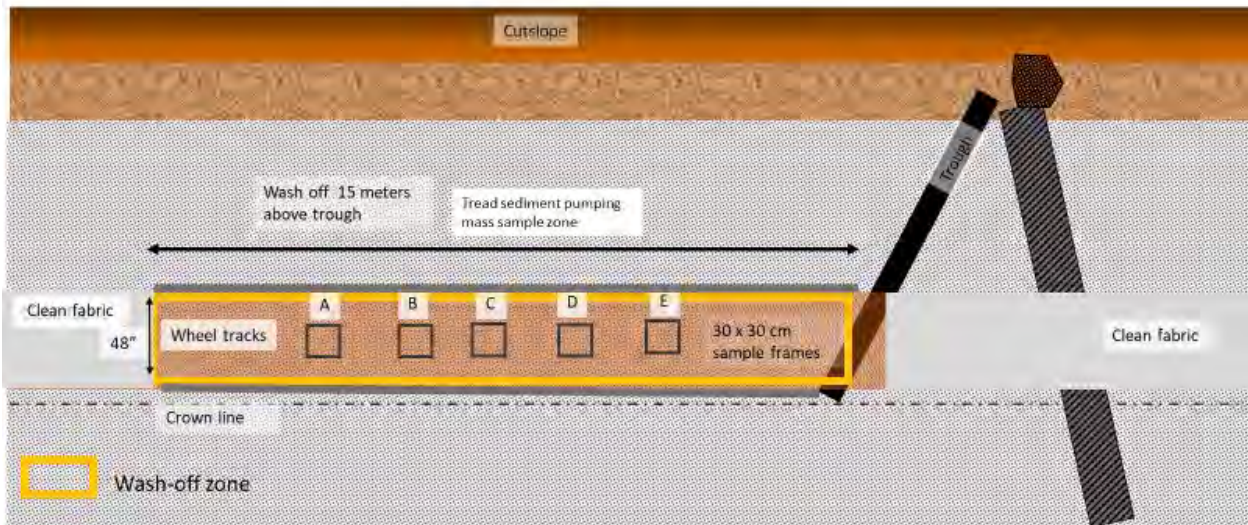


Figure 6.4 The location of the 5 sampling frames within the study plot.

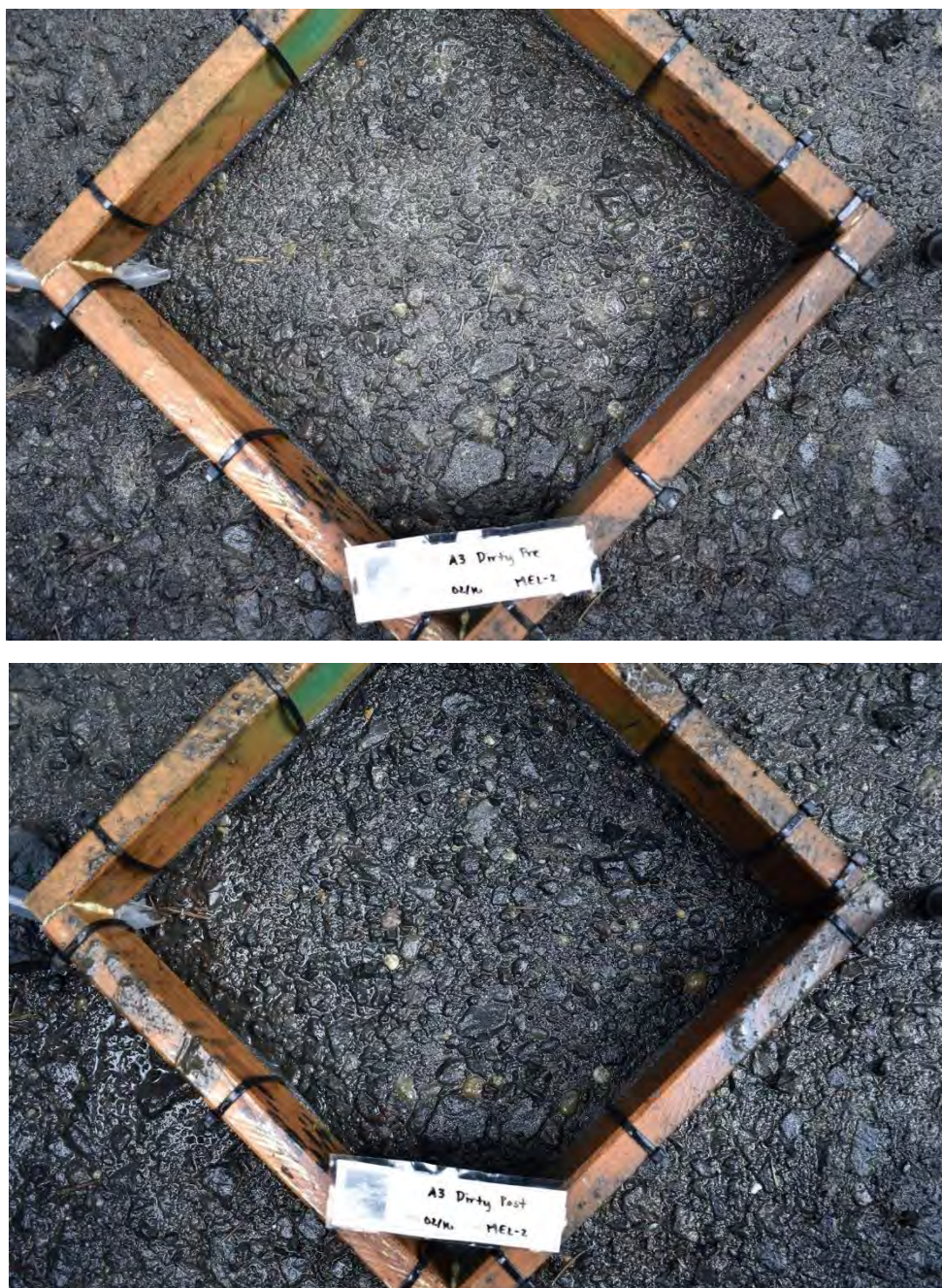


Figure 6.5 Sampling frame before the truck passes and after the truck passes at Mel-2

The differences between the pre and post traffic fine sediment was determined. For example, at the Mel 12 and Mel 4 locations the 6 truck passes mobilized between 4 and 6 grams of sediment per 30-centimeter by 30-centimeter sampling frame (Figure 6.6). Assuming that the truck tires are about 30 cm in width, this equates to about 2.8 grams of sediment per meter of wheel track length per truck pass.

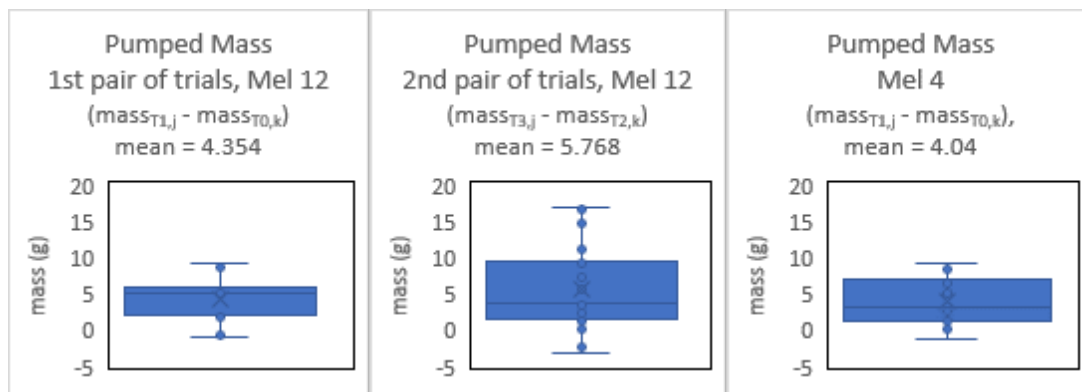


Figure 6.6 Fine sediment mass sampled from 5 sample locations at Mel 12 on 2/14/ 2023 and Mel 4 on 2/19/23. Box plots show differences between the pre-truck pass and the post truck mass associated with 6 passes of a loaded truck.

6.2 SHORT-TIME-SCALE TURBIDITY EXPERIMENT

The S-T-S Turbidity Experiment is designed to monitor the spatiotemporal evolution of discrete sediment pulses moving off the road as they relate to traffic and rainfall. To accomplish this, we collected discretely timed and located samples of sediment after six truck passes and during sufficient rainfall to cause sediment to flow off the road. Sample locations, represented in Figure 6.7, are specifically: A) the outlet of the steel trough (from the Major Experiment, capturing all water flowing down the 80-meter segment); B) the lower end of a 4.7-m concrete gutter placed just below the steel trough; C) the ditch upstream of the trough; and D) the outlet of the cross-drain culvert as it flows into the Major Experiment tub. Sample A is capturing all water flowing down the 80-m segment that does not contribute to the ditch. Sample B, not part of the segment total, helps us understand capture from the edge of the road tread where crowned flow is facilitated to occur as it would in a perfectly crowned road segment without rutting. Sample C is the ditch concentration as it occurs from crown flow plus the cutslope contribution during rainfall. Sample D, for comparison purposes, should be the total contribution from the 80-m segment. Total water volume is estimated from the tipping bucket record as Sample D flows through the tub, and a rain gage with an expanded catchment surface accurately records rainfall during the experiment.

Table 6.2 Table of STE Turbidity runs dates and data quality.

Site	Sample Date	Data quality	Comment
Mel 1	3/14/2022	Good, but not complete	.42" rain in 4 hrs., 8-15 l/min, missed trough turbidity peaks
Mel 14	3/12/2023	poor	Broken datalogger, Insufficient rain/runoff
Mel 14	4/1/2023	poor	Insufficient rain/runoff
Mel 14	1/18/2024	Good but partial data	.45" in 5 hrs. 2 turbidity sensors unstable

We have made steady progress in developing the experimental procedures and sampling equipment required to carry out the S-T-S Turbidity Experiment, but we have not yet completed a single perfect run.

The S-T-S Turbidity Experiment has been run 4 times so far with good but imperfect results on two of the runs. Our main challenge has been having the personnel and equipment on site when the ideal rainfall and runoff conditions finally occur, given the complexity of the experiment and the home locations of the staff. The turbidity equipment has also presented challenges. We began the work using NTS turbidity sensors that had a maximum reading of 2,500 FNU, and we learned in 2022 that the turbidity associated with the road surface quickly exceeded that value after the six truck passes in each experimental run.

As such, we identified and procured 4 Campbell Scientific ClariVue 10 turbidity sensors that have an upper threshold of 4,000 FNU and began using these sensors with a CR6 data logger and a Toughbook field computer. In 2023, we had some success testing the ClariVue sensors, but the weeks we had identified in the field were not optimal for rain. We also had an electrical problem with the CR6 datalogger that prevented data collection when we did have sufficient rainfall and runoff on the afternoon of 3/12/2023.

On January 18, 2024, we had excellent rainfall and runoff conditions at Mel 14, but a delay occurred with the arrival of the loaded truck. The turbidity equipment appeared to be working well at the low turbidity levels associated with little traffic, but when the truck arrived the sensors at the trough location and the lateral sampler became unstable. We tested and switched samplers around to try to accommodate the problem but were not able to get a complete set of turbidity measurements with the existing sensors.

Short Time-Scale Experiment Plot Layout

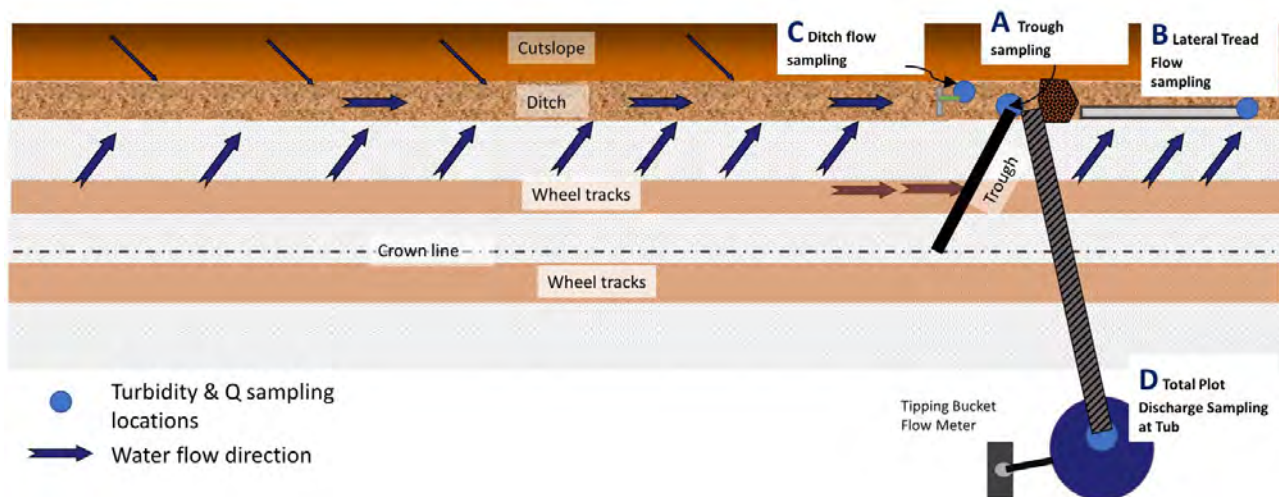


Figure 6.7 General layout of the water and sediment sampling locations for the turbidity experiments. Water and sediment were sampled at the Trough A, Lateral Gutter B, Ditch Line Dam C, and then Tub D integrates the entire plot.



Figure 6.8 Gutter is sheltered from direct rainfall with a cover so that the sample is not diluted.

In addition to locating a turbidity sensor with a suitable range, one of the key developments has been the creation of a flow-through cell that allows the sensor to remain submerged in the sample flow without becoming fouled by sediment or getting interference from light or the sample container. Figure 6.9 shows the current design of P-trap style sampler where the side looking ClariVue 10 sites submerged in a sample volume of water flowing through the trap. A 1 mm screen removes coarse sand from the flow as it enters the trap below the trough, ditch, and lateral sampling locations. This sand is collected,

dried, and weighed separately. The lower portion of the P-trap can be removed to clean out any fine sand that accumulates at high sediment concentrations. The inlet of the sampler in the pipe above the tub has an in-line sand filter that isolates the sand that makes it to the tub sampler.



Figure 6.9 Turbidity sampling locations below the trough and ditch in the upper photo and at the Tub in the lower photo.

Suspended sediment concentration and flow were manually measured periodically at all 4 sample locations in addition to turbidity on January 18, 2024. The average suspended sediment concentration coming off the road at the trough was 8,613 mg/l and the lateral SSC was 4,761 mg/l. The ditch flow had an average SSC of 163 mg/l and the combined flow at the tub had an SSC of 1,044 mg/l (see Figure 6.10).

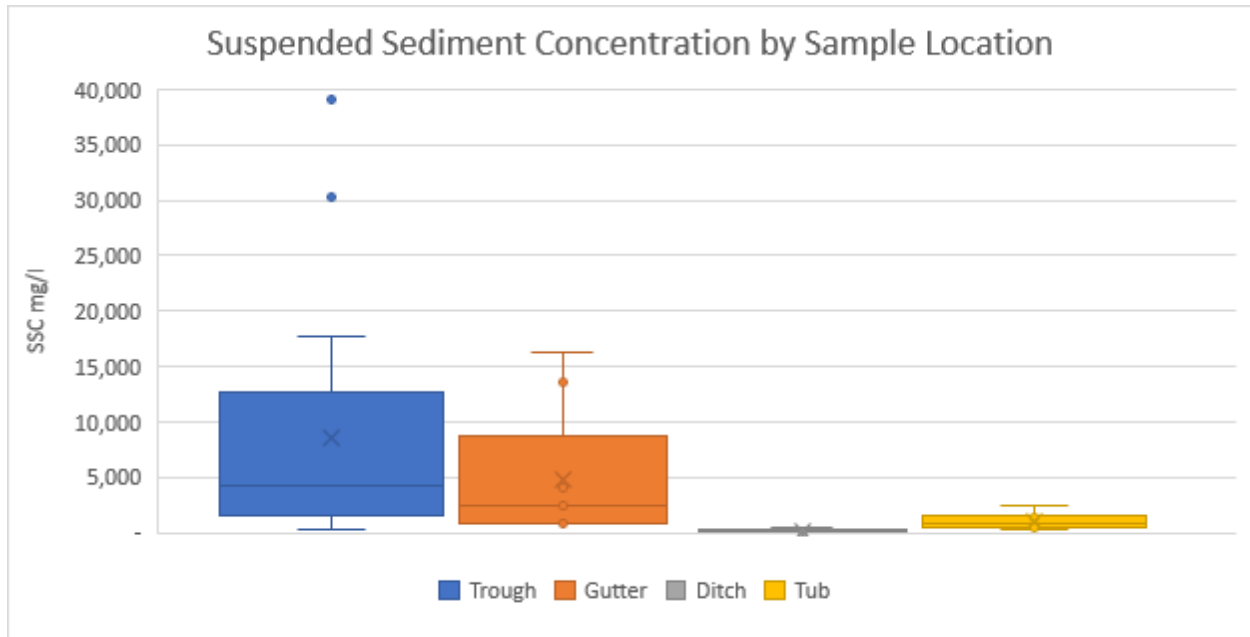


Figure 6.10 Suspended sediment concentrations from sample locations at Mel 14 on Jan 18, 2024, following truck traffic.

The water samples that were taken to determine SSC were used to test the 4 different ClariVue 10 sensors in the lab. It was determined that the sensors that had been sampling the Lateral gutter, and the Trough were reading in an unstable manner and were returned to the manufacturer for service and repair. These sensors were positioned at the locations with the highest sediment concentrations following the truck passes. Some of the record peaks may be out of the range of any turbidity sensor due to the optical opacity of the thick suspension of fine sediment directly washing off the road.

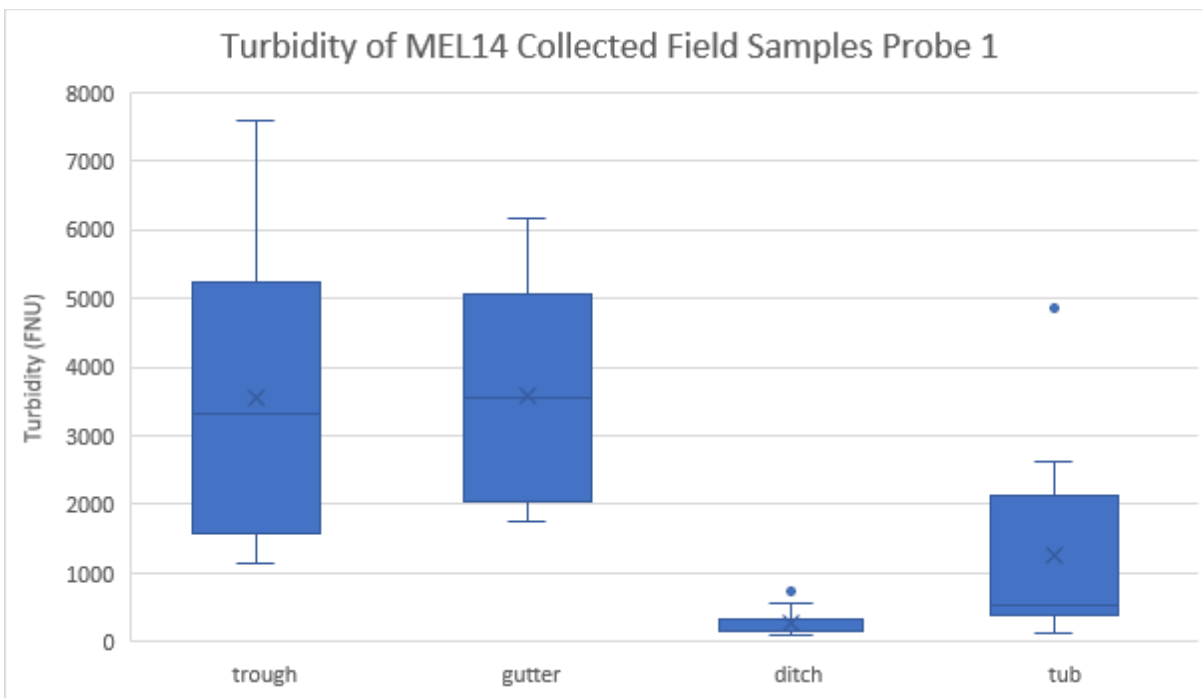


Figure 6.11 Turbidity of samples collected for SSC from the Trough, Gutter, Ditch and Tub on 1/18/24 using a reliable ClariVue 10 in the lab. The calibrated range is 0-4,000 FNU.

Rainfall and runoff conditions were ideal on January 18, 2024, with consistent rainfall of 2-5 mm/hr and plot runoff measured at the tub of 10-17 liters per minute.

Truck passes began at 14:15 and again at 15:23. The data for SSC, discharge, and rainfall were collected successfully. The turbidity data were reasonable for the ditch (C) and tub (D) which had mean values of 272 FNU and 1,257 FNU respectively (Figure 6.11). The turbidity data for the trough (A) and the gutter (B) were not used as they were unsteady, and the sensors demonstrated problems when tested in the lab.

Because of the moderate runoff rate from the road, the sediment responded rapidly to the truck passes, reaching a peak concentration at the tub in about 19 minutes after the first truck pass and 23 minutes after the first truck pass on the second run. The turbidity declines substantially within 45 minutes (to about 900 FNU) but had not returned to baseline (400-600 FNU) in either case before the second run or before the experiment was ended (Figure 6.12).

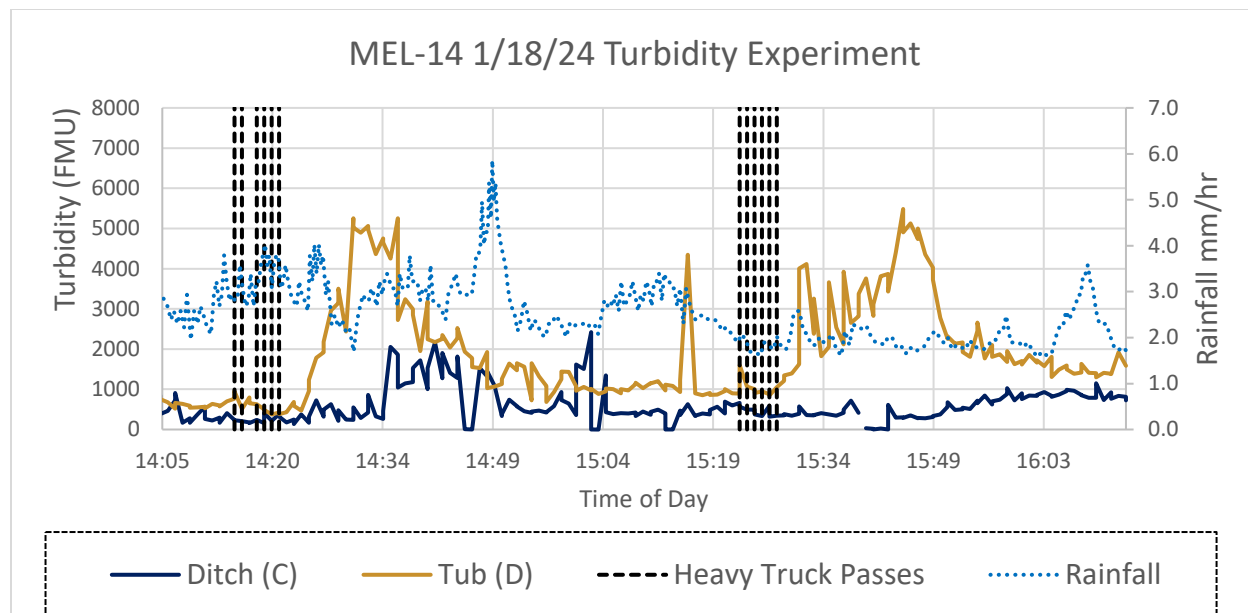


Figure 6.12 Turbidity results from the Ditch and Tub locations on January 18, 2024, with two periods of truck passes.

7 DITCH LINE HYDRAULICS EXPERIMENT

This experiment was carried out between May 2021 and October 2022. The results of the experiment were published in *Earth Surface Processes and Landforms* in early 2024. Please see Appendix B for the full paper.

8 MICRO-TOPOGRAPHY EXPERIMENT

This experiment was carried out between November 2020 and June 2022. The results of the experiment will be submitted as a paper for publication within the next month. Please see Appendix C for the full paper.

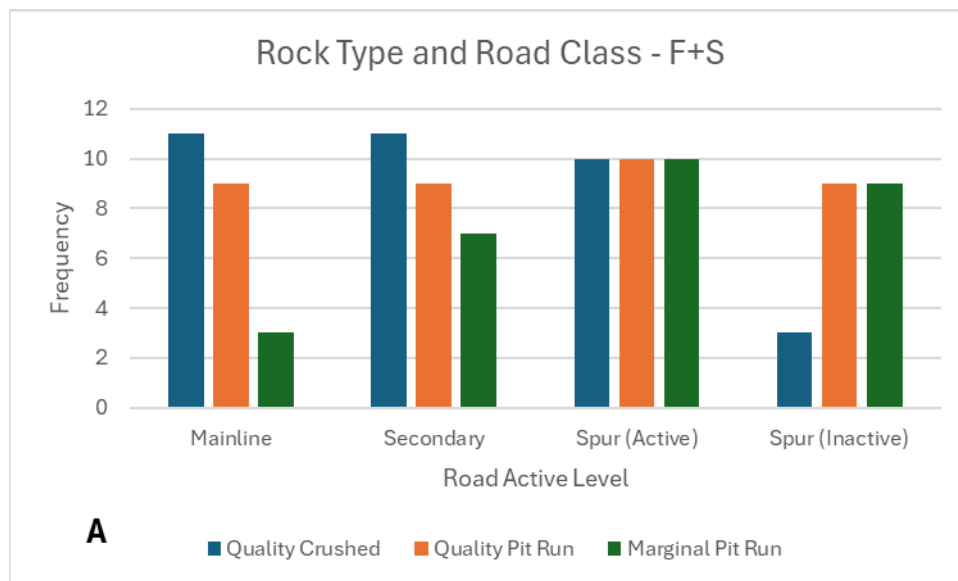
9 COST VS. MAINTENANCE SURVEY

In April-May, 2023, a Cost Vs. Maintenance Survey was distributed to private industrial landowners in Washington State by Project Team members through the Washington Forest Protection Association and to other, targeted entities that maintain forest roads. The survey was designed to determine which surfacing, tread, traffic management, and ditch line BMP are in common use and to be able to estimate the cost of implementation. Frequency of use, by road activity level, is asked in broad categories of Frequent, Sometimes and Never. Cost is not directly requested in the survey, as this may be somewhat proprietary, but equipment needs and time of installation/maintenance are asked for and can be used to estimate costs using federal prevailing rates. In addition to wanting this information in the broad context of the project, these results were needed to inform the ditch line BMP changeover for the Major Experiment. The survey is attached to this document (Appendix D).

Eleven responses were received—eight from industrial tree farms in Washington State (some landowners sent in multiple responses but from different tree farms), one from a State Lands region of Washington State, and two from the United States Forest Service in Idaho and Montana. The 2 responses from the United States Forest Service may represent roads in a drier climate with limited log haul, so the results may be less applicable to the haul routes of western Washington. Results presented below are preliminary, particularly as a few responses require follow-up questions, and we will re-solicit from a couple of key landowners who did not submit responses. However, the answers that were received were sufficient to assist in the identification and implementation of elevated ditch line BMP in the Major Experiment.

9.1.1 Surfacing

Asphalt and surface binding agents are rarely to never used on forest roads; the occasional applications are for very site-specific and reason-specific applications (and the exception is that USFS in Idaho frequently uses binding agents on heavier haul roads). Surfacing of quality crushed road, quality pit run, and marginal pit run are in common use, and there is a predictable trend between rock quality and traffic levels such that better rock is placed on higher traffic roads (Figure 9.1). In the “other” category, a couple of landowners noted that “round rock” is also used—drain style rock from glacial outwash or river terrace pits.



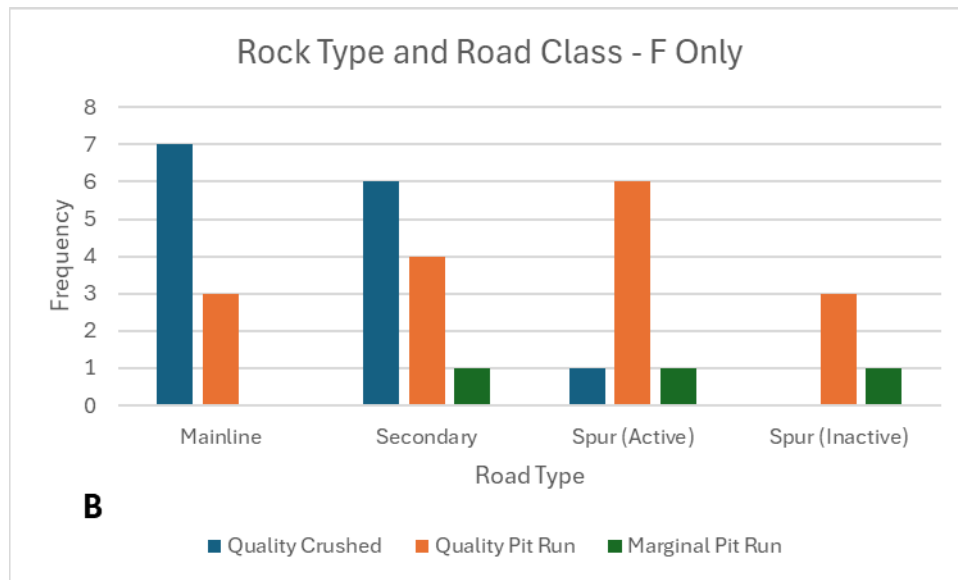


Figure 9.1 Number of responders out of 11 for rock quality by road traffic level – A) frequent and sometimes used; B) frequent use only.

9.1.2 Tread BMP

Grading is done frequently or sometimes on all active roads. Landowners picked “weekly,” “biweekly,” and “monthly” when asked how often grading occurs during heavy haul, but many picked “other” or additionally picked “other” and wrote that they graded when necessary. Rolling dips are frequently used by the USFS in Idaho and Montana on active roads, but on forest lands in Washington State they are only used sometimes by some landowners, and then on roads with lower levels of traffic. Flappers (i.e., waterbars constructed of conveyor belt) are used by some landowners, particularly on mainline roads with less use on lower traffic roads; estimates for installation vary from 1 to 3 hours, and there is some agreement that they require maintenance once or twice a year. Geotechnical fabric is in occasional use on all road traffic levels by most landowners, with 2 hours being the common estimate of installation time; it might be worthwhile during a phone follow up to ask why it is being used. Two “other” tread BMP described are: 1) Concrete Open Top Culverts (COTS) which are being implemented on a trial basis in Montana to replace flappers—photos and specifications were provided with the survey; however, these seem impractical for the mainline traffic levels on industrial timberland. And 2) the filling of potholes with clean, crushed rock as soon as they develop to avoid growth and splash—this tread BMP has been called “pot holing.”

9.1.3 Traffic Management

The survey results suggest that reduction of tire pressure is not in use in Washington State; however, one of the landowners failing to respond is known to use this BMP. Most landowners shut-down haul during wet weather “sometimes” or “frequently.”

9.1.4 Ditch Line BMP

Table 9.1 displays the survey answers from the eleven responders for each ditch line BMP for each of the four road types – in each cell, the first number is the number of responders answering “frequent” or “sometimes” (F+S) and the second number is only those responders answering “frequent.” The rows are roughly organized in descending order of use. Sediment traps are the most common BMP, utilized by

most landowners on all road types, and the only BMP to be frequently used (winner, winner, chicken dinner!); with fairly tight installation times ranging from 10 to 30 minutes. All other ditch line BMP in the survey are used by many landowners, but generally this use is preferential to higher traffic roads and not frequent. Silt fence use ranges from “frequent” to “never,” and is more commonly used parallel to the stream crossing (i.e., slowing the ditch line water down) than it is across the stream crossing (i.e., to prevent tread water to flow off a fillslope into a stream). There is some agreement that silt fencing typically takes 1 to 2 hours to install. Rock check dams are sometimes used by most landowners, again across all traffic levels; time to install varied from 10 minutes to 4 hours, which might reflect people answering for one dam or for a length of road with several dams (follow-up opportunity). Both hay/straw bales and scattered material are in common use in Washington State on industrial timberland, for all traffic levels and with a range of installation times from 20 to 60 minutes. Bales are usually maintained annually (perhaps reflecting that they are being used as an elevated ditch line BMP), while scattered material is not maintained (perhaps reflecting that it is used as cover after work is accomplished). Wattles are sometimes used by most landowners, with use more common on roads of higher traffic levels; installation times vary from 10 to 60 minutes, probably for the same reason hypothesized above for rock check dams (follow-up opportunity). Grass/hydro seeding is sometimes used by most landowners, across all road traffic levels. Rocking the ditch is sometimes used by some landowners, again across all traffic levels (this is more common than we would have predicted—see the ditch line hydraulics paper in Appendix B to see the effectiveness of this BMP). And one landowner described double ditching under “other” - the practice of piping ditch line water across a stream crossing, to reach a better cross-drain location.

Table 9.1 Number of responders out of 11 for each ditch line BMP by road traffic level. The first number in each cell is F+S (frequent plus sometimes responses). The second number is F only.

	Mainline	Secondary	Spur (Active)	Spur (Inactive)
Sediment Traps	11 / 9	11 / 9	11 / 9	10 / 5
Silt Fence Parallel	11 / 3	10 / 2	7 / 1	4 / 0
Rock Check Dams	9 / 2	9 / 0	8 / 0	6 / 0
Hay/Straw Bundled	10 / 1	9 / 0	9 / 0	7 / 0
Hay/Straw Scattered	8 / 1	9 / 0	9 / 0	8 / 0
Wattles	8 / 0	7 / 0	6 / 0	3 / 0
Settling Pond	8 / 3	7 / 3	6 / 2	6 / 2
Grass/Hydro	7 / 1	6 / 1	6 / 1	5 / 1
Silt Fence Across	6 / 3	6 / 2	6 / 2	5 / 0
Rocking the Ditch	6 / 0	5 / 0	4 / 0	4 / 0

We chose sediment traps, wattles, and rocking the ditch as the elevated ditch line BMP studied in the Ditch Line Hydraulic Experiment, the Sediment Trap Efficiency Experiment, and the Major Experiment. These foci reflect that sediment traps are in very common use, and that wattles and rocking the ditch are used by approximately half of the landowners. Hay/straw bales, in common use, are quite similar in function to wattles; we have not separately studied them. Scattered hay/straw is used to address short-term erosion after work but does not appear to be a haul-related BMP. Although in fairly common use,

we have not studied silt fencing effectiveness, as others have tested them and found them sensitive to site conditions and installation methods (Schussler et al., 2021).

10 GRAIP/WARSEM

This experiment is expected to be carried out between November 2024 and May 2025. The GRAIP/WARSEM Parameterization Experiment will evaluate the degree to which the distance a forest road lies from a stream affects the probability of sediment from a drainage structure reaching the stream. Several factors in addition to absolute distance may influence the results and will be evaluated as covariates. The length of road draining to the drainage structure and total drainage area of that road segment are closely related and have been shown to strongly influence the probability of delivery. For example, related survey work on stream connectivity shows an effect of the contributing length of road on the probability of delivery at different distances for a large Idaho dataset (Luce et al., 2014). Other factors, such as hillslope gradient, did not strongly influence the results (Luce et al., 2014), but greater amounts of woody debris on the forest floor and better soil development, particularly greater accumulation of the humus layer, may cause western Washington results to be different from those observed in Idaho. In addition to contributing road length, contributing drainage area, and hillslope gradient below the drainage structure, ditch line gradient and lithology will be evaluated for potential influence. Emphasis will be placed on data collection along HTNS roads. These will be evaluated as a subset because large volumes of fine sediment produced by high-traffic road segments may travel farther than is generally observed in other circumstances. This is partially because high-traffic roads are wider and, for a given length of road, contribute more water to a cross-drain culvert. Delivery distances are shorter for smaller contributing road lengths and widths, which is relevant to the use of crowning or outslipping, to reduce the area of roads contributing to stream crossings. These results will help landowners identify those segments of HTNS roads that cannot be disconnected from the channel network with just the installation of drainage structures (i.e., usually cross-drain culverts in western Washington) and focus the use of tread and ditch line BMP to those road segments with the most critical need. The data will also inform future landscape-scale modeling efforts.

For this analysis, we will use a sediment delivery survey developed in a manner that facilitates comparisons with pre-existing datasets such as in Luce et al. (2014) which was collected using the GRAIP methodology (Black et al., 2012). It may also be possible to augment our dataset with the Washington Road Sub-Basin Scale Effectiveness Monitoring First Sampling Event (2006-2008) dataset (Dubé et al., 2010) which was collected using the WARSEM methodology (Dubé et al., 2004). The process of preparing a sampling protocol that integrates both GRAIP and WARSEM sediment delivery sampling methodologies is currently underway.

Crews will travel down a road, measuring the spacing and nature of road drainage features and follow the outlets of road drainage to see where evidence of sediment transport, such as scouring of the hillslope or deposition of fresh sediment, stops and whether it reaches the stream. They will measure hillslope and ditch line gradient, and map three points—top of the road segment, drainage feature, and last sediment/scour observed. Lithology and contributing drainage area will be GIS evaluations and will not be field measured.

11 REFERENCES

- Alvis, A. D., Luce, C. H., & Istanbuluoglu, E. (2023). How does traffic affect erosion of unpaved forest roads? *Environmental Reviews*, 31(1), 182–194. <https://doi.org/10.1139/er-2022-0032>
- Alvis, A. D., Luce, C. H., Istanbuluoglu, E., Black, T., Dieu, J., & Black, J. (2024). Using additional roughness to characterize erosion control treatment effectiveness in roadside ditch lines. *Earth Surface Processes and Landforms*, 49(4), 1255–1272. <https://doi.org/10.1002/esp.5763>
- Barnhart, K. R., Hutton, E. W. H., Tucker, G. E., Gasparini, N. M., Istanbuluoglu, E., Hobbey, D. E. J., et al. (2020). Short communication: Landlab v2.0: a software package for Earth surface dynamics. *Earth Surface Dynamics*, 8(2), 379–397. <https://doi.org/10.5194/esurf-8-379-2020>
- Black, T. A., & Luce, C. H. (2013). *Measuring water and sediment discharge from a road plot with a settling basin and tipping bucket* (No. RMRS-GTR-287) (p.44). Ft. Collins, CO: U.S. Department of Agriculture, Forest Service, Rocky Mountain Research Station. <https://doi.org/10.2737/RMRS-GTR-287>
- Black, T. A., Cissel, R. M., & Luce, C. H. (2012). *The Geomorphic Road Analysis and Inventory Package (GRAIP) Volume 1: Data Collection Method* (No. RMRS-GTR-280) (p.110). Fort Collins, CO: U.S. Department of Agriculture, Forest Service, Rocky Mountain Research Station. <https://doi.org/10.2737/RMRS-GTR-280>
- CMER. (2017). *Empirical and Modeled Evaluation of Forest Road BMP Effectiveness in Western Washington* (Study Design).
- Dubé, K., Megahan, W., & McCalmon, M. (2004). *Washington Road Surface Erosion Model*. Olympia, Washington, USA: Washington Department of Natural Resources.
- Dubé, K., Shelly, A., Black, J., & Kuzis, K. (2010). *Washington road sub-basin scale effectiveness monitoring first sampling event (2006–2008) report*. Olympia, Washington, USA: Washington Department of Natural Resources.
- Foltz, R. B., & Truebe, M. A. (2003). Locally available aggregate and sediment production. *Transportation Research Record*, 1819(1), 185–193.
- Govers, G. (1992). Evaluation of transporting capacity formulae for overland flow. In *Overland Flow: Hydraulics and Erosion Mechanics* (pp. 243–273). New York: Chapman and Hall.
- Hirano, M. (1971). RIVER-BED DEGRADATION WITH ARMORING. *Proceedings of the Japan Society of Civil Engineers*, 1971(195), 55–65. https://doi.org/10.2208/jscej1969.1971.195_55
- Hobbey, D. E. J., Adams, J. M., Nudurupati, S. S., Hutton, E. W. H., Gasparini, N. M., Istanbuluoglu, E., & Tucker, G. E. (2017). Creative computing with Landlab: an open-source toolkit for building,

- coupling, and exploring two-dimensional numerical models of Earth-surface dynamics. *Earth Surface Dynamics*, 5(1), 21–46. <https://doi.org/10.5194/esurf-5-21-2017>
- Luce, C. H., & Black, T. A. (2001). Effects of traffic and ditch maintenance on forest road sediment production. In *Proceedings of the Seventh Federal Interagency Sedimentation Conference* (pp. V67–V74). Reno, Nevada.
- Luce, C. H., Black, T. A., Cissel, R., & Nelson, N. (2014, October). *Assessing Controls on Sediment Delivery from Forest Roads*. Salt Lake City, UT.
- Martin, D. (2009). *Forest Road Runoff Disconnection Survey of Private Timberlands in Washington*. 724 Columbia Street NW, Suite 250, Olympia, WA 98501: Washington Forest Protection Association.
- Minor, C. E. (1960). Degradation of mineral aggregates. In *Symposium on Road and Paving Materials* (pp. 109–121). San Francisco, CA: American Society for Testing Materials. <https://doi.org/10.1520/STP38775S>
- PRISM Climate Group. (2023). Mean annual precipitation time series [Data set]. Oregon State University. Retrieved from <https://prism.oregonstate.edu>
- Reid, L. M., & Dunne, T. (1984). Sediment production from forest road surfaces. *Water Resources Research*, 20(11), 1753–1761. <https://doi.org/10.1029/WR020i011p01753>
- Rhee, H., Fridley, J., & Page-Dumroese, D. (2018). Traffic-Induced Changes and Processes in Forest Road Aggregate Particle-Size Distributions. *Forests*, 9(4), 181. <https://doi.org/10.3390/f9040181>
- Schussler, J. C., Kazaz, B., Perez, M. A., Blake Whitman, J., & Cetin, B. (2021). Field Evaluation of Wattle and Silt Fence Ditch Checks. *Transportation Research Record: Journal of the Transportation Research Board*, 2675(6), 281–293. <https://doi.org/10.1177/0361198121992073>
- Suttle, K. B., Power, M. E., Levine, J. M., & McNeely, C. (2004). HOW FINE SEDIMENT IN RIVERBEDS IMPAIRS GROWTH AND SURVIVAL OF JUVENILE SALMONIDS. *Ecological Applications*, 14(4), 969–974. <https://doi.org/10.1890/03-5190>
- Van Meerveld, H. J., Baird, E. J., & Floyd, W. C. (2014). Controls on sediment production from an unpaved resource road in a Pacific maritime watershed. *Water Resources Research*, 50(6), 4803–4820. <https://doi.org/10.1002/2013WR014605>
- Ziegler, A. D., Sutherland, R. A., & Giambelluca, T. W. (2001). Interstorm surface preparation and sediment detachment by vehicle traffic on unpaved mountain roads. *Earth Surface Processes and Landforms*, 26(3), 235–250.

12 APPENDICES

Appendix A. Synthesis paper

Appendix B. Ditch Line Hydraulics paper

Appendix C. Micro-Topography draft paper

Appendix D. Cost Vs. Maintenance survey

Appendix E. Defining Watershed Hydraulic Attributes for DNR High Traffic Near Stream Roads

How does traffic affect erosion of unpaved forest roads?

Amanda D. Alvis^a, Charles H. Luce^b, and Erkan Istanbuluoglu^a

^aDepartment of Civil and Environmental Engineering, University of Washington, Seattle, WA, USA; ^bRocky Mountain Research Station, USDA Forest Service, Boise, ID, USA

Corresponding author: Amanda D. Alvis (email: amanaste@uw.edu)

Abstract

The relationship between traffic and forest road erosion has been studied for decades, and the answer to the question “what happens when traffic is present on unpaved forest roads?” is simple: erosion increases. However, the answer to the question “why does it increase?” is complex and requires us to consider forest road erosion through an integrated lens. Fully understanding how traffic affects forest road erosion will allow us to control forest road erosion effectively. In this synthesis, we look at forest road erosion literature and focus the discussion on the interactions between traffic and erosion. Specifically, we explore four main hypotheses that have been proposed to explain how traffic affects erosion. These hypotheses are discussed in detail, including what data and information are required to evaluate them. In addition to the specific traffic-erosion interactions, we review important factors that interact with traffic to enhance erosion. Finally, we propose a framework that describes forest road erosion as a combination of all limiting factors. This framework can help guide future data collection needs, allow us to form a more holistic understanding of forest road erosion, and ultimately improve predictions of erosion from forest roads.

Key words: Resource roads, erosion, traffic, sediment, rut, runoff

1. Introduction

Erosion from forest roads is a long-standing environmental problem (e.g., Trimble and Sartz 1957; Trimble 1959; Packer 1967; Kochenderfer 1970; Megahan and Kidd 1972; Bilby, Sullivan and Duncan 1989; Lane and Sheridan 2002; Sheridan and Noske 2007), with ongoing contention over how best to prevent road-derived sediments from entering streams (e.g., Boston 2012; Aust, Bolding and Barrett 2015; Brown et al. 2015). Forest streams are generally cleaner than their counterparts in urban, suburban, and agricultural settings, making the impacts of turbid water from forest roads readily apparent. The set of standard best practices for managing sediment from roads includes protecting ditches with vegetation, placing sturdier rock on road surfaces, limiting traffic, and placing roads as far from streams as practical. Even so, locations exist where roads must cross or are located close to streams, and some of these near-stream roads carry substantial traffic. In these locations, options for erosion control are more limited, resulting in impacts that, from a practical standpoint, seem unavoidable. However, where protected fish species are affected, this unavoidability is better framed as an issue of economics and tradeoffs.

Erosion control solutions are commonly presented as two potential options: paving the road surface and limiting traffic on the road. These solutions have been applied to varying locations where the value of both timber and fisheries are high (e.g., Cederholm and Reid 1987). However, these two practices are expensive for forest land managers (e.g., Edwards, Wood

and Quinlivan 2016). Framing the management choices as stopping traffic or paving roads is too coarse, and more gradations in treatment choices need to be articulated. Certainly, we could express degrees of traffic limitation, such as an acceptable number of loaded trucks per unit time (e.g., Croke and Hairsine 2006) or condition traffic on other factors, such as precipitation (e.g., Dent, Mills and Robben 2003). Similarly, engineering approaches like reduced tire pressure (e.g., Foltz 1994; Foltz and Elliot 1997), geotextiles placed in the subgrade (e.g., Visser, Brown and Tinnelly 2017), and harder rock (e.g., De Witt, Boston and Leshchinsky 2020) have all been shown to help reduce sediment production and erosion on forest roads.

Unfortunately, the substantial literature covering the interactions between traffic and erosion lacks a holistic treatment of the various ways in which traffic influences sediment and runoff production from forest roads. Research does indicate that the presence of traffic increases forest road erosion (e.g., Reid and Dunne 1984; Luce and Black 2001; Ziegler, Sutherland and Giambelluca 2001; Sheridan et al. 2006; Sugden and Woods 2007) though in a broad sense and with little quantitative accounting for context. Multiple hypotheses have been put forth regarding what traffic-induced processes are driving sediment production and erosion, including pumping, scattering, rutting, and crushing. However, these hypotheses are typically invoked—often individually—as potential explanations of erosion (e.g., Reid and Dunne 1984; Swift, Jr. 1984; Foltz, Evans and Truebe 2000), sometimes without a

detailed mechanism being defined or providing quantitative expectations of effect. Some authors have gone further than others, but research is still missing how these mechanisms interact with one another and how they are affected by other treatments for sediment reduction. If we want to address sediment production from high traffic roads in a more fine-tuned and efficient way, it is necessary to advance our understanding of these different effects on roads. The hypotheses that have been put forth require more specific definition, particularly so that quantitative models can be constructed to guide the data collection needed to test the models and hypotheses.

In this synthesis, we focus on the relationship between traffic and erosion by examining the current state of the literature and including a discussion of hypotheses and knowledge gaps. Additionally, we present a potential contextual framing for the erosion process with respect to traffic and other factors and discuss how we can further our understanding of erosion on unpaved forest roads. We begin by focusing on the specific ways in which traffic affects erosion from roads; we then discuss the ways in which erosion is enhanced by the interactions between traffic and contextual climate, topographic, and road characteristics; and we complete the discussion with a conceptualization that generalizes forest road erosion in terms of sediment supply and transport energy to quantify contextual interactions and expectations for treatments.

2. Traffic-induced, erosion-enhancing processes

Traffic is one of the most frequently cited drivers of erosion on unpaved forest roads. Disturbance of the road surface by heavy vehicles—leading to an increase in fine sediment supply and changes in the energy available for sediment transport—has been observed in many studies (e.g., Reid 1981; Swift, Jr. 1984; Bilby, Sullivan and Duncan 1989; Coker, Fahey and Payne 1993; Luce and Black 2001; MacDonald, Sampson and Anderson 2001; Ziegler, Sutherland and Giambelluca 2001; Van Meerveld, Baird and Floyd 2014; Reid, Hassan and Floyd 2016). These studies investigate the effects of traffic on erosion from a broad perspective, generally noting that erosion is highly correlated with the presence of traffic. This general understanding has motivated the development of hypotheses regarding the mechanics of traffic-induced erosion processes.

Observations and anecdotal evidence of the influence of traffic on erosion are multitudinous, but more information is needed to understand how and why traffic has such an influence, particularly if erosion caused by traffic is to be accurately represented in a model. Researchers have hypothesized multiple traffic-induced erosion processes: (1) crushing, (2) pumping, (3) scattering, and (4) flow rerouting. However, available data sets to evaluate these hypotheses are limited. In the next few sections, we address these processes in more depth and present a discussion of what we know and what we have yet to learn.

2.1. Crushing

Crushing occurs when a heavy vehicle, such as a loaded logging truck, drives over an aggregate-covered road surface, and the aggregate breaks down. The downward force exerted by the vehicle onto a brittle material causes breakage, increasing the supply of fine sediment available for transport (Fig. 1A). Shifting of grains against one another under heavy loading causes chipping and abrasion of particles, which we lump conceptually in the term crushing. Crushing is posited to be influenced by aggregate quality, as well as frequency and type of traffic. Because of its relation to other factors and plentiful anecdotal evidence (Fig. 1B), crushing is one of the most cited traffic-induced erosion mechanisms in the literature (e.g., Reid and Dunne 1984; Foltz and Truebe 1995, 2003; Luce and Black 2001; Ziegler, Sutherland and Giambelluca 2001; Dawson and Kolisoja 2006; Dubé et al. 2010; Toman and Skaugset 2011; Kemp, Leshchinsky and Boston 2016; Rhee, Fridley and Page-Dumroese 2018).

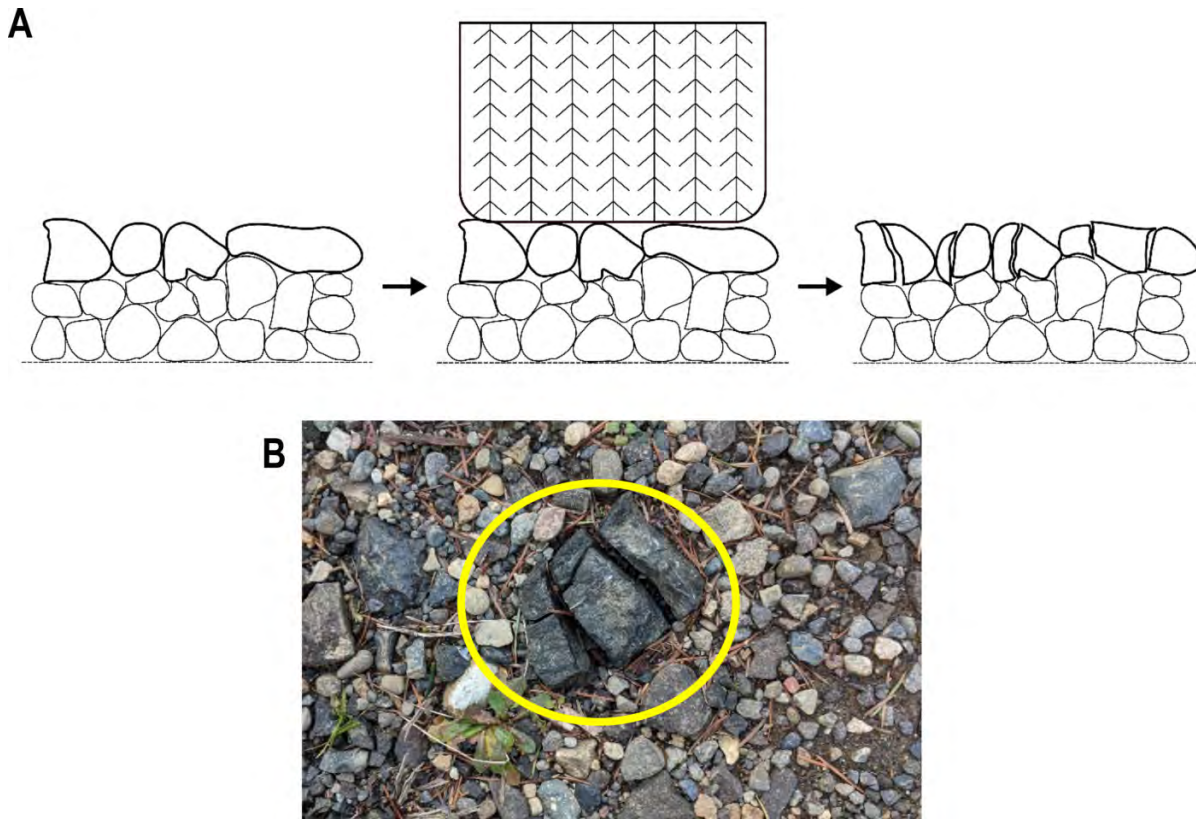
Crushing is so closely connected with other factors affecting erosion that few data regarding the process of crushing—why and how it occurs—have been collected. Most field studies related to crushing focus on aggregate strength rather than the role that traffic plays with respect to aggregate. However, in a recent paper, De Witt et al. (2020) describe a field experiment in which they isolated different qualities of road surface aggregate in cylindrical geotextile bags to observe degradation after traffic had driven over the segment. The cylindrical geotextile parcels of aggregate were placed within the road surface and were subject to a different number of truck passes. The authors looked at the aggregate after 500, 950, and 1500 passes of a loaded dump truck and found that most of the degradation occurred within the first 500 truck passes for all aggregate qualities.

The results of this study confirm that crushing relates to traffic volume and frequency, but the observation resolution is still too low to capture the nonlinearities in the crushing rate. The authors recommend a future experiment with earlier and more frequent observations (i.e., check the aggregates after 100, 250, and 350 truck passes) to capture the initial aggregate degradation rate and how it changes. Such an understanding would allow us to represent this diminishing rate process more accurately in a model.

2.2. Pumping

Pumping is the process by which fine sediment is forced upwards toward the surface of the road. When a vehicle passes over a gravel road surface, larger sediment is pushed down, which, in turn, displaces fine sediment, moving it upwards (Fig. 2A). As this process is repeated, fine sediment makes its way to the surface of the road where it is readily available for sediment transport, thus increasing the supply. Pumping has been suggested as a traffic-induced erosion process in many studies (e.g., Reid 1981; Swift, Jr. 1984; Luce and Black 2001; Ziegler, Sutherland and Giambelluca 2001; Foltz and Truebe 2003; Ramos-Scharrón and Macdonald 2005; Dawson and Kolisoja 2006) and anecdotal evidence is abundant (Fig. 2B).

Fig. 1. (A) Schematic of the crushing process. On a typical road surface aggregate (left) when vehicles drive over the road (center), the larger sediment breaks down into finer sediment (right). Image not to scale. (B) Image of forest road with evidence of crushing (circled in yellow).



Because pumping is a difficult process to isolate, only a few studies investigated the process further than qualitative field observations and conjecture. One study attempted to investigate pumping by examining the utility of three different treatments to reduce fine sediment production, which was hypothesized to be caused by pumping at the surfacing-subgrade interface (Toman and Skaugset 2011). The three different treatments included: (1) placing geotextile between the subgrade and road surfacing; (2) increasing the depth of the road surfacing; and (3) installing a geocell pavement structure. All three treatments were meant to hinder the pumping process at the surfacing-subgrade interface and were compared to control segments.

This study was carried out on recently built spur roads designed for short-term use in three locations. Measurements of sediment runoff were made over a single winter haul season. The authors concluded that pumping was not a significant source of fine material on the roads they tested based on the fact that sediment production did not differ significantly between treated and control road segments. Rather, they concluded that the fine material was either already present in the new road surface aggregate or was generated by crushing of the surface aggregate.

Extrapolation of these findings to more established roads may not be applicable because the study focused on short-term use roads that were recently built and were monitored for only one winter season. Recently built roads have a set-

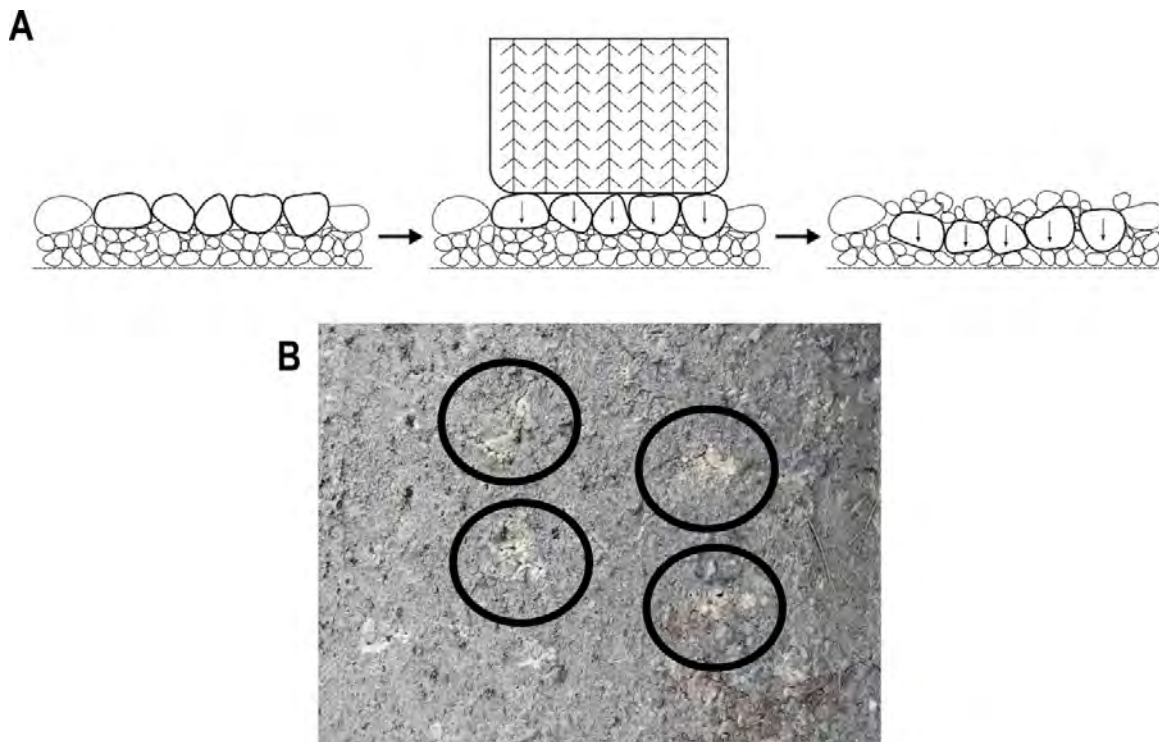
ling period in which existing fine sediment is flushed away, armoring the road surface (Megahan 1974). This armoring phenomenon is also observed in roads that have been disturbed by other means, such as road maintenance (Luce and Black 2001). As such, the study's findings—that the road surface aggregate was the main source of fine material—may well be a feature of the newly-built road's settling period.

Experimental evidence for pumping has been demonstrated on more established unpaved forest roads. Rhee et al. (2018) carried out a study in Clearwater National Forest, Idaho in which they inferred different processes (i.e., crushing, pumping, and scattering) from changes in the particle size distribution of different vertical layers of the road after varying amounts of traffic (i.e., none, light, and heavy). Coarsening of the middle and bottom layers of these roads provides evidence of pumping, while fining provides evidence of crushing. Significant evidence of pumping (i.e., a coarsened particle size distribution) was found in the bottom layer of the heavy traffic road. Further investigation is warranted to help us understand the rate at which pumping occurs under different conditions.

2.3. Scattering

Road surface armoring occurs when readily available fine sediment is flushed away, leaving only larger sediment that forms a protective layer (Megahan 1974). Scattering is the displacement of the larger sediments that have armored the

Fig. 2. (A) Schematic of the pumping process. Larger sediment over finer sediment (left) gets pushed down due to the weight of the vehicles (center), which forces the finer sediment upwards (right). Image not to scale. (B) Image of forest road with evidence of pumping, light colored deposits of fine sediments around edges of holes (circled in black).



road surface and is caused by a disturbance thereof, such as traffic. Disturbing this armor layer exposes the fine sediments below, increasing the amount of sediment that is readily available for transport (Fig. 3).

This process has been both posited by researchers and observed in the field (e.g., Gnanendran and Beaulieu 1999; Foltz, Evans and Truebe 2000; Johnson 2003). Rhee et al. (2018) is one of the few studies that demonstrated the scattering process in a field study—referred to as “sweeping” in their study. They were able to infer that scattering was a dominant process on the shoulder section of the light traffic road in their study based on an increase in the particle size distribution (i.e., coarsening) at that location on the road. They note that evidence of scattering outside of the tire tracks (i.e., the coarsening of material outside the tire tracks) is more significant than evidence of scattering inside the tire tracks (i.e., the fining of material inside the tire tracks). This suggests that reduced erosion of medians and shoulders can be attributed to traffic but that increased erosion in tire tracks—caused by reduced rock cover therein—might be less clearly attributable to scattering of an armor layer by traffic.

Most other evidence of scattering is largely anecdotal (Fig. 4). More empirical evidence of scattering, as well as quantification thereof, is required if we are to separate the effects of different processes on the supply of fine sediments and to prescribe treatments to mitigate traffic effects. Quantification of scattering under different circumstances (e.g., weather, traffic speed, tire pressure) will help us further understand the process and potential solutions.

2.4. Flow rerouting

Flow rerouting occurs when traffic deforms a road surface and diverts the flow pathways. On a non-deformed road, runoff leaves the road as sheet flow and flows either into a roadside ditch line or onto the fill slope below the road. Traffic-induced road deformation, however, reroutes the flow and changes its hydraulics. One specific traffic-induced road surface deformation is the development of wheel ruts. Ruts are small channels—like rills on a hillslope—that form on an unpaved road surface due to traffic. The formation of ruts is posited to be caused by a combination of factors, including, but not limited to, scattering, compaction, and plastic deformation of the surface (Dawson 1997). Ruts tend to develop on either side of the crown of the road due to traffic straddling the center of the road (Fig. 5A).

Once a rut has formed, a feedback loop begins where concentrated water flows in the rut (Fig. 5B), leading to higher shear stress and, thus, more erosion and further channelization. This advective process would typically produce deep rill- or gully-like features in a strongly consolidated material, but on heavily trafficked roads, the traffic acts as a diffusive process due to its spatially stochastic nature, which allows the ruts to maintain a relatively hydraulically wide shape. Even with the diffusive nature of traffic, the ruts that develop still have a greater capacity and competence to move sediment. This feedback loop of a dominant advective process and an ancillary diffusive process causes the hydraulically wide ruts to persist and deepen unless an outside force, such as grading of the road surface, occurs.

Fig. 3. The road surface develops an armor layer of larger sediments (left). Once the road is disturbed by traffic (center), the armor layer is scattered, exposing fine sediments below (right). Image not to scale.

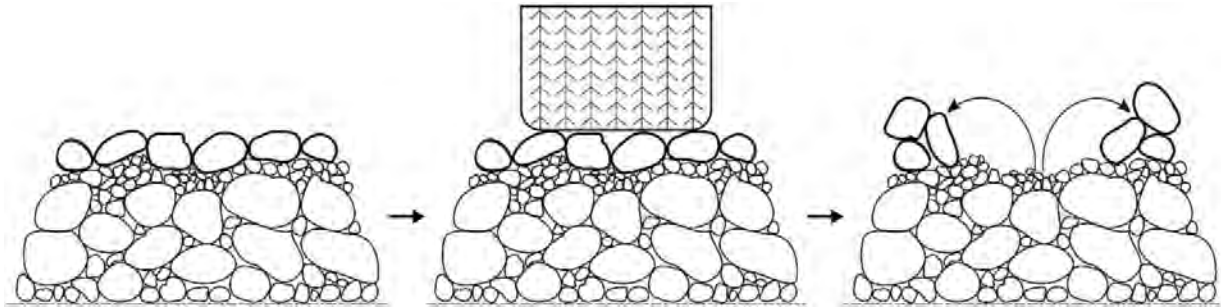


Fig. 4. Image of a forest road with evidence of scattering.



The presence of wheel ruts can cause an effective increase in the supply of fine sediment available to be transported and an effective increase in the energy available to transport the sediment. This traffic-driven change in topology tends to route flow along the road surface instead of to the sides, which has its own implications for erosion. Where wheel ruts prevent out-slope drainage, they directly add to potential delivery through concentration of flow along the road instead of diffuse flow. Where wheel ruts capture flow bound for a ditch, they prevent the potential utility of ditchline best management practices (BMPs)—such as grass lining, wattles, or rock lining—that could reduce transport capacity and potentially yield less erosion.

The presence of ruts and their influence on erosion are anecdotally abundant (Fig. 6). Additionally, empirical studies have found that roads with ruts can produce anywhere from 2 to 5 times more sediment than freshly graded roads (Foltz and Burroughs 1990). However, distributing the weight of logging vehicles over a larger surface area (i.e., reducing tire pressure) can decrease rut development and, thus, erosion (Bradley 1994; Foltz 1994). Additionally, consistent maintenance of roads can minimize the impacts of ruts (Sheridan et al. 2006). Though we have some knowledge about how to decrease rut development, additional information is needed about the formation of wheel ruts and other road surface

deformations. Learning the rate at which the road deforms and the conditions under which the road deforms can give us more insight into how to prevent these deformations.

3. Important contextual covariates for traffic effects

Other factors that influence the erosion of unpaved forest roads include rainfall intensity, road topography and topology, aggregate quality, and subgrade strength. These factors can fall into one of two categories: supply-related or energy-related. As discussed in Section 2, traffic is one of the most-cited and least-understood factors affecting the erosion of forest roads that is both supply- and energy-related. Many other processes and characteristics of roads that influence forest road erosion exist and can be either supply-related or energy-related, but these factors also affect how traffic affects erosion. These additional factors are largely related to traffic and each other, and as such, a discussion of all factors and their interaction is warranted to fully frame a discussion of unpaved forest road erosion and the dominant role of traffic therein.

3.1. Rainfall intensity

Rainfall initiates sediment transport on forest roads because it quickly turns into runoff due to low infiltration rates (e.g., Luce and Cundy 1994; Ziegler, Sutherland and Giambelluca 2000). The energy from the rain can contribute to displacement of sediment on the road through rain splash erosion as well. Thus, erosion caused by rainfall can be partitioned into two interconnected processes: hydraulic erosion and rain splash erosion.

Hydraulic erosion is largely energy-related and occurs due to Hortonian overland flow, which is frequently seen on unpaved forest roads. As these roads are used, they can become heavily compacted, allowing for less infiltration, and thus increasing the amount of overland flow (Ziegler and Giambelluca 1997). Hydraulic erosion is the agent through which sediment is transported away from the road prism. For areas in which sediment is readily available prior to a storm—through traffic, road maintenance, or other means—hydraulic erosion tends to be the dominant process at the beginning of a storm (Ziegler, Sutherland and Giambelluca 2000).

Fig. 5. (A) Image of a rutted forest road. (B) Image of a rutted forest road with water flowing in one of the ruts rather than off to the ditch line.

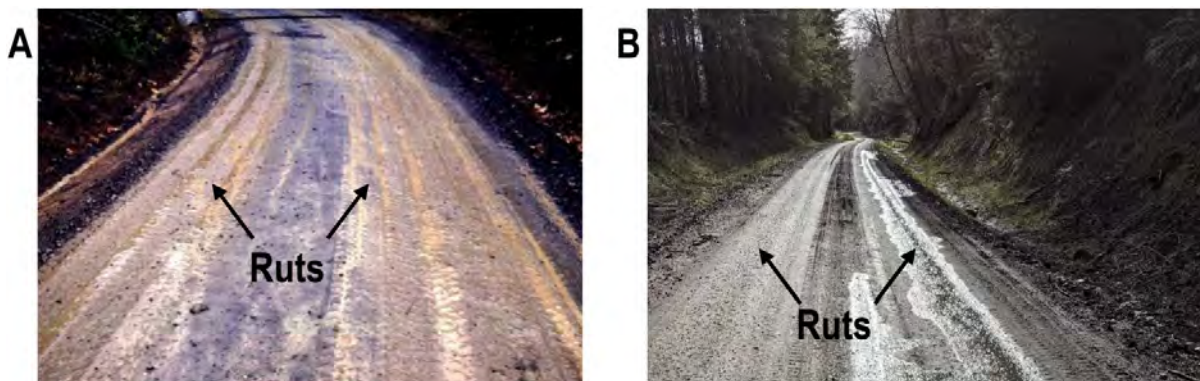
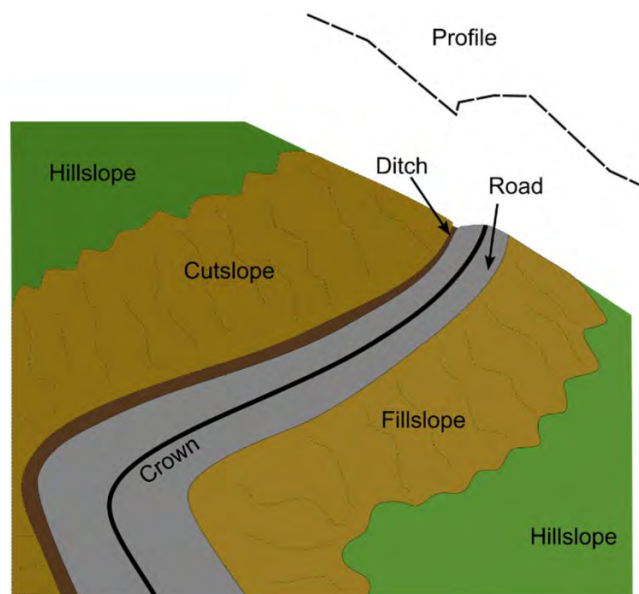


Fig. 6. Image of an extremely rutted road that receives little traffic.



Fig. 7. Schematic of a typical forest road and its surroundings.



Though hydraulic erosion is the transporter of sediment, rain splash erosion is another important supply-related piece in the rainfall-driven erosion process. Rain splash erosion increases the sediment supply that is readily available to be transported due to sediment displacement via rain drop impact, and once sediment is available for transport, hydraulic erosion occurs. For areas in which sediment is not immediately loose enough for overland flow transport alone (i.e., roads that have not been disturbed) rain splash erosion tends to dominate at the beginning of a storm (Ziegler, Sutherland and Giambelluca 2000).

3.2. Road topography and topology

Road topography refers to the geometry, slope, and other spatial characteristics of the road (Fig. 7). Topographical features such as road length and gradient are among the most

cited and studied influences on road surface erosion and largely impact erosion from an energy perspective. Road length and gradient are interconnected topographical features that represent the space over which erosion can occur. Assuming a constant road length, increasing the road gradient significantly increases erosion (Arnáez, Larrea and Ortigosa 2004). The interaction between road length and gradient leads to different effects on erosion. For example, increasing the length of a low gradient road has a smaller impact on erosion than increasing the length of a high gradient road. This relationship has been observed on established mainline logging roads (Luce and Black 1999) and less-used unpaved forest roads (Ramos-Scharrón and Macdonald 2005).

Related to topography is the topology of the road. We can think of topology as how water navigates the topography of the road (e.g., across the road vs. along the road). Some roads are out-sloped, where sheet flow that forms during rainfall events is directed primarily toward the fillslope, with some

along-road movement that depends on the road's slope. Similarly, some roads are in-sloped, where the water flows toward an inboard ditch that runs alongside the road until a drainage feature, like a culvert, relieves the ditch. For maintenance and traffic reasons, many roads are crowned, with half of the road draining to the fillslope and half to the inboard ditch. A point of special interest discussed in [Section 2.4](#) is that traffic can form wheel ruts that favor flow along the road surface before it reaches either the outer edge or the inboard ditch. Flow coming off out-sloped roads does not travel far because the road contributing area per unit discharge width is small. In contrast, runoff travelling along a road in a ditch or wheel rut becomes concentrated. When this concentrated runoff is discharged from a drainage feature, the likelihood of delivery to a stream increases ([Wemple, Jones and Grant 1996](#)).

In addition to water flow along and off of the road, cut-slopes along the side of the road and their spatial characteristics have also been shown to affect erosion. [Arnáez, Larrea and Ortigosa, \(2004\)](#) point to mass-wasting and freeze-thaw cycles as being important processes that provide transportable sediment from cut slopes. Additionally, an increase in the cut slope gradient causes erosion to increase (e.g., [Jordán and Martínez-Zavala 2008](#); [Jordán-López, Martínez-Zavala and Bellinfante 2009](#)). However, cutslope height is not necessarily a significant influence on sediment yield from roads in some areas, perhaps because of vertical heterogeneity in cutslope material ([Luce and Black 1999](#); [Megahan, Wilson and Monsen 2001](#)). Cutslopes are also often sources of water, either as direct overland flow during high rainfall intensity events or through interception of subsurface flow ([Ziegler, Sutherland and Giambelluca 2000](#); [Luce 2002](#); [Wemple and Jones 2003](#)). This water flows along the ditch when one is present, which lends itself to carrying sediment towards drainage features.

Some topographical and topological features of roads are commonly used to model road erosion because the features are easily obtained, either through field measurements or GIS software computations, and their relations to erosion are computationally simple. Modeling studies most often incorporate road drainage area and gradient, which are closely related to the concept of the slope-area product in geomorphology (e.g., [Istanbulluoglu et al. 2002, 2003](#)). Because these features are easily extracted using GIS technologies and are shown to be correlated with road erosion, they are the basis of multiple models that use empirically based equations to estimate such erosion (e.g., [Anderson and Macdonald 1998](#); [Akay et al. 2008](#)). Coefficients for these relationships can be empirically determined using existing data and, with additional experimentation, can be tied to climate, soil, and level of road disturbance.

3.3. Aggregate quality

Aggregate refers to the material used to surface an unpaved forest road (see surfacing in [Fig. 8A](#)). This surfacing aggregate provides a layer of protection to the native material underneath and decreases the amount of erosion that would otherwise be present without such protection (e.g., [Kochenderfer and Helvey 1987](#); [Brown, Aust and McGuire 2013](#)). Though the

presence of surfacing aggregate decreases erosion, aggregate quality must also be considered where traffic occurs. In general, aggregate quality is defined by how much the aggregate breaks down when it is exposed to different stressors, such as water, air, or traffic. The quality of surfacing aggregates is an important factor influencing erosion via the supply of fine sediment. Studies have observed that lower quality aggregate leads to more erosion because of its susceptibility to breakdown (e.g., [Foltz and Truebe 1995](#); [Foltz, Evans and Truebe 2000](#)).

What aggregate is used to surface a forest road depends on the landowner's main goal—cost reduction or erosion reduction—though that goal may change based on local availability of material. Generally, lower quality aggregates will be used to decrease cost, whereas higher quality aggregates will be used to reduce sediment loss. The quality of aggregate can be determined via either road managers' recommendations based on experience or physical tests of the aggregate. However, [Hanna and Boston \(2018\)](#) carried out a series of physical tests on aggregate obtained from quarries that road managers were also asked to classify as good or marginal sources of material. Results showed that road manager-recommended aggregates rarely met quality thresholds as established based on literature review, emphasizing the importance of testing aggregate prior to placing it on roads.

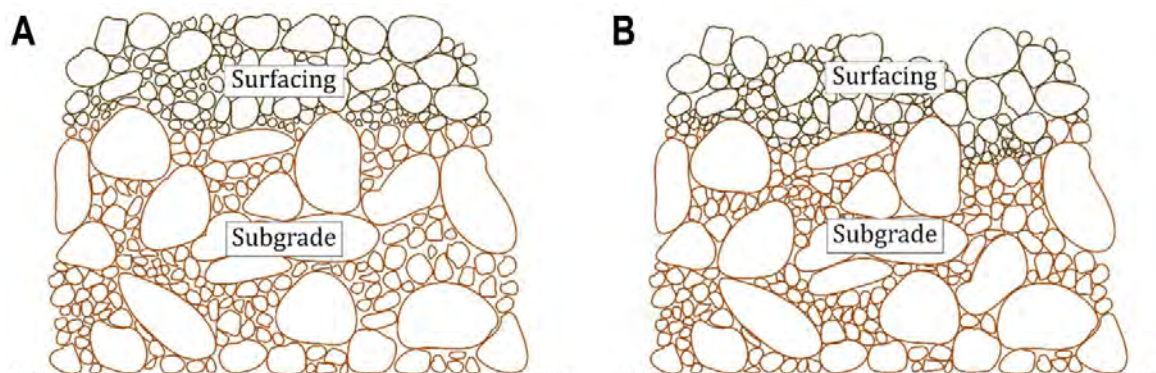
Two of the best tests to predict aggregate quality are the P20 portion of the Oregon air degradation test and the sand equivalent test ([Foltz and Truebe 2003](#)). The P20 portion of the Oregon air degradation test assigns an index indicating the breakage resistance of the aggregate when exposed to both water and a jet of air, and the sand equivalent test assigns an index to the aggregate based on the amount of fine material present. The sand equivalent test is more common as it is less time- and equipment-intensive and is therefore easier to carry out in the field.

3.4. Subgrade strength

The subgrade is the base upon which forest roads are built and is generally composed of native soil and rock (see subgrade in [Fig. 8A](#)). Multiple studies have looked at the importance of subgrade strength with respect to the durability of the road. Overall, these studies have found that deformation of the road surface—poor aggregate performance and quality aside—can occur when the integrity of the subgrade is compromised ([Fig. 8B](#)) and that road surface deformation is positively correlated with erosion. Therefore, lower subgrade strength can lead to increased erosion (e.g., [Bloser and Scheetz 2012](#)). As such, subgrade strength influences erosion from a supply perspective.

The strength of the subgrade is highly dependent on both the level of compaction during road construction and the durability of the materials therein. Different levels of compaction can lead to different levels of material breakage, with an optimal range of compaction existing to minimize material degradation (e.g., [Indraratna, Lackenby and Christie 2005](#); [Lackenby et al. 2007](#)). Additionally, proper compaction of the subgrade can optimize subgrade strength and

Fig. 8. (A) Schematic of a road cross section. The surfacing (top layer) is the aggregate used to cover the forest road, and the subgrade (bottom layer) is the packed excess fill material from road excavation as well as the native material. (B) Schematic of a road cross section where the integrity of the subgrade has been compromised, causing surfacing deformation. This example demonstrates a case where the subgrade was improperly compacted (i.e., weak) when the road was installed, and repeated outside stressors (traffic) caused further subgrade compaction that deformed the road surface. Images not to scale.



decrease the required amount of surface aggregate—and, therefore, cost—without compromising the integrity of the road (Boston, Pyles and Bord 2008). Easy field measurements of subgrade strength in tandem with a simple correlation model can aid in the proper compaction of the road subgrade (Pattison, Boston and Pyles 2010).

In addition to compaction of the subgrade, other reinforcements—such as geogrids or geotextiles—can be installed in or on the subgrade to increase road strength while decreasing the required amount of road surface aggregate (Giroud and Han 2004). Geotextiles are permeable textiles placed at the subgrade-aggregate interface to increase soil stability; geogrids are synthetic materials that reinforce the subgrade. Visser, Brown and Tinnelly (2017) looked at the cost-benefit of using geogrids with less road surface aggregate and found that doing so may be viable, specifically in cases which would otherwise require expensive or exorbitant amounts of road surface aggregate to maintain similar road strength.

4. A framework for future research

The role of traffic in forest road erosion is still poorly understood, which limits our ability to efficiently reduce its effects on erosion. The studies discussed in previous sections have given us tantalizing individual hints that further our understanding, but they are poorly integrated with one another and form a fragmented field of knowledge. As a result, we are left with many fundamental questions: How does the rate of traffic affect these erosion processes? Which of these traffic-induced erosion processes is the most dominant under different field and climate conditions? Why do some heavily trafficked roads accumulate fine sediment on the surface while others do not? What is the role of compaction in traffic-induced erosion processes? Is the pumping process solely a function of traffic, or are time and moisture variables to be considered as well? What other factors contribute to the importance of these traffic-induced erosion processes? In other

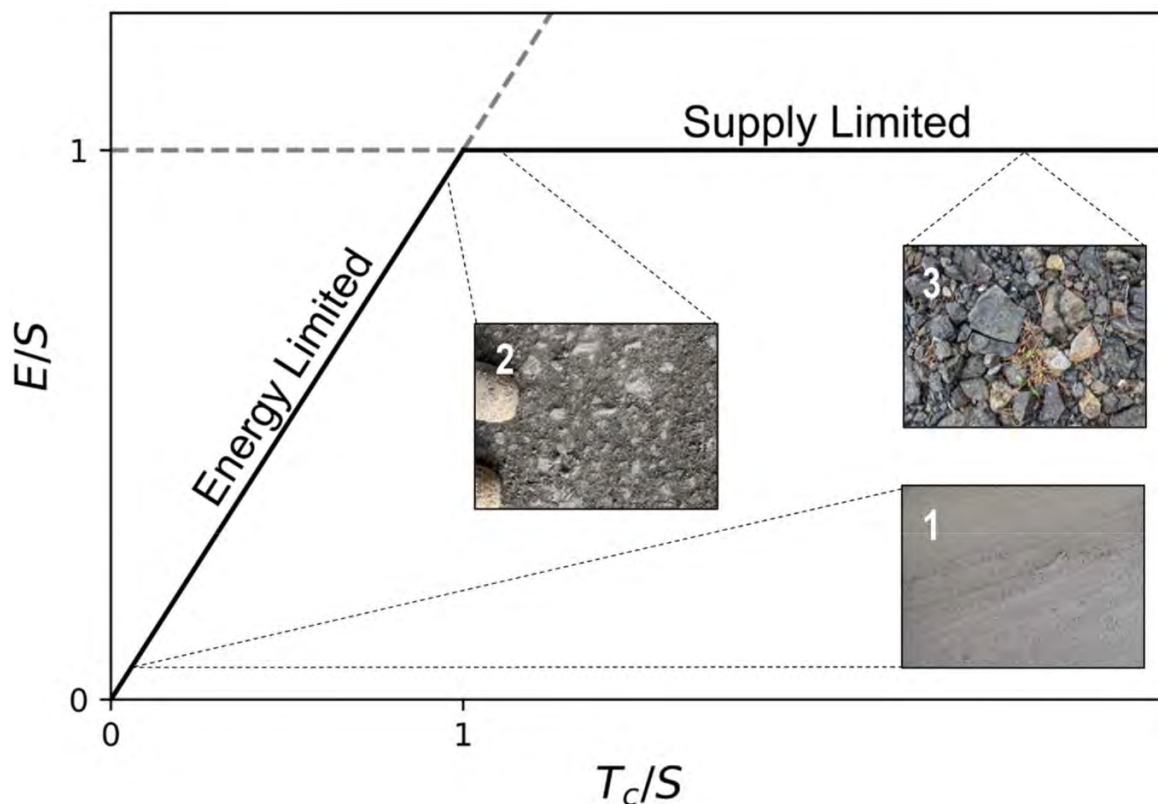
words, we want to know how much sediment is coming from which mechanisms under what circumstances—a three-fold problem. To answer these questions, we need an efficient path forward.

We can think of forest road erosion through the lens of supply and energy limitations, a framework commonly used in geomorphology. In the classic geomorphological sense and a very long time perspective, this framework would characterize forest roads as energy limited only. However, if we view a forest road as a closed system that exists under specific conditions, we can characterize the system as either supply or energy limited. Supply limiting factors include traffic (Section 2), aggregate quality (Section 3.3), and subgrade strength (Section 3.4), while energy limiting factors include traffic (Section 2), road topography (Section 3.2), and rainfall (Section 3.1), and all these factors are markedly interconnected. These factors, both individually and combined, determine where a forest road falls on an energy- vs. supply-limited spectrum.

At any point in time, depending on the context, a forest road, even the same segment of forest road, can be considered either a supply-limited or an energy-limited system, and under different contexts, the state of the system may change. As such, we posit that the relationship between erosion, supply, and energy can be described using the concept of limiting factors (Fig. 9). If the energy is less than the supply, the erosion of the system will be dependent on energy, making the erosion process energy limited (e.g., a muddy road storing fine sediment on the surface that has not yet been transported off the road). However, once the energy surpasses the supply, the erosion of the system will be equal to the supply available, making the erosion process supply limited (e.g., a rocky road).

A subset of this relationship can be seen in preliminary sediment and flow data collected in Washington state (Fig. 10) as part of an ongoing study conducted by the Cooperative Monitoring Evaluation and Research Committee within the Washington Department of Natural Resources Adaptive

Fig. 9. A limiting factor diagram for conceptualizing the relationship between erosion, energy, and supply. When the energy (T_c) is less than the supply (S), the erosion (E) depends on energy, and data from this road would plot along the energy limited line. When T_c surpasses S , E is equal to the supply, and data would fall along the supply limited line. Three examples of a forest road in different states are shown: (1) an energy limited road surface; (2) a road surface that is on the cusp between energy and supply limited; and (3) a supply limited road surface.



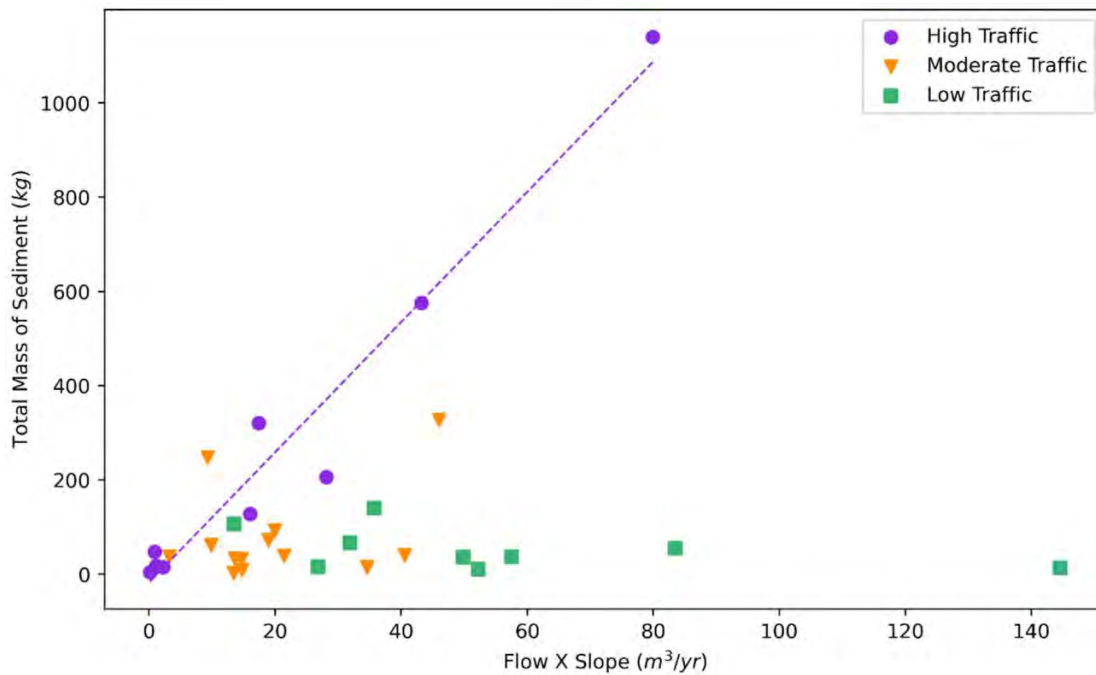
Management Program. In this ongoing study, a number of covariates are being measured. These covariates include the total annual flow of a road segment, which is measured using tipping buckets, and the total annual sediment mass, which is collected in settling basins connected to the same road segment. These preliminary data show the relationship between average annual flow \times slope (a surrogate for transport capacity or “energy”, T_c) and total annual mass of sediment (a measure of erosion, E) as a function of traffic level (a surrogate for supply, S). At field sites where traffic levels are high (purple circles in Fig. 10), sediment supply is also high and the data show that E depends on T_c . These locations would plot near the energy-limited line in the limiting factor space presented above. In contrast, the low traffic field sites (green squares in Fig. 10) have a lower supply and the data show that E does not depend on T_c . These locations would plot close to the supply-limited line in the limiting factor space. In this limiting factor space—where the response variable (i.e., erosion) is affected by multiple factors (i.e., the energy-supply balance and level of traffic)—quantile regression would be helpful to examine these data (Cade and Noon 2003).

The framing of forest road erosion as a function of both supply and energy can help us focus further research, specifically with respect to the influence of traffic. As discussed above, we know that the role of traffic in this framework

can be found in both the supply and energy limitations. For example, pumping and crushing can increase the available supply explicitly, while scattering can affect the available supply implicitly by either revealing or covering existing fine sediment on the road surface. Additionally, scattering can affect the available energy through road surface deformation, similar to rutting. Both rutting and scattering lead to flow rerouting, which effectively increases the energy directed to transporting fine sediments. Rerouted flow will not necessarily reach the roadside ditches, which tend to offer more resistance to flow—through installation of grass or other ditch line BMPs—and, therefore, sediment transport. However, these effects depend on context, such as surfacing quality; subgrade strength; underlying geology; spatial characteristics of the road; wet weather; or freeze-thaw processes.

Thinking of traffic-induced erosion as a function of supply and energy and remembering context dependencies allows for interpretation and synthesis of targeted experiments to test hypotheses regarding these processes. One example experiment could include looking at short-time-scale interactions between traffic and an established mainline road to measure the magnitude of the pumping process. Another segment-scale experiment could include looking at changes in the hydraulics of flow in roadside ditch lines and road

Fig. 10. Preliminary data from western Washington field study showing the total annual mass of sediment (kg) vs. total annual flow x slope (m^3) for three different traffic levels. These data show that for high traffic sites (i.e., high supply sites; purple circles in figure), total annual mass of sediment (surrogate for erosion) is linearly related to total annual flow x slope (surrogate for transport capacity), whereas low traffic sites (i.e., low supply sites; green squares) show no significant dependence.



surface ruts to help characterize the effects of rutting on flow rerouting and, ultimately, erosion.

An important next step would be to use our current understanding and hypotheses to develop a process-based model that incorporates mathematical conceptualizations for the aforementioned processes. The development of such a model can, in turn, help us develop field studies to further understand these processes and parameterize our models. Currently, no model exists that looks at the multiple specific traffic-induced erosion processes. Some previous models incorporate the role of traffic via a traffic factor that changes erosion based on average road use (e.g., [Dubé, Megahan and McCalmon 2004](#); [Akay et al. 2008](#)) or via increasing road “erodibility” with traffic over time ([Ziegler, Giambelluca and Sutherland 2001](#)), while other models note the importance of traffic but do not consider it quantitatively. Therefore, a process-based unpaved forest road erosion model incorporating the four different traffic-driven processes ([Section 2](#)) and their context dependencies ([Section 3](#)) is warranted to guide data collection and analysis needs.

Advancing research regarding traffic-induced road erosion has multiple implications. Understanding how much supply is increased by pumping or crushing, and their dependencies on aggregate quality and subgrade integrity, can improve guidelines for traffic levels under particular conditions. Additionally, understanding how much energy increases by scattering or flow rerouting, and their dependencies on spatial road characteristics and weather, can allow for more informed recommendations regarding road maintenance. Overall, increased knowledge of traffic-specific processes

and related factors will enable us to determine the most cost-effective steps to take to reduce forest road erosion.

5. Conclusion

The influence of traffic on forest road erosion has been studied from a broad and somewhat qualitative perspective, with the literature commonly focusing on increased erosion due to traffic and the effects thereof, without detailing and quantifying underlying mechanisms. Current research lacks comprehensive consideration of these mechanisms and related contextual covariates, but this research has provided the groundwork for development of quantitative hypotheses regarding four main traffic-induced erosion-enhancing processes: crushing, pumping, scattering, and flow rerouting. Quantifying these processes, and their relation to other important contextual covariates, is integral to furthering our understanding of forest road erosion. To quantify these processes and covariates, we should start framing traffic and other influencing factors in terms of their roles in supply- and energy-limitations. If we focus future research using this framework, our capacity to evaluate the current hypotheses of traffic-induced erosion-enhancing processes will increase, and we will be able to establish the most effective and efficient ways to control forest road erosion.

Acknowledgements

This review was made possible by funding from the Cooperative Monitoring, Evaluation, and Research Committee

within the Washington State Department of Natural Resources Adaptive Management Program.

Article information

History dates

Received: 4 April 2022

Accepted: 31 August 2022

Accepted manuscript online: 13 October 2022

Version of record online: 2 February 2023

Copyright

© 2022 Copyright remains with the author(s) or their institution(s). This work is licensed under a [Creative Commons Attribution 4.0 International License](https://creativecommons.org/licenses/by/4.0/) (CC BY 4.0), which permits unrestricted use, distribution, and reproduction in any medium, provided the original author(s) and source are credited.

Data availability

The data shown in Fig. 10 of this manuscript are not publicly available due to an agreement with the authors' funding agency but are available from the corresponding author upon reasonable request and approval from the funding agency.

Author information

Author ORCIDs

Amanda D. Alvis <https://orcid.org/0000-0002-9662-1121>

Author contribution

Conceptualization: ADA, CHL, EI

Funding acquisition: ADA, CHL, EI

Investigation: ADA

Supervision: CHL, EI

Project administration: CHL, EI

Visualization: ADA, CHL

Writing – original draft: ADA, CHL

Writing – review & editing: ADA, CHL, EI

Competing interests

The authors declare there are no competing interests.

References


- Akay, A.E., Erdas, O., Reis, M., and Yuksel, A. 2008. Estimating sediment yield from a forest road network by using a sediment prediction model and GIS techniques. *Build. Environ.* **43**(5): 687–695. doi:10.1016/j.buildenv.2007.01.047.
- Anderson, D.M., and Macdonald, L.H. 1998. Modelling road surface sediment production using a vector geographic information system. *Earth Surf. Process. Landf.* **23**(2): 95–107. doi:10.1002/(SICI)1096-9837(199802)23:2%3C95::AID-ESP849%3E3.0.CO;2-1.
- Arnáez, J., Larrea, V., and Ortigosa, L. 2004. Surface runoff and soil erosion on unpaved forest roads from rainfall simulation tests in north-eastern Spain. *Catena* **57**(1): 1–14. doi:10.1016/j.catena.2003.09.002.
- Aust, W.M., Bolding, M.C., and Barrett, S.M. 2015. Best management practices for low-volume forest roads in the piedmont region: summary and implications of research. *Transp. Res. Rec.* **2472**(1): 51–55. doi:10.3141/2472-06.

- Bilby, R.E., Sullivan, K., and Duncan, S.H. 1989. The generation and fate of road-surface sediment in forested watersheds in southwestern Washington. *For. Sci.* **35**(2): 453–468.
- Bloser, S., and Scheetz, B.E. 2012. Sediment production from unpaved oil well access roads in the Allegheny National Forest. The Center for Dirt and Gravel Road Studies at Pennsylvania State University. University Park, PA. p. 62.
- Boston, K. 2012. Impact of the ninth circuit court ruling (*Northwest Environmental Defense Center v. Brown*) regarding forest roads and the Clean Water Act. *J. For.* **110**(6): 344–346. doi:10.5849/jof.11-069.
- Boston, K., Pyles, M., and Bord, A. 2008. Compaction of forest roads in northwestern Oregon—room for improvement. *Int. J. For. Eng.* **19**(1): 24–28. doi:10.1080/14942119.2008.10702556.
- Bradley, A.H. 1994. Reducing tire pressures lessens rutting on thawing forest roads: results of two field trials. SAE Technical Paper No. 942246. SAE International. United States. doi:10.4271/942246.
- Brown, K.R., Aust, W.M., and McGuire, K.J. 2013. Sediment delivery from bare and graveled forest road stream crossing approaches in the Virginia piedmont. *For. Ecol. Manag.* **310**: 836–846. doi:10.1016/j.foreco.2013.09.031.
- Brown, K.R., McGuire, K.J., Aust, W.M., Hession, W.C., and Dolloff, C.A. 2015. The effect of increasing gravel cover on forest roads for reduced sediment delivery to stream crossings. *Hydrol. Process.* **29**(6): 1129–1140. doi:10.1002/hyp.10232.
- Cade, B.S., and Noon, B.R. 2003. A gentle introduction to quantile regression for ecologists. *Front. Ecol. Environ.* **1**(8): 412–420. doi:10.1890/1540-9295(2003)001%5b0412:AGITQR%5d2.0.CO;2.
- Cederholm, C.J., and Reid, L.M. 1987. Impact of forest management on coho salmon (*Oncorhynchus kisutch*) populations of the Clearwater River, Washington: a project summary. In E.O. Salo and T.W. Cundy(Eds.). *Streamside Management: Forestry and Fishery Interactions*. Proceedings of a Symposium held at University of Washington, 12–14 February 1986. Contribution no. 57. Institute of Forest Resources. Seattle, WA. pp. 373–398.
- Coker, R.J., Fahey, B.D., and Payne, J.J. 1993. Fine sediment production from truck traffic, Queen Charlotte Forest, Marlborough Sounds, New Zealand. *J. Hydrol.: N. Z.* **31**(1): 56–64.
- Croke, J.C., and Hairsine, P.B. 2006. Sediment delivery in managed forests: a review. *Environ. Rev.* **14**(1): 59–87. doi:10.1139/a05-016.
- Dawson, A. 1997. Rutting in unsurfaced roads - materials and structure interaction effects. In Proceedings of the International Symposium on Thin Pavements, Surface Treatments, Unbound Roads. University of New Brunswick, Fredericton, New Brunswick, Canada. pp. 101–108.
- Dawson, A., and Kolisoja, P. 2006. Managing Rutting in Low Volume Roads: Executive Summary. Roadex III Project Report. Swedish Road Administration, Northern Region, Luleå, Sweden.
- De Witt, A., Boston, K., and Leshchinsky, B. 2020. Predicting aggregate degradation in forest roads in northwest Oregon. *Forests* **11**(7): 729. doi:10.3390/f11070729.
- Dent, E.F., Mills, K.A., and Robben, J. 2003. Turbidity off of forest roads in Oregon. In Saleh(Ed.). *Total Maximum Daily Load (TMDL) Environmental Regulations II*. Proceedings of the 8-12 November 2003 Conference. American Society of Agricultural and Biological Engineers, Albuquerque, NM, USA. pp. 191–197. doi:10.13031/2013.15557.
- Dubé, K., Megahan, W., and McCalmon, M. 2004. *Washington Road Surface Erosion Model*. Washington Department of Natural Resources, Olympia, WA, USA.
- Dubé, K., Shelly, A., Black, J., and Kuzis, K. 2010. *Washington Road Sub-basin Scale Effectiveness Monitoring First Sampling Event (2006–2008) Report*. Washington Department of Natural Resources, Olympia, WA, USA.
- Edwards, P.J., Wood, F., and Quinlivan, R.L. 2016. *Effectiveness of Best Management Practices that Have Application to Forest Roads. General Technical Report NRS-163*. USDA Forest Service Northern Research Station, Parsons, WV, USA.
- Foltz, R.B. 1994. Sediment reduction from the use of lowered tire pressures. SAE Technical Paper No. 942244. SAE International. United States. doi:10.4271/942244.
- Foltz, R.B., and Burroughs, E.R. 1990. Sediment production from forest roads with wheel ruts. In R.E. Riggins, E.B. Jones, R. Singh and P.A. Rechar(Eds.). *Watershed Planning and Analysis in Action Symposium*. Proceedings of IR Conference Watershed Mgt/IR Div/ASCE, in Durango,

- Colorado, 9–11 July 1990. American Society of Civil Engineers. Durango, Colorado. pp. 266–275.
- Foltz, R.B., and Elliot, W.J. 1997. Effect of lowered tire pressures on road erosion. *Transp. Res. Rec.* **1589**(1): 19–25. doi:10.3141/1589-03.
- Foltz, R.B., Evans, G.L., and Truebe, M. 2000. Relationship of forest road aggregate test properties to sediment production. In M. Flug, D. Frevert and D.W. Watkins, Jr.(Eds.). *Watershed Management and Operations Management 2000 in Fort Collins, Colorado, 20–24 June 2000*. American Society of Civil Engineers, Reston, VA, USA. pp. 1–10.
- Foltz, R.B., and Truebe, M.A. 1995. Effect of aggregate quality on sediment production from a forest road. In Proceedings of the Sixth International Conference on low-volume roads. Transportation Research Board, National Research Council: Washington, DC, USA. pp. 49–57.
- Foltz, R.B., and Truebe, M.A. 2003. Locally available aggregate and sediment production. *Transp. Res. Rec.* **1819**(1): 185–193. doi:10.3141/1819b-24.
- Giroud, J.P., and Han, J. 2004. Design method for geogrid-reinforced unpaved roads. I. Development of design method. *J. Geotech. Geoenviron. Eng.* **130**(8): 775–786. doi:10.1061/(ASCE)1090-0241(2004)130:8(775).
- Gnanendran, C., and Beaulieu, C. 1999. On the behaviour of low-volume unpaved resource access roads: effects of rehabilitation. *Can. J. Civil Eng.* **26**(3): 262–269. doi:10.1139/j98-064.
- Hanna, S., and Boston, K. 2018. Aggregate performance on forest roads in the Pacific Northwest. *Eur. J. For. Eng.* **4**(2): 43–49. doi:10.33904/ejfe.458287.
- Indraratna, B., Lackenby, J., and Christie, D. 2005. Effect of confining pressure on the degradation of ballast under cyclic loading. *Geotechnique* **55**(4): 325–328. doi:10.1680/geot.2005.55.4.325.
- Istanbulluoglu, E., Tarboton, D.G., Pack, R.T., and Luce, C. 2002. A probabilistic approach for channel initiation. *Water Resour. Res.* **38**(12): 61–1–61–14. doi:10.1029/2001WR000782.
- Istanbulluoglu, E., Tarboton, D.G., Pack, R.T., and Luce, C. 2003. A sediment transport model for incision of gullies on steep topography. *Water Resour. Res.* **39**(4): 6–1–6–15, doi:10.1029/2002WR001467.
- Johnson, G. 2003. Minnesota's experience with thin bituminous treatments for low-volume roads. *Transp. Res. Rec.* **1819**(1): 333–337. doi:10.3141/1819b-42.
- Jordán, A., and Martínez-Zavala, L. 2008. Soil loss and runoff rates on unpaved forest roads in southern Spain after simulated rainfall. *For. Ecol. Manag.* **255**(3–4): 913–919. doi:10.1016/j.foreco.2007.10.002.
- Jordán-López, A., Martínez-Zavala, L., and Bellinfante, N. 2009. Impact of different parts of unpaved forest roads on runoff and sediment yield in a Mediterranean area. *Sci. Total Environ.* **407**(2): 937–944. doi:10.1016/j.scitotenv.2008.09.047. PMID: 18992920.
- Kemp, E., Leshchinsky, B., and Boston, K. 2016. Case study: evaluating road performance and sediment generation during simulated wet weather hauling. *Eur. J. For. Eng.* **2**(1): 22–34.
- Kochenderfer, J.N. 1970. *Erosion Control on Logging Roads in the Appalachians*. Research Paper NE-158. U.S. Department of Agriculture, Forest Service, Northeastern Forest Experiment Station, Upper Darby, PA. p. 28.
- Kochenderfer, J.N., and Helvey, J.D. 1987. Using gravel to reduce soil losses from minimum-standard forest roads. *J. Soil Water Conserv.* **42**(1): 46–50.
- Lackenby, J., Indraratna, B., McDowell, G., and Christie, D. 2007. Effect of confining pressure on ballast degradation and deformation under cyclic triaxial loading. *Géotechnique* **57**(6): 527–536. doi:10.1680/geot.2007.57.6.527.
- Lane, P.N., and Sheridan, G.J. 2002. Impact of an unsealed forest road stream crossing: water quality and sediment sources. *Hydrol. Process.* **16**(13): 2599–2612. doi:10.1002/hyp.1050.
- Luce, C.H. 2002. Hydrological processes and pathways affected by forest roads: what do we still need to learn?. *Hydrol. Process.* **16**(1): 2901–2904. doi:10.1002/hyp.5061.
- Luce, C.H., and Black, T.A. 1999. Sediment production from forest roads in western Oregon. *Water Resour. Res.* **35**(8): 2561–2570. doi:10.1029/1999WR900135.
- Luce, C.H., and Black, T.A. 2001. Effects of traffic and ditch maintenance on forest road sediment production. In Proceedings of the Seventh Federal Interagency Sedimentation Conference, in Reno, Nevada, 25–29 March 2001. U.S. Interagency Committee on Water Resources, Subcommittee on Sedimentation. Washington, D.C. pp. V67–V74.
- Luce, C.H., and Cundy, T.W. 1994. Parameter identification for a runoff model for forest roads. *Water Resour. Res.* **30**(4): 1057–1069. doi:10.1029/93WR03348.
- MacDonald, L.H., Sampson, R.W., and Anderson, D.M. 2001. Runoff and road erosion at the plot and road segment scales, St John, US Virgin Islands. *Earth Surf. Process. Landf.* **26**(3): 251–272. doi:10.1002/1096-9837(200103)26:3%3c251::AID-ESP173%3e3.0.CO;2-X.
- Megahan, W.F. 1974. *Erosion over Time on Severely Disturbed Granitic Soils: A Model*. Research Paper INT-156. U.S. Department of Agriculture Forest Service Intermountain Forest and Range Experiment Station, Ogden, UT. p. 20.
- Megahan, W.F., and Kidd, W.J. 1972. *Effect of Logging Roads on Sediment Production Rates in the Idaho Batholith*. Research Paper INT-123. U.S. Department of Agriculture Forest Service Intermountain Forest and Range Experiment Station, Ogden, UT. p. 23. doi:10.5962/bhl.title.68728.
- Megahan, W.F., Wilson, M., and Monsen, S.B. 2001. Sediment production from granitic cut-slopes on forest roads in Idaho, USA. *Earth Surf. Process. Landf.* **26**(2): 153–163. doi:10.1002/1096-9837(200102)26:2(153::AID-ESP172)3.0.CO;2-O.
- Packer, P.E. 1967. Criteria for designing and locating logging roads to control sediment. *For. Sci.* **13**(1): 2–18. doi:10.1093/forestscience/13.1.2.
- Pattison, J., Boston, K., and Pyles, M. 2010. Development of a correlation model between a 20-kg clegg hammer and field CBR for measuring subgrade strength in forest roads in western Oregon. *Int. J. For. Eng.* **21**(1): 12–19. doi:10.1080/14942119.2010.10702586.
- Ramos-Scharrón, C.E., and Macdonald, L.H. 2005. Measurement and prediction of sediment production from unpaved roads, St John, US Virgin islands. *Earth Surf. Process. Landf.* **30**(10): 1283–1304. doi:10.1002/esp.1201.
- Reid, D.A., Hassan, M.A., and Floyd, W. 2016. Reach-scale contributions of road-surface sediment to the Honna river, Haida Gwaii, BC. *Hydrol. Process.* **30**(19): 3450–3465. doi:10.1002/hyp.10874.
- Reid, L.M. 1981. *Sediment Production from Gravel-Surfaced Roads, Clearwater Basin, Washington*. University of Washington. Seattle, Washington.
- Reid, L.M., and Dunne, T. 1984. Sediment production from forest road surfaces. *Water Resour. Res.* **20**(11): 1753–1761. doi:10.1029/WR020i011p01753.
- Rhee, H., Fridley, J., and Page-Dumroese, D. 2018. Traffic-induced changes and processes in forest road aggregate particle-size distributions. *Forests* **9**(4): 181. doi:10.3390/f9040181.
- Sheridan, G.J., and Noske, P.J. 2007. A quantitative study of sediment delivery and stream pollution from different forest road types. *Hydrol. Process. Int. J.* **21**(3): 387–398. doi:10.1002/hyp.6244.
- Sheridan, G.J., Noske, P.J., Whipp, R.K., and Wijesinghe, N. 2006. The effect of truck traffic and road water content on sediment delivery from unpaved forest roads. *Hydrol. Process. Int. J.* **20**(8): 1683–1699. doi:10.1002/hyp.5966.
- Sugden, B.D., and Woods, S.W. 2007. Sediment production from forest roads in western Montana. *J. Am. Water Resour. Assoc.*, **43**(1): 193–206. doi:10.1111/j.1752-1688.2007.00016.x.
- Swift, L.W., Jr. 1984. Gravel and grass surfacing reduces soil loss from mountain roads. *For. Sci.* **30**(3): 657–670. doi:10.1093/forestscience/30.3.657.
- Swift, L.W., Jr. 1984. Soil losses from roadbeds and cut and fill slopes in the southern Appalachian Mountains. *South. J. Appl. For.* **8**(4): 209–216. doi:10.1093/sjaf/8.4.209.
- Toman, E.M., and Skaugset, A.E. 2011. Reducing sediment production from forest roads during wet-weather hauling. *Transp. Res. Rec.* **2203**(1): 13–19. doi:10.3141/2203-02.
- Trimble, G.R. 1959. Logging roads in northeastern municipal watersheds. *Am. Water Works Assoc.* **51**(3): 407–410. doi:10.1002/j.1551-8833.1959.tb15759.x.
- Trimble, G.R., and Sartz, R.S. 1957. How far from a stream should a logging road be located? *J. For.* **55**(5): 339–341. doi:10.1093/jof/55.5.339.
- Van Meerveld, H., Baird, E.J., and Floyd, W.C. 2014. Controls on sediment production from an unpaved resource road in a Pacific maritime watershed. *Water Resour. Res.* **50**(6): 4803–4820. doi:10.1002/2013WR014605.
- Visser, R., Brown, K., and Tinnelly, B. 2017. Geogrid for unsealed forest roads: installation considerations and bearing capacity testing in New Zealand. *Int. J. For. Eng.* **28**(2): 106–115. doi:10.1080/14942119.2017.1317132.

- Wemple, B.C., and Jones, J.A. 2003. Runoff production on forest roads in a steep, mountain catchment. *Water Resour. Res.* **39**(8): 17. doi:[10.1029/2002WR001744](https://doi.org/10.1029/2002WR001744).
- Wemple, B.C., Jones, J.A., and Grant, G.E. 1996. Channel network extension by logging roads in two basins, western cascades, Oregon. *J. Am. Water Resour. Assoc.* **32**(6): 1195–1207. doi:[10.1111/j.1752-1688.1996.tb03490.x](https://doi.org/10.1111/j.1752-1688.1996.tb03490.x).
- Ziegler, A.D., and Giambelluca, T.W. 1997. Importance of rural roads as source areas for runoff in mountainous areas of northern Thailand. *J. Hydrol.* **196**(1–4): 204–229. doi:[10.1016/S0022-1694\(96\)03288-X](https://doi.org/10.1016/S0022-1694(96)03288-X).
- Ziegler, A.D., Giambelluca, T.W., and Sutherland, R.A. 2001. Erosion prediction on unpaved mountain roads in northern Thailand: validation of dynamic erodibility modelling using KINEROS2. *Hydrol. Process.* **15**(3): 337–358. doi:[10.1002/hyp.96](https://doi.org/10.1002/hyp.96).
- Ziegler, A.D., Sutherland, R.A., and Giambelluca, T.W. 2000. Partitioning total erosion on unpaved roads into splash and hydraulic components: the roles of interstorm surface preparation and dynamic erodibility. *Water Resour. Res.* **36**(9): 2787–2791. doi:[10.1029/2000WR900137](https://doi.org/10.1029/2000WR900137).
- Ziegler, A.D., Sutherland, R.A., and Giambelluca, T.W. 2001. Interstorm surface preparation and sediment detachment by vehicle traffic on unpaved mountain roads. *Earth Surf. Process. Landf.* **26**(3): 235–250. doi:[10.1002/1096-9837\(200103\)26:3%3c235::AID-ESP171%3e3.0.CO;2-T](https://doi.org/10.1002/1096-9837(200103)26:3%3c235::AID-ESP171%3e3.0.CO;2-T).

Using additional roughness to characterize erosion control treatment effectiveness in roadside ditch lines

Amanda D. Alvis¹  | Charles H. Luce² | Erkan Istanbuluoglu¹ | Thomas Black² | Julie Dieu³ | Jenelle Black⁴

¹Department of Civil and Environmental Engineering, University of Washington, Seattle, Washington, USA

²Rocky Mountain Research Station, USDA Forest Service, Boise, Idaho, USA

³Pacific Resource Unit, Rayonier, Hoquiam, Washington, USA

⁴CMER Science Staff, Northwest Indian Fisheries Commission, Olympia, Washington, USA

Correspondence

Amanda D. Alvis, Department of Civil and Environmental Engineering, University of Washington, Seattle, WA, USA.
Email: amanaste@uw.edu

Funding information

Cooperative Monitoring, Evaluation, and Research (CMER) Committee within the Washington State Department of Natural Resources Adaptive Management Program

Abstract

Forest roadside ditch lines capture and redirect road runoff and typically have erosion control treatments installed therein. Existing methods used to determine the effectiveness of roadside ditch line erosion control treatments estimate fixed fractional reductions in sediment yield. However, fixed fractional reductions do not describe dependence on any measurable physical property of treatment, climate, and the environment. Here, we use additional flow roughness induced by erosion control treatments as a metric that can be used as the basis of estimating treatment effectiveness in varying contexts. We investigate its utility in small-scale field experiments in western Washington. We measured the physical characteristics of each ditch (e.g., shape, soil texture, and slope) and flow velocities and sediment concentrations for each treatment under multiple experimental discharges. We then used the concept of shear stress partitioning to relate sediment yield from the ditch line erosion treatments to grain shear stress, which is a function of flow roughness (Manning's n) of the respective treatment. We found that (1) a given erosion control treatment produced consistent Manning's n values across multiple replications and sites, with a bare ditch (no treatment) yielding the lowest roughness ($n = 0.05$) and a densely watted ditch yielding the highest roughness ($n = 0.75$); (2) sediment load and calculated grain shear stress data yielded a single positive relationship when data from each experiment were combined, which suggests the effect of additional roughness on grain shear stress is a main driver in the reduction of ditch line sediment load; and (3) in our dataset, fractional erosion reduction had a variable and nonlinear sensitivity to low flow rates (99% of observed flows) for lower roughnesses. Our results demonstrate how additional flow roughness can be used as a general metric to help evaluate the effectiveness of ditch line erosion control treatments for a variety of physical conditions.

KEYWORDS

erosion, erosion control treatments, forest roads, hydrology, sediment transport, shear stress

1 | INTRODUCTION

Roadside ditch lines are crucial conduits for capturing and redirecting forest road runoff to mitigate the effects of forest road erosion. Erosion control treatments for dirt and gravel roads—especially those that are installed in roadside ditch lines—are essential to the protection of

both transportation infrastructure and downstream water quality and aquatic habitat (e.g., Cristan et al., 2016). Accurate estimates of erosion reduction from forest road surfaces and ditch lines are critical to developing regulations and assessing the cost effectiveness of erosion control treatments (e.g., wattles, gravel, and vegetation; see, e.g., Boston, 2016; Dangle et al., 2019). Most of the current research

This is an open access article under the terms of the [Creative Commons Attribution](https://creativecommons.org/licenses/by/4.0/) License, which permits use, distribution and reproduction in any medium, provided the original work is properly cited.

© 2024 The Authors. *Earth Surface Processes and Landforms* published by John Wiley & Sons Ltd.

evaluating the efficacy of these treatments has been done in the vein of randomized control trials (*sensu* Cartwright, 2007) and relies on empirical methods that quantify a fixed fractional reduction of sediment transport (e.g., Aust et al., 2015; Burroughs et al., 1984; Burroughs & King, 1989; Cristan et al., 2019; Edwards et al., 2016; Luce & Black, 1999; Megahan, 1974; Megahan et al., 2001). The choice to use randomized control trials—rather than developing physics-based models and testing those models using experiments—is likely driven by a few key factors. For one, each erosion control treatment involves distinct mechanisms for reducing ditch line erosion. Rather than focussing on details of different process representations in models, empirical field methods can be used to determine reduction factors. Additionally, multiple treatments are commonly used within a single project to assess their efficacy, and the interactions among these treatments pose challenges for modelling due to their complex nature. Finally, a large portion of the motivation behind this research originates from practitioners rather than academics. Practitioners have preferred methods that can be easily implemented without the need for vast data collection and site characterization.

A major challenge in using fixed fractional reductions in erosion is in the generalization of the effects of the erosion control treatments to other contextual settings. For example, the fixed fractional reduction in sediment estimated from an experiment conducted in a place where high intensity rainstorms occur may not apply in places where snow melt generated runoff is more common. The results that are calculated from an experiment on a steep road will likely not be equivalent to those of a low-gradient road. The general applicability of limited experimental results to a wide range of ditch conditions and treatments is hindered by the presence of thresholds and nonlinearities in the sediment entrainment and transport process (e.g., Al-Hamdan et al., 2013; Buffington & Montgomery, 1997; Govers, 1992; Nearing et al., 1989). To address the need for erosion predictions in a wide range of field conditions, differences in experimental controls or premises need to be accounted for in the development of models and/or methods. These differences can be considered either through conducting more randomized control trials in various experimental settings (a potentially slow and expensive process) or through a more process-based approach, where a simple physical parameter is used. We advocate for the latter by proposing to use additional roughness imparted by different ditch line erosion treatments as that simple physical parameter. Additional flow roughness is the increment in roughness affecting flowing water caused by placement or growth of materials/vegetation in the ditch. We then partition the shear stress acting on the water column between particles on the bed versus the added roughness elements. The concept of shear stress partitioning is a well-known method in sediment transport literature to represent how additional flow roughness elements on the bed reduce the shear stress acting on sediment particles (Einstein & Banks, 1950; Einstein & Barbarossa, 1952).

In practice, three main mechanisms help erosion control treatments reduce sediment transport and erosion in ditch lines: (1) increasing flow roughness, (2) binding, and (3) filtering. Increasing the roughness of the flow by placing additional roughness elements, such as grass and wattles, to slow down the flow velocity is well-grounded in observational evidence (e.g., Donald et al., 2013; Edwards et al., 2016; Li et al., 2020; Li, Zhang, et al., 2022; Prosser et al., 1995; Schussler et al., 2021; Whitman et al., 2021). Other erosion control

treatments approach erosion reduction through binding and filtering, both of which may involve additional physical mechanisms that decrease the erodibility of the bed material or reduce erosivity of flows. Binding refers to treatments that functionally increase the size of particles that would need to be transported. Examples of binding treatments include concrete lining, maintaining vegetative root mats, or spreading a binding agent (e.g., Edwards et al., 2016; Likitlersuang et al., 2020; Sojka et al., 2007). Filtering treatments seek to capture particles that are in transport by passing them through some kind of sieving or settling element along a flow path. Examples of filtering treatments include constructed wetlands, straw bales, and rock check dams (e.g., Collins & Johnston, 1995; Edwards et al., 2016; Tollner et al., 1977; Wright, 2010). In the context of controlling erosion in the roadside ditches of rural and forest roads, most common treatments combine two or more of these effects to some degree. Not all erosion control treatments utilize binding and/or filtering, but all treatments do impart some degree of additional flow roughness, which affects shear stress partitioning. As a result, investigating the role of additional roughness—and therefore that of shear stress—on flow and sediment loads is a logical first step towards developing process-based modelling tools and conceptual frameworks to interpret field observations. Shear stress partitioning is a well-established method in the soil erosion literature of rangelands, landscape evolution, and fluvial geomorphology (e.g., Al-Hamdan et al., 2022; Darby et al., 2010; Foster et al., 1989; Istanbuluoglu et al., 2002, 2003; Li, Venditti, et al., 2022; Yager et al., 2007; Yetemen et al., 2019). However, such a method has not seen much attention in erosion control practices literature.

The idea of shear stress partitioning and its theory as developed by multiple researchers, particularly in fluvial environments (e.g., Buffington & Montgomery, 1997; Einstein & Banks, 1950; Einstein & Barbarossa, 1952; Ferguson et al., 2019; Manga & Kirchner, 2000), provides the basis for quantification of changes in total versus effective shear stress on grains with application of different treatments. Increased flow roughness (i.e., the addition of erosion control treatments) leads to deeper flows and thereby higher shear stress or stream power for sediment entrainment and transport. Consequently, a proportion of this shear stress is imparted on the added roughness elements rather than the bed sediment due to increases in friction around the immobile roughness elements. Effectively, the addition of erosion control treatments reduces the shear stress available for the bed, which decreases the frequency and magnitude of sediment mobilization and transport under a variable climate. A substantial body of literature already exists on shear stress partitioning and its effects on sediment transport that supports the use of additional roughness as a metric to determine reduction in sediment mobilization (e.g., Istanbuluoglu & Bras, 2005; Le Bouteiller & Venditti, 2015).

Critically, the roughness contributions from common ditch line erosion control treatments are unknown, and the literature provides scant recommendations to estimate additional flow roughness (i.e., Manning's n) contributed by erosion control treatments. Roughness is typically used as a calibration parameter in models (Lane, 2014) and is based on approximate guidelines (e.g., Arcement & Schneider, 1989) offering large ranges in values. However, we posit that incremental roughness added by an erosion control treatment—a simple physical parameter—can be used as a measure or index of erosion control treatment effectiveness. We are left with multiple

questions: What is the additional Manning's roughness due to different treatments? What is the influence of increased roughness on sediment load? Is increasing additional flow roughness the dominant mechanism for reducing sediment yields in select roadside ditch line erosion control treatments? Can additional flow roughness be used as a simple physical metric to generalize the effects of the treatments to other contextual settings?

In this paper, we examine several ditch line erosion control treatments through estimating their added roughness as well as measuring sediment transport in field experiments in western Washington. Using these measurements, as well as established theory around shear stress partitioning, we evaluate the utility of roughness as a quantitative characterization of ditch line erosion control treatments. Overall, this study offers potential simplification of determining erosion control treatment effectiveness through the leveraging of theory in hydraulics and sediment transport to reduce the dimensionality of the experimental measurements.

2 | MATHEMATICAL THEORY

2.1 | Shear stress partitioning

Sediment transport has been related to grain shear stress τ_g (the shear stress acting on sediment grains) in excess of critical shear stress τ_c (the shear stress threshold at which sediment will begin to move) in a power-function form:

$$Q_s \sim (\tau_g - \tau_c)^m. \quad (1)$$

When there are other obstructions in the channel aside from the substrate grains, the portion of shear stress acting on the sediment grains is responsible for transport. A shear stress partitioning ratio, f_g , can be used to determine this portion of the total boundary shear stress that acts on the channel bed substrate grains (e.g., Tiscareno-Lopez et al., 1994).

$$\tau_g = \tau_t * f_g. \quad (2)$$

Einstein and Barbarossa (1952) proposed to partition τ_t into various components such as τ_g and τ_a :

$$\tau_t = \tau_g + \tau_a, \quad (3)$$

where τ_a is the shear stress acting on additional roughness in the channel (e.g., bed forms and vegetation). We write the total shear stress based on a force-balance derivation and equate it to the sum of drag forces acting on grains and additional roughness components (Manga & Kirchner, 2000).

$$\rho_w g R S = \rho_w C_{dg} U^2 + \rho_w C_{da} U^2, \quad (4)$$

where ρ_w is the density of water, g is the acceleration of gravity, R is the hydraulic radius of flow, S is the slope, C_{dg} is the drag coefficient for the sediment grains, C_{da} is the drag coefficient for additional

roughness components, and U is the flow velocity. When additional roughness is not present, the equation can be solved for C_{dg} :

$$C_{dg} = \frac{g R_g S}{U^2}, \quad (5)$$

where C_{dg} is assumed to remain constant within the same channel (ditch), even with the addition of any roughness elements. Here, we would like to relate C_{dg} to Manning's n , which is widely used to represent channel roughness in hydraulic engineering applications. If we use Manning's equation for U ($U = \frac{1}{n} R^{2/3} S^{1/2}$), assume parabolic channel geometry, and express R from the equation of parabola, C_{dg} takes the following form (Appendix A):

$$C_{dg} = g n_g^{24/13} Q^{-2/13} S^{1/13} \left(\frac{6}{a}\right)^{1/13}, \quad (6)$$

where n_g is grain roughness, a is a parabolic shape factor, and Q is channel flow. Following the logic of (3) and (4), the drag coefficient of the bare ditch can be added to the drag coefficient for added roughness elements to obtain a total drag coefficient (i.e., $C_{dg} + C_{da} = C_{dt}$). As such, we can write an equation for the total drag coefficient in a similar form:

$$C_{dt} = g n_t^{24/13} Q^{-2/13} S^{1/13} \left(\frac{6}{a}\right)^{1/13}. \quad (7)$$

Substituting (6) and (7) into (4) to write equations for grain and total shear stress, we express the shear stress partitioning ratio in (2) as (8). Upon cancelling the identical terms in the fraction, (8) reduces to (9):

$$f_g = \frac{\tau_g}{\tau_t} = \frac{\rho_w g n_g^{24/13} Q^{-2/13} S^{1/13} \left(\frac{6}{a}\right)^{1/13} U^2}{\rho_w g n_t^{24/13} Q^{-2/13} S^{1/13} \left(\frac{6}{a}\right)^{1/13} U^2}, \quad (8)$$

$$\frac{\tau_g}{\tau_t} = f_g = \left(\frac{n_g}{n_t}\right)^{24/13}. \quad (9)$$

In Appendix A, we show several methods for characterizing flow hydraulics in parabolic channels and derive variations of (9) with the exponent in the shears stress partitioning ratio ranging from 3/2 to 15/8 (1.5 to 1.875).

To obtain the shear stress partitioning ratio, we can characterize n_g from bare ditch lines and n_t from ditch lines with different erosion control treatments. The flow roughness (i.e., Manning's n or Manning's roughness) can be calculated by

$$n = \frac{1}{U} R^{2/3} S^{1/2}. \quad (10)$$

Again, if the channel geometry is assumed to be parabolic, R can be written in terms of other hydraulic and geometric properties (Appendix A), which turns (10) into

$$n = \frac{Q^{4/9} S^{1/2}}{U^{13/9} (\frac{6}{a})^{2/9}}. \quad (11)$$

Given fixed Q , S , and a , U becomes the main variable that differentiates the actual roughness values for bare or erosion control treatment conditions, which can then be used in (9). Using (11), Manning's n obtained for a bare ditch gives us n_g , while that which is obtained for ditches with erosion control treatments gives us n_t .

As discussed above, the total shear stress can be divided into various components such as τ_g and τ_a (Equation 3). Combining (3) and (9) and noting that $n_t = n_a + n_g$, we can visualize total shear stress and its division into various components as a function of additional channel roughness, n_a (Figure 1; see also fig. 4 in Manga & Kirchner, 2000, for a related perspective).

2.2 | Transport capacity of ditch flow

To evaluate the reductions of sediment transport of different erosion control treatments relative to bare ditch lines, we use an excess-shear-stress-dependent sediment transport equation developed for rills and overland flow on a noncohesive substrate (Govers, 1992):

$$T_c = \frac{10^{-4.348}}{d_{50}^{0.811}} (\tau_g - \tau_c)^{2.457}, \quad (12)$$

where T_c is the sediment transport capacity of the flow, d_{50} is the median grain size, τ_g is the grain shear stress, and τ_c is the critical shear stress.

2.3 | Indicators of erosion control treatment effectiveness

To examine the effectiveness of erosion control treatments, we look at the contextually determined fractional reduction in grain shear

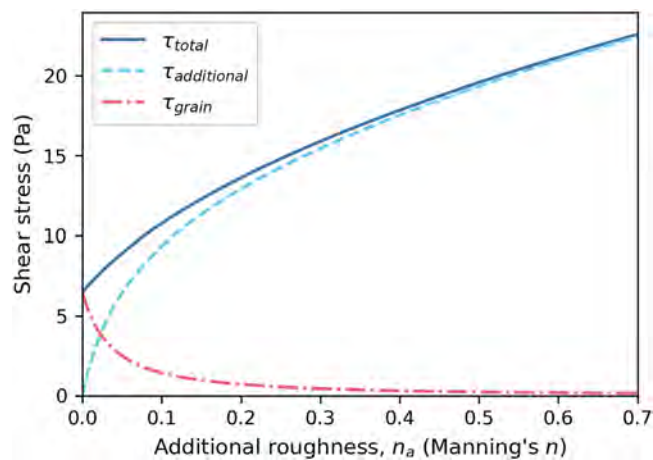


FIGURE 1 The theoretical effect of additional immobile roughness elements on shear stress and its partitioning. [Color figure can be viewed at wileyonlinelibrary.com]

stress and the contextually determined fractional reduction in sediment transport capacity (henceforth referred to in this experiment as “fractional reductions” as opposed to “contextually determined fractional reductions,” for clarity). We define the fractional reduction in grain shear stress, ϕ , as

$$\phi = \frac{\tau_{g,bare} - \tau_{g,ect}}{\tau_{g,bare}}, \quad (13)$$

where $\tau_{g,bare}$ is the bed shear stress of a bare ditch, or the shear stress acting on the sediment grains in a bare ditch, and $\tau_{g,ect}$ is the shear stress acting on the sediment grains in a ditch with additional roughness from installed erosion control treatments. This metric allows us to quantify the proportion of reduction of $\tau_{g,bare}$ achieved by an erosion control treatment.

Similar to (13), we define the fractional reduction in sediment transport capacity, θ , as

$$\theta = \frac{T_{c,bare} - T_{c,ect}}{T_{c,bare}}, \quad (14)$$

where $T_{c,bare}$ is the transport capacity of flow in a bare ditch and $T_{c,ect}$ is the transport capacity of flow in a ditch with additional roughness from installed erosion control treatments.

3 | FIELD STUDY

3.1 | Study area

We carried out an experiment to measure the Manning's roughness and sediment load of multiple roadside ditch line erosion control treatments in two regions of southwest Washington state: (1) a volcanic lithology near Mount Saint Helens and (2) a siltstone lithology near Aberdeen, WA. These regions contain multiple field sites with different ditch line treatments, which were selected to be on mainline logging roads as part of a broader study conducted by the Cooperative Monitoring Evaluation and Research Committee within the Washington Department of Natural Resources Adaptive Management Program. Each field site for this experiment consists of a 40 m length of ditch line with a cross-drain culvert at the bottom of the ditch segment and has a slope between 4% and 6% (Figure 2a). The field sites in the volcanic lithology experience, on average, 1560 mm of annual precipitation, and the field sites in the siltstone province experience, on average, 2400 mm of annual precipitation (PRISM Climate Group, 2023), with most of the precipitation occurring between October and April.

The experimental runs were carried out in the volcanic region in May 2021 and May 2022 and in the siltstone region in May 2021, May 2022, and October 2022. In each region, multiple ditch treatments were tested (Table 1 and Figure 2b).

Additionally, in the siltstone region, we performed the same experiment on a rut in the road surface to observe the hydraulic properties of ruts as well as their sediment-carrying effectiveness.

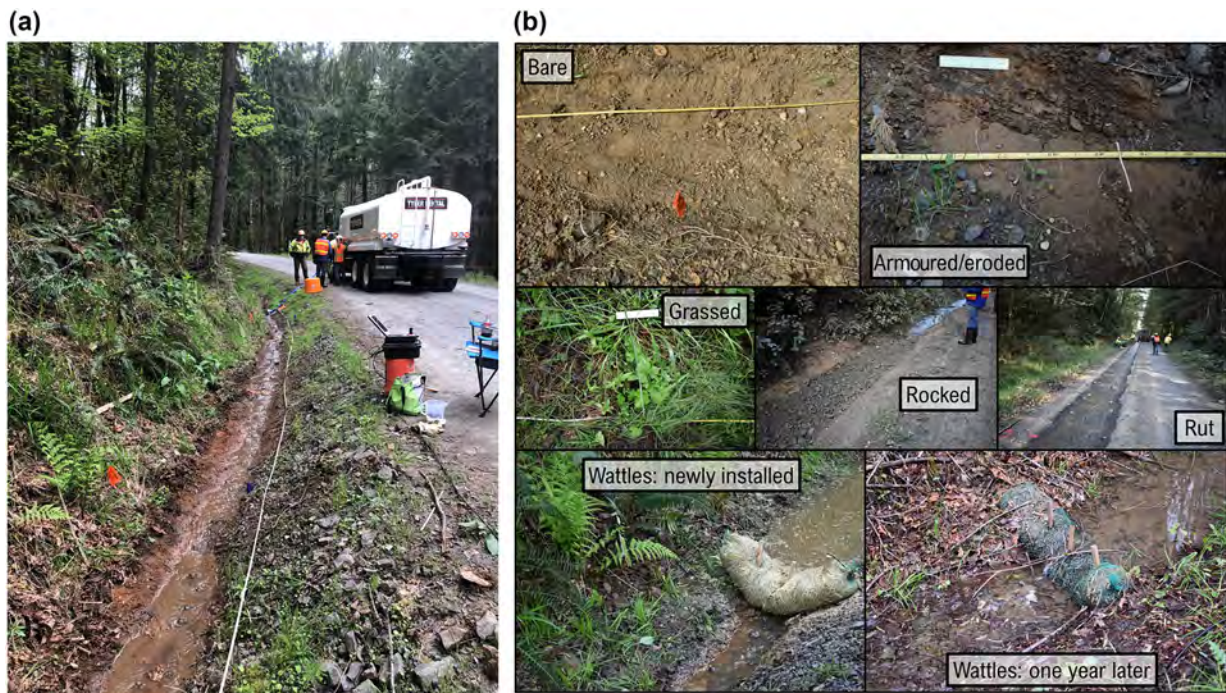


FIGURE 2 (a) Example experimental setup showing the roadside ditch line and water truck and (b) example photos of each ditch line treatment tested. [Color figure can be viewed at [wileyonlinelibrary.com](https://onlinelibrary.wiley.com/doi/10.1002/esp.5763)]

TABLE 1 Descriptions and locations for each ditch treatment tested.

Treatment	Description	Siltstone region	Volcanic region
Bare subsoil	Freshly ditched and no treatment	x	x
Eroded/armoured	Not recently ditched with minimal grass recovery	x	
Grassed	Not recently ditched with good grass recovery		x
Sparse wattles, initial installation	10 straw wattles		x
Sparse wattles, 1 year post-installation	10 straw wattles		x
Dense wattles, initial installation	19 straw wattles	x	
Rocked	3" minus rock covering bottom of ditch	x	

3.2 | Experiment

The goal of the experiment was to estimate Manning's roughness and sediment load for each ditch treatment. We examined changes in the hydraulics of flow, as well as sediment production and transport, in roadside ditch lines for multiple roughness-varying erosion control treatments. Each experimental run consisted of the following:

1. Measurements of the physical characteristics of the ditch line (e.g., shape, soil texture, and slope).
2. Collection of surface sediment samples at each of five cross sections (measurement stations) in the ditch.
3. Use of a salt tracer to determine the velocity of flow for three given flow rates (Moore, 2005; United States Bureau of Reclamation, 2001).
4. Collection of sediment samples at the downstream end of the ditch line throughout each experimental run.

We determined the longitudinal profile (i.e., slope) of the ditch using a survey rod and a survey level and established measurement

stations at 4 m intervals from the ditch relief cross-drain culvert at the bottom of the ditch segment (origin; 0 m) to the top of the experimental segment (40 m up-ditch). Cross-sectional channel profiles were measured at every other measurement station from the bottom of ditch line (4 m above the pipe inlet and 12, 20, 28, and 36 m) using a level and a metric ruler, with elevation-drop measurements being made at 0.1 m intervals from the cutslope side of the ditch (0 m) to the side of the road (1.1–1.2 m) (Figure 3a).

Sediment was sampled at each of the five cross sections noted above to determine the existing grain size distribution in each experimental ditch. Sediment samples were taken from the surface because the expected transported sediment comes from the surface of the ditch, as flow was provided upstream of each ditch. These samples were originally processed such that we obtained a dispersed grain size distribution. However, because the material in our ditch lines had some cohesion, we took additional samples to obtain a water-stable aggregate grain size distribution for each site following the methods of Kemper and Rosenau (1986). The resulting median grain size was approximately 1 mm, which was used as the median grain size for further analysis (see Section 4). Photographs were taken at each of the

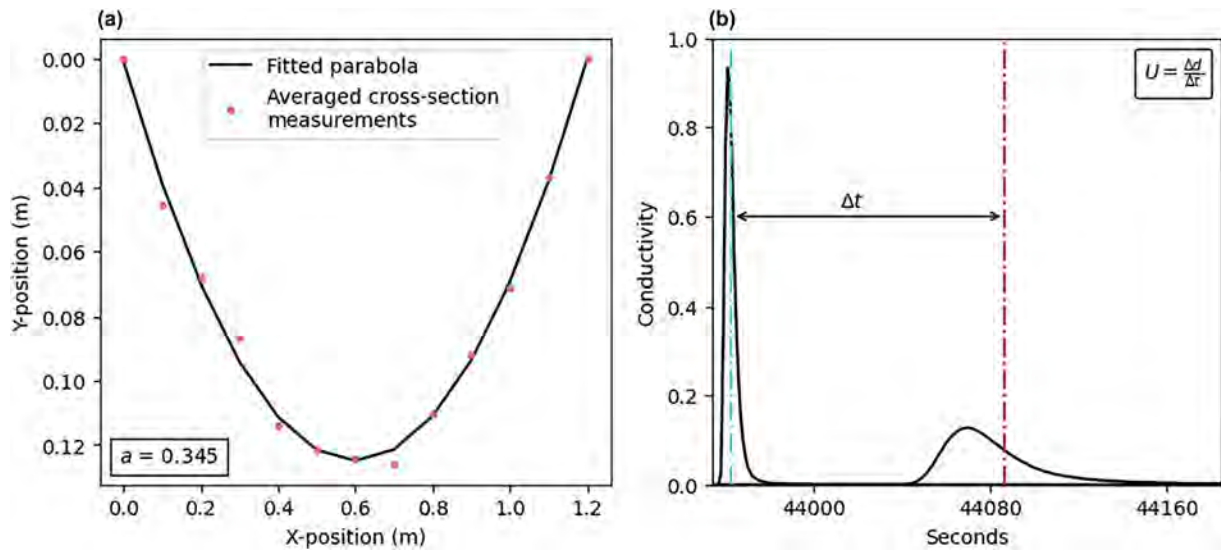


FIGURE 3 Examples of (a) average ditch cross-section measurements with a fitted parabola and shape factor and (b) a conductivity plot for two sensors from the salt tracer experiment. Δt is the time it takes for the salt tracer to get from the upper sensor to the lower sensor (average rate taken as one half area under the curve) and is determined from the plot, and Δd is known. [Color figure can be viewed at [wileyonlinelibrary.com](https://onlinelibrary.wiley.com/doi/10.1002/esp.5763)]

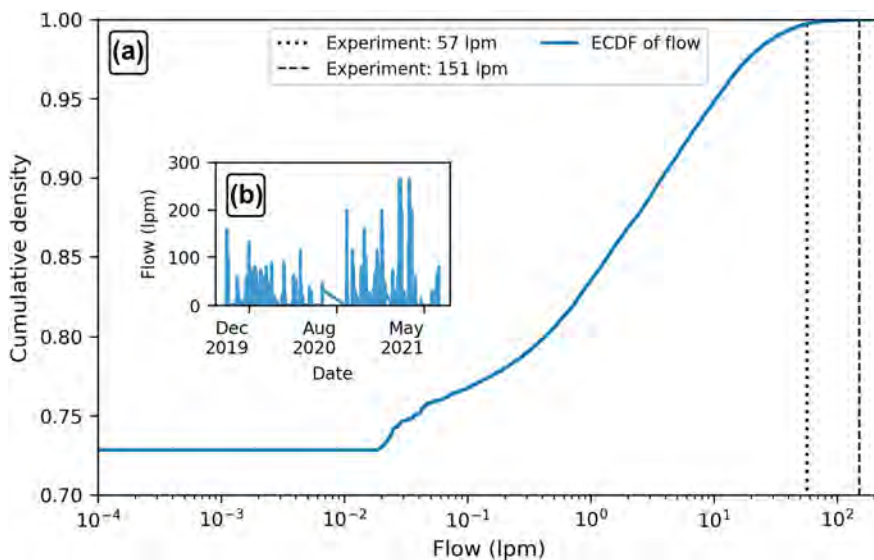


FIGURE 4 (a) Empirical cumulative distribution function (ECDF) of flow data from one of our siltstone lithology field sites in western Washington with vertical lines denoting two of the flows used in the small-scale experiment in litres per minute (57 and 151 lpm). For this site, 57 lpm flows exist in the 99th percentile and 151 lpm flows exist in the 100th percentile. (b) The corresponding tipping bucket flow hydrograph for the 2020 and 2021 water years. [Color figure can be viewed at [wileyonlinelibrary.com](https://onlinelibrary.wiley.com/doi/10.1002/esp.5763)]

five cross sections noted above to document the physical changes of the ditch line before and after the experimental runs (if any). Finally, to ensure minimal loss of water flow to infiltration during experimental runs, the ditch line was wetted by a water tank truck providing flow at a slow rate (Figure 2a).

To provide known flow rates, we utilized a flow meter (Flomec G2 AI Turbine Flow Meter Model G2A15NQ9GMB) and hose attached at the water tanker outlet. The experimental runs were carried out at three flow rates for each ditch treatment, twice to thrice per flow rate: 57, 95, and 151 L min⁻¹ (lpm). These three flow rates were chosen to reflect flows that have been observed in our broader study dataset of these magnitudes. More specifically, these three flow rates exist within the 99th to 100th percentile of empirical flow data recorded at one of our siltstone lithology sites between 2019 and 2021 (Figure 4). Those years experienced slightly drier-than-average climatic conditions (PRISM Climate Group, 2023). We used the high end of the flow rates as most sediment is transported within the wettest few days in ditch lines.

Conductivity probes (Campbell Scientific Model CS547A with a Campbell Scientific CR 1000 Data Logger) were placed in the ditch at just below 4 m and just above 36 m. The conductivity probes measured the passage of salt tracers, used to determine the velocity of the flow during our experimental runs.

Once the flow from the water tank truck stabilized in the ditch line, a known quantity of NaCl was added to the system, signalling the start of the experimental run, and was monitored via conductivity probes. The conductivity probes logged a reading every second. Once the NaCl level for both conductivity probes returned to their original values, the experimental run was considered complete. We repeated the addition of NaCl for each flow and treatment combination twice.

For each experimental run, a grab sample for sediment concentration was collected at the downstream end of the ditch line once the flow rate stabilized. We collected one main sediment concentration sample per run to give us an estimate of sediment transport occurring for each treatment prior to any ditch armoring occurring.

3.3 | Data analysis

In order to calculate Manning's roughness values for each experimental run, we first estimated flow velocities from our salt tracer experiments. We measured the time it takes for the NaCl to travel from the upper sensor to the lower sensor (Figure 3b). With a known distance between the two sensors and the time of travel, we calculated the average velocity of the flow between the two sensors, which is taken as the average velocity for the ditch line flow.

The cross-sectional shape of our ditches for the experimental runs was mostly parabolic (e.g., Figure 3a). Given the estimated U and measured Q , we then characterized the parabolic shape factor, a . To calculate this shape factor, we took the average of the measurements of the ditch line cross-sectional channel profiles and characterized a representative cross-sectional shape of the ditch line. We fit each ditch with an equation for a parabola and estimated the shape factor a .

Given U , Q , a , and the measured mean profile slope of the ditch line, n is obtained from (11). For each erosion control treatment (Figure 2b), we estimated the corresponding n (i.e., n_t) using the steps outlined above. We carried out an ordinary least squares regression analysis to help describe the observed relationship between n_t and flow (Table 2). Ultimately, we were interested in the response of the grain shear stress (i.e., shear stress partitioning) and the sediment transport capacity of the ditch line to additional Manning's roughness,

which we calculated based on our measured and calculated experimental values following the logic in Section 2.

In addition to the roughness of each ditch and the grain shear stress of each experimental run, we used our sediment concentration grab samples from each experimental run to corroborate our estimates of shear stress partitioning and sediment transport capacity and test for whether additional factors other than roughness appeared to affect sediment transported along the bottom of the ditch line. Sediment concentrations were converted to sediment transport per unit flow width, which is calculated as $\text{sediment concentration} \times \frac{Q}{w}$ where Q is flow discharge and w is flow width obtained from the parabolic channel cross section assumption at the measured cross-sectional area (Figure 3a).

We used 2 years of measured flow data (1 October 2019–30 September 2021) from one of our field sites to calculate flow durations to be applied (Figure 4) in estimating grain shear stress and sediment transport capacity. This allowed us to address questions about how much of the time sediment might be expected to be produced from the ditch, the expected distribution of sediment export rates, and the fractional reduction in sediment yields as a function of a treatment specified in terms of its added roughness. These flows were used to calculate grain shear stress (τ_g), sediment transport capacity (T_c), the fractional reduction in grain shear stress (ϕ), and the fractional reduction in sediment transport capacity (θ) for different erosion control treatments using their respective Manning's roughness values.

TABLE 2 Statistical analysis results of trend lines shown that relate total roughness and flow.

Treatment	Slope	Coefficient of variance	P-value
Dense wattles, initial installation	0.000 ^a	1.000 ^a	N/A ^a
Grassed	−0.004	0.748	0.026
Sparse wattles, 1 year post-installation	−0.003	0.953	0.003
Sparse wattles, initial installation	0.000	0.021	0.907
Rocked	−0.002	0.890	0.057
Armoured	0.000	0.099	0.319
Bare	0.000	0.405	0.035
Rut	0.000	0.240	0.402

^aOnly two data points.

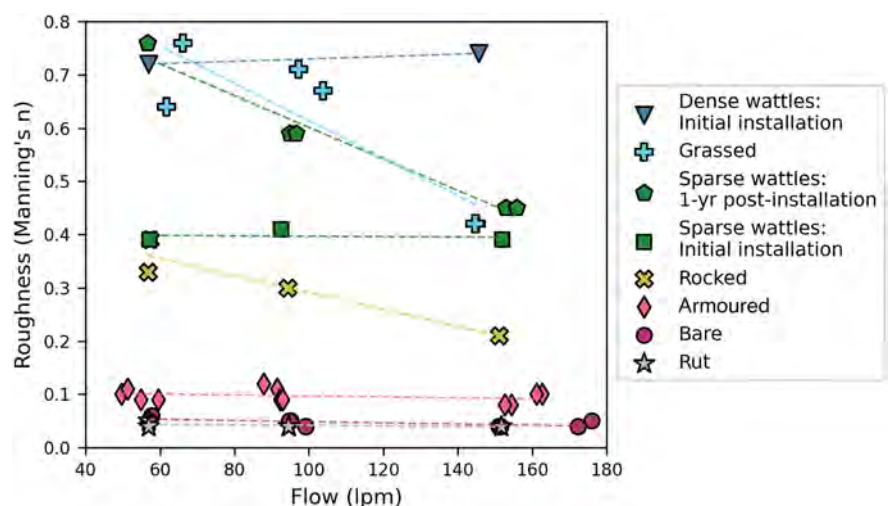


FIGURE 5 Roughness values (Manning's n) for each ditch condition and their relationship to flow. [Color figure can be viewed at wileyonlinelibrary.com]

4 | RESULTS

4.1 | Inferences from field observations

To address our first research question, we report estimated total roughness values (Manning's n) from our experiments (Figure 5). Erosion control treatment installation and natural armoring of a ditch line increased n_t as compared with a bare (recently disturbed) ditch. Three erosion control treatments—rocked, grassed, and sparse wattles 1 year post-installation—demonstrated a linearly decreasing relationship between the total roughness and flow (Table 2). Additionally, we performed the same experiment on a heavily defined wheel rut on the road surface (Figure 2b) and found that the rut had similar roughness to a bare (recently disturbed) ditch. The observed increase in Manning's roughness with added erosion control treatments is consistent with the literature and the shear stress partitioning theory, further elaborated in Section 5. The next logical question to address here is as follows: What is the influence of increased roughness on sediment load? We address this question through our sediment concentration data.

Our grab samples provided us with sediment concentration values (Figure 6a) and sediment transport per unit width (Figure 6b) for each

treatment and flow. All of our ditch treatments yielded some amount of sediment transport. The bare ditch and rut yielded the highest sediment concentrations and sediment transport, with an armoured ditch yielding at least one order of magnitude less sediment. To provide a more direct comparison, we plot sediment transport from each erosion control treatment staged from low to high n_t , with nominal flow rates denoted by colour (Figure 6c). As the roughness due to each treatment increases, sediment transport decreases, with the highest flow rate showing the most consistent reductions with increased roughness (Figure 6c).

One goal of this experiment was ultimately to determine the sediment reduction effects of erosion control treatments in roadside ditch lines using the concept of shear stress partitioning. To do so, we calculated—for each of the treatments—the total shear stress using the denominator of (8) and the grain shear stress using (9) solved for τ_g (Figure 7b). The merit of using shear stress partitioning to determine sediment reduction effects is well-illustrated by our data: The relationship between total shear stress and sediment transport is disjointed (Figure 7a). Despite a consistent increase in calculated total shear stress for different erosion control treatments, their associated sediment transport estimates were consistently lower than bare

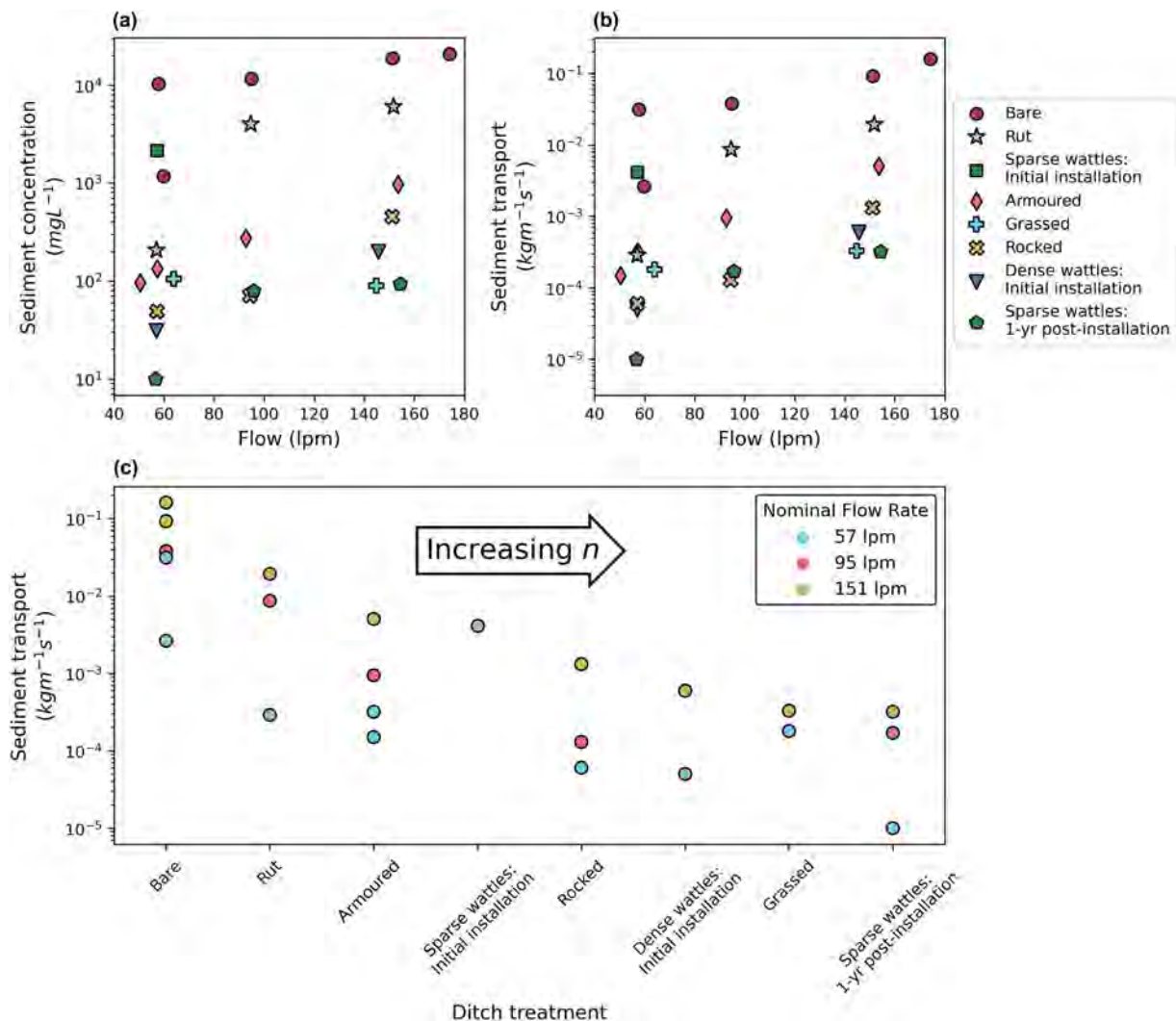


FIGURE 6 (a) Sediment concentration values for each ditch condition and their relationship to flow. (b) Sediment transport values for each ditch condition based on sediment concentration and flow width. (c) Strip plot showing the spread of sediment transport values for each ditch treatment. The nominal flow rates for each sediment transport value are denoted by different colours. [Color figure can be viewed at wileyonlinelibrary.com]

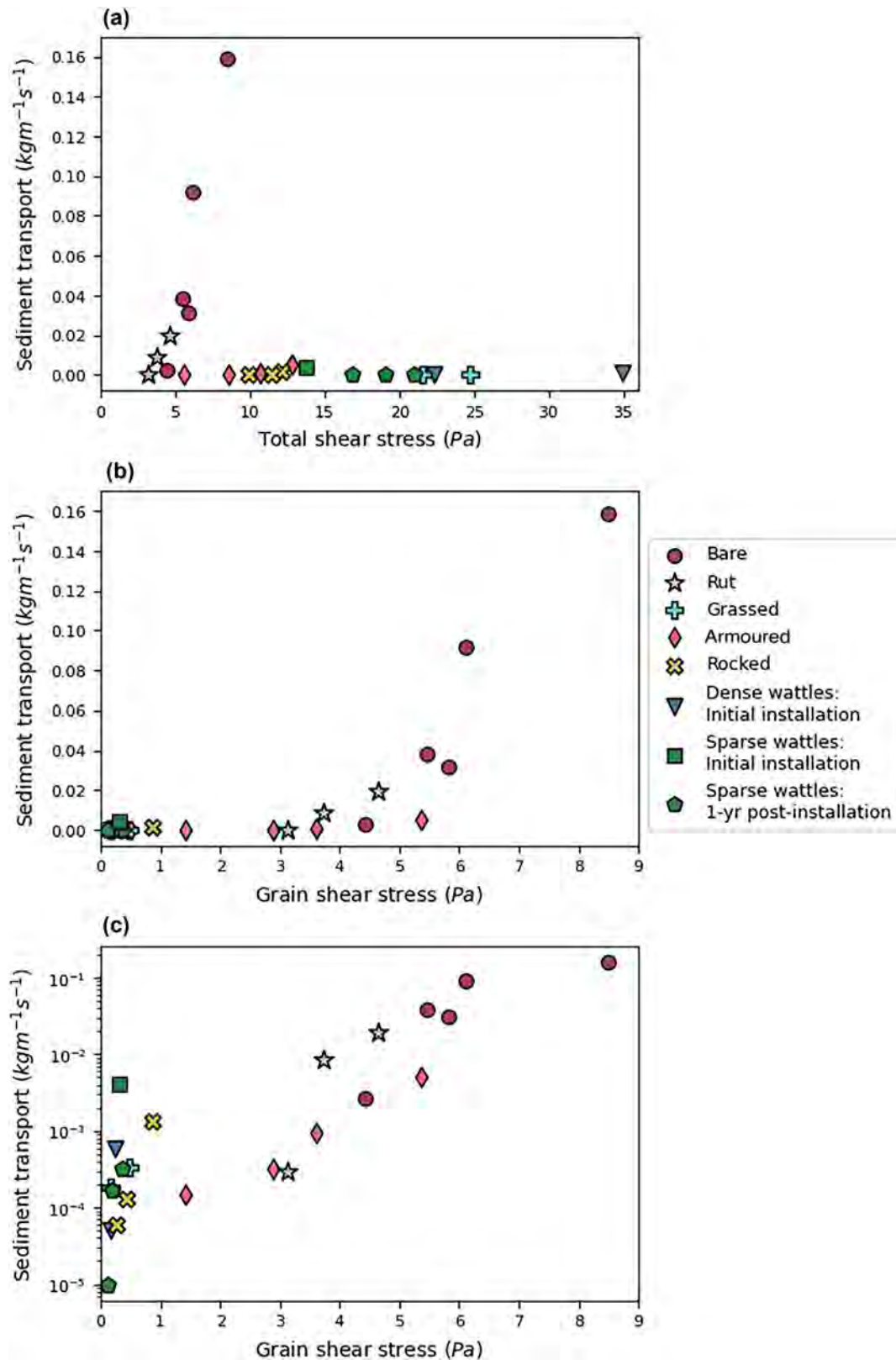


FIGURE 7 (a) Measured sediment transport values as a function of total shear stress, (b) measured sediment transport values as a function of grain shear stress, and (c) measured sediment transport values as a function of grain shear stress with a log-scale y-axis. [Color figure can be viewed at wileyonlinelibrary.com]

ditches and ruts (only under higher flow). This seemingly counterintuitive behaviour can only be explained when effective (grain) shear stress is used, organizing the data points consistently along a curve, where all the erosion control treatment sediment fluxes are now pushed back to consistently small values, largely less than 1 Pa, while bare plots remain constant ($\tau_g = \tau_t$). The relationship between grain

shear stress and sediment transport aligns with the expectation that increased roughness results in decreased sediment transport (Figure 7b,c). Furthermore, if filtering were an additional effect of some erosion control treatments, sediment yield from filtering treatments (grass, initial installation of wattles, and rocking) might be systematically lower than the mean expectation based on the pattern of

points (e.g., a fitted curve). No such pattern is observed in Figure 7c. As discussed above (Section 1), adding roughness elements to the ditch line (i.e., erosion control treatments) increases the total shear stress acting on the ditch due to the deepening and slowing of water flow. However, as also discussed previously, the resulting increase in friction around immobile roughness elements reduces the amount of grain shear stress available for sediment transport, which is illustrated by plotting total shear stress as a function of Manning's n due to additional roughness elements (Figure 1).

4.2 | Erosion control treatment effectiveness in context of climate

Because sediment transport is a strongly nonlinear function of grain shear stress, we must consider potential sediment yield reductions from treatments in the context of not just a few flows, as done with the field study. Rather, we should consider potential sediment yield reductions in the context of an ensemble of flows as might be seen over a season of runoff (e.g., Figure 4).

We can see that with higher roughness values, the exceedance probabilities of grain shear stress decrease in a relatively consistent nature (Figure 8a), with substantial reductions in the fraction of time

that sediment would likely be transported. The d_{50} of soil aggregate particles in the field sites is approximately 1 mm, which has a relatively high critical shear stress based on Shield's criteria (0.566 Pa) as compared with the distribution of grain shear stresses estimated from observed flows and, as such, only yields modelled sediment transport for Manning's roughness values of up to 0.25 (Figure 8a). In Figures 4 and 8a, water flows (considered nonzero at a rate greater than 0.02 lpm) about 27% of the time, and in freshly disturbed ditches, grain shear stress exceeds the critical shear stress about 22% of the time (or about 80% of the time that water is flowing). In contrast, by increasing the roughness to $n=0.10$ (armoured condition), runoff from the ditch would be expected to transport sediment only about 12% of the time (or 44% of the time there is runoff), and with $n=0.25$ (rocked ditch), grain shear stress would exceed critical shear stress less than 2% of the time (or 7% of the time that runoff occurs). The fractional reduction in grain shear stress is constant for roughness values that do not vary with flow, whereas a slight decrease occurs for roughness values that linearly decrease with flow (Figure 8b).

From our calculated grain shear stresses, and using (12) in Section 2, we modelled the sediment transport capacity of ditch flow—when there was ditch flow—for different roughness values. The resulting sediment transport capacity exceedance probabilities decrease dramatically as a function of increasing roughness

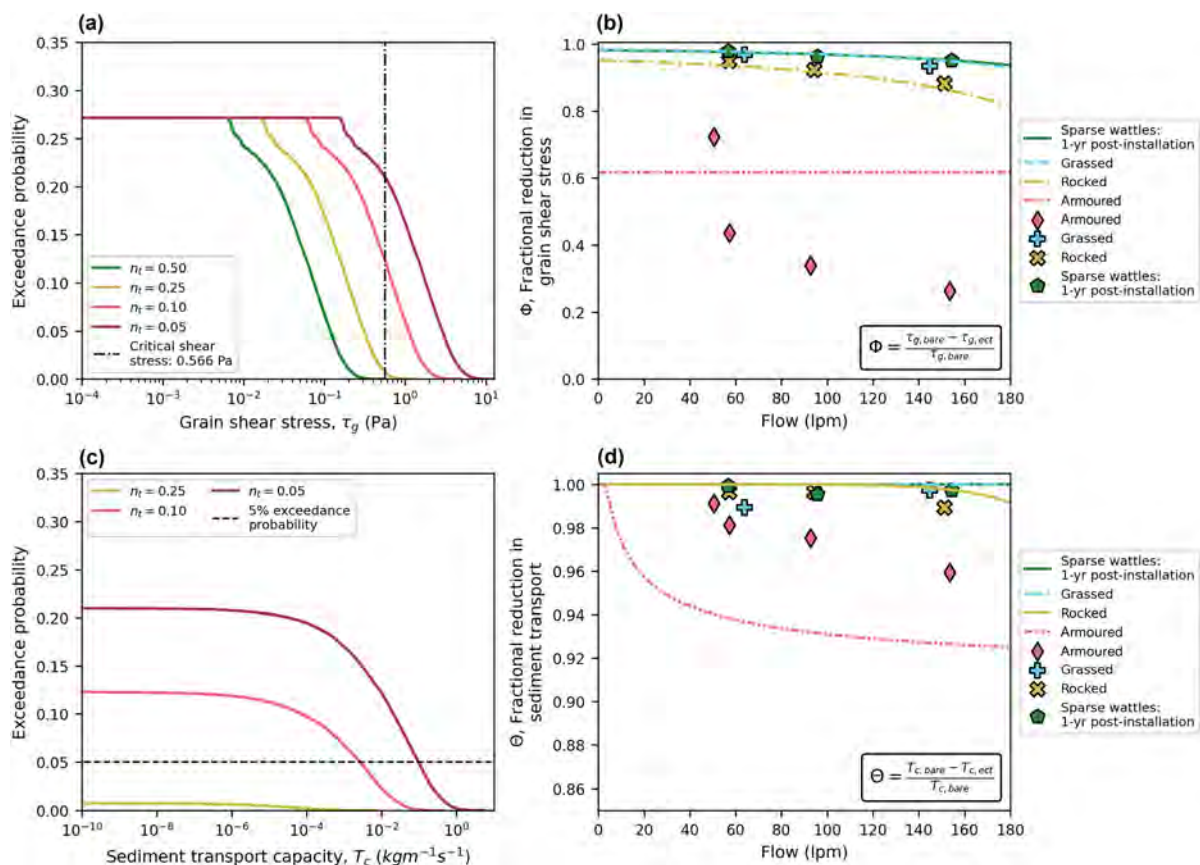


FIGURE 8 (a) Exceedance probabilities of grain shear stress, τ_g , for multiple n_t values calculated from (2) using observed ditch line flow hydrographs. Higher n_t values decrease grain shear stress. The critical shear stress threshold for a d_{50} of 1 mm is denoted by the vertical line. (b) Fractional reduction in grain shear stress, ϕ , for multiple ditch erosion control treatments. Erosion control treatments with n_t values that vary with flow provide less reduction in grain shear stress with higher flows. Experimental fractional reductions in grain shear stress are shown as points. (c) Exceedance probabilities of sediment transport capacity, T_c , for multiple n_t values. An exceedance probability of 5% is denoted by the horizontal line. (d) Theoretical fractional reduction in sediment transport capacity, θ , for multiple ditch erosion control treatments. Experimental fractional reductions in sediment transport are shown as points. [Color figure can be viewed at [wileyonlinelibrary.com](https://onlinelibrary.wiley.com/terms-and-conditions)]

(Figure 8c). For 5% of the time (about 18 days per year), the transport capacity in a bare ditch ($n=0.05$) would exceed $0.1 \text{ kg m}^{-1} \text{ s}^{-1}$, a rate that is almost never expected to occur in an armoured ditch ($n=0.10$). At the same time, in an armoured ditch, 5% of the time, transport capacity would be expected to exceed $0.002 \text{ kg m}^{-1} \text{ s}^{-1}$, which is about 2% of the rate in a bare ditch for that exceedance probability. Integrating over the ensemble of flows, the bare ditch ($n=0.05$) would have a transport capacity, T_c , of $61 \text{ Mg m}^{-1} \text{ year}^{-1}$, an armoured ditch ($n=0.10$) would have a T_c of $2.8 \text{ Mg m}^{-1} \text{ year}^{-1}$, and the higher roughness of a rocked ditch ($n=0.25$) would have a T_c of about $0.04 \text{ Mg m}^{-1} \text{ year}^{-1}$. Actual erosion collected from a ditch would be smaller because available sediment would eventually be depleted, but the contrast in transport capacity integrated over the year gives a more concrete sense of the effect of added roughness on sediment yield. One notable point is that for low flows (common), a total roughness of $n=0.10$ transitions from nearly complete reduction in sediment transport at 4 lpm or less to around 94% reduction at 57 lpm in a nonlinear way (Figure 8d). The modelled reductions are nearly 100% for a ditch with installed erosion control treatments (rocked ditch or stronger; $n \geq 0.25$). In other studies, measurements of sediment yield from road segments with recently disturbed versus armoured ditches over a few months to years showed reductions ranging from 85% (Luce & Black, 1999, 2001b) to nearly complete reduction (Luce & Black, 2001a).

5 | DISCUSSION

Shear stress partitioning offers an effective way of characterizing the effect of forest road erosion control treatments in reducing sediment transport through the use of their associated Manning's roughness. Because Manning's roughness associated with shallow flow is typically an empirical value coming from limited studies with varying conditions and contexts and few, if any, studies use Manning's n to evaluate erosion control treatment effectiveness, comparing all our measured Manning's roughness values to the literature is challenging. Our measured roughness values for bare soil ($n \approx 0.05$), grass ($n \approx 0.45$ to 0.75), and a rocked surface ($n \approx 0.25$ to 0.35) are reasonably consistent with previously established values for shallow flow (Figure 5; e.g., Arcement & Schneider, 1989; Barros & Colello, 2001; Emmett, 1970; Engman, 1986). While not comparable with established roughness values due to limited studies, wattles do show comparable roughness values to grass. Measuring the roughness of a ditch line erosion control treatment offers an efficient and more general way to estimate the effectiveness of a given erosion control treatment, when used in a sediment transport equation driven by discharge, for differing conditions and contexts.

This final point is important—99% of observed flows that were >0.02 lpm in this dataset were less than 57 lpm, and in this range of flows, there is a variable and nonlinear sensitivity of fractional sediment transport capacity reduction (θ) as a function of flow rate (Figure 8d). Any experiment that reports a fractional sediment reduction from a treatment equivalent to an armoured ditch would need to qualify that the reduction is applicable to the particular flow rate used, and any study integrating sediment over a season would need to report the ensemble probability distribution of precipitation or flow. Directly transferring a fractional reduction from a mild rainy climate (e.g., northwest

United States and northern Europe) to one where high intensity storms are more common (e.g., tropics and southeast United States) or places where snowmelt is more common is not necessarily a reasonable expectation. The change in roughness associated with an erosion control treatment, however, should be transferable through the use of shear stress partitioning in a sediment transport model.

While most erosion control treatments maintained constant total roughness with varying flow, three erosion control treatments had roughness decrease as flow increased (Figure 5): rocking, grass, and 1 year-old wattles. Each of these treatments had unique physical characteristics that we hypothesize contribute to their decreasing relationship between roughness and flow (Figure 9).

For the site with a rocked ditch (approximately $d_{50} = 38 \text{ mm}$), the decrease in roughness as flow increased can likely be attributed to the fraction of the cross-sectional area of flow navigating the immobile roughness elements. With low flow, the majority of the water is moving through the subsurface (the interstitial spaces between the rocks) of the channel, with minimal surface flow (Figure 9a). As the flow increases, the fraction of the water being slowed due to immobile roughness elements decreases (e.g., Barros & Colello, 2001; Chen et al., 2015).

For the grassed site, the decrease in roughness with higher flows is similar to the rocked site: a decrease in the fraction of the cross-sectional area of flow experiencing immobile elements, but due to different mechanics. With lower flows, the water must flow through grass and vegetation stems. As the flow increases, the vegetation begins to bend, which effectively “smooths” these immobile roughness elements, causing the total roughness to decrease (Figure 9b; e.g., Chen et al., 2015; Jordanova & James, 2003; Nepf, 2012).

The decrease in roughness with an increase in flow for the 1 year-old sparse wattles site can likely be attributed to both the fraction of the cross-sectional area of flow navigating immobile roughness elements and the dam-and-reservoir effect seen during the experiment. The wattles at this site were initially installed in May 2020. During those initial wattle experimental runs, the flow never overtopped any of the wattles; rather, the flow went under or through the wattles (Figure 9c), which led to relatively consistent roughness values for varying flows. One year later, however, the wattles had not experienced any maintenance. Sediment and debris had built up inside of and behind each wattle, and, as such, the wattles acted like a series of dams and reservoirs (see Edwards et al., 2016). The initially high roughness values for the 1 year-old wattles can likely be attributed to the severe slowing of water as it built up behind each wattle before spilling over. As the flow increased, that slowing had less of an effect, and the fraction of the flow seeing the immobile roughness element decreased (Figure 9d).

In conjunction with the roughness, the sediment concentration grab samples validated the use of shear stress partitioning to evaluate reduced sediment transport effects due to erosion control treatment installation. This is demonstrated by the relationship between measured sediment transport and total shear stress (Figure 7a) and measured sediment transport and grain shear stress (Figure 7b). The trend between sediment transport and grain shear stress (Figure 7c) indicates that the increase in flow roughness due to additional immobile elements is likely the key driver in the reduction of sediment transport, rather than other mechanisms, such as binding effects of vegetation roots or filtering by wattles (which leads to rapid clogging with little internally retained sediment in any event).

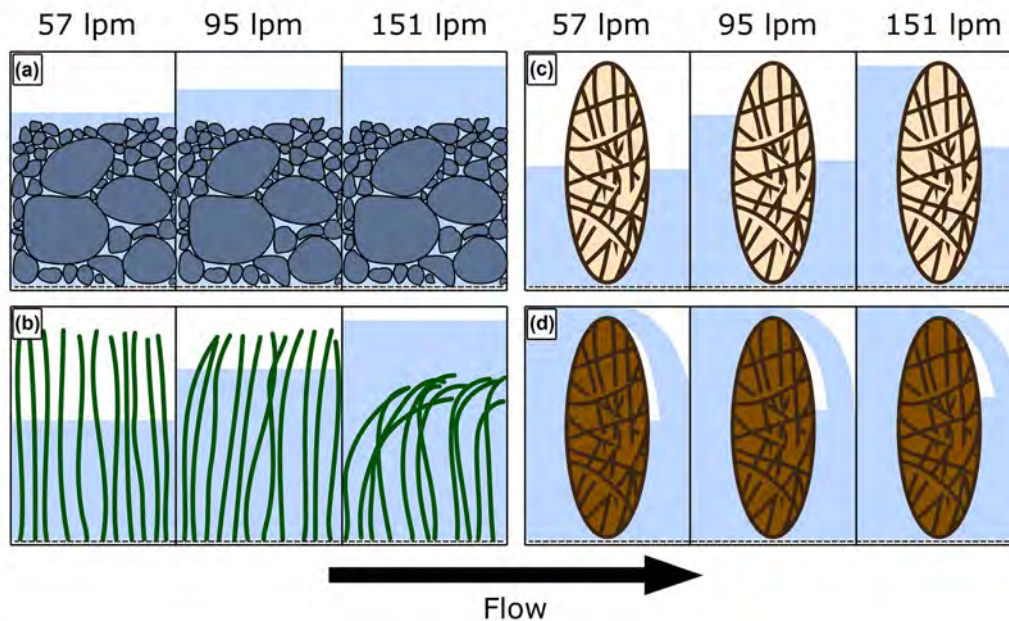


FIGURE 9 Drawings showing side views of the following: (a) The rocked ditch as flow increases. Once the flow gets to 151 lpm, the water far overtops the rocking, causing the fraction of the flow cross-sectional area being slowed by the immobile roughness to decrease. (b) The grassed ditch as flow increases. The highest flow causes the vegetation to bend, effectively smoothing the cross section. (c) The initial installation of straw wattles, where the flow went under or through the wattles, as they were brand new. (d) The wattles after they had been in the field for a year without any maintenance, causing them to become clogged with sediment. At all flow rates, the space behind the wattles fills up with water then overtops, producing a reservoir-and-dam effect, which slows the water down. [Color figure can be viewed at wileyonlinelibrary.com]

We estimated that a majority of ditch line erosion control treatments decreased calculated grain shear stress, and therefore modelled sediment transport, by almost 100%, producing fractional reductions near 1 (Figure 8d). In terms of measured sediment transport, we found that all treatments in our experimental runs produced some amount of sediment transport, including those with high roughness values. One site had a higher-than-expected sediment concentration value: sparse wattles during the initial installation (Figure 6). In the case of the sparse wattle initial installation, the measured sediment concentration value is high likely due to three factors: (1) The small amount of ditch below the final wattle had some erosion; (2) the ditch in which the wattles were installed had been recently disturbed and therefore had a larger amount of easily accessible sediment for transport; and (3) the wattles had a tendency to slightly float immediately after installation and, again, had a larger amount of easily accessible sediment for transport. Additionally, the sparse wattle installation had enough space between wattles that erosion and suspension of fine material was possible therein, especially at lower flows. Indeed, the spatial heterogeneity in grain shear stress is not fully accounted for in our modelling approach, which assumes uniform roughness and grain shear stress.

Overall, the decrease in measured sediment transport and calculated sediment transport capacities with erosion control treatment installation emphasizes the importance of ditch line erosion control treatment installation both from the perspective of ditch erosion reduction and potential mitigation of sediment transport from other elements within the road prism. Erosion control treatment installation can help reduce large ditch line erosion events, particularly immediately after road ditch grading (e.g., Luce & Black, 2001b) or new road construction (e.g., Megahan, 1974). Additionally, roads that are crowned or insloped allow for sediment from the road surface to

travel to the ditch line where erosion control treatments can mitigate the tread-derived sediment. However, due to traffic and road deformation, wheel ruts tend to form on the road surface, which can cause water and sediment to bypass ditch line erosion control treatments (Alvis et al., 2023). As discussed above, a rut on the road (Figure 2b) has a similar roughness to a bare (recently disturbed) ditch and therefore has a high likelihood of carrying sediment in its rill-like flow. The interaction between the ditch line and other elements of the road prism is more complex and requires further exploration.

While the results from our experiment are promising, we have a limited number of observations for a limited number of erosion control treatments. However, we are not in the realm of conjecture, as both ample theory and empirical evidence exist for estimating the link between added roughness and sediment mobility and transport (e.g., Kothiyari et al., 2009; Prosser et al., 1995; Thompson et al., 2004). Geomorphologically, both shear stress partitioning and the relationship between roughness and sediment transport are commonly utilized to estimate erosion and sedimentation in rivers and on vegetated hillslopes (e.g., Darby et al., 2010; Ferguson et al., 2019; Istanbuluoglu & Bras, 2005; Li, Venditti, et al., 2022). Regardless, future studies to empirically validate the relationship between roughness measurements and ditch line erosion control treatment sediment reduction, especially for a larger range of contexts and conditions, are warranted.

6 | CONCLUSION

Using the notion that the additional roughness of ditch line erosion control treatments can be used to examine their effectiveness—in

conjunction with existing theory surrounding shear stress partitioning—we evaluated several ditch line erosion control treatments. We found that (1) each erosion control treatment yielded consistent Manning's n values across multiple replications and sites, with a bare ditch (no treatment) having the lowest roughness ($n = 0.05$) and a densely wattled ditch having the highest roughness ($n = 0.75$); (2) when combined from each experiment, the sediment load and calculated grain shear stress data yielded a single positive relationship, which suggests the effect of additional roughness on grain shear stress is a main driver in the reduction of ditch line sediment load; and (3) our data demonstrated that fractional erosion reduction had a variable and nonlinear sensitivity to low flow rates (99% of observed flows) for lower roughnesses, which emphasizes the importance of context (i.e., climate and other conditions) in terms of fractional erosion reduction for a given treatment.

In contrast to the fixed sediment reductions determined through traditional engineering trials, the use of Manning's n and relevant established theory can allow for more rigorous extrapolation to other contexts and climates. Our study demonstrated that Manning's n , in tandem with shear stress partitioning in a sediment transport model, can be used in such a way for a few conditions and contexts. However, further research should be done to establish the use of roughness as a physical metric to evaluate erosion control treatment effectiveness for a wider range of conditions and contexts. Additionally, being able to characterize erosion control treatments with continuous numerical values would also pave the way for later empirical testing of the effect of additional ditch line roughness on overall road segment sediment production.

AUTHOR CONTRIBUTIONS

Conceptualization: Amanda D. Alvis, Charles H. Luce, Erkan Istanbuluoglu, Thomas Black, Julie Dieu, and Jenelle Black. **Data curation:** Amanda D. Alvis, Charles H. Luce, Thomas Black, and Jenelle Black. **Formal analysis:** Amanda D. Alvis, Charles H. Luce, Erkan Istanbuluoglu, and Thomas Black. **Funding acquisition:** Amanda D. Alvis, Charles H. Luce, Erkan Istanbuluoglu, Thomas Black, Julie Dieu, and Jenelle Black. **Investigation:** Amanda D. Alvis, Charles H. Luce, Erkan Istanbuluoglu, Thomas Black, Julie Dieu, and Jenelle Black. **Methodology:** Amanda D. Alvis, Charles H. Luce, Erkan Istanbuluoglu, Thomas Black, Julie Dieu, and Jenelle Black. **Project administration:** Charles H. Luce, Thomas Black, and Julie Dieu. **Resources:** Amanda D. Alvis, Charles H. Luce, Erkan Istanbuluoglu, Thomas Black, Julie Dieu, and Jenelle Black. **Software:** Amanda D. Alvis and Charles H. Luce. **Supervision:** Charles H. Luce, Erkan Istanbuluoglu, Thomas Black, and Julie Dieu. **Validation:** Amanda D. Alvis and Thomas Black. **Visualization:** Amanda D. Alvis and Charles H. Luce. **Writing—original draft preparation:** Amanda D. Alvis, Charles H. Luce, and Erkan Istanbuluoglu. **Writing—review and editing:** Amanda D. Alvis, Charles H. Luce, Erkan Istanbuluoglu, Thomas Black, Julie Dieu, and Jenelle Black.

ACKNOWLEDGEMENTS

This research was made possible by public funding through the Cooperative Monitoring, Evaluation, and Research (CMER) Committee within the Washington State Department of Natural Resources Adaptive Management Program. The authors thank Sam Calahan, Lauren Wittkopf, Bob Danehy, and Teresa Miskovic for helping with field

data collection and Alexander Prescott for helping with field data collection and logistical support.

CONFLICT OF INTEREST STATEMENT

The authors declare that there are no competing interests.

DATA AVAILABILITY STATEMENT

The data presented in this manuscript are not currently publicly available due to an agreement with the Cooperative Monitoring, Evaluation, and Research (CMER) Committee within the Washington State Department of Natural Resources Adaptive Management Program but are available from the corresponding author upon reasonable request and approval from CMER. Additionally, the data will be made publicly available in the future upon completion of the overarching project and CMER's approval of the final report.

ORCID

Amanda D. Alvis  <https://orcid.org/0000-0002-9662-1121>

REFERENCES

- Al-Hamdan, O.Z., Pierson, F.B., Nearing, M.A., Williams, C.J., Stone, J.J., Kormos, P.R., et al. (2013) Risk assessment of erosion from concentrated flow on rangelands using overland flow distribution and shear stress partitioning. *Transactions of the ASABE*, 56(2), 539–548. Available from: <https://doi.org/10.13031/2013.42684>
- Al-Hamdan, O.Z., Pierson, F.B., Robichaud, P., Elliot, W.J. & Williams, C.J. (2022) New erodibility parameterization for applying WEPP on rangelands using ERMIT. *Journal of the ASABE*, 65(2), 251–264. Available from: <https://doi.org/10.13031/ja.14564>
- Alvis, A.D., Luce, C.H. & Istanbuluoglu, E. (2023) How does traffic affect erosion of unpaved forest roads? *Environmental Reviews*, 31(1), 182–194. Available from: <https://doi.org/10.1139/er-2022-0032>
- Arcement, G.J. & Schneider, V.R. (1989) *Guide for selecting Manning's roughness coefficients for natural channels and flood plains*. USGS Numbered Series 2339. Washington, D.C.: U.S. Geological Survey. Available from: <https://doi.org/10.3133/wsp2339>.
- Aust, W.M., Bolding, M.C. & Barrett, S.M. (2015) Best management practices for low-volume forest roads in the Piedmont region: summary and implications of research. *Transportation Research Record*, 2472(1), 51–55. Available from: <https://doi.org/10.3141/2472-06>
- Barros, A.P. & Colello, J.D. (2001) Surface roughness for shallow overland flow on crushed stone surfaces. *Journal of Hydraulic Engineering*, 127(1), 38–52. Available from: [https://doi.org/10.1061/\(ASCE\)0733-9429\(2001\)127:1\(38\)](https://doi.org/10.1061/(ASCE)0733-9429(2001)127:1(38))
- Boston, K. (2016) The potential effects of forest roads on the environment and mitigating their impacts. *Current Forestry Reports*, 2(4), 215–222. Available from: <https://doi.org/10.1007/s40725-016-0044-x>
- Buffington, J.M. & Montgomery, D.R. (1997) A systematic analysis of eight decades of incipient motion studies, with special reference to gravel-bedded rivers. *Water Resources Research*, 33(8), 1993–2029. Available from: <https://doi.org/10.1029/96WR03190>
- Burroughs, E.R. & King, J.G. (1989) *Reduction of soil erosion on forest roads*. Ogden, UT: U.S. Department of Agriculture, Forest Service, Intermountain Research Station Available from: 10.2737/INT-GTR-264.
- Burroughs, E.R., Watts, F.J., King, J.G., Haber, D.F., Hansen, D. & Flerchinger, G. (1984) Relative effectiveness of rocked roads and ditches in reducing surface erosion. In: *21st Annual Engineering, Geology, and Soils Engineering Symposium*. Moscow, ID: University of Idaho, pp. 251–263.
- Cartwright, N. (2007) Are RCTs the gold standard? *BioSocieties*, 2(1), 11–20. Available from: <https://doi.org/10.1017/S1745855207005029>
- Chen, Y., Xing-nian, L. & Xie-kang, W. (2015) Effects of roughness elements distribution on overland flow resistance. *Journal of Mountain Science*, 12(5), 1145–1156. Available from: <https://doi.org/10.1007/s11629-014-3391-8>

- Collins, L.M. & Johnston, C.E. (1995) Effectiveness of straw bale dams for erosion control in the Oakland Hills following the fire of 1991. In: Keeley, J.E. & Scott, T. (Eds.) *Brushfires in California wildlands: ecology and resource management*. Fairfield, WA: International Association of Wildland Fire, pp. 171–183.
- Cristan, R., Aust, W.M., Bolding, M.C. & Barrett, S.M. (2019) Estimated sediment protection efficiencies for increasing levels of best management practices on forest harvests in the Piedmont, USA. *Forests*, 10(11), 997. Available from: <https://doi.org/10.3390/f10110997>
- Cristan, R., Aust, W.M., Bolding, M.C., Barrett, S.M., Munsell, J.F. & Schilling, E. (2016) Effectiveness of forestry best management practices in the United States: literature review. *Forest Ecology and Management*, 360, 133–151. Available from: <https://doi.org/10.1016/j.foreco.2015.10.025>
- Dangle, C.L., Bolding, M.C., Aust, W.M., Barrett, S.M. & Schilling, E.B. (2019) Best management practices influence modeled erosion rates at forest haul road stream crossings in Virginia. *JAWRA Journal of the American Water Resources Association*, 55(5), 1169–1182. Available from: <https://doi.org/10.1111/1752-1688.12762>
- Darby, S.E., Trieu, H.Q., Carling, P.A., Sarkkula, J., Koponen, J., Kumm, M., et al. (2010) A physically based model to predict hydraulic erosion of fine-grained riverbanks: the role of form roughness in limiting erosion. *Journal of Geophysical Research*, 115(F4), F04003. Available from: <https://doi.org/10.1029/2010JF001708>
- Donald, W.N., Zech, W.C., Fang, X. & LaMondia, J.J. (2013) Evaluation of wheat straw wattles for velocity reduction in ditch check installations. *Transportation Research Record: Journal of the Transportation Research Board*, 2358(1), 69–78. Available from: <https://doi.org/10.3141/2358-08>
- Edwards, P.J., Wood, F. & Quinlivan, R.L. (2016) *Effectiveness of best management practices that have application to forest roads*. General Technical Report NRS-163. Parsons, West Virginia, USA: USDA Forest Service Northern Research Station.
- Einstein, H.A. & Banks, R.B. (1950) Fluid resistance of composite roughness. *Transactions of the American Geophysical Union*, 31(4), 603–610. Available from: <https://doi.org/10.1029/TR031i004p00603>
- Einstein, H.A. & Barbarossa, N.L. (1952) River channel roughness. *Transactions of the American Society of Civil Engineers*, 117(1), 1121–1132. Available from: <https://doi.org/10.1061/TACEAT.0006666>
- Emmett, W.W. (1970) *The hydraulics of overland flow on hillslopes*. Report 662A. Washington, D.C.: U.S. Government Publishing Office. Available from: <https://doi.org/10.3133/pp662A>
- Engman, E.T. (1986) Roughness coefficients for routing surface runoff. *Journal of Irrigation and Drainage Engineering*, 112(1), 39–53. Available from: [https://doi.org/10.1061/\(ASCE\)0733-9437\(1986\)112:1\(39](https://doi.org/10.1061/(ASCE)0733-9437(1986)112:1(39)
- Ferguson, R.I., Hardy, R.J. & Hodge, R.A. (2019) Flow resistance and hydraulic geometry in bedrock rivers with multiple roughness length scales. *Earth Surface Processes and Landforms*, 44(12), 2437–2449. Available from: <https://doi.org/10.1002/esp.4673>
- Foster, G.R., Lane, L.J., Nearing, M.A., Finkner, S.C. & Flanagan, D.C. (1989) Erosion component. In: Lane, L.J. & Nearing, M.A. (Eds.) *USDA-water erosion prediction project: hillslope profile model documentation*. West Lafayette, IN: National Soil Erosion Research Lab (NSERL Report, 2), pp. 1–12.
- Govers, G. (1992) Evaluation of transporting capacity formulae for overland flow. In: *Overland flow: hydraulics and erosion mechanics*. New York: Chapman and Hall, pp. 243–273.
- Istanbulluoglu, E. & Bras, R.L. (2005) Vegetation-modulated landscape evolution: effects of vegetation on landscape processes, drainage density, and topography. *Journal of Geophysical Research*, 110(F2), F02012. Available from: <https://doi.org/10.1029/2004JF000249>
- Istanbulluoglu, E., Tarboton, D.G., Pack, R.T. & Luce, C. (2002) A probabilistic approach for channel initiation. *Water Resources Research*, 38(12), 611–614. Available from: <https://doi.org/10.1029/2001WR000782>
- Istanbulluoglu, E., Tarboton, D.G., Pack, R.T. & Luce, C. (2003) A sediment transport model for incision of gullies on steep topography. *Water Resources Research*, 39(4), 1103. Available from: <https://doi.org/10.1029/2002WR001467>
- Jordanova, A.A. & James, C.S. (2003) Experimental study of bed load transport through emergent vegetation. *Journal of Hydraulic Engineering*, 129(6), 474–478. Available from: [https://doi.org/10.1061/\(ASCE\)0733-9429\(2003\)129:6474](https://doi.org/10.1061/(ASCE)0733-9429(2003)129:6474)
- Kemper, W.D. & Rosenau, R.C. (1986) Aggregate stability and size distribution. In: Klute, A. (Ed.) *Methods of soil analysis*. Madison, WI: American Society of Agronomy-Soil Science Society of America, pp. 425–442. Available from: <https://doi.org/10.2136/sssabookser5.1.2ed.c17>
- Kothiyari, U.C., Hashimoto, H. & Hayashi, K. (2009) Effect of tall vegetation on sediment transport by channel flows. *Journal of Hydraulic Research*, 47(6), 700–710. Available from: <https://doi.org/10.3826/jhr.2009.3317>
- Lane, S.N. (2014) Acting, predicting and intervening in a socio-hydrological world. *Hydrology and Earth System Sciences*, 18(3), 927–952. Available from: <https://doi.org/10.5194/hess-18-927-2014>
- Laursen, E.M. (1958) The total sediment load of streams. *Journal of the Hydraulics Division*, 84(1), 1–36. Available from: <https://doi.org/10.1061/JYCEAJ.0000158>
- Le Bouteiller, C. & Venditti, J.G. (2015) Sediment transport and shear stress partitioning in a vegetated flow. *Water Resources Research*, 51(4), 2901–2922. Available from: <https://doi.org/10.1002/2014WR015825>
- Li, L., Nearing, M.A., Polyakov, V.O., Nichols, M.H., Pierson, F.B. & Cavanaugh, M.L. (2020) Evolution of rock cover, surface roughness, and its effect on soil erosion under simulated rainfall. *Geoderma*, 379, 114622. Available from: <https://doi.org/10.1016/j.geoderma.2020.114622>
- Li, T., Venditti, J.G., Rennie, C.D. & Nelson, P.A. (2022) Bed and bank stress partitioning in bedrock rivers. *Journal of Geophysical Research - Earth Surface*, 127(2), e2021JF006360.
- Li, X., Zhang, Y., Ji, X., Strauss, P. & Zhang, Z. (2022) Effects of shrub-grass cover on the hillslope overland flow and soil erosion under simulated rainfall. *Environmental Research*, 214(Pt 1), 113774. Available from: <https://doi.org/10.1016/j.envres.2022.113774>
- Likitlersuang, S., Kounyou, K. & Prasetyaningtiyas, G.A. (2020) Performance of geosynthetic cementitious composite mat and vetiver on soil erosion control. *Journal of Mountain Science*, 17(6), 1410–1422. Available from: <https://doi.org/10.1007/s11629-019-5926-5>
- Luce, C.H. & Black, T.A. (1999) Sediment production from forest roads in western Oregon. *Water Resources Research*, 35(8), 2561–2570. Available from: <https://doi.org/10.1029/1999WR900135>
- Luce, C.H. & Black, T.A. (2001a) Effects of traffic and ditch maintenance on forest road sediment production. In: *Proceedings of the Seventh Federal Interagency Sedimentation Conference*. Nevada: Reno, pp. V67–V74.
- Luce, C.H. & Black, T.A. (2001b) *Spatial and temporal patterns in erosion from forest roads*. Land use and watersheds: Human influence on hydrology and geomorphology in urban and forest areas, pp. 165–178.
- Manga, M. & Kirchner, J.W. (2000) Stress partitioning in streams by large woody debris. *Water Resources Research*, 36(8), 2373–2379. Available from: <https://doi.org/10.1029/2000WR900153>
- Megahan, W.F. (1974) *Erosion over time on severely disturbed granitic soils: a model*. Research Paper INT-156. Ogden, Utah: U.S.: Department of Agriculture Forest Service Intermountain Forest and Range Experiment Station, p. 20.
- Megahan, W.F., Wilson, M. & Monsen, S.B. (2001) Sediment production from granitic cut slopes on forest roads in Idaho, USA. *Earth Surface Processes and Landforms*, 26(2), 153–163. Available from: [https://doi.org/10.1002/1096-9837\(200102\)26:2<153::AID-ESP172>3.0.CO;2-0](https://doi.org/10.1002/1096-9837(200102)26:2<153::AID-ESP172>3.0.CO;2-0)
- Moore, R.D. (2005) Slug injection using salt in solution. *Streamline Watershed Management Bulletin*, 8(2), 1–6.
- Moore, I.D. & Burch, G.J. (1986) Sediment transport capacity of sheet and rill flow: application of unit stream power theory. *Water Resources Research*, 22(8), 1350–1360. Available from: <https://doi.org/10.1029/WR022i008p01350>
- Nearing, M.A., Foster, G.R., Lane, L.J. & Finkner, S.C. (1989) A process-based soil erosion model for USDA-water erosion prediction project

- technology. *Transactions of ASAE*, 32(5), 1587–1593. Available from: <https://doi.org/10.13031/2013.31195>
- Nepf, H.M. (2012) Flow and transport in regions with aquatic vegetation. *Annual Review of Fluid Mechanics*, 44(1), 123–142. Available from: <https://doi.org/10.1146/annurev-fluid-120710-101048>
- PRISM Climate Group. (2023) *Oregon State University*, <https://prism.oregonstate.edu>, data created 7 Feb 2023, accessed 7 Feb 2023.
- Prosser, I.P., Dietrich, W.E. & Stevenson, J. (1995) Flow resistance and sediment transport by concentrated overland flow in a grassland valley. *Geomorphology*, 13(1–4), 71–86. Available from: [https://doi.org/10.1016/0169-555X\(95\)00020-6](https://doi.org/10.1016/0169-555X(95)00020-6)
- Schussler, J.C., Kazaz, B., Perez, M.A., Blake Whitman, J. & Cetin, B. (2021) Field evaluation of wattle and silt fence ditch checks. *Transportation Research Record: Journal of the Transportation Research Board*, 2675(6), 281–293. Available from: <https://doi.org/10.1177/0361198121992073>
- Sojka, R.E., Bjorneberg, D.L., Entry, J.A., Lentz, R.D. & Orts, W.J. (2007) Polyacrylamide in agriculture and environmental land management. In: Sparks, D.L. (Ed.) *Advances in agronomy*. United States: Academic Press Inc., pp. 75–162. Available from: [https://doi.org/10.1016/S0065-2113\(04\)92002-0](https://doi.org/10.1016/S0065-2113(04)92002-0)
- Thompson, A.M., Wilson, B.N. & Hansen, B.J. (2004) Shear stress partitioning for idealized vegetated surfaces. *Transactions of ASAE*, 47(3), 701–709. Available from: <https://doi.org/10.13031/2013.16102>
- Tiscareno-Lopez, M., Lopes, V.L., Stone, J.J. & Lane, L.J. (1994) Sensitivity analysis of the WEPP watershed model for rangeland applications II: channel processes. *Transactions of ASAE*, 37(1), 151–158. Available from: <https://doi.org/10.13031/2013.28065>
- Tollner, E.W., Barfield, B.J., Vachirakornwatana, C. & Haan, C.T. (1977) Sediment deposition patterns in simulated grass filters. *Transactions of ASAE*, 20(5), 0940–0944. Available from: <https://doi.org/10.13031/2013.35679>
- United States Bureau of Reclamation. (2001) *Water measurement manual*. Washington, D.C.: U.S. Government Printing Office. Available at: <http://www.usbr.gov/tsc/techreferences/mands/wmm/> (Accessed: 7 September 2023).
- Whitman, J.B., Schussler, J.C., Perez, M.A. & Liu, L. (2021) Hydraulic performance evaluation of wattles used for erosion and sediment control. *Journal of Irrigation and Drainage Engineering*, 147(7), 04021028. Available from: [https://doi.org/10.1061/\(ASCE\)IR.1943-4774.0001586](https://doi.org/10.1061/(ASCE)IR.1943-4774.0001586)
- Wright, K.N. (2010) *Evaluation of check dams for sediment control on disturbed land surfaces*. M.S. Thesis. Urbana, IL: University of Illinois at Urbana-Champaign.
- Yager, E.M., Kirchner, J.W. & Dietrich, W.E. (2007) Calculating bed load transport in steep boulder bed channels. *Water Resources Research*, 43(7), W07418. Available from: <https://doi.org/10.1029/2006WR005432>
- Yetemen, O., Saco, P.M. & Istanbuluoglu, E. (2019) Ecohydrology controls the geomorphic response to climate change. *Geophysical Research Letters*, 46(15), 8852–8861. Available from: <https://doi.org/10.1029/2019GL083874>

How to cite this article: Alvis, A.D., Luce, C.H., Istanbuluoglu, E., Black, T., Dieu, J. & Black, J. (2024) Using additional roughness to characterize erosion control treatment effectiveness in roadside ditch lines. *Earth Surface Processes and Landforms*, 49(4), 1255–1272. Available from: <https://doi.org/10.1002/esp.5763>

APPENDIX A: SHEAR STRESS PARTITIONING RATIOS

As discussed in Section 2.1 of the main text, Einstein and Barbarossa (1952) proposed to partition shear stress into various components such as the shear stress that acts upon sediment grains and the shear stress that acts upon forms in the channel (e.g., bed forms and vegetation).

$$\tau_t = \rho_w g R S, \quad (\text{A1})$$

$$\tau_t = \tau_g + \tau_a, \quad (\text{A2})$$

where τ_g is the grain shear stress and τ_a is the additional shear stress. ρ_w is the density of water, g is the acceleration due to gravity, R is the hydraulic radius, and S is the channel slope.

In this appendix, we take this knowledge and look at the partitioning ratio of grain shear stress to total bed shear stress (Section 2.1 and Equation 2) using different approximations.

A.1 | General form with velocity term

Starting with Manning's equation and rearranging, we can obtain the hydraulic radius, R , of the channelized flow as a function of flow velocity, U , roughness, n , and slope, S :

$$U = \frac{R^{2/3} S^{1/2}}{n} \quad (\text{Manning}),$$

$$\Rightarrow R = \left(n \frac{U}{S^{1/2}} \right)^{3/2}. \quad (\text{A3})$$

Following the logic of Laursen (1958), Equation (A3) can be used for obtaining the grain component hydraulic radius, R_g , given an average flow velocity in the channel:

$$R_g = \left(n_g \frac{U}{S^{1/2}} \right)^{3/2}, \quad (\text{A4})$$

where n_g is the grain roughness.

In the same form as Equation (A1), the effective shear stress acting on the grains, τ_g , can be written as

$$\tau_g = \rho_w g R_g S,$$

$$\tau_g = \rho_w g n_g^{3/2} U^{3/2} S^{1/4}, \quad (\text{A5})$$

where ρ_w is the density of water and g is the acceleration of gravity.

For the shear stress partitioning ratio ($f_g = \frac{\tau_g}{\tau_t}$), we combine Equations (A1), (A3), and (A5) to get

$$\frac{\tau_g}{\tau_t} = \frac{n_g^{3/2} \rho_w g U^{3/2} S^{1/4}}{n_t^{3/2} \rho_w g U^{3/2} S^{1/4}},$$

$$\frac{\tau_g}{\tau_t} = \left(\frac{n_g}{n_t} \right)^{3/2}. \quad (\text{A6})$$

Using this standard form of shear stress partitioning ratio maintains a dependency on constant velocity, and the resulting shear stress partitioning ratio is proportional to the ratio of grain roughness to total roughness raised to the 1.5 power.

A.2 | General form with no velocity term

In this subsection, we take the general form of the shear stress partitioning ratio and remove the dependency on constant velocity to get the equation in terms of fewer dependent variables. To do so, we write velocity as $U = \frac{Q}{A}$ and substitute in $A = \frac{R^2}{C}$ (sensu Istanbuloglu et al., 2003; Moore & Burch, 1986), where C is a constant that is based on channel shape:

$$U = \frac{QC^2}{R^2}. \quad (\text{A7})$$

Using these substitutions, we can rewrite Manning's equation for Q and solve for R :

$$Q = \frac{1}{nC^2} R^{8/3} S^{1/2},$$

$$\Rightarrow R = \left[\frac{nC^2}{S^{1/2}} \right]^{3/8} Q^{3/8}. \quad (\text{A8})$$

Again, following the logic of Laursen (1958), R can be written for grain or total roughness as

$$R_g = \left[\frac{n_g C^2}{S^{1/2}} \right]^{3/8} Q^{3/8},$$

$$R_t = \left[\frac{n_t C^2}{S^{1/2}} \right]^{3/8} Q^{3/8}. \quad (\text{A9})$$

Recalling Equation (A7), we can now express U as a function of Q , n , and S :

$$U = \frac{C^{1/2}}{n^{3/4}} Q^{1/4} S^{3/8}. \quad (\text{A10})$$

We now have all the pieces needed to calculate the shear stress partitioning ratio. From Equation (A2) and Manga and Kirchner (2000), we have

$$\tau_t = \tau_g + \tau_a,$$

$$\rho_w g R_t S = \rho_w C_{dg} U^2 + \rho_w C_{da} U^2,$$

or

$$\rho_w g R_t S = \rho_w C_{dt} U^2, \quad (\text{A11})$$

where $C_{dt} = C_{dg} + C_{da}$. And for bare conditions, we have

$$\tau_t = \tau_g,$$

$$\rho_w g R_g S = \rho_w C_{dg} U^2, \quad (\text{A12})$$

which we can use to solve for C_{dg} (and C_{dt}):

$$C_{dg} = \frac{g R_g S}{U^2}. \quad (\text{A13})$$

Substituting Equations (A9) and (A10):

$$C_{dg} = \frac{g \left[\frac{n_g C^2}{S^{1/2}} \right]^{3/8} Q^{3/8} S}{\left[\frac{C^{1/2}}{n_g^{3/4}} Q^{1/4} S^{3/8} \right]^2},$$

$$C_{dg} = \frac{g \left[\frac{n_g^{3/8} C^{3/4}}{S^{1/16}} \right] Q^{3/8} S}{\frac{C}{n_g^{3/2}} Q^{1/2} S^{3/4}},$$

$$C_{dg} = g n_g^{15/8} C^{-1/4} Q^{-1/8} S^{1/16}. \quad (\text{A14})$$

And it follows that C_{dt} takes on the same form:

$$C_{dt} = n_t^{15/8} C^{-1/4} Q^{-1/8} S^{1/16} g. \quad (\text{A15})$$

Our shear stress partitioning ratio, then, is

$$\frac{\tau_g}{\tau_t} = \frac{\rho_w g n_g^{15/8} C^{-1/4} Q^{-1/8} S^{1/16} U^2}{\rho_w g n_t^{15/8} C^{-1/4} Q^{-1/8} S^{1/16} U^2},$$

$$\frac{\tau_g}{\tau_t} = \left(\frac{n_g}{n_t} \right)^{15/8}. \quad (\text{A16})$$

The resulting shear stress partitioning ratio here is proportional to the ratio of grain roughness to total roughness raised to the 1.875 power.

A.3 | Parabolic channel approximation with reduced dimensionality

In this subsection, we again take the general form of the shear stress partitioning ratio and remove the dependency on constant velocity to get the equation in terms of fewer dependent variables. Additionally, we use a parabolic approximation to further reduce the required variables.

In this case, we will follow a similar set of steps to Section A.2, but instead of using $A = \frac{R^2}{C^2}$ to calculate A , we instead use two simplifications: one for a parabolic channel's area, A , and one for the parabolic approximation of wetted perimeter, P , and hydraulic radius, R , assuming that the shape of water flow is wide and shallow:

$$A = \frac{a}{6} w^3, \quad (\text{A17})$$

$$P \approx w, \quad (\text{A18})$$

$$R = \frac{A}{P} \approx \frac{a}{6} w^2, \quad (\text{A19})$$

where a is the parameter that determines the shape of a parabola and w is the top width of the channel flow.

We can substitute $w =$ into Equation (A17):

$$A = \frac{a}{6} \left(\frac{6}{a} R \right)^{3/2},$$

$$A = \sqrt{\frac{6}{a}} R^{3/2}, \quad (\text{A20})$$

which we can substitute into Manning's equation and solve for R :

$$Q = \frac{1}{n} \sqrt{\frac{6S}{a}} R^{3/2} R^{2/3} = \frac{1}{n} \sqrt{\frac{6S}{a}} R^{13/6}, \quad (\text{A21})$$

$$\Rightarrow R = \left(\frac{nQ}{\sqrt{\frac{6S}{a}}} \right)^{6/13}. \quad (\text{A22})$$

Plugging Equation (A22) back into Equation (A20) to get A in terms of n , Q , S , and a :

$$A = \sqrt{\frac{6}{a}} \left(\frac{nQ}{\sqrt{\frac{6S}{a}}} \right)^{6/13+3/2} = \sqrt{\frac{6}{a}} \left(\frac{nQ}{\sqrt{\frac{6S}{a}}} \right)^{9/13}. \quad (\text{A23})$$

Getting the velocity, U , in the same terms:

$$U = \frac{Q}{A} = Q \sqrt{\frac{a}{6}} \left(\frac{nQ}{\sqrt{\frac{6S}{a}}} \right)^{-9/13}. \quad (\text{A24})$$

And calculating U^2 for ease of future arithmetic:

$$U^2 = Q^2 \frac{a}{6} \left(\frac{nQ}{\sqrt{\frac{6S}{a}}} \right)^{-18/13}$$

$$U^2 = \frac{Q^2 S^{9/13} \left(\frac{6}{a} \right)^{9/13}}{n^{18/13} Q^{18/13} \left(\frac{6}{a} \right)}$$

$$U^2 = \frac{Q^{8/13} S^{9/13}}{n^{18/13} \left(\frac{6}{a} \right)^{4/13}} \quad (\text{A25})$$

Following the logic of Section A.2 and using the forms of Equations (A12) through (A14), we can get C_{dg} in terms of n , Q , S , and a , too:

$$\begin{aligned}
 C_{dg} &= \frac{gR_g S}{U^2} \\
 C_{dg} &= \frac{g \left(\frac{n_g Q}{\sqrt{\frac{\delta}{a}}} \right)^{6/13} S}{Q^{8/13} S^{9/13} n_g^{18/13} \left(\frac{\delta}{a} \right)^{4/13}} \\
 C_{dg} &= \frac{g n_g^{6/13} Q^{6/13} S n_g^{18/13} \left(\frac{\delta}{a} \right)^{4/13}}{Q^{8/13} S^{9/13} S^{3/13} \left(\frac{\delta}{a} \right)^{3/13}} \\
 C_{dg} &= g n_g^{24/13} Q^{-2/13} S^{1/13} \left(\frac{\delta}{a} \right)^{1/13}
 \end{aligned} \tag{A26}$$

And it follows that C_{dt} takes on the same form:

$$C_{dt} = n_t^{24/13} Q^{-2/13} S^{1/13} \left(\frac{\delta}{a} \right)^{1/13} g. \tag{A27}$$

Our shear stress partitioning ratio, then, is

$$\begin{aligned}
 \frac{\tau_g}{\tau_t} &= \frac{\rho_w g n_g^{24/13} Q^{-2/13} S^{1/13} \left(\frac{\delta}{a} \right)^{1/13} U^2}{\rho_w g n_t^{24/13} Q^{-2/13} S^{1/13} \left(\frac{\delta}{a} \right)^{1/13} U^2} \\
 \frac{\tau_g}{\tau_t} &= \left(\frac{n_g}{n_t} \right)^{24/13}
 \end{aligned} \tag{A28}$$

The resulting shear stress partitioning ratio here is proportional to the ratio of grain roughness to total roughness raised to the 1.85 power.

Spatiotemporal evolution of forest road rutting and flow pathways

(Draft)

Amanda D. Alvis, Charles Luce, Friedrich Knuth, Lauren Wittkopf, David Shean, Gregory Stewart, Erkan Istanbulluoglu

Abstract

Ruts are one of the most common types of surface deformation seen on unpaved forest roads. Historically, the rate and magnitude of rut development have been studied using cross-sectional analyses. While elevational cross sections are a straightforward way to examine the development of ruts, this type of analysis lacks spatial distribution. More recently, remote sensing techniques, such as structure-from-motion (SfM), have demonstrated their utility in detecting ruts on forest roads but applications of these data are limited. Here we used SfM, with validation from terrestrial LiDAR scanning (TLS), to examine the development of ruts on forest roads in a spatially-comprehensive manner. We carried out a small-scale field experiment at two field sites in western Washington using unoccupied aerial vehicles (UAVs) to obtain digital elevation models (DEMs) of mainline logging road surfaces over three seasons. These UAV-derived (SfM) DEMs were used in an elevation change analysis and in a simple flow routing model to examine the evolution of ruts, especially with respect to the road surface flow pathways and erosion potential. We found that: (1) the relationship between our measure of rut incision and time since grading was nonlinear at both sites for all seasons with sufficient data; (2) as ruts develop, the overall flow pathways shift down-road; and (3) the erosion potential of our road surfaces tended to increase overall as ruts developed, with maximum increases of 30-120%. Our results demonstrate the advantage of using SfM DEMs for analysis of rut evolution over cross-sections alone. Additionally, our results give us insight into how rutting may affect the utilization of erosion control treatments in roadside ditch lines and the sediment yield of the road surface.

1. Introduction

Forest roads are subject to a number of stressors that lead to road deformation, such as heavy traffic and rainfall. Road surface deformation commonly presents as ruts and rill-like incisions typically formed by traffic that straddles the centerline or crown of a road surface. Forest roads are typically crowned to allow water to drain as sheetflow to either side of the road (Figure 1a; Figure 2a). However, when ruts develop due to traffic, water on the road surface is instead diverted down the road (Figure 1b), which has multiple implications regarding forest road erosion. One problem is that, water diverted down the road is unable to make use of any erosion control treatments in the roadside ditch lines (e.g., Sheridan et al., 2006; Figure 2b). Additionally, ruts cause channelized flow, and thus have more capacity to carry sediment (Foltz & Truebe, 1995; Ziegler et al., 2001; Figure 2c).

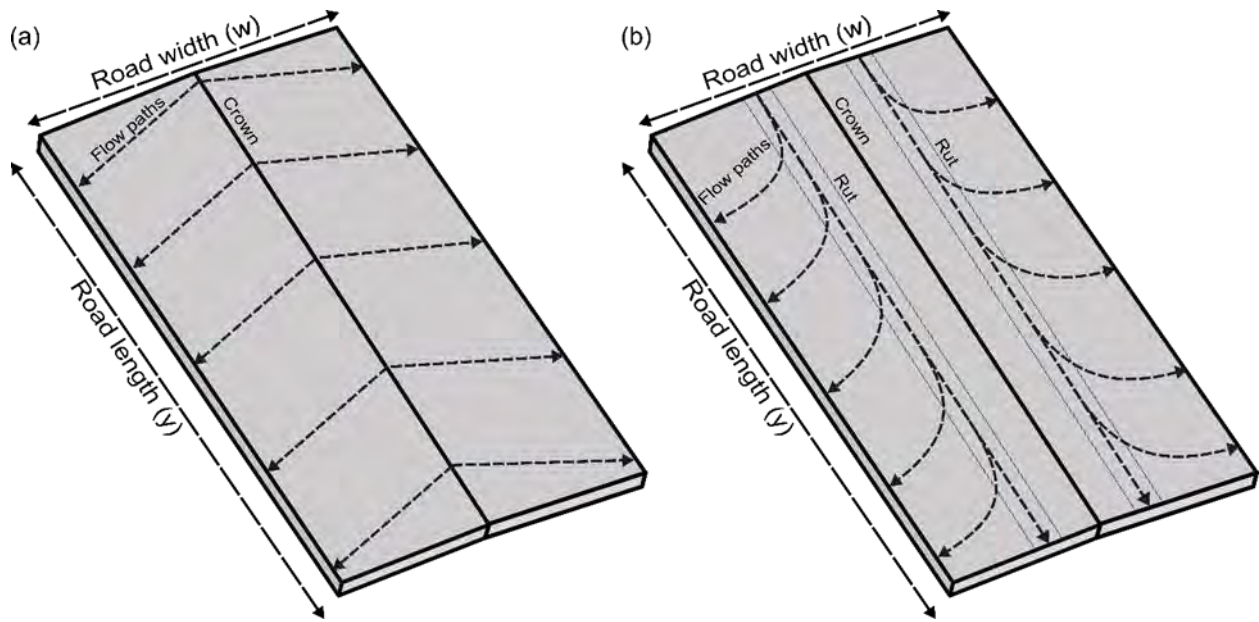


Figure 1. Schematic of a crowned road segment showing the flow pathways for (a) an idealized (i.e., perfectly smooth) road surface and (b) a rutted road surface.



Figure 2. Example photos of (a) an un-rutted road with flow heading to the ditch line from the center of the road; (b) water traveling down-road in a wheel rut instead of being directed to the roadside ditch; and (c) a heavily rutted road with channelized, sediment-laden flow heading down-road. The road widths seen in each of these photos are approximately 5 meters.

The development and impact of rutting on forest roads has been the topic of study for decades. As early as the 1980s, ruts were denoted as a source of increased fine sediment on forest roads (e.g., Burroughs & King, 1989; Reid & Dunne, 1984), with later studies looking at maintenance techniques to mitigate rutting (e.g., Bradley, 1994; Fannin & Sigurdsson, 1996; Foltz & Elliot, 1997; Sugden & Woods, 2007). In more recent years, studies have shifted to focus on the development of rutting, specifically looking at how quickly or to what depth ruts form (e.g., Akgul et al., 2017; Nevalainen et al., 2017). In just the last few years, studies have begun to use remote sensing techniques, such as terrestrial LiDAR scanning (TLS) or photogrammetry techniques (e.g., Cao et al., 2021; Yurtseven et al., 2019), rather than more traditional physical measurements (e.g., Fannin & Sigurdsson, 1996; Foltz, 1994).

Most studies evaluating ruts are either carried out on recently-built roads, or roads with soft soils where ruts develop deep and fast (e.g., Fannin & Sigurdsson, 1996; Toman & Skaugset, 2011), or on non-mainline roads such as skid trails or forest soils for logging operations (e.g., Cambi et al., 2015; Machuga et al., 2023; Uusitalo et al., 2020; Venanzi et al., 2023). Even if the studies are carried out on more established forest roads, their focus is typically on the advancement of data collection methods (e.g., Aydin et al., 2019; Dobson et al., 2014; El Issaoui et al., 2021; Hrůza et al., 2018; Türk et al., 2022). Additionally, earlier studies use cross-sectional analyses to examine the magnitude (i.e., depth) of ruts (e.g., Fannin & Sigurdsson, 1996; Foltz, 1994), but such techniques offer no information regarding the flow pathways on the road surface. Understanding the flow pathways on the road surface is critical for

determining the effectiveness of maintaining the road surface to reduce sediment delivery from the established road network.

Mainline logging roads have heavy traffic and are some of the largest sources of anthropogenic sediment in nearby streams (Cissel et al., 2014; W. F. Megahan & Kidd, 1972; Reid & Dunne, 1984), and roads with ruts can produce 2 to 5 times more sediment than roads without ruts (Foltz & Burroughs, 1990). We lack detailed, quantifiable information about rut formation and their impacts on mainline logging roads, specifically with respect to the alteration of flow pathways on the road surface. Thus, information regarding rut formation and the alteration of flow pathways is important to plan for mainline logging road maintenance to reduce fine sediment yields and assess the effectiveness of roadside ditch lines in trapping sediment.

To bridge this knowledge gap, we carried out a series of unoccupied aerial vehicle (UAV) structure-from-motion (SfM) surveys, with validation from TLS, to examine how wheel ruts evolve on mainline logging roads following road grading. We used differences between digital elevation models (DEMs) to assess the evolution of these ruts in terms of their incision and used a basic flow routing model to assess their impacts on the drainage system and erosion potential of the road segment. This paper presents the results from the aforementioned surveys to help us answer the following questions:

1. What are the temporal trends of rut formation on mainline logging roads?
2. How does rut evolution affect road surface flow pathways?
3. How do ruts affect the erosion potential of the road surface?

We first discuss the field study area and data acquisition methods, followed by the creation of DEMs and analyses of the elevation change, drainage system, and erosion potential. We present our results and finish with a discussion of the implications of this work.

2. Methods and data

2.1. Field study area

We carried out UAV and TLS surveys in two regions of southwest Washington state: (1) a volcanic lithology near Mount Saint Helens and (2) a siltstone lithology near Aberdeen, WA (Figure 3). Each region contains multiple field sites located on mainline logging roads as part of a broad study conducted by the Cooperative Monitoring Evaluation and Research Committee within the Washington Department of Natural Resources Adaptive Management Program. One field site in each of the aforementioned regions was chosen for our UAV SfM and TLS surveys (KID-13 in the volcanic lithology and MEL-14 in the siltstone lithology). The field sites are relatively straight 80-meter segments of road delineated by 4.572-meter water bars placed at the top and bottom thereof to help drain the road surface to the roadside ditch line. KID-13 has an average gradient of 6% and is located approximately 278 meters (911 feet) above sea level. MEL-14 has an average gradient of 10% and is located approximately 185 meters (606 feet) above sea level. From our broader study, we obtained preliminary traffic count data for October 2021 to April 2022 at MEL-14 and November 2021 to June 2022 at KID-13. Over their respective durations, MEL-14 received heavy traffic (on average, 7 trucks per day), where heavy traffic is defined as five or more logging truck passes per day (Reid, 1981), and KID-13 received light traffic, where light traffic is defined as no logging trucks but some light vehicles (Reid, 1981). On average, KID-13 receives 1560 mm of annual precipitation, and MEL-14 receives 2400 mm of annual precipitation (PRISM Climate Group, 2023), with most of the precipitation occurring between October and April.

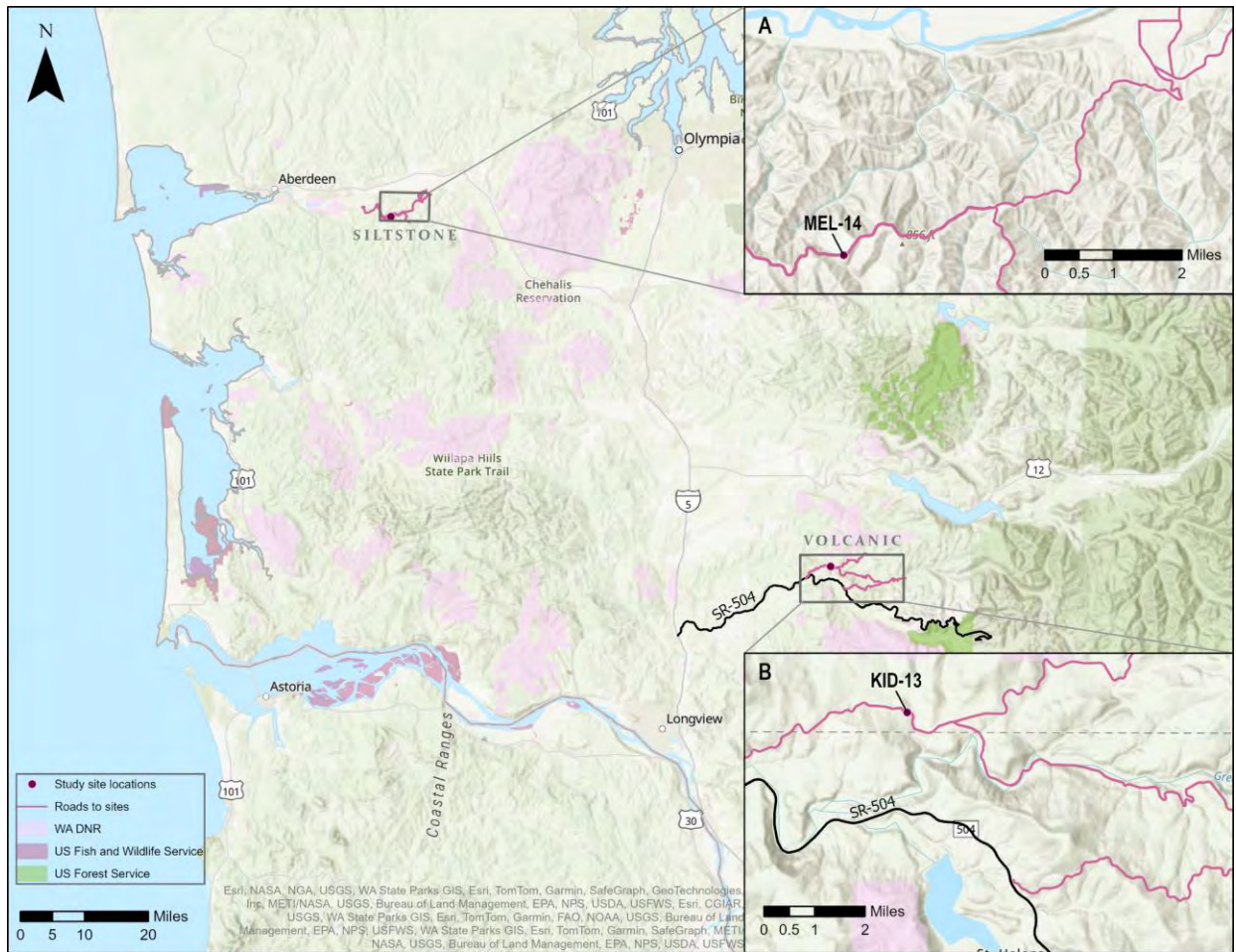


Figure 3. Map of field site locations in Washington state. Inset A shows MEL-14, the field site in the siltstone lithology and inset B shows KID-13, the field site in the volcanic lithology.

2.2. Data acquisition

UAV and TLS surveys were conducted over three subsequent seasons (wet, dry, wet) between November 2020 and June 2022 (Table 1). At the beginning of the first wet season (wet season year 1, Wet1), each site had good quality aggregate added to the surface and was graded. Subsequent seasons (dry season year 1, Dry1; wet season year 2, Wet2) began once the road segments were regraded. At KID-13, all three seasons of surveys consisted of longer time periods between surveys (i.e., a range of 1-4 months between surveys) to look at the longer-term temporal trends of rut development on a road segment. At MEL-14, the first two seasons consisted of longer time periods between surveys whereas the final season consisted of more frequent surveys (i.e., a range of 1-5 weeks between surveys) to look at the shorter-term temporal trends of rut development on a road segment.

For ground-truthing of the UAV surveys and to align and coregister surveys at different time slices, 24 ground control points (GCP) were installed at each site. These ground control points were 10-inch nails hammered in along the sides of the road segments—12 on each side—and spray painted for extra visibility. The spatial coverage of GCPs was limited to the sides of the road segment as we could not guarantee the safety of traffic nor the stability of the GCPs if they were placed in the road prism itself. Two additional monuments were installed off the road at each site for TLS survey use.

The locations of the GCPs were measured in an arbitrary coordinate system at the beginning and end of a season using a Trimble SX10 Scanning Total Station to ensure that the GCPs had not migrated. At KID-13, the variation in repeat survey GCP locations was small (on average, less than 1 mm) and was assumed to be random error. As such, the mean survey location for each GCP was used for data processing at KID-13. At MEL-14, multiple GCPs were ripped out between seasons during grading, so the GCPs had to be reset at the beginning of each season. As such, locations recorded at the beginning of each season were used for data processing at MEL-14.

To map rut formation on these road segments, UAV and TLS surveys were conducted in tandem. Multiple UAV surveys were conducted within each season, whereas the TLS surveys were conducted only at the beginning and end of each season (Table 1). The main goal was to use UAV SfM for analysis, with the initial TLS survey for each season serving as a reference baseline dataset, due to TLS inherently providing validated data (e.g., Wilkinson et al., 2016). The TLS surveys used a Trimble SX10 Scanning Total Station and required three locations for scanning the full road surface. Each TLS survey yielded high-resolution point cloud data.

The UAV SfM surveys were carried out with a Phantom 4 Pro DJI drone with RC controller and all flights were done manually due to high tree cover and lack of good global navigation satellite system (GNSS) lock. Each UAV survey consisted of three flights: (1) lower flight elevation (~5 meters above ground level) up and down the road segment with the camera nadir; (2) lower flight elevation (~5 m agl) around the road segment with the camera at an angle; and (3) higher flight elevation (~10-15 m agl) up the road segment with the camera nadir. The UAV SfM surveys collected high-overlap, high-resolution photographs to be processed using photogrammetric techniques.

Table 1. Survey seasons, dates, types, and times since baseline at each field site.

Site	Season	Date of survey	Type of survey	Time since baseline (months)
KID-13	Wet season year 1 (Wet1)	11/09/2020	UAV; TLS	0
		02/08/2021	UAV	3
		04/06/2021	UAV	5
		05/13/2021	UAV; TLS	6
	Dry season year 1 (Dry1)	06/04/2021	UAV; TLS	0
		08/19/2021	UAV	2.5
		09/13/2021	UAV; TLS	3.5
	Wet season year 2 (Wet2)	10/07/2021	UAV; TLS	0
		02/08/2022	UAV	4
		05/03/2022	UAV	7
		05/31/2022	UAV; TLS	8
	MEL-14	Wet1	12/03/2020	UAV; TLS
02/24/2021			UAV	2.5
04/12/2021*			UAV*	4.5*
Dry1		06/03/2021	UAV; TLS	0
		09/14/2021	UAV; TLS	3.5
Wet2		03/09/2022	UAV; TLS	0
		03/16/2022	UAV	0.25
		03/24/2022	UAV	0.5
		04/11/2022	UAV	1
		04/28/2022	UAV	1.75
		06/01/2022	UAV; TLS	3

*This survey was rendered unusable due to unforeseen interim road work.

2.3. TLS and UAV DEM post-processing

Post-processing of TLS and UAV data was done using CloudCompare and Pix4DMapper, respectively. The TLS data were processed such that the DEMs of the road surface had 1 cm resolution in an arbitrary coordinate system. To process the UAV data and ensure accurate representation of the road surface, we manually selected high-precision GCP locations collected at each site. The data products of the UAV data

post-processing included high-resolution orthoimages and UAV-derived DEMs with 1 cm resolution in an arbitrary coordinate system (Figure 4).

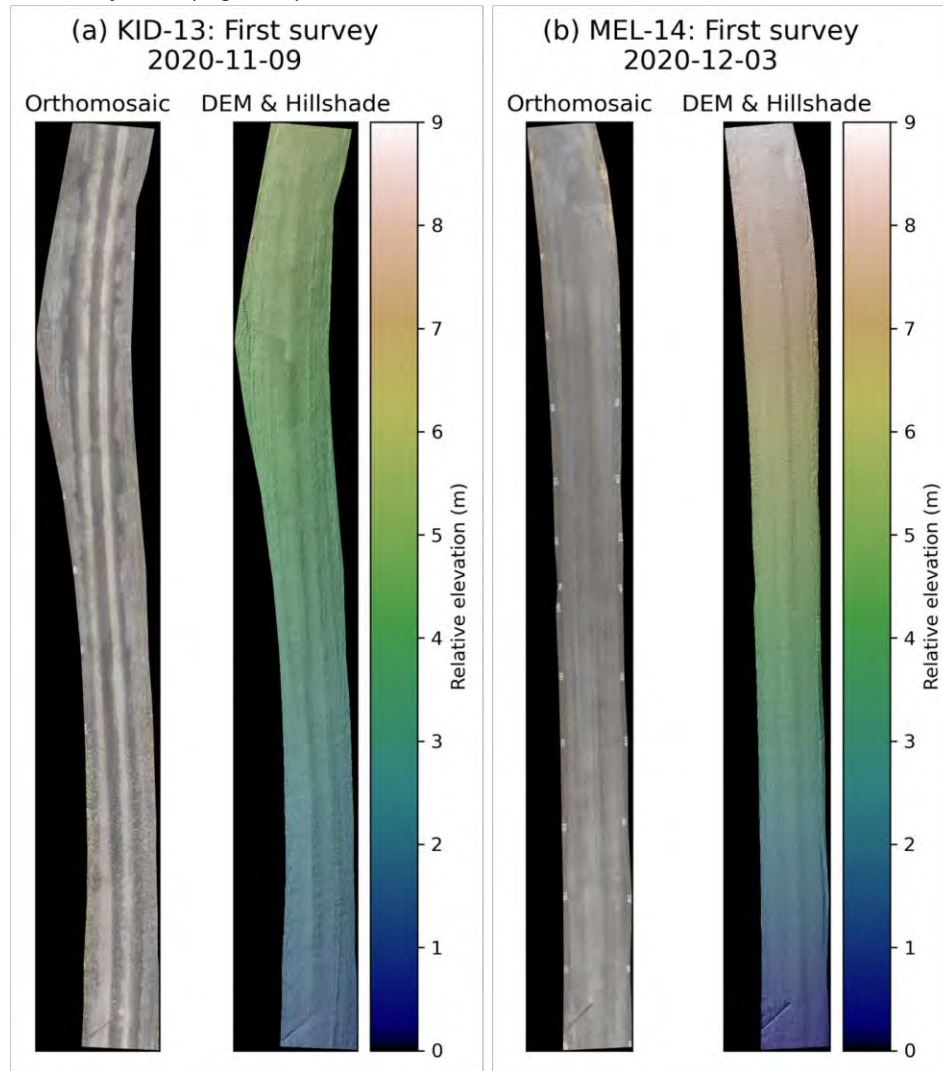


Figure 4. Example orthomosaic (left) and color-shaded relief map (right) for the first UAV SfM survey at the (a) KID-13 and (b) MEL-14 sites.

To analyze the development of wheel ruts over time, DEMs were reprojected on a common grid and subtracted from one another. The initial TLS-derived (LiDAR) DEM for each season was used as a reference dataset to coregister all UAV-derived (SfM) DEMs. Following co-registration, the SfM DEMs were subtracted from the baseline SfM survey of each season (Figure 5). We also examined the season-spanning LiDAR DEM difference maps for additional validation (Figure 5, far right panel). Initial difference maps of the SfM DEMs showed systematic error in the form of a longitudinal undulation pattern (Figure 5a). The longitudinal undulation artifacts seen in our SfM datasets are likely introduced during the initial alignment and camera model optimization step of data processing and create errors that can propagate to subsequent analysis steps (Tarekegn & Sayama, 2013). These artifacts likely arose from our SfM survey geometry (i.e., very low altitude flights due to canopy, e.g., Mueller et al., 2023). Here we used a high-pass Gaussian filter, which is a common signal-processing technique used to remove undulation artifacts through attenuating low-frequency waveforms such that only the high-frequency waveforms (i.e., the elevation change signals) remain (Figure 5b).

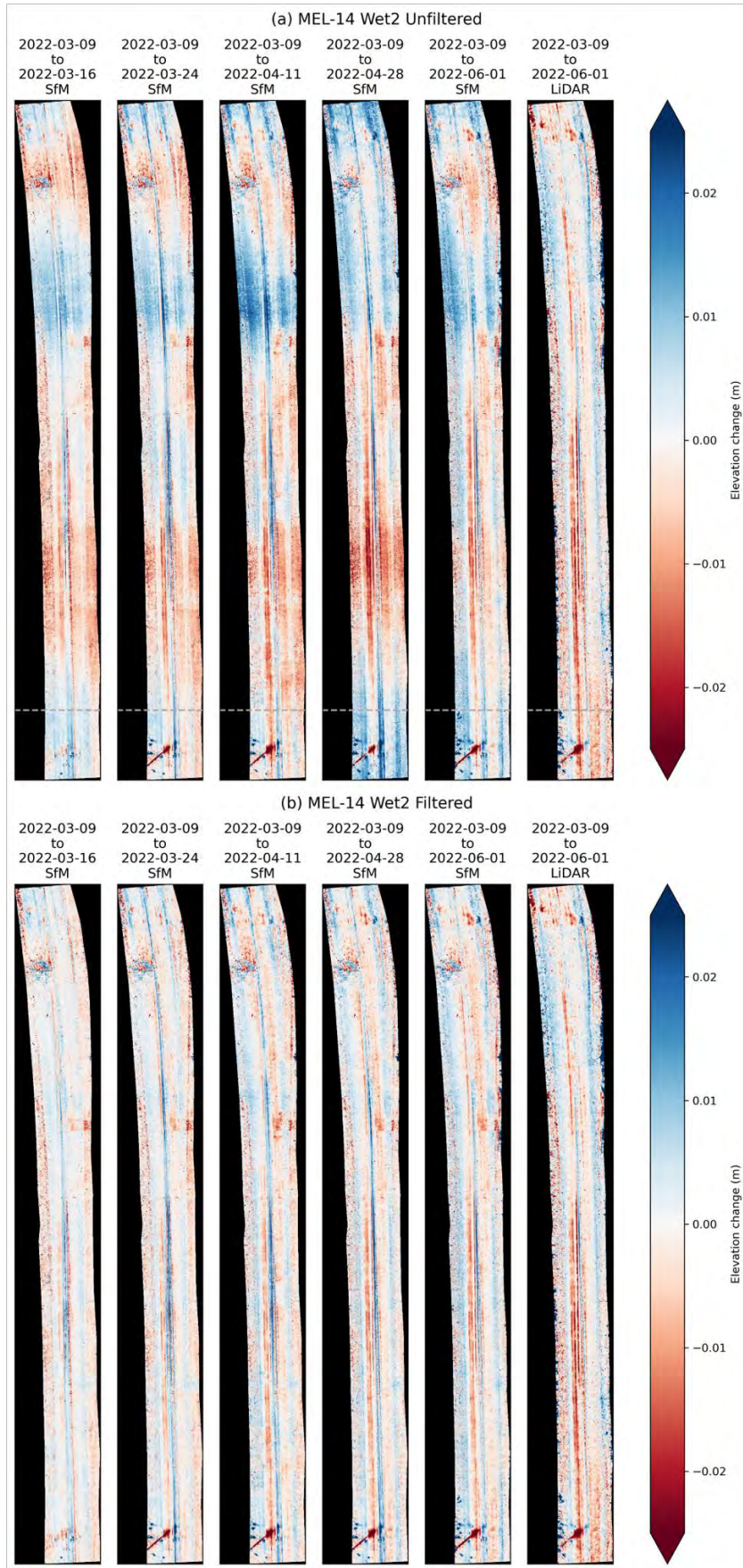


Figure 5. Example elevation change maps for the time series of the (a) original and (b) filtered surveys at MEL-14 during the second wet season (Wet2). The gray dashed lines in (a) denote the location of the cross section in Figure 6. The LiDAR data (far right panel) are shown for comparison and were not processed using a high-pass Gaussian filter.

2.4. UAV DEM elevation change analysis

One potential method to examine the depth of wheel ruts is to look at cross-sectional profiles of the road surface at different longitudinal locations, such as in Fannin & Sigurdsson (1996). While the cross-sectional profiles do show the development of ruts (e.g., Figure 6), this method is insufficient and problematic for analyzing our surveys for several reasons. The vertical scale of ruts developing on our survey segments is small and highly variable along the longitudinal axis of the road (i.e., different cross sections have different rut magnitudes and shapes). This variation precludes a succinct description of road surface behavior with respect to rut development using cross sections alone. Additionally, the artificial longitudinal undulation pattern seen in Figure 5a is present in the cross-sectional profiles: where we expect the profile of 03-09-2022 to be the highest elevation, we instead see 03-16-2022 and 04-28-2022 plotting above 03-09-2022 (Figure 6). And lastly, cross-sectional analysis does not take advantage of the entire high-resolution data.

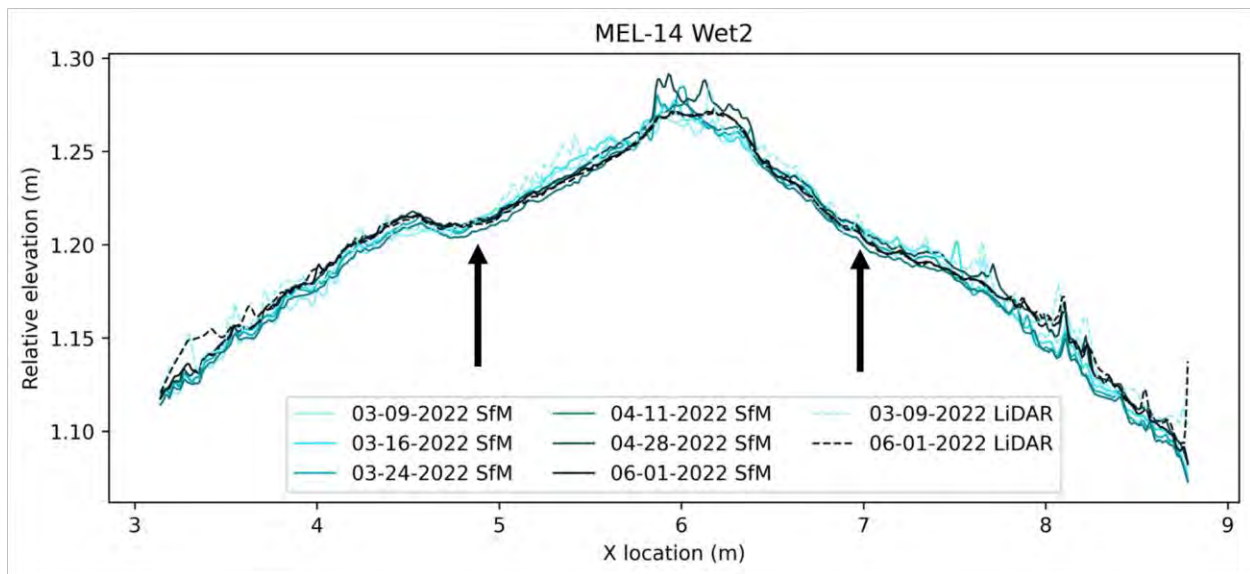


Figure 6. Cross-sectional profiles (location denoted by gray dashed line in Figure 5b) of unoccupied aerial vehicle (UAV)-derived digital elevation model (DEM) and terrestrial LiDAR scanning (TLS)-derived DEM time series' at MEL-14 during the second wet season (Wet2). The development of ruts is denoted by the black arrows on either side of the road crown.

To examine how the entire road surface evolves over time, we used the filtered differenced DEMs to determine the empirical cumulative distribution functions (eCDFs) of elevation change across the full domain (Figure 7). For shorter survey time periods, the eCDF has a smaller variance, indicating minimal change to the road surface. Longer survey time periods, however, have a larger variance, indicating that the micro-topography of the road surface has become more heterogeneous.

Though we removed the longitudinal undulation pattern artifact with our high-pass Gaussian filter, other artifacts and random errors (i.e., noise) are still present in the differenced SfM DEMs. To avoid these artifacts and errors—which exist on the extreme ends of our eCDFs of elevation change—we used the

5th percentile of the eCDF of elevation change as a measure for rut incision of a given time period. We chose the 5th percentile to represent rut incision as ruts tend to constitute the largest incisions in elevation change data and their depths are more uniform than rills caused by overland flow. As such, the cumulative rut incision depth over a given season is assumed to be the 5th percentile of elevation change for the final survey of the season.

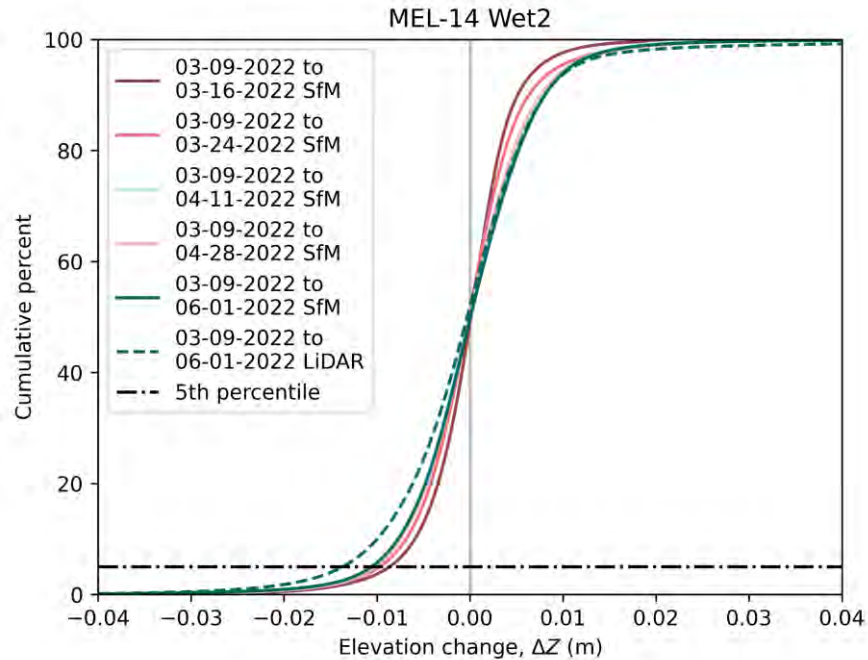


Figure 7. Empirical cumulative distribution function (eCDF) of elevation change for the full domain at MEL-14 during the second wet season (Wet2). As the length of time between surveys increases, the variance of the elevation change also increases, indicating more heterogeneity in the micro-topography of the road surface. The 5th percentile of elevation change (denoted by the black dash-dotted line) is used as a measure of cumulative rut incision for a given survey time period. The LiDAR data are shown for comparison.

2.5. Drainage system analysis

To examine the impacts of rutting on road surface flow pathways, we routed flow on the SfM and LiDAR DEMs using Landlab, a Python toolkit for modeling earth surface processes (Hobley et al., 2017; Barnhart et al., 2020). In this drainage system analysis, we were less concerned with the longitudinal undulation pattern artifacts due to their relatively small impact on the slope of the road surface. As such, we resampled both the raw SfM and LiDAR DEMs from 0.01 m to 0.25 m resolution to attenuate excess noise, to smooth other potential artifacts, and to aid in maintaining reasonable processing times. Using a D8 flow routing algorithm, we routed runoff to the nodes of the survey grids. Each model run resulted in maps of the drainage system on the road surface (Figure 8).

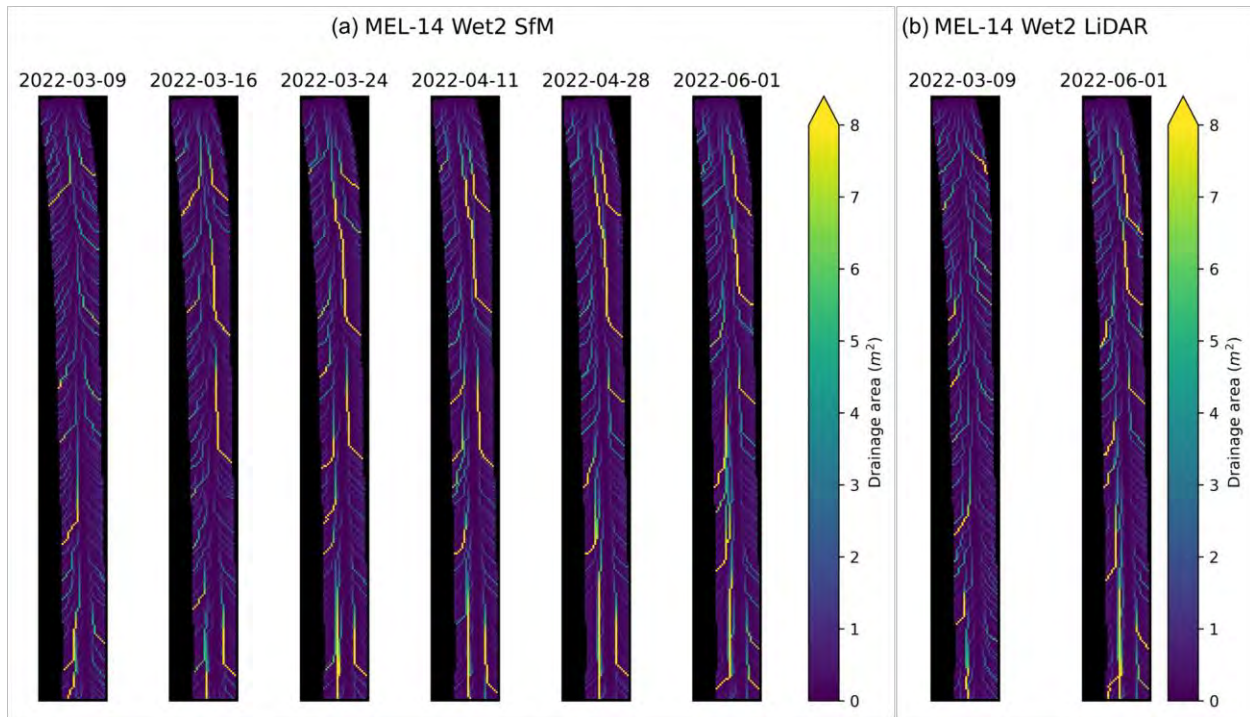


Figure 8. Time series maps of road surface drainage area at MEL-14 during the second wet season (Wet2) for both (a) SfM DEMs and (b) LiDAR DEMs. As time progresses, the drainage pathways increase in length and move farther down-road before veering off to the sides, which demonstrates the impacts of ruts on the road surface. The LiDAR data are shown as a comparison.

As discussed in Section 2.1, a water bar is located near the bottom of each site’s road segment. Without the presence of these water bars, water heading down road in a rut would continue down road and is thus considered part of our lowest boundary drainage for the following analyses. Note that these water bars were not always empty during a given UAV survey and therefore did not always have water draining through them.

We used the derived drainage areas for each survey to analyze the geomorphic outcome of rut incision (i.e., how wheel ruts evolve the drainage pattern of the road surface). To do so, we determined the average longitudinal location at which water leaves the road surface, weighted by drainage area at the edge of each longitudinal location. Because drainage area is proportional to discharge, we can use drainage area as a surrogate for discharge, and as such, the average longitudinal location at which water leaves the road surface can be thought of as the center of mass of the drainage areas at the edges of the road surface. This center of mass of drainage areas at the edges of the road surface allows us to quantify the down-road shift due to rutting (see Section 1).

On a perfectly smooth (i.e., un-rutted), crowned road with no longitudinal slope, we expect the center of mass of the drainage areas to be in the longitudinal middle of the road. In this case, water would drain directly from the centerline to the sides as sheet flow. On an un-rutted, crowned road with longitudinal slope, though, the center of mass of the drainage areas will be shifted slightly down-road. The flow paths for this case would look more like Figure 1a. Because the roads we used in this study have both longitudinal slope and crown slope, we defined our “idealized” center of mass (i.e., the baseline to which we can compare the actual center of mass) using the latter geometry. We use the width of the road at each longitudinal location as a weight value for the center of mass calculation:

$$CM_{ideal} = \frac{\sum(w_y * y)}{a_{total}} - \frac{w_{avg} S_L}{4 S_x} \quad (1)$$

where CM_{ideal} is the idealized center of mass; w_y is the road width at a longitudinal location along the road segment, y ; a_{total} is the total road segment area; w_{avg} is the average road width; S_L is the longitudinal slope of the road; and S_x is the average slope of the crown of the road (approx. 6% at both KID-13 and MEL-14). The first term in Eq. 1 is used to calculate the center of mass assuming no longitudinal slope. The second term in Eq. 1 is used to shift CM_{ideal} down-road to account for the effect of slope. That shift can be derived using basic trigonometry by taking the longitudinal slope and the crown slope as vectors to determine the downward shift angle and is a function of the average width of the road.

However, as roads rut, and with the natural roughness and longitudinal slope of the road, the drainage patterns tend to move downslope before curving toward the ditch, as can be seen in Figure 8. This leads to an even larger down-road shift of the center of mass of drainage areas than that of an idealized surface. As stated above, we use the sum of the drainage areas at the edge of each longitudinal location as a weight value for this center of mass calculation:

$$CM_a = \frac{\sum(a_y * y)}{a_{total}} \quad (2)$$

where CM_a is the center of mass of the drainage areas along the edges, a_y is the drainage area at a longitudinal location along the road segment y , and a_{total} is the total road segment area (i.e., the total drainage area).

To convert the center of mass values from an arbitrary coordinate system, we normalized both CM_a and CM_{ideal} by road location. These normalized values are dimensionless and on a scale of 0 to 1. We then compared CM_a to CM_{ideal} to give an approximation of the effect of ruts on the road flow pathways (i.e., downwards shift due to rutting; Figure 1b).

Additionally, we determined the fraction of the total drainage area leaving the road through the bottom edge (i.e., leaving in ruts):

$$R_a = \frac{\sum(a_{bot}) + a_{wb}}{a_{total}} \quad (3)$$

where R_a is the fraction metric, a_{bot} is the drainage area along the bottom edge of the road segment, a_{wb} is the drainage area at the water bar, and a_{total} is the total road segment area.

2.6. Erosion potential analysis

As an additional examination of the impacts of ruts on forest roads, we carried out a brief analysis of the relative erosion potential of the flow pathways as ruts evolve. To do so, we used an index of erosion potential based on excess shear stress. In excess shear stress formulations of sediment transport and erosion, the excess shear stress is proportional to both erosion and sediment transport potential:

$$\varepsilon_p \propto (\tau - \tau_c)^n \quad (4)$$

where ε_p is erosion potential, τ is the shear stress, τ_c is the critical shear stress (i.e., the threshold at which sediment will start moving), and n is a constant. The value of n generally ranges between 1.5 and 2.5 in the literature (e.g., Govers, 1992; Meyer-Peter & Müller, 1948). For our analysis, we defined the index of potential erosion as in Eq. 4, where n is taken to be 2.0, and τ_c is taken to be 0.566 Pa based on an assumed d_{50} of 1 mm.

The formulation of shear stress we used (Istanbulluoglu et al., 2002) brings in discharge, which, as discussed in Section 2.5, is proportional to drainage area:

$$\begin{aligned}\tau &= \beta q_o^m S^n \\ \Rightarrow \beta &= \rho_w g n_b^{0.6}\end{aligned}\tag{5}$$

where q_o is overland flow per unit width, S is slope, $m = 0.6$, $n = 0.7$, ρ_w is the density of water, g is the acceleration due to gravity, and n_b is Manning's roughness of the surface, which we take to be 0.05, based on results from Alvis et al. (2024).

Once we calculated the shear stress, we summed the indices of erosion potential for each survey in a time period and divided the summed index of a given survey ($t = t_n$) by the summed index for the initial survey ($t = t_0$) to obtain a normalized index of erosion potential, ε_i :

$$\varepsilon_i = \frac{\sum(\tau - \tau_c)^2_{t=t_n}}{\sum(\tau - \tau_c)^2_{t=t_0}}\tag{6}$$

This normalized index allows us to see the effect of ruts on the erosion potential of the road surface over time. A normalized index greater than 1 indicates an increase in erosion potential as compared to the initial time period, and a normalized index less than 1 indicates a decrease.

3. Results

3.1. Temporal evolution of rutting

To address our first question of temporal trends of rutting on these mainline logging roads, we looked at elevation change data from three seasons at both KID-13 and MEL-14. Using the 5th percentile from our eCDFs of elevation change, we show how our measure of cumulative rut incision changes over time (Figure 9).

We plotted the 5th percentile of elevation change in centimeters (i.e., the cumulative rut incision) with respect to time since grading in months. The measures of cumulative rut incisions (i.e., final data points) are variable across seasons and sites, falling between approximately 1.0 cm and 2.5 cm for the SfM DEMs. At KID-13, we see the largest cumulative rut incision for SfM of 2.5 cm during Wet1. With subsequent seasons, the cumulative incision of rutting decreases (i.e., a “shallowing” of rutting). At MEL-14, the largest cumulative rut incision for SfM occurs during Dry1 with a depth of 1.6 cm. Unlike KID-13, however, MEL-14 shows no discernible pattern between subsequent seasons. The lack of a similar pattern is likely due to the fact that only two surveys were usable for Wet1. Interim road grading was carried out without our knowledge between 02/24/2021 and 04/12/2021, which led to 04/12/2021 being an unusable survey for our analyses. For most of the seasons, we see the measures of cumulative rut incisions for the LiDAR DEMs fall below those of the SfM DEMs.

In terms of temporal trends, at KID-13, we see that cumulative rut incision development has a nonlinear relationship with time since grading during all three seasons, with Wet2 showing the rut depth approximately approaching an asymptote of the deepest cumulative rut incision for that season. At MEL-14, we see a similar nonlinear relationship between cumulative rut incision and time since grading for Wet2, which is the only season for which we had sufficient data at that site.

Note that the time since grading generally differs between field sites. The time between surveys at KID-13 was overall longer than that of MEL-14, which was intentional, specifically for Wet2 at MEL-14. We noticed that rut development tended to occur quickly, and we wanted to capture a finer temporal resolution at one of our field sites.

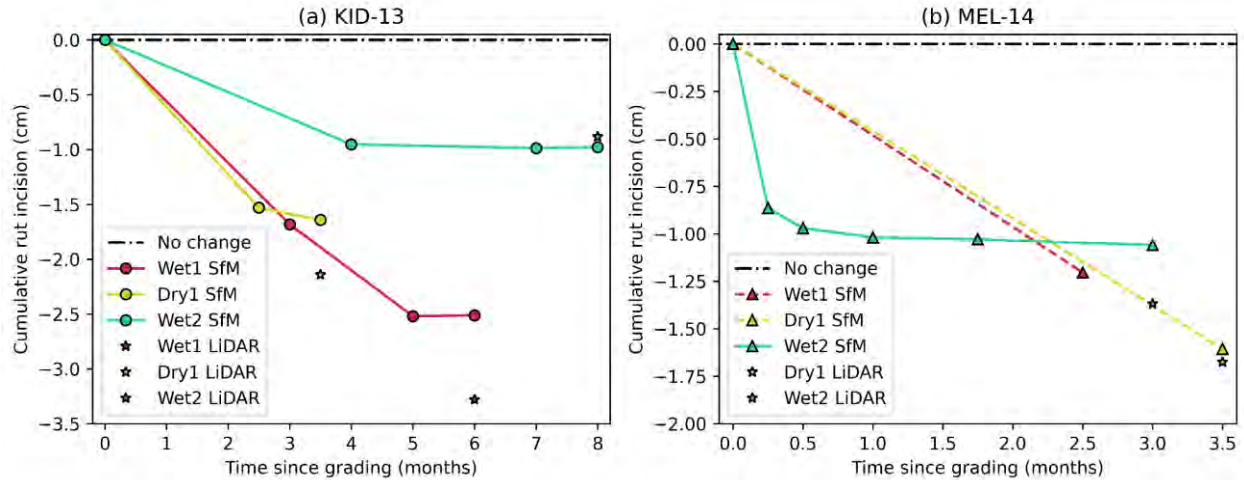


Figure 9. Relationship between cumulative rut incision depth in centimeters with respect to time since grading in months for the full domain at (a) KID-13 and (b) MEL-14. Both KID-13 and MEL-14 demonstrate a nonlinear relationship between the variables. The LiDAR data are provided for comparison.

3.2. Metrics of the drainage system

The cumulative incision depth and rate of rutting are important, but we are also interested in the implications: if ruts are present, what happens to the flow pathways on the road surface and how does that impact the drainage of the system? The capacity to measure this is a key advantage of aerial surveys over cross sections alone. To answer this question, we examined the results of our drainage area center of mass analysis discussed in Section 2.5. Specifically, we looked at where the center of mass of an idealized surface is located as compared to our rutted road surfaces, and we looked at the fraction of the road surface area that is draining through the lowest boundary of the road segment.

For our idealized road surfaces at KID-13 and MEL-14, the normalized values of CM_{ideal} are located at 0.501 and 0.482, respectively. For all seasons at both KID-13 and MEL-14, the normalized values of CM_a for SfM data fall below the normalized values of CM_{ideal} (Figure 10), indicating a down-road shift due to rutting. The LiDAR data provided for comparison show somewhat variable shifts at KID-13 and more consistent down-road shifts at MEL-14, but all normalized values of CM_a fall below the normalized values of CM_{ideal} . The magnitude of the downward shift at KID-13 is less than that of MEL-14.

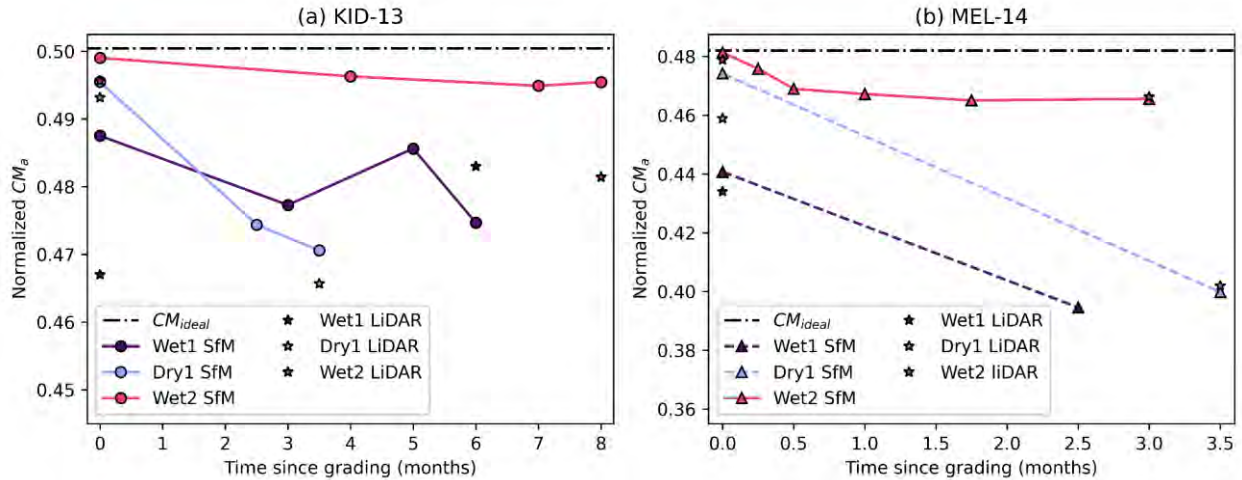


Figure 10. Relationship between the normalized drainage area center of mass and time since grading for (a) KID-13 and (b) MEL-14. Values falling below the ideal center of mass (CM_{ideal}) indicate a down-road shift due to rutting. The LiDAR data are provided for comparison.

While our center of mass analysis utilized the drainage areas along all edges of the road surface, we were also interested in determining how much of the road surface contributed to only the lowest boundary. To show that we plotted the fraction of the total drainage area leaving the road through the bottom edge and included any drainage area exiting the plot through the lower water bar (see Section 2.5 for explanation). In this, we found that as ruts developed, the fraction of road surface draining through the lowest boundary of the road segment increased, with maximum fractions at KID-13 and MEL-14 for SfM data being around 0.20 and 0.30, respectively (Figure 11). The LiDAR data provided for comparison showed somewhat similar maximum fractions of around 0.15 and 0.20 for KID-13 and MEL-13, respectively (Figure 11). For less pronounced rut incisions (i.e., Wet2 at both sites), this fraction is the smallest.

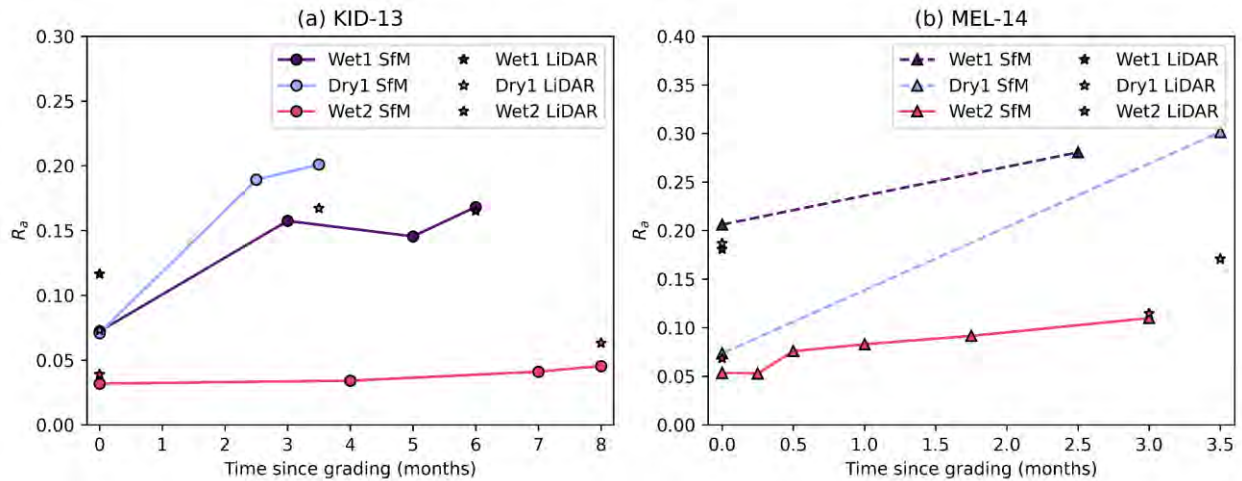


Figure 11. Relationship between fraction of total drainage exiting through the lowest boundary of the road segment and time since grading for (a) KID-13 and (b) MEL-14. The LiDAR data are provided for comparison.

3.3. Erosion potential of the road surface

For the final piece of our analysis, we wanted to examine how rutting and drainage areas relate to erosion, since erosion is a key concern for forest roads. Our evaluation of the normalized index of

potential erosion, ε_i , yielded somewhat similar patterns of results at each site (Figure 12). KID-13 (Figure 12a) presented interesting behavior where ε_i fell below 1 in both Wet1 and Wet2 for the SfM data, which indicates a decrease in erosion potential as compared to the initial surface. During Wet2 at KID-13, that index of erosion potential remained below 1. For Wet1 and Dry1, however, KID-13 exhibited a net increase in erosion potential. MEL-14 (Figure 12b) demonstrated behavior more consistent with the expectation that rutting can cause an increase in erosion and overall exhibited higher relative erosion potentials for all seasons. At their maxima, KID-13 saw a 30% increase in erosion potential and MEL-14 saw a 120% increase in erosion potential for the SfM data, while the LiDAR data provided a maximum of 100% increase in erosion potential at KID-13 and 60% increase in erosion potential at MEL-14. The LiDAR data showed overall increases in erosion potential for all seasons.

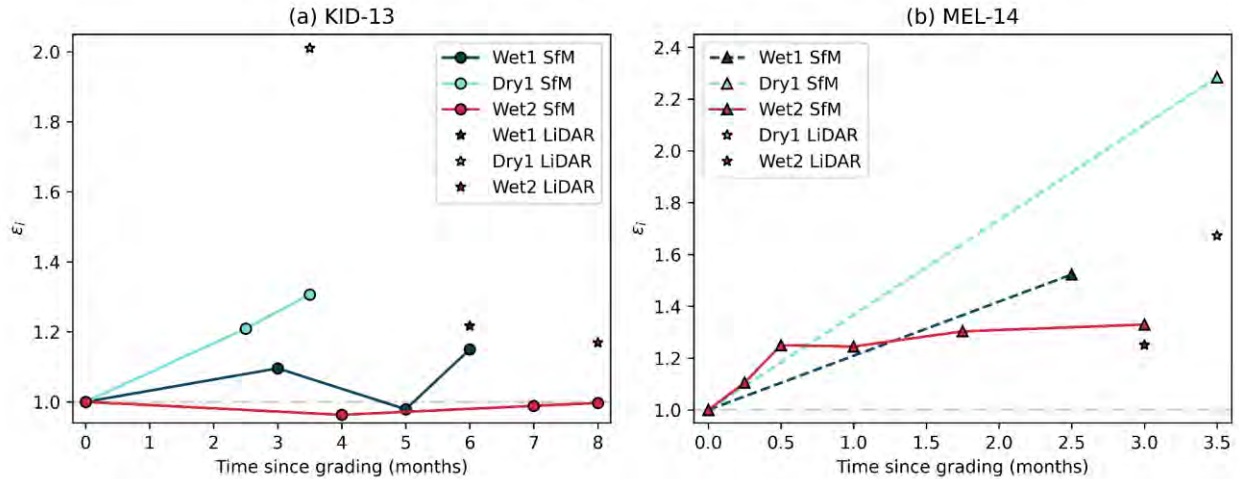


Figure 12. Relationship between the normalized index of erosion potential, ε_i , (Equation 6) and time since grading at (a) KID-13 and (b) MEL-14. The dot-dashed gray line on both panels shows the threshold where the normalized index of erosion potential switches from a decrease to an increase as compared to the initial road surface. The LiDAR data are provided for comparison.

4. Discussion

We found that our measure of cumulative rut incision depth for the SfM DEMs over the duration of a given survey season at both sites varied between approximately 1.0 cm and 2.5 cm (Figure 9). The magnitude of these depths is not as large as compared to other studies (e.g., Fannin & Sigurdsson, 1996; Machuga et al., 2023; Marra et al., 2018), but those studies were carried out on roads built in softer soils (sometimes with the intention of evaluating methods to control rutting in soft soils) or on non-mainline roads. On well-established mainline logging roads like these study sites, however, rut development appears to be less severe, probably because the subgrade of the road has been well-compacted by years of traffic.

At KID-13, all three seasons demonstrated a “slower” nonlinear relationship between cumulative rut incision and time since grading than that of Wet2 at MEL-14 (Figure 9). The rate of rutting is likely slower at KID-13 than MEL-14 due to the difference of longitudinal slopes at each site—MEL-14 is steeper than KID-13—and differences in traffic level at each of the sites—MEL-14 had, on average, more traffic than KID-13. The exponential decrease and subsequent asymptotic approach of the cumulative rut incision depth seen in a season is due to a feedback loop created by erosion processes and traffic. While traffic and rainfall/channelized flow both contribute to development and persistence of ruts, the expected

continuing incision is negated by traffic serving as a stochastic variable that “smooths” the ruts and the large amount of compaction occurring (Alvis et al., 2023).

Additionally, at KID-13 (and, to an extent, MEL-14), we see a “shallowing” of rut incisions with subsequent survey seasons (Figure 9), which is likely due to the fact that, while the road was graded between seasons, no additional rock was added. The road hardened over time due to additional compaction from traffic.

While our measure of rut depth magnitudes is relatively small, their impact is still noticeable. Both our center of mass analysis and our lowest boundary contribution analysis demonstrate the effects of ruts on road surface flow pathways. In an idealized situation, no ruts would exist, and flow would be directed off of the road surface to either side as sheet flow (e.g., Figure 1a, 2a). With the development of ruts, the flow is directed down-road before being directed off to the sides or is not directed off to the sides and instead continues out of the lowest boundary of the road segment (e.g., Figure 1b, 2b, 2c). Essentially, the net vector of flow direction shifts down slope. All surveys for both KID-13 and MEL-14 demonstrate this downward shift, even the initial surveys for each season (Figure 10, Figure 11). The initial surveys were all carried out as soon as possible after grading the road surface. On average, the surveys occurred the day of or day after grading. The first survey at KID-13, however, was an exception, with the survey occurring one week after grading due to weather. Regardless, in most instances, rut development was in its beginning stages due to traffic running over the road surface and resulted in a down-road shift in the center of mass.

The center of mass metric not only tells us the shift of the average location at which water leaves the road surface, it also gives us an approximation of ditch line erosion control treatment effectiveness. Flow that is directed down the road instead of into the roadside ditch does not utilize erosion control treatments present therein. Erosion control treatments in roadside ditch lines have been shown to be largely effective (e.g., Aust et al., 2015; Burroughs et al., 1984; Luce & Black, 1999; Megahan et al., 2001). However, if flow is not traveling in the ditch, erosion control treatments are unable to aid in sediment transport reduction. With the down-road shift of flow pathways due to rutting, erosion control treatments in the ditch have less effectiveness potential as less of the ditch is utilized, as demonstrated in our results in Section 3.2 (Figure 10, Figure 11).

Additionally, flow that is channelized on the road surface due to rutting has a larger capacity for erosion than that of diffuse sheet flow (e.g., Elliot et al., 1999; Foltz & Burroughs, 1990). We see evidence of a net increase in erosion potential as rut incision increases in our results (Figure 12). MEL-14 had a largely consistent increase in erosion potential over all three seasons. KID-13, however, demonstrated a slightly different story: for Wet1 and Wet 2, the erosion potential decreased as compared to the first survey of the seasons during at least one subsequent survey. A couple possible reasons for this exist: 1) the indices of erosion potential we calculated are a function of the entire road surface and not the ruts alone, so the road surface aside from the ruts played an important role and 2) KID-13 demonstrated very clear evidence of sediment displacement, so even though the rut incision depth increased, the rest of road surface could have smoothed out. Another important piece to note is that the model of shear stress used for our calculations assumes overland flow. This assumption does not necessarily hold for the ruts and rills on the road surface. If we included a more sophisticated rill hydraulics model, we would likely have predicted more erosion potential both overall and, more specifically, at KID-13.

All told, the results of our analyses emphasize the importance of road maintenance on a regular basis. Ruts are quick to develop, especially if a new layer of aggregate is added to the road surface, but frequent grading can minimize the impacts of these ruts with respect to flow pathway alteration. However,

as discussed in Luce & Black (2001), road maintenance can also produce higher sediment yields shortly thereafter. As such, further work should be conducted to determine the relative increase in sediment yields due to rutting as compared to the increase in sediment yields due to road maintenance.

5. Conclusion

Overall, our two field sites yielded important information regarding rut formation on a sampling of mainline logging roads, especially with respect to flow pathways on the road surface. Our results demonstrate the advantage of using UAV-derived (SfM) DEMs for analysis over cross-sections alone. Using UAV SfM surveys, with validation from TLS, we examined the evolution of ruts on two segments of mainline logging roads in western Washington. We found that:

1. the relationship between rut incision and time since grading is nonlinear at both sites for all seasons with sufficient data, with MEL-14 having a generally quicker rate of rutting than that of KID-13;
2. as ruts develop, the overall flow pathways shift down-road, which has implications on how much of the erosion control treatments in the roadside ditch lines are utilized; and
3. the erosion potential of our road surfaces tended to increase overall as ruts developed, with KID-13 seeing a maximum increase of 30% and MEL-14 seeing a maximum increase of 120%.

6. References

- Akgul, M., Yurtseven, H., Akburak, S., Demir, M., Cigizoglu, H. K., Ozturk, T., et al. (2017). Short term monitoring of forest road pavement degradation using terrestrial laser scanning. *Measurement*, 103, 283–293. <https://doi.org/10.1016/j.measurement.2017.02.045>
- Alvis, A. D., Luce, C. H., & Istanbuluoglu, E. (2023). How does traffic affect erosion of unpaved forest roads? *Environmental Reviews*, 31(1), 182–194. <https://doi.org/10.1139/er-2022-0032>
- Alvis, A. D., Luce, C. H., Istanbuluoglu, E., Black, T., Dieu, J., & Black, J. (2024). Using additional roughness to characterize erosion control treatment effectiveness in roadside ditch lines. *Earth Surface Processes and Landforms*, 49(4), 1255–1272. <https://doi.org/10.1002/esp.5763>
- Aust, W. M., Bolding, M. C., & Barrett, S. M. (2015). Best Management Practices for Low-Volume Forest Roads in the Piedmont Region: Summary and Implications of Research. *Transportation Research Record*, 2472(1), 51–55. <https://doi.org/10.3141/2472-06>
- Aydin, A., Turk, Y., & Eker, R. (2019). Pros and Cons of the Manual and Autonomous UAV Flights in Mapping of the Forest Road Surface Deformations: Preliminary Results. In *2nd International Symposium of Forest Engineering and Technologies* (pp. 47–52). Tirana, Albania.
- Barnhart, K. R., Hutton, E. W. H., Tucker, G. E., Gasparini, N. M., Istanbuluoglu, E., Hobley, D. E. J., et al. (2020). Short communication: Landlab v2.0: a software package for Earth surface dynamics. *Earth Surface Dynamics*, 8(2), 379–397. <https://doi.org/10.5194/esurf-8-379-2020>
- Bradley, A. H. (1994). *Reducing tire pressures lessens rutting on thawing forest roads: Results of two field trials* (SAE Technical Paper No. No. 942246). Warrendale, PA: Society of Automotive Engineers.
- Burroughs, E. R., & King, J. G. (1989). *Reduction of soil erosion on forest roads*. Ogden, UT: U.S. Department of Agriculture, Forest Service, Intermountain Research Station. <https://doi.org/10.2737/INT-GTR-264>
- Burroughs, E. R., Watts, F. J., King, J. G., Haber, D. F., Hansen, D., & Flerchinger, G. (1984). Relative Effectiveness of Rocked Roads and Ditches in Reducing Surface Erosion. In *21st annual engineering, geology, and soils engineering symposium* (pp. 251–263). Moscow, ID: University of Idaho.
- Cambi, M., Certini, G., Neri, F., & Marchi, E. (2015). The impact of heavy traffic on forest soils: A review. *Forest Ecology and Management*, 338, 124–138. <https://doi.org/10.1016/j.foreco.2014.11.022>
- Cao, L., Wang, Y., & Liu, C. (2021). Study of unpaved road surface erosion based on terrestrial laser scanning. *CATENA*, 199, 105091. <https://doi.org/10.1016/j.catena.2020.105091>
- Cissel, R., Black, T., Nelson, N., & Luce, C. (2014). *Southwest Crown of the Continent GRAIP Roads Assessment: Center Horse and Morrell/Trail Project Area, Poorman Creek, and Cold Creek. Lolo, Helena, and Flathead National Forests, Montana* (Report to Southwest Crown Collaborative). Boise, ID: US Department of Agriculture, Forest Service Rocky Mountain Research Station.
- Dobson, R. J., Colling, T., Brooks, C., Roussi, C., Watkins, M. K., & Dean, D. (2014). Collecting Decision Support System Data through Remote Sensing of Unpaved Roads. *Transportation Research Record: Journal of the Transportation Research Board*, 2433(1), 108–115. <https://doi.org/10.3141/2433-12>
- El Issaoui, A., Feng, Z., Lehtomäki, M., Hyypä, E., Hyypä, H., Kaartinen, H., et al. (2021). Feasibility of

- Mobile Laser Scanning towards Operational Accurate Road Rut Depth Measurements. *Sensors*, 21(4), 1180. <https://doi.org/10.3390/s21041180>
- Elliot, W. J., Foltz, R. B., & Luce, C. H. (1999). Modeling Low-Volume Road Erosion. *Transportation Research Record*, 1652(1), 244–249. <https://doi.org/10.3141/1652-64>
- Fannin, R. J., & Sigurdsson, O. (1996). Field Observations on Stabilization of Unpaved Roads with Geosynthetics. *Journal of Geotechnical Engineering*, 122(7), 544–553. [https://doi.org/10.1061/\(ASCE\)0733-9410\(1996\)122:7\(544\)](https://doi.org/10.1061/(ASCE)0733-9410(1996)122:7(544))
- Foltz, R. B. (1994). *Sediment Reduction from the Use of Lowered Tire Pressures* (SAE Technical Paper No. No. 942244) (pp. 47–52). Warrendale, PA: Society of Automotive Engineers.
- Foltz, R. B., & Burroughs, E. R. (1990). Sediment production from forest roads with wheel ruts. In R. E. Riggins, E. B. Jones, R. Singh, & P. A. Rechar (Eds.), *Watershed Planning and Analysis in Action Symposium. Proceedings of IR Conference Watershed Mgt/IR Div/ASCE in Durango, Colorado, July 9-11, 1990*. (pp. 266–275). American Society of Civil Engineers.
- Foltz, R. B., & Elliot, W. J. (1997). Effect of lowered tire pressures on road erosion. *Transportation Research Record*, 1589(1), 19–25.
- Foltz, R. B., & Truebe, M. A. (1995). Effect of aggregate quality on sediment production from a forest road. In *Proceedings of the Sixth International Conference on low-volume roads*. (Vol. 1, pp. 49–57). Washington, DC, USA: Transportation Research Board, National Research Council.
- Govers, G. (1992). Evaluation of transporting capacity formulae for overland flow. In *Overland Flow: Hydraulics and Erosion Mechanics* (pp. 243–273). New York: Chapman and Hall.
- Hobley, D. E. J., Adams, J. M., Nudurupati, S. S., Hutton, E. W. H., Gasparini, N. M., Istanbuluoglu, E., & Tucker, G. E. (2017). Creative computing with Landlab: an open-source toolkit for building, coupling, and exploring two-dimensional numerical models of Earth-surface dynamics. *Earth Surface Dynamics*, 5(1), 21–46. <https://doi.org/10.5194/esurf-5-21-2017>
- Hrůza, P., Mikita, T., Tyagur, N., Krejza, Z., Cibulka, M., Procházková, A., & Patočka, Z. (2018). Detecting Forest Road Wearing Course Damage Using Different Methods of Remote Sensing. *Remote Sensing*, 10(4), 492. <https://doi.org/10.3390/rs10040492>
- Istanbuluoglu, E., Tarboton, D. G., Pack, R. T., & Luce, C. (2002). A probabilistic approach for channel initiation. *Water Resources Research*, 38(12), 61-1-61–14. <https://doi.org/10.1029/2001WR000782>
- Luce, C. H., & Black, T. A. (1999). Sediment production from forest roads in western Oregon. *Water Resources Research*, 35(8), 2561–2570.
- Luce, C. H., & Black, T. A. (2001). Spatial and Temporal Patterns in Erosion from Forest Roads. *Land Use and Watersheds: Human Influence on Hydrology and Geomorphology in Urban and Forest Areas*, 165–178.
- Machuga, O., Shchupak, A., Styranivskiy, O., Krilek, J., Helexa, M., Kováč, J., et al. (2023). Field and Laboratory Research of the Rut Development Process on Forest Roads. *Forests*, 15(1), 74. <https://doi.org/10.3390/f15010074>
- Marra, E., Cambi, M., Fernandez-Lacruz, R., Giannetti, F., Marchi, E., & Nordfjell, T. (2018). Photogrammetric estimation of wheel rut dimensions and soil compaction after increasing numbers of forwarder passes. *Scandinavian Journal of Forest Research*, 33(6), 613–620.

<https://doi.org/10.1080/02827581.2018.1427789>

- Megahan, W. F., & Kidd, W. J. (1972). Effects of logging and logging roads on erosion and sediment deposition from steep terrain. *Journal of Forestry*, 70(3), 136–141.
- Megahan, Walter F., Wilson, M., & Monsen, S. B. (2001). Sediment production from granitic cutslopes on forest roads in Idaho, USA. *Earth Surface Processes and Landforms*, 26(2), 153–163. [https://doi.org/10.1002/1096-9837\(200102\)26:2<153::AID-ESP172>3.0.CO;2-0](https://doi.org/10.1002/1096-9837(200102)26:2<153::AID-ESP172>3.0.CO;2-0)
- Meyer-Peter, E., & Müller, R. (1948). Formulas for bed-load transport. In *IAHSR 2nd meeting*. Stockholm, Sweden: IAHSR.
- Mueller, M. M., Diitenberger, S., Nestler, M., Hese, S., Ziemer, J., Bachmann, F., et al. (2023). Novel UAV Flight Designs for Accuracy Optimization of Structure from Motion Data Products. *Remote Sensing*, 15(17), 4308. <https://doi.org/10.3390/rs15174308>
- Nevalainen, P., Salmivaara, A., Ala-Illomäki, J., Launiainen, S., Hiedanpää, J., Finér, L., et al. (2017). Estimating the Rut Depth by UAV Photogrammetry. *Remote Sensing*, 9(12), 1279. <https://doi.org/10.3390/rs9121279>
- PRISM Climate Group. (2023). Mean annual precipitation time series [Data set]. Oregon State University. Retrieved from <https://prism.oregonstate.edu>
- Reid, L. M. (1981). *Sediment Production from Gravel-Surfaced Roads, Clearwater Basin, Washington*. University of Washington, Seattle, Washington.
- Reid, L. M., & Dunne, T. (1984). Sediment production from forest road surfaces. *Water Resources Research*, 20(11), 1753–1761. <https://doi.org/10.1029/WR020i011p01753>
- Sheridan, G. J., Noske, P. J., Whipp, R. K., & Wijesinghe, N. (2006). The effect of truck traffic and road water content on sediment delivery from unpaved forest roads. *Hydrological Processes*, 20(8), 1683–1699. <https://doi.org/10.1002/hyp.5966>
- Sugden, B. D., & Woods, S. W. (2007). Sediment Production From Forest Roads in Western Montana. *JAWRA Journal of the American Water Resources Association*, 43(1), 193–206. <https://doi.org/10.1111/j.1752-1688.2007.00016.x>
- Tarekegn, T. H., & Sayama, T. (2013). Correction of SRTM DEM Artefacts by Fourier Transform for Flood Inundation Modeling. *Journal of Japan Society of Civil Engineers, Ser. B1 (Hydraulic Engineering)*, 69(4), I_193-I_198. https://doi.org/10.2208/jscejhe.69.I_193
- Toman, E. M., & Skaugset, A. E. (2011). Reducing Sediment Production from Forest Roads during Wet-Weather Hauling. *Transportation Research Record: Journal of the Transportation Research Board*, 2203(1), 13–19. <https://doi.org/10.3141/2203-02>
- Türk, Y., Aydin, A., & Eker, R. (2022). Comparison of Autonomous and Manual UAV Flights in Determining Forest Road Surface Deformations. *European Journal of Forest Engineering*, 8(2), 77–84. <https://doi.org/10.33904/ejfe.1206846>
- Uusitalo, J., Ala-Illomäki, J., Lindeman, H., Toivio, J., & Siren, M. (2020). Predicting rut depth induced by an 8-wheeled forwarder in fine-grained boreal forest soils. *Annals of Forest Science*, 77(2), 42. <https://doi.org/10.1007/s13595-020-00948-y>
- Venanzi, R., Latterini, F., Civitarese, V., & Picchio, R. (2023). Recent Applications of Smart Technologies for Monitoring the Sustainability of Forest Operations. *Forests*, 14(7), 1503.

<https://doi.org/10.3390/f14071503>

Wilkinson, M. W., Jones, R. R., Woods, C. E., Gilment, S. R., McCaffrey, K. J. W., Kokkalas, S., & Long, J. J. (2016). A comparison of terrestrial laser scanning and structure-from-motion photogrammetry as methods for digital outcrop acquisition. *Geosphere*, 12(6), 1865–1880. <https://doi.org/10.1130/GES01342.1>

Yurtseven, H., Akgul, M., Akay, A. O., Akburak, S., Cigizoglu, H. K., Demir, M., et al. (2019). High accuracy monitoring system to estimate forest road surface degradation on horizontal curves. *Environmental Monitoring and Assessment*, 191(1), 32. <https://doi.org/10.1007/s10661-018-7155-8>

Ziegler, A. D., Sutherland, R. A., & Giambelluca, T. W. (2001). Interstorm surface preparation and sediment detachment by vehicle traffic on unpaved mountain roads. *Earth Surface Processes and Landforms*, 26(3), 235–250.

CMER Roads Prescription-Scale Effectiveness Monitoring Project – Survey

The survey provides information about the frequency of use of Best Management Practices, the results of which will be summarized in the final CMER report. It also informs which ditch line Best Management Practices will be studied during the second half of this CMER Project.

- Please fill-in your contact information on this page.
- Please email either this Word File or a scan of the completed document to julie.dieu@rayonier.com, and call her at (360) 580-0088 if you have any questions about or problems with the survey.
- Please submit by May 31st if at all possible, but we will accept submissions until June 30th.
- Please send this survey to a person generally in charge of road management/maintenance on each of your company's tree farms. And in particular to anyone who is installing creative solutions.
- Please carefully read the instructions at the top of the table on the second page. Understand that we are asking about use of BMP's at individual stream crossings (which is why items like rock quality and grading have "X's" in some boxes – we know those activities are conducted on longer pieces of road).
- Answers about time and equipment will be calculated into \$ using state rates, and no landowner-specific information will be published.
- For those of you who would like to know more about the project, an overview is provided on the last page.

Name: Click or tap here to enter text.

Phone Number: Click or tap here to enter text.

Job Title: Click or tap here to enter text.

Email: Click or tap here to enter text.

Company: Click or tap here to enter text.

Counties: Click or tap here to enter text.

Tree Farm Name: Click or tap here to enter text. **Approx Acres of Tree Farm:** Click or tap here to enter text.

These answers are for an individual stream crossing.

For haul categories,

- F = Frequent if the BMP is commonly used at stream crossings,
- S = Sometimes if the BMP is used at some stream crossings,
- N = Never if you don't use or maintain the BMP on that type of road.

- Enter minutes into Time to Install.
- Enter number of times/year in the Maintenance Frequency (can use 0.5 for maintenance every other year).
- Check the equipment used for each BMP. You are not expected to use boxes with an "X" already in place.

		Main Line	Secondary	Spur (active)	Spur (no logging)	Time (minutes) to Install	Maintenance Frequency (#/yr)	Small Excavator (e.g., 220)	Big Excavator (e.g., 330)	Dump Truck	Skid Cat	Ground Crew
Surface Prep	Asphalt					X	X	X	X	X	X	X
	Surface Binding Agent							X	X	X	X	X
	Quality Crushed					X	X	X	X	X	X	X
	Quality Pit Run					X	X	X	X	X	X	X
	Marginal Pit Run					X	X	X	X	X	X	X
	Other											
Tread BMPs	Grading					X	X	X	X	X	X	X
	Rolling Dips							<input type="checkbox"/>	<input type="checkbox"/>	<input type="checkbox"/>	<input type="checkbox"/>	<input type="checkbox"/>
	Flappers							<input type="checkbox"/>	<input type="checkbox"/>	<input type="checkbox"/>	<input type="checkbox"/>	<input type="checkbox"/>
	Geo Fabric							<input type="checkbox"/>	<input type="checkbox"/>	<input type="checkbox"/>	<input type="checkbox"/>	<input type="checkbox"/>
	Other							<input type="checkbox"/>	<input type="checkbox"/>	<input type="checkbox"/>	<input type="checkbox"/>	<input type="checkbox"/>
Traffic Mgmt	Tire Pressure Reductions					X	X	X	X	X	X	X
	Weather Shut-Downs					X	X	X	X	X	X	X
	Other					X	X	X	X	X	X	X
Ditchline BMPs	Grass Seed/Hydro Seed							<input type="checkbox"/>	<input type="checkbox"/>	<input type="checkbox"/>	<input type="checkbox"/>	<input type="checkbox"/>
	Rocking the Ditch							<input type="checkbox"/>	<input type="checkbox"/>	<input type="checkbox"/>	<input type="checkbox"/>	<input type="checkbox"/>
	Rock Check Dams							<input type="checkbox"/>	<input type="checkbox"/>	<input type="checkbox"/>	<input type="checkbox"/>	<input type="checkbox"/>
	Silt Fence (parallel)							<input type="checkbox"/>	<input type="checkbox"/>	<input type="checkbox"/>	<input type="checkbox"/>	<input type="checkbox"/>
	Silt Fence (across)							<input type="checkbox"/>	<input type="checkbox"/>	<input type="checkbox"/>	<input type="checkbox"/>	<input type="checkbox"/>
	Hay/Straw Bundled							<input type="checkbox"/>	<input type="checkbox"/>	<input type="checkbox"/>	<input type="checkbox"/>	<input type="checkbox"/>
	Hay/Straw Scattered							<input type="checkbox"/>	<input type="checkbox"/>	<input type="checkbox"/>	<input type="checkbox"/>	<input type="checkbox"/>
	Wattles							<input type="checkbox"/>	<input type="checkbox"/>	<input type="checkbox"/>	<input type="checkbox"/>	<input type="checkbox"/>
	Sediment Traps/Catch Basin							<input type="checkbox"/>	<input type="checkbox"/>	<input type="checkbox"/>	<input type="checkbox"/>	<input type="checkbox"/>
	Settling Pond							<input type="checkbox"/>	<input type="checkbox"/>	<input type="checkbox"/>	<input type="checkbox"/>	<input type="checkbox"/>
	Other							<input type="checkbox"/>	<input type="checkbox"/>	<input type="checkbox"/>	<input type="checkbox"/>	<input type="checkbox"/>

QUESTION 2: For either tread or ditchline BMPs, please describe any others you find useful that have not been listed above. Please provide photos or a diagram of same.

Click or tap here to enter text.

QUESTION 3: How frequently are roads graded during heavy haul?

- Weekly Monthly Bi-Monthly
 Other (Describe): Click or tap here to enter text.

QUESTION 4: How frequently are mainline roads ditched, assuming well-grassed conditions that are capturing sediment?

- Annual Every 2nd Year Every 3rd Year
 Other (Describe): Click or tap here to enter text.

QUESTION 5: May we contact you to clarify any information and/or inquire further about unique BMPs you have described in Question 2?

- YES No

Thank you from the Project Team: Amanda Alvis (UW - PhD Candidate), Jenelle Black (NWIFC - CMER Staff Scientist), Tom Black (USFS - Hydrologist), Sam Calahan (USFS - Hydrologic Technician), Julie Dieu (Rayonier - Geomorphologist, CMER), Erkan Istanbuluoglu (UW - Professor), Charlie Luce (USFS - Research Hydrologist, Principal Investigator), Alexander Prescott (WADNR - Project Manager), West Fork Environmental.

OVERVIEW

CMER Roads Prescription-Scale Effectiveness Monitoring Project

Roads play an important role in our society, providing efficient links for transportation of people and materials. Forest roads provide many functions such as allowing timber products to be transported to mills, providing emergency access, and providing access for recreationists, hunters, and fishermen. However, road erosion can be a large source of anthropogenic sediment in watersheds managed for timber production. In particular, fine-grained sediment has the potential to adversely affect water quality and aquatic resources at the site, the channel reach, and the watershed scales.

Recognizing that roads are persistent sources of fine sediment to forest streams, forest managers have made substantial improvements in water quality in recent decades through their diligent application of best management practices (BMP). Initial monitoring results in western Washington indicate that 10-11% of the total forested road length directly delivers sediment to the channel network (Dube et al., 2010; Martin, 2011). Installation of cross-drain culverts, to relieve ditch water before it reaches a stream crossing, has become a common practice and remains an effective and low-maintenance BMP. The 10-11% of the total forest road length that is hydrologically connected to streams is stream-adjacent, cannot be successfully drained onto a hillslope, and, where this situation coincides with heavy traffic, leads to increased delivery of sediment to streams. A focal question in this project is: *What combinations of surfacing, ditch line management, traffic control, and drainage management will most efficiently and effectively mitigate sediment yields from high-traffic, near-stream (HTNS) road segments?*

Currently, one of the most significant challenges for evaluating BMP effectiveness experimentally is a lack of theoretical and modeling basis with which to: a) analyze and interpret data, b) generate hypotheses for new locations, and c) explore what-if scenarios for comparison of BMP alternatives on water and sediment budgets. This limitation results in strained applicability to locations other than where BMP effectiveness was empirically tested. Therefore, to advance our understanding and predictive capability, a critical need exists for joint development of extensive field studies and complementary process-based numerical modeling approaches to investigate the effects of single and multiple BMP on runoff and sediment production and transport from roads. To fulfill this need, we are investigating sediment production and delivery by conducting extensive empirical field research of BMP impacts on road erosion, complemented by a process-based geomorphic modeling framework developed using a Python-based Earth Surface modeling toolkit called Landlab (<http://landlab.github.io/#/>).

For the Major Experiment, we are measuring rainfall, runoff, and sediment production from the road surface and ditch line over several years for a large sample of individual road segments using sediment tubs, tipping buckets, and turbidity tanks. Our field study effort focuses on 39 road segments in each of two distinct lithologies. Across each set of 39 sites, similar ranges in rainfall that are generally typical of forested Western Washington are being sampled. We have sampled the 78 sites for three years to understand relationships between rainfall, traffic, surfacing, and grading, in the context of the distinct lithologic attributes and all with no ditch line BMP's present except grass seeding. We will be sampling the 78 sites for three more years with tread and ditch line BMP of interest installed at some of the sites to quantify their benefits.

We are also conducting smaller, targeted Parameterization Experiments. Most of these are to quantify specific sediment production and transport processes to aid in model development. However, the Cost Versus Maintenance Survey will provide the Project Team with insight into BMPs, both common and unique, and their relative costs in installation time and maintenance requirements. The results from this survey will influence our ditch line BMP choices that we will assess during the second three-year period of the Major Experiment.

Defining Watershed Hydraulic Attributes for DNR High Traffic Near Stream Roads

Prepared By:

Kimberlee Vezzetti

Green River College

12401 SE 320th Street

Auburn, WA 98092

kavezzetti@outlook.com

(253) 397-9542

Table of Contents

Project Sponsor 3

Project Partners 3

Project Background..... 4

Methods..... 4

Deliverables 12

Discussion 13

Conclusion 14

References..... 15

Appendicies..... 16

 Appendix A – Sub-meter GPS Points 16

 Appendix B – File Geodatabase Contents Key..... 19

 Appendix C – Watershed Areas 20

 Appendix D – Watershed Slope Statistics..... 22

 Appendix E – Final Watershed Area Polygon Model..... 24

 Appendix F – Watershed Slope Statistics Model..... 25

SPONSER AND CONTACT INFORMATION

Gavin Nishiyori

West Fork Environmental – Natural Resources Technician

Address: 2350 Mottman Rd SW, Tumwater, WA 98512

Email: Gavin@westforkenv.com

Office: 360-753-0485

Cell: 253-282-1753

PROJECT PARTNERS AND CONTACT INFORMATION

Jenelle Black

Cooperative Monitoring, Evaluation, and Research (CMER) – Staff Manager / Northwest Indian Fisheries Commission – Lead Scientist

Email: JBlack@nwifc.org

Tom Black

United States Forest Service (USFS) Rocky Mountain Research Station – Hydrologist

Email: Thomas.Black1@usda.gov

Alexander Prescott

WA Department of Natural Resources (DNR) – Project Manager

Email: Alexander.Prescott@dnr.wa.gov

PROJECT BACKGROUND

Across Washington, forest roads provide many functions including transportation of timber products to mills, emergency medical service access, and forest access to recreationalists, hunters, and fishermen. While there are many benefits to forest roads, they can also be a large source of sediment delivery to nearby watersheds and streams. This sediment delivery can affect fish, amphibians, and stream primary production. Recognizing that roads are persistent sources of fine sediment to forest streams, forest managers have made substantial improvements in water quality management in recent decades through their diligent application of Best Management Practices (BMP).

West Fork Environmental, Washington State Department of Natural Resources (DNR) Adaptive Management Program (AMP) and the US Forest Service are working together to monitor sediment runoff and define the extent of watersheds to better understand the relationship between forest road management, application of road BMP, and road sediment generation. To do this, they need to understand the relationship between contributing watershed characteristics including area and slope, and total water discharge and timing.

A focal question in their project is: *What combinations of surfacing, ditch line management, traffic control, and drainage management will most efficiently and effectively mitigate sediment yields from high-traffic, near-stream (HTNS) roads?*

Gaining a better understanding of these relationships would assist in the development of process-based numerical modeling framework that can be used to generate field-testable hypotheses, as well as open future avenues for road sediment and BMP research. A greater process-based understanding, rooted in scientific evidence, will ensure that the most effective BMP are being applied.

METHODS

Sub-Meter GPS Points

125 Sub-Meter GPS points were collected representing the top and bottom points for each of the 79 watershed areas in this study. Each point was collected using the JAVAD Mobile Tools app on tablets provided by West Fork Environmental using the Static Survey method for twenty minutes at each location. Three tablets and TRIUMPH-2 JAVAD GNSS devices were used to collect three sub-meter GPS points simultaneously. Once collected, West Fork Environmental uploaded the

GPS points from their tablets onto their computer, which I then shared with project partners via a Box Drive folder in .JPS format. Alexander Prescott returned these to me in decimal degree format in an Excel sheet.

Upon investigation, forty of the one hundred twenty-five GPS points had error codes and needed to be corrected. After conducting research and emailing with JAVAD Technical Support, I did this by converting the .JPS files to RINEX format using JAVAD's JPS2RIN software. RINEX files can be corrected using the NOAA Online Positioning User Service (OPUS) by using rapid-static processing to correct them against the CORS network or Base Stations near the collected points (NOAA, 2010). After many tries, each attempt at correcting these resulted in error codes. I reached out to Nathan Waldren with the WA DNR for further guidance and assistance. He found that one of the three TRIUMPH-2 JAVAD GNSS devices was originally set up incorrectly by the DNR, meaning I would be unable to correct these points on my own, as I do not have access to JAVAD's NetView & Modem software. Nathan was able to input the original .JPS files with error codes and correct them for me, sending back CSV files with the corrected coordinates in Washington south state plane format.

Using Earth Point (Tools for Google Earth) I converted these coordinates from the Washington south state plane coordinate system to decimal degree coordinates. These coordinates were added to the final Watershed Attributes Excel workbook (Appendix A), which was then saved as a CSV to be used in ArcPro. Using the XY Table to Point (Data Management) tool in ArcPro, all sub-meter GPS points were output into a single shapefile. The Split by Attribute (Analysis) tool was used to separate each point as individual feature classes located in the Sub_Meter_GPS_Points feature dataset in the WatershedAttributes.gdb file geodatabase.

File Geodatabase

The WatershedAttributes.gdb file geodatabase contains feature datasets and raster mosaics with all relevant layers and tool outputs for all sub-meter GPS points and watershed areas. Tools from both internal ArcPro toolboxes and external TauDEM toolbox scripts were used to create file geodatabase contents. The TauDEM 5.3.7 Complete Windows Installer can be accessed at the Utah State Universities Hydrogeology Research Group's website, where you can also find installation

instructions (Tarboton et al., 2015). Feature datasets include sub-meter GPS point plot locations, moved to stream points, final individual watershed areas, merged final watershed areas, and points area polygons. Raster mosaics include WA DTM tiles, WA DTMHS tiles, pit filled DTM tiles, D8 flow direction outputs, D8 slope grid outputs, D8 contributing area outputs, point D8 contributing areas, dissolved raster outputs, slope raster outputs, and flow accumulation outputs. A contents key with descriptions for all feature datasets and mosaic datasets can be referenced in the Watershed Attributes Excel workbook (Appendix B). Methods for creating each feature dataset and raster mosaic are listed below:

Sub-meter GPS Plot Locations: Methods for Sub-meter GPS Plot Locations are described in the above section, “Sub-Meter GPS Points”. Points are located in the Sub_Meter_GPS_Points feature dataset in the WatershedAttributes.gdb file geodatabase.

WA DTM Tiles: Washington State Digital Terrain Model (DTM) tiles were acquired from the Washington State Department of Natural Resources Washington Lidar Portal. Southwest_wa_opsw_2019 was used for sites DELE, MEL, NEWS, BISH, and NASE, cascades_south_3deop_2019 was used for east KID sites, swwa_foothills_2017 was used for west KID sites, and Abby Gleason with the WA DNR provided new lidar tiles for TOUT sites via the Box Drive. The WA_DNR_Lidar_2022_St_Helens_MTI shapefile provided by Abby was used to determine the correct TOUT lidar tiles to use for the study area. Manual sorting of all tiles was used to determine the correct lidar tiles for the DELE, MELE, NEWS, BISH, NASE, and KID area. Once gathered, the Add Rasters to Mosaic Dataset (Data Management) tool was used to add appropriate raster tiles to the DTM_Rasters mosaic located in the WatershedAttributes.gdb file geodatabase.

WA DTMHS Tiles: Washington State Digital Terrain Model Hill Shade (DTMHS) tiles were acquired from the Washington State Department of Natural Resources Washington Lidar Portal. Southwest_wa_opsw_2019 was used for DELE, MEL, NEWS, BISH, and NASE sites, cascades_south_3deop_2019 was used for TOUT and east KID sites, and swwa_foothills_2017 was used for west KID sites. Manual sorting of all tiles was used to determine the correct lidar tiles for all areas. Once gathered, the Add Rasters to Mosaic Dataset (Data Management) tool was used to add

appropriate raster tiles to the DTMHS_Rasters mosaic located in the WatershedAttributes.gdb file geodatabase.

Pit Filled DTM Tiles: Pit filled elevation grids are the required input for the TauDEM D8 Flow Direction script. I used the Pit Remove script located in the TauDEM Basic Grid Analysis toolset to create pit filled elevation grids. The Pit Remove script works by identifying all pits in a DEM or DTM and raises their elevation to the lowest pour point around surrounding cell edges (Tarboton et al., 2015). Input files were DTM mosaics located in the DTM_Rasters mosaic, and output rasters were saved to a folder located on my computer. Once created, the Add Rasters to Mosaic Dataset (Data Management) tool was used to add appropriate rasters to the Pit_Filled_Rasters mosaic located in the WatershedAttributes.gdb file geodatabase.

D8 Flow Direction Outputs: D8 flow direction grids are the required input for the TauDEM D8 Contributing Area and Move Outlets to Streams scripts. I used the D8 Flow Direction script located in the TauDEM Basic Grid Analysis toolset to create D8 flow direction grids. The D8 flow direction script works by identifying one of eight adjacent or diagonal neighboring cells with the steepest downward slope, assigning a single direction to that cell (Tarboton et al., 2015). Input files were pit filled elevation grids located in the Pit_Filled_Rasters mosaic, and output rasters were saved to a folder located on my computer. Once created, the Add Rasters to Mosaic Dataset (Data Management) tool was used to add appropriate rasters to the D8_Flow_Directions mosaic located in the WatershedAttributes.gdb file geodatabase.

D8 Slope Grid Outputs: D8 slope grids are a second output of the D8 Flow Direction script located in the TauDEM Basic Grid Analysis toolset. This output is a grid giving slope in the D8 flow direction, measured as drop and distance (Tarboton et al., 2015). Input files were pit filled elevation grids located in the Pit_Filled_Rasters mosaic, and output rasters were saved to a folder located on my computer. Once created, the Add Rasters to Mosaic Dataset (Data Management) tool was used to add appropriate rasters to the D8_Slope_Grids mosaic located in the WatershedAttributes.gdb file geodatabase.

D8 Contributing Area Outputs: D8 contributing area grids are the required input for the TauDEM Stream Definition by Threshold script. I used the D8 Contributing Area script located in the TauDEM Basic Grid Analysis toolset to create D8 contributing area grid. The D8 Contributing Area script works by calculating the total of a cells own contribution, plus the contribution from neighboring upslope cells that drain into it according to the D8 flow direction models (Tarboton et al., 2015). Input files were D8 flow direction grids located in the D8_Flow_Directions mosaic, and output rasters were saved to a folder located on my computer. Once created, the Add Rasters to Mosaic Dataset (Data Management) tool was used to add appropriate rasters to the D8_Contributing_Areas mosaic located in the WatershedAttributes.gdb file geodatabase.

Flow Accumulation Outputs: Stream raster grids are one of the required inputs for the TauDEM Move Outlets to Streams script. I used the Stream Definition by Threshold script located in the TauDEM Stream Network Analysis toolset to create stream raster grids. The Stream Definition by Threshold script works by indicating the location of streams, using a value of 1 for stream cells and 0 for all other cells within the raster (Tarboton et al., 2015). Input files were D8 contributing area grids located in the D8_Contributing_Area mosaic, and output rasters were saved to a folder located on my computer. Once created, the Add Rasters to Mosaic Dataset (Data Management) tool was used to add appropriate rasters to the Flow_Accumulation mosaic located in the WatershedAttributes.gdb file geodatabase.

Moved to Stream Points: Sub-meter GPS points need to be moved to stream locations in order to determine the D8 Contributing Area flowing to each point. I used the Move Outlets to Streams script located in the TauDEM Stream Network Analysis toolset. To save time and labor, I batch ran this script for each of the sub-meter GPS points at once by creating a batch tool. The Move Outlets to Streams script works by moving points downslope according to the D8 flow direction grid until it has reached a stream, according to the stream rasters grid. Points that are already located on streams will not be moved (Tarboton et al., 2015). Input files were sub-meter GPS points located in the Sub_Meter_GPS_Points feature dataset and stream raster grids located in the Flow_Accumulation mosaic. Output points were saved to a folder on my computer, then exported to the Moved_to_Streams_GPS_Points feature dataset located in the WatershedAttributes.gdb file geodatabase.

Points D8 Contributing Areas: Determining the D8 contributing area for each individual point is the first step in defining each plot's watershed area, defined by a top and bottom point. I used the D8 Contributing Area script located in the TauDEM Basic Grid Analysis toolset to create D8 contributing area grids for the watershed area contributing to each individual point. This script was unable to be ran in batch form, so I manually ran it for each individual point. The D8 Contributing Area script works by calculating the total of a cells own contribution, plus the contribution from neighboring upslope cells that drain into a single point according to the D8 flow direction models (Tarboton et al., 2015). Input files were D8 flow direction grids located in the D8_Flow_Directions mosaic and moved to stream points located in the Moved_to_Streams_GPS_Points feature dataset. Output rasters were saved to a folder on my computer, then exported to the Point_D8_Contributing_Areas mosaic located in the WatershedAttributes.gdb file geodatabase.

Dissolved Rasters: In order to create polygons from the point D8 contributing areas, these rasters needed to be dissolved so each cell had the same value of 0. I used Raster Calculator (Spatial Analyst Tools) in ArcPro and input the following equation with each point D8 contributing area raster, located in the Point_D8_Contributing_Areas mosaic, to create dissolved raster outputs.

Int ("Point_D8_Contributing_Area raster name" * 0)

Output rasters were saved to a folder on my computer, then added to the Dissolved_Rasters mosaic located in the WatershedAttributes.gdb file geodatabase using the Add Rasters to Mosaic Dataset (Data Management) tool in ArcPro.

Point Area Polygons: Point area polygons for each top and bottom point are needed to determine the watershed area for each plot in this study. I used Raster to Polygon (Conversion Tools) in ArcPro to do this. To save time, I batch ran this tool for each of the dissolved rasters at once by creating a batch tool. Input files were the dissolved rasters located in the Dissolved_Rasters mosaic and output polygons were saved to a folder on my computer, the exported to the Point_Watershed_Areas feature dataset in the WatershedAttributes.gdb file geodatabase using the Feature Class to Geodatabase (geoprocessing tools) in ArcPro.

Final Individual Watershed Areas: Final watershed areas are defined by the area between top and bottom points for each site in this study. I used Erase (Analysis Tools) in ArcPro to erase the top point area polygon from the bottom point area polygon to create a polygon that contains only the area between these two points. Input files were the bottom point area polygons for each site and erase features were the top point area polygons for each site, both located in the Point_Watershed_Areas feature dataset. Output polygons were saved to a folder on my computer, then exported to the Final_Watershed_Areas feature dataset located in the WatershedAttributes.gdb file geodatabase using the Feature Class to Geodatabase (geoprocessing tools) in ArcPro. Please note that not all top and bottom area polygons reached each other and needed manual edits to complete the final watershed area polygons. Watershed areas in question (BISH 4, BISH 7, MEL 4, MEL 5, NASE 8, TOUT 4, and TOUT 5) were manually determined by using point area polygons, WA DTMHS tiles, and flow accumulation rasters to determine the correct extent of these watersheds. I used the Edit Vertices tool on the Edit Ribbon in ArcPro to manually edit the final individual watershed polygon shape before exporting final feature classes to the WatershedAttributes.gdb file geodatabase.

Merged Final Watershed Areas: Final watershed area polygons for each study area (BISH, DELE, KID, MEL, NASE, NEWS, and TOUT) needed to be merged into one feature class to quickly calculate slope statistics for each watershed within a study area at once. I used Merge (Data Management Tools) in ArcPro to combine all final watershed area polygons into one feature class. Input features were the final individual watershed areas located in the Final_Watershed_Areas feature dataset. Output features were saved to a folder on my computer. I created a new field within the attribute table for each merged feature for the name of each individual watershed area. Once complete, the merged watershed areas were exported to the Merged_Watershed_Areas feature dataset located in the WatershedAttributes.gdb file geodatabase.

Slope Rasters: Slope rasters for each study area (BISH, DELE, KID, MEL, NASE, NEWS, and TOUT) needed to be created in order to calculate slope statistics for each individual watershed. I used Slope (Spatial Analyst Tools) in ArcPro to create final slope rasters. Input rasters were the pit filled DTM rasters located in the Pit_Filled_Rasters mosaic, and output slope rasters were saved

to my computer. Once created, the Add Rasters to Mosaic Dataset (Data Management) tool was used to add appropriate rasters to the Slope_Rasters mosaic located in the WatershedAttributes.gdb file geodatabase.

Watershed Attributes

Watershed attributes were calculated for each of the 79 individual watershed areas in this study. Watershed attributes include watershed area (square meters) and slope statistics (min, max, range, mean, STD, SUM, Median, and PCT90). To calculate the area for each individual watershed polygon I created a Shape_Area field within the Merged_Watershed_Areas feature class's attribute table. Once created, I used Calculate Geometry within the attribute table to find the area of each individual polygon. The area unit for this field is square meters. I copied all area value to the Watershed Attributes Excel Workbook (Appendix C).

To calculate the slope statistics for each watershed polygon I used Zonal Statistics as Table (Spatial Analyst Tools) in ArcPro. Input feature zone data files were the Merged_Watershed_Areas feature classes, input zone fields were "name", and input value rasters were the Slope_Rasters, located in the WatershedAttributes.gdb. I saved output tables to my computer then copied the information for all individual watershed within all study areas (BISH, DELE, KID, MEL, NASE, NEWS, and TOUT) to the Watershed Attributes Excel workbook (Appendix D).

Models & Scripts

ESRI's ModelBuilder was used in ArcPro to create the Final Watershed Area Polygon model (Appendix E) and the Watershed Slope Statistics model (Appendix F). Tools from both the ArcPro toolbox and scripts from the TauDEM toolbox's toolsets were used to create the Final Watershed Area Polygon model while only tools from the ArcPro toolbox were used to create the Watershed Slope Statistics model. Both Models were exported from ArcPro into Python files, that will be shared with project partners. *Please note that exported Python files may not be functioning due to TauDEM tools not working in ModelBuilder. See more information in the Discussion section.*

DELIVERABLES

Sub-Meter GPS Points

125 Sub-Meter GPS points represent the top and bottom points for each of the 79 watershed areas in this study. GPS point data is available in decimal degree format in the Watershed Attributes Excel workbook (Appendix A) and as individual feature classes located in the Sub_Meter_GPS_Points feature dataset in the WatershedAttributes.gdb file geodatabase.

File Geodatabase

The WatershedAttributes.gdb file geodatabase contains feature datasets and raster mosaics with all relevant layers and tool outputs for all sub-meter GPS points and watershed areas. datasets include sub-meter GPS point plot locations, moved to stream points, final individual watershed areas, merged final watershed areas, and points area polygons. Raster mosaics include WA DTM tiles, WA DTMHS tiles, pit filled DTM tiles, D8 flow direction outputs, D8 slope grid outputs, D8 contributing area outputs, point D8 contributing areas, dissolved raster outputs, slope raster outputs, and flow accumulation outputs. When using the Edit Vertices tool to manually determine watershed areas, I created both minimum and maximum area polygons for TOUT 4 and TOUT 5 watersheds. Due to the planar slopes and forest roads that may or may not contribute water to these watersheds, it was hard to determine the exact extent of these watershed areas. In-field reconnaissance will be the best way to determine whether or not the upslope forest roads are contributing to these areas. A contents key with descriptions can be referenced in the Watershed Attributes Excel workbook (Appendix B).

Watershed Attributes

Watershed attributes were calculated for each of the 79 individual watershed areas in this study are available in the Watershed Attributes Excel workbook. Watershed attributes include watershed area (square meters) (Appendix C) and slope statistics (min, max, range, mean, STD, SUM, Median, and PCT90) (Appendix D).

Models & Scripts

Two ModelBuilder models were created for the Final Watershed Area Polygon (Appendix E) and Watershed Slope Statistics (Appendix F) processes. Models included tools from both the ArcPro

Toolbox and scripts from the TauDEM toolbox's toolsets. Python files were exported from ArcPro for both model that will be shared with project partners. *Please note that exported Python files may not be functioning due to TauDEM tools not working in ModelBuilder. See more information in the Discussion section.*

DISCUSSION

Working with the TRIUMPH-2 JAVAD GNSS was a new experience and had some limiting factors associated with it, as a non-DNR employee. The output file type from the TRIUMPH-2 JAVAD GNSS is a .JPS file, which is only readable by JAVAD NetView & Modem software. This did not present any issues for the collected GPS points that Alexander Prescott originally shared with me, as he had converted those into decimal degree format. However, when it came to correcting the .JPS files he could not get coordinates for, or to using the additional .JPS files sent to me from West Fork Environmental throughout this project, I needed to rely on Nathan Waldren with the WA DNR for assistance. As mentioned in the methods section, JAVAD's NetView & Modem software is required to correct .JPS files and convert them into decimal degree format. This should be noted in future projects where Javad NetView & Modem software is required to prevent time being spent on troubleshooting how to work with, access, or correct these file types.

In future projects that require the use of the TauDEM ArcGIS Toolbox, it should be noted that TauDEM 5.3 has been tested for ArcGIS versions 10.0, 10.2.2, and 10.3.1, but not ArcPro (Tarboton et al., 2015). While I was able to use all "D8" tool scripts to reach the end goal for this project, I was unable to use any "D-Infinity" tool scripts. I was also unable to run batch versions of any TauDEM tools or use them in ModelBuilder. TauDEM scripts may need to be modified in some way to be used in ArcPro or ModelBuilder in conjunction with other tools, but fully troubleshooting this was beyond the scope of my project. Please note that this may cause exported Python files not to function correctly. Another thing I had to troubleshoot with TauDEM was file path and naming practices. The TauDEM scripts do not always work when working out of a geodatabase. Nathan Nelson with the US Forest Service gave me guidance on making sure to save all working rasters and feature classes to folders on my computer's drive and keep file names to a maximum of 13 characters. I experienced no further problems with input datasets after making sure these two steps were followed, and exporting feature classes and rasters to the file geodatabase after they were created and used as inputs for other tools.

CONCLUSION

Both the TRIUMPH-2 JAVAD GNSS and TauDEM Toolbox scripts were new tools that required learning and troubleshooting throughout the entirety of this project. Through the support of my project sponsor, project partners, WA DNR employees, instructors at Green River College and strangers on internet help forms, I was able to successfully complete the required deliverables and have gained a better understanding of spatial analysis processes and problem solving. The final individual watershed polygons and watershed attributes will be used in conjunction with sediment runoff data to better understand the relationship between contributing watershed characteristics and total water discharge and timing. Gaining a better understanding of these relationships will assist in the development of process-based numerical modeling framework that can be used to generate field-testable hypotheses, as well as open future avenues for road sediment and BMP research. A greater process-based understanding, rooted in scientific evidence, will ensure that the most effective BMP are being applied in our forests.

REFERENCES

NOAA. (2010, August 13). *Opus: The online positioning user service, process your GNSS data in the National Spatial Reference System*. OPUS: the Online Positioning User Service, process your GNSS data in the National Spatial Reference System. <https://geodesy.noaa.gov/OPUS/about.jsp#:~:text=OPUS%20uses%20the%20same%20software,will%20be%20emailed%20to%20you>.

Tarboton, D. G., Sazib, N., & Dash, P. (2015, October). *QUICK START GUIDE TO USING THE TAUDEM ARCGIS TOOLBOX*. Utah State University Hydrology Research Group. <https://hydrology.usu.edu/taudem/taudem5/documentation.html>

APPENDECIES

Appendix A – Sub-meter GPS Points

Name:	Latitude:	Longitude:
BISH_1_BOT	46.7985374	-123.7499527
BISH_1_TOP	46.7989848	-123.7491944
BISH_10_BOT	46.7864873	-123.8003547
BISH_10_TOP	46.78599368	-123.801126
BISH_11_BOT	46.7854264	-123.8053296
BISH_11_TOP	46.78524228	-123.8043112
BISH_12_TOP	46.78546777	-123.805527
BISH_2_BOT	46.7912459	-123.7762603
BISH_2_TOP	46.79108234	-123.7773141
BISH_3_BOT	46.7911451	-123.7815305
BISH_3_TOP	46.7911965	-123.7805073
BISH_4_BOT	46.79157532	-123.787659
BISH_4_TOP	46.7908805	-123.7878624
BISH_5_BOT	46.7909121	-123.7888055
BISH_5_TOP	46.7911801	-123.7897307
BISH_6_BOT	46.79174842	-123.7907272
BISH_6_TOP	46.791646	-123.7917135
BISH_7_BOT	46.79150203	-123.793269
BISH_7_TOP	46.79081772	-123.7934367
BISH_9_BOT	46.7867736	-123.7994351
DELE_10_BOT	46.9225262	-123.4419445
DELE_10_TOP	46.9219769	-123.442566
DELE_4_BOT	46.9343424	-123.4081817
DELE_4_TOP	46.933857	-123.4089429
DELE_6_BOT	46.9308028	-123.4144599
DELE_6_TOP	46.93088502	-123.4155216
DELE_8_BOT	46.9249649	-123.436363
DELE_8_TOP	46.92467625	-123.4372953
DELE_9_BOT	46.9215047	-123.4460218
DELE_9_TOP	46.92145589	-123.444972
KID_1_BOT	46.38458782	-122.5984045
KID_13_BOT	46.391601	-122.557462
KID_13_TOP	46.3916432	-122.5585037
KID_14_BOT	46.3912605	-122.5566409
KID_15_BOT	46.3906031	-122.5564646
KID_16_BOT	46.38989235	-122.5567774
KID_2_BOT	46.3848211	-122.5974233
KID_26_BOT	46.36295368	-122.5006144
KID_26_TOP	46.3629703	-122.5016086
KID_27_BOT	46.36158945	-122.4993331
KID_28_BOT	46.36144795	-122.4983569
KID_29_BOT	46.3608967	-122.4976854
KID_3_BOT	46.3848288	-122.5963756
KID_30_BOT	46.3603472	-122.4967052

Capstone in Natural Resources

KID_30_TOP	46.36079585	-122.4975107
KID_31_BOT	46.3596262	-122.4957399
KID_32_BOT	46.3575383	-122.4899692
KID_32_TOP	46.35822843	-122.49027
KID_33_BOT	46.3568487	-122.4874774
KID_33_TOP	46.35666641	-122.48848
KID_34_BOT	46.3570943	-122.486478
KID_37_BOT	46.3656273	-122.4436852
KID_37_TOP	46.36493322	-122.4438921
KID_38_BOT	46.36601784	-122.4428881
KID_39_BOT	46.36609334	-122.4418723
KID_4_BOT	46.3849433	-122.5954331
KID_40_BOT	46.3660355	-122.4406962
KID_40_TOP	46.36603782	-122.4396478
KID_43_BOT	46.3712207	-122.4204362
KID_44_BOT	46.3717454	-122.4197408
KID_44_TOP	46.3722309	-122.4189888
KID_46_BOT	46.37275914	-122.4161399
KID_46_TOP	46.37268649	-122.4152079
KID_5_BOT	46.38544701	-122.5947623
KID_5_TOP	46.38607631	-122.5942997
KID_52_BOT	46.35919009	-122.4943903
KID_52_TOP	46.35946823	-122.4953689
KID_7_BOT	46.38729743	-122.5927025
KID_7_TOP	46.3876582	-122.5918025
MEL_1_BOT	46.95819936	-123.4843746
MEL_11_BOT	46.9354304	-123.5491059
MEL_11_TOP	46.9357978	-123.5481933
MEL_12_BOT	46.9335661	-123.5511113
MEL_12_TOP	46.9341555	-123.5505196
MEL_13_TOP	46.93319031	-123.551697
MEL_14_BOT	46.93308337	-123.5530309
MEL_2_BOT	46.9580894	-123.4833447
MEL_2_TOP	46.9575719	-123.4830434
MEL_4_BOT	46.9568476	-123.4816725
MEL_4_TOP	46.9561793	-123.4813952
MEL_5_BOT	46.95582117	-123.481131
MEL_5_TOP	46.95543653	-123.4813507
NASE_1_BOT	46.30673506	-123.7856328
NASE_1_TOP	46.30652543	-123.7846902
NASE_10_BOT	46.3167035	-123.7377639
NASE_11_BOT	46.31668856	-123.7387752
NASE_11_TOP	46.3166792	-123.7398307
NASE_12_BOT	46.3181238	-123.7441204
NASE_12_TOP	46.3181324	-123.7450879
NASE_13_BOT	46.31079513	-123.7590563
NASE_13_TOP	46.31135494	-123.7584195

Capstone in Natural Resources

NASE_2_BOT	46.30608649	-123.7824245
NASE_3_BOT	46.3057214	-123.7815996
NASE_4_BOT	46.30517168	-123.7809504
NASE_4_TOP	46.3047398	-123.7802036
NASE_5_BOT	46.31755605	-123.7234482
NASE_5_TOP	46.3172522	-123.7243853
NASE_6_BOT	46.31670504	-123.7269248
NASE_6_TOP	46.31635825	-123.7260464
NASE_7_BOT	46.31588819	-123.7282922
NASE_7_TOP	46.31644505	-123.7276557
NASE_8_BOT	46.31615521	-123.7293046
NASE_9_BOT	46.31521424	-123.7306717
NEWS_19_BOT	46.86353627	-123.7377783
NEWS_19_TOP	46.8641737	-123.7374317
NEWS_20_BOT	46.86745085	-123.7393133
NEWS_20_TOP	46.8681494	-123.7392001
TOUT_10_BOT	46.2350384	-122.5063342
TOUT_11_BOT	46.2355534	-122.5070499
TOUT_12_BOT	46.2360697	-122.5077769
TOUT_13_BOT	46.23647934	-122.5085863
TOUT_13_TOP	46.2366557	-122.5095757
TOUT_15_BOT	46.23705596	-122.513527
TOUT_15_TOP	46.2369833	-122.5125094
TOUT_19_BOT	46.24197653	-122.5236771
TOUT_19_TOP	46.24142228	-122.5230843
TOUT_20_BOT	46.2424813	-122.5244268
TOUT_22_BOT	46.2435113	-122.5275721
TOUT_22_TOP	46.24312137	-122.5267418
TOUT_24_BOT	46.2492406	-122.5459729
TOUT_24_TOP	46.2497442	-122.5453224
TOUT_4_BOT	46.2299887	-122.4835691
TOUT_5_BOT	46.2300027	-122.4846094
TOUT_5_TOP	46.2300231	-122.4856436
TOUT_9_BOT	46.23452085	-122.5056664

Appendix B – File Geodatabase Contents Key

WatershedAttributes.gdb Contents		
Name:	Type:	Description:
Final_Watershed_Areas	Feature Dataset	Final watershed polygons of individual watersheds between plot top and bottom points
Merged_Watershed_Areas	Feature Dataset	Final watershed polygons for each study area (BISH, DELE, KID, MEL, NASE, NEWS, TOUT)
Moved_to_Streams_GPS_Points	Feature Dataset	Output points of TauDEM Move Outlets To Streams tool for each plot point
Point_Watershed_Areas	Feature Dataset	Individual watershed polygons per point (prior to erasing top polygon from bottom polygon)
Sub_Meter_GPS_Points	Feature Dataset	Actual Plot Locations (prior to using TauDEM Move Outlets To Streams tool)
D8_Contributing_Areas	Mosaic Dataset	Output D8 Contributing Area Grid of TauDEM D8 Contributing Area tool for each study area (BISH, DELE, KID, MEL, NASE, NEWS, TOUT)
D8_Flow_Directions	Mosaic Dataset	Output Flow Direction Grid of TauDEM D8 Flow Directions tool for each study area (BISH, DELE, KID, MEL, NASE, NEWS, TOUT)
D8_Slope_Grids	Mosaic Dataset	Output Slope Grid of TauDEM D8 Flow Directions tool for each study area (BISH, DELE, KID, MEL, NASE, NEWS, TOUT)
Dissolved_Rasters	Mosaic Dataset	Dissolved Point D8 Contributing Area rasters (input for Point Watershed Areas)
DTM_Rasters	Mosaic Dataset	WA State Lidar DTM tiles for each study area (BISH, DELE, KID, MEL, NASE, NEWS, TOUT)
DTMHS_Rasters	Mosaic Dataset	WA State Lidar Hillshade tiles for each study area (BISH, DELE, KID, MEL, NASE, NEWS, TOUT)
Flow_Accumulation	Mosaic Dataset	Output Stream Raster Grid of TauDEM Stream Definition By Thershold tool for each study area (BISH, DELE, KID, MEL, NASE, NEWS, TOUT)
Pit_Filled_Rasters	Mosaic Dataset	Output Pit Removed Elevation Grid of TauDEM Pit Remove tool for each study area (BISH, DELE, KID, MEL, NASE, NEWS, TOUT)
Point_D8_Contributing_Areas	Mosaic Dataset	Output D8 Contributing Area Grid of TauDEM D8 Contributing Area tool for each plot top and bottom points
Slope_Rasters	Mosaic Dataset	Output Raster of Slope (Spatial Analysis Tool) for each study area (BISH, DELE, KID, MEL, NASE, NEWS, TOUT)

Appendix C – Watershed Areas

Name:	Area (sq meters):
BISH_1	1349.41
BISH_2	5246.26
BISH_3	5707.05
BISH_4	2828.75
BISH_5	12586
BISH_6	3040.33
BISH_7	3143.24
BISH_10	2979.18
BISH_11	12330.13
BISH_12	1020.48
DELE_4	6792.52
DELE_6	2884.08
DELE_8	2382.76
DELE_9	8613.80
DELE_10	16376.98
KID_1	10670.08
KID_2	27454.81
KID_3	16977.62
KID_4	10050.98
KID_5	5220.45
KID_7	9427.99
KID_13	7469.51
KID_14	4021.17
KID_15	1917.53
KID_16	6064.11
KID_26	6916.88
KID_27	15072.02
KID_28	10117.99
KID_29	9908.69
KID_30	9418.74
KID_31	12234.55
KID_32	2590.09
KID_33	19159.31
KID_34	14750.47
KID_37	3863.91
KID_38	6792.92
KID_39	9103.43
KID_40	36035.56
KID_43	22148.81
KID_44	19297.55
KID_46	8187.61
KID_52	17271.19
MEL_1	10937.60
MEL_2	1331.35

MEL_4	2947.93
MEL_5	1154.30
MEL_11	1818.66
MEL_12	2661.53
MEL_13	2233.55
MEL_14	4319.23
NASE_1	5141.97
NASE_2	16501.10
NASE_3	15519.69
NASE_4	5986.48
NASE_5	2770.00
NASE_6	5752.60
NASE_7	24134.16
NASE_8	6777.81
NASE_9	11301.25
NASE_10	2584.95
NASE_11	2386.91
NASE_12	6074.41
NASE_13	1135.89
NEWS_19	3371.94
NEWS_20	4713.93
TOUT_4_min	28648.25
TOUT_4_max	29391.88
TOUT_5_min	24547.29
TOUT_5_max	139833.37
TOUT_9	7528.38
TOUT_10	21048.39
TOUT_11	12262.87
TOUT_12	19287.43
TOUT_13	19449.99
TOUT_15	9999.79
TOUT_19	4221.51
TOUT_20	26392.05
TOUT_22	7329.28
TOUT_24	2666.98

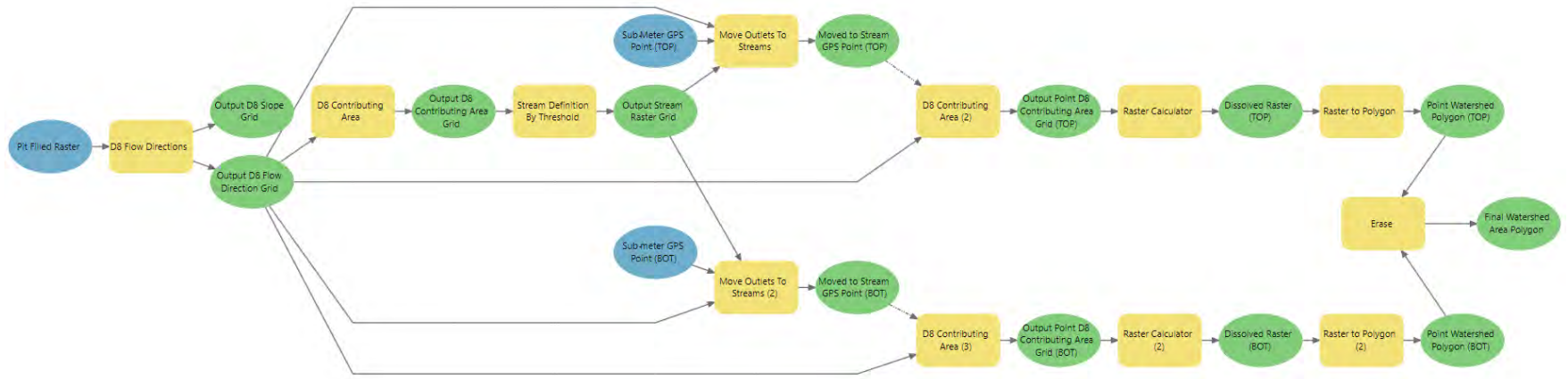
Appendix D – Watershed Slope Statistics

Name:	Min:	Max:	Range:	Mean:	STD:	SUM:	Median:	PCT90:
BISH_1	0.38	74.59	74.21	33.13	18.68	78045.31	33.95	57.94
BISH_2	0.16	75.39	75.24	36.60	14.62	335161.54	37.23	54.18
BISH_3	0.24	74.59	74.35	29.05	14.59	289538.56	27.49	47.65
BISH_4	0.46	76.73	76.27	34.73	14.42	171539.93	34.46	53.74
BISH_5	0.34	77.53	77.19	44.27	15.66	972888.86	45.83	63.61
BISH_6	0.00	81.39	81.39	48.26	20.31	255948.43	50.73	72.97
BISH_7	0.00	76.65	76.65	41.28	13.94	226684.26	41.45	58.73
BISH_10	0.14	72.12	71.99	32.85	17.22	170801.65	30.64	59.88
BISH_11	0.14	79.00	78.86	42.99	14.40	925092.20	44.26	60.30
BISH_12	2.90	79.03	76.13	52.83	14.61	94035.77	55.07	68.86
DELE_4	1.02	76.90	75.88	54.64	15.34	411707.25	58.96	68.90
DELE_6	0.36	77.79	77.43	39.69	20.36	126805.40	43.42	64.29
DELE_8	0.19	72.74	72.55	46.69	19.46	123128.07	52.27	67.19
DELE_9	0.89	79.88	78.99	48.64	14.66	463876.70	50.65	65.66
DELE_10	0.00	75.50	75.50	47.83	16.40	868413.72	51.75	65.33
KID_1	2.25	75.77	73.53	46.65	10.97	862504.61	48.73	57.83
KID_2	0.00	77.41	77.41	34.76	16.08	1654203.07	35.65	55.12
KID_3	0.00	78.34	78.34	31.20	12.68	917959.80	31.20	46.74
KID_4	0.16	73.91	73.75	31.24	11.49	544280.03	31.16	45.39
KID_5	0.96	75.04	74.09	29.83	13.19	269881.91	28.50	47.26
KID_7	0.00	76.15	76.15	27.81	15.25	454321.04	25.60	49.47
KID_13	0.00	62.53	62.53	25.43	11.18	329466.22	25.17	40.30
KID_14	0.00	69.04	69.04	25.06	12.06	174966.03	24.04	39.82
KID_15	0.00	69.83	69.83	28.34	13.73	94170.54	27.02	47.07
KID_16	0.00	67.18	67.18	28.46	12.28	299152.78	27.93	45.02
KID_26	0.00	75.49	75.49	37.78	17.12	452922.72	38.52	60.02
KID_27	0.00	77.03	77.03	31.44	18.20	820586.57	28.54	58.18
KID_28	0.00	78.59	78.59	33.96	16.27	595882.59	32.14	55.99
KID_29	0.00	76.42	76.42	39.59	15.26	679461.86	41.37	57.88
KID_30	0.00	73.83	73.83	41.80	14.04	682508.42	43.96	57.68
KID_31	0.00	75.55	75.55	35.52	15.89	752610.53	35.01	57.09
KID_32	1.79	76.59	74.81	39.11	17.88	175375.18	39.39	61.08
KID_33	0.00	76.21	76.21	48.50	11.21	1609646.84	49.58	60.85
KID_34	0.00	76.17	76.17	44.60	11.99	1139330.95	44.93	59.08
KID_37	0.97	76.56	75.58	28.42	13.93	190140.72	26.30	47.34
KID_38	0.34	76.31	75.98	29.71	14.19	349650.01	28.26	47.94
KID_39	0.12	75.61	75.49	35.74	14.04	564039.69	36.34	51.49
KID_40	0.00	78.91	78.91	30.98	14.69	1934349.94	29.56	51.47
KID_43	0.00	78.46	78.46	38.81	14.21	1488970.53	40.12	56.13
KID_44	0.07	72.04	71.97	36.69	11.77	1226753.87	37.49	51.09
KID_46	0.00	73.99	73.99	34.00	13.61	482239.69	34.56	50.37
KID_52	0.00	77.00	77.00	31.60	15.91	945171.51	29.48	53.08
MEL_1	0.00	76.66	76.66	40.34	12.92	772646.34	43.11	54.00
MEL_2	7.95	77.72	69.78	45.71	16.79	106495.44	46.39	69.19
MEL_4	0.00	78.50	78.50	42.30	18.40	218420.44	44.62	64.53
MEL_5	0.31	77.72	77.41	23.61	15.25	47734.73	19.47	43.93
MEL_11	0.31	80.44	80.13	40.29	22.46	128296.41	40.85	71.01
MEL_12	1.92	80.86	78.94	49.69	19.33	231696.95	53.41	72.81
MEL_13	0.48	77.80	77.32	38.98	18.70	152394.58	36.96	69.86
MEL_14	0.00	75.70	75.70	31.89	13.64	240970.60	30.80	51.89
NASE_1	0.12	75.10	74.98	34.21	16.17	304128.04	33.92	56.71
NASE_2	0.00	76.34	76.34	32.43	15.63	926000.39	31.60	53.92
NASE_3	0.00	75.75	75.75	28.22	15.51	758483.94	26.56	50.02
NASE_4	0.00	78.51	78.51	34.82	15.08	360734.33	35.18	54.21
NASE_5	0.08	80.00	79.92	52.38	19.51	251047.81	58.63	71.98
NASE_6	0.34	78.71	78.37	34.69	14.72	345323.00	35.19	52.73
NASE_7	0.00	79.98	79.98	28.70	14.28	1198934.39	27.20	48.71

Capstone in Natural Resources

NASE_8	0.17	80.19	80.03	37.13	19.54	435294.61	35.32	64.36
NASE_9	0.00	79.49	79.49	31.73	15.68	620698.02	30.19	52.84
NASE_10	0.00	79.27	79.27	50.10	19.93	223864.59	57.43	71.10
NASE_11	0.43	80.20	79.77	45.37	21.88	187153.41	50.73	73.10
NASE_12	0.62	73.75	73.13	38.39	15.87	403568.78	38.54	59.45
NASE_13	1.30	81.53	80.23	46.06	20.82	90961.74	50.95	71.27
NEWS_19	1.48	72.49	71.01	47.01	16.99	175097.31	51.78	64.97
NEWS_20	0.00	72.79	72.79	32.57	17.19	169632.37	30.16	59.13
TOUT_4_min	0.00	83.08	83.08	54.46	15.17	10785640.24	58.25	69.93
TOUT_4_max	0.00	83.08	83.08	53.92	15.46	10956247.04	57.77	69.86
TOUT_5_min	0.00	84.14	84.14	53.74	16.60	9117627.01	58.94	69.89
TOUT_5_max	0.00	84.14	84.14	34.26	16.15	33116469.46	32.67	58.72
TOUT_9	0.00	75.92	75.92	37.10	12.02	1931526.80	37.64	51.97
TOUT_10	0.00	77.39	77.39	40.18	12.32	5847488.56	40.51	55.94
TOUT_11	0.00	77.67	77.67	41.41	13.36	3510793.25	42.75	58.31
TOUT_12	0.00	78.19	78.19	39.87	15.41	5317167.43	43.06	57.34
TOUT_13	0.00	79.35	79.35	39.14	15.94	5264138.50	40.14	60.02
TOUT_15	0.00	78.31	78.31	39.37	15.84	2722196.35	39.43	60.12
TOUT_19	0.74	79.86	79.12	45.88	16.75	1339840.92	45.45	70.28
TOUT_20	0.00	80.66	80.66	31.39	18.08	5729579.89	28.32	58.45
TOUT_22	0.00	79.41	79.41	38.77	15.29	1966111.87	39.46	58.18
TOUT_24	0.41	77.69	77.28	33.29	17.26	614044.12	31.26	58.39

Appendix E – Final Watershed Area Polygon Model



Appendix F – Watershed Slope Statistics Model

